THÈSE DE DOCTORAT

de l'Université de recherche Paris Sciences et Lettres
PSL Research University

Préparée à MINES Paristech

Aspects thermodynamiques du captage des gaz acides à partir du gaz naturel

Ecole doctorale n°432

Science des Métiers de l'ingénieur

Spécialité Energétique et procédés

COMPOSITION DU JURY :

M. WESTACOTT Robin
Heriot-Watt University, Rapporteur

M. DE WEIRELD Guy
Mons University, Rapporteur

M. KONTOGEORGIS Georgios
Technical University of Denmark,
Président du jury

M. CADOURS Renaud
Total, Membre du jury

M. COQUELET Christophe
Mines ParisTech, PSL Research
University, Membre du jury

Mme. EL AHMAR Elise
Mines ParisTech, PSL Research
University, Membre du jury

Soutenue par Tianyuan **WANG**
le 07 12 2017

Dirigée par **Christophe Coquelet**
Encadrée par **Elise El Ahmar**

To Qiao,

And our parents

ACKNOWLEDGMENTS

I would first like to thank my two thesis supervisors, Christophe Coquelet and Elise El Ahmar for their generosity in CTP, for our many exchanges and for their support during these three years of thesis.

I would like to thank Pr. Guy Weireld, Dr.Robin Westacott, Pr. Georgios, Kontogeorgis, Dr. Renaud Cadours for accepting to review my thesis and for their advices. I would also like to thank Pr. Georgios, Kontogeorgis not only for accepting to be the chairman of the thesis committee but also for our discussions during the meetings we had in DTU when I spent unforgettable three months in Denmark thanks to a great team in CERE.

I express in these lines all my thanks for the members of the CTP: Jocelyne and Marie-Claude for helping me on administrative things; Alain, Pascal, Eric, David and Hervé for helping me on the experimental. PhDs, Marco, Fan, Jamal, Martha, and Mauro for our discussions.

Thanks to my colleagues and friends, I enjoyed my stay in Fontainebleau.

Thanks to Qiao, and thanks to our family for their support since we were born.

List of Symbols

Abbreviations

AAD	*Average absolute deviation*
ARD	*Average absolute relative deviation*
BIP	*Binary interaction parameter*
CPA	*Cubic Plus Association*
CR	*Combining Rule*
DEA	*Diethanolamine*
DMS	*Dimethyl sulfide*
DM	*Deshmuch Mather model*
EM	*Ethyl mercaptan*
E-NRTL	*Electrolyte Non random two liquids model*
EoS	*Equation of State*
FID	*Flame ionization detector*
Func	*Objective function*
HETP	*Height Equivalent to a Theoretical Plate*
GC	*Gas Chromatography*
MEA	*Monoethanolamine*
MDEA	*Methyl diethanolamine*
MM	*methyl mercaptan*
n-PM	*n-Propyl mercaptan*

n-BM	*n-Butyl mercaptan*
NRTL	*Non random two liquids*
PR	*Peng Robinson*
ppm	*Part per million*
ROLSI	*Rapid online sampler injector*
SRK	*Soave – Riedlich - Kwong*
SAFT	*Statistical Associating Fluid Theory*
TCD	*Thermal conductivity detector*
UNIFAC	*Universal quasi chemical*
UNIQUAC	*Universal quasi chemical model Functional activity coefficient model*
VLE	*Vapour – liquid equilibrium*
VLLE	*Vapour – liquid – liquid equilibrium*
vdW	*van der Waals*

Latin letter

a	*energy parameter*
a_o	*parameter in energy term*
a_i	*activity of component i*
A	*Debye and Hückel parameter*
B	*Debye and Hückel parameter*
b	*co-volume parameter*
c	*Parameter of the equation of state*
d	*Temperature dependent segment diameter*
f	*Fugacity*

f_L	*Fugacity in solution*
G	*Gibbs energy*
g^E	*Excess Gibbs energy*
$g(d)$	*radial distribution function*
h	*Enthalpy*
H	*Henry's law constant*
I	*Ionic strength based on ionic strength*
K	*Equilibrium constant*
ρ	*Density*
k_{ij}	*Binary interaction parameter in mixing rule*
l_{ij}	*Dimensionless constant for binary interaction parameter for the asymmetric term*
m_i	*Molality of species i*
M	*molar mass*
N	*Number of moles*
N_A	*Avogadro's number, [1/mol]*
Nc	*Number of components*
P^v	*Vapour pressure*
P	*Pressure*
R	*Universal gas constant*
S	*Entropy*
T	*Temperature [K]*
v	*Molar volume [cm^3/ mol]*

v^l	*Saturated liquid volume*
x	*Liquid mole fraction*
X^{Ai}	*Mole fraction of component not bonded at site A of component i*
y	*Vapour mole fraction*
z	*initial composition*
Z_i	*number of charge of specie i*
z	*Coordination number in the UNIQUAC model of Abrams and Prausnitz (1975)*

Greek letters:

ϕ	*Fugacity coefficient*
$\hat{\phi}$	*Fugacity coefficient in solution*
γ	*Activity coefficient*
γ_i^{∞}	*Infinite dilution activity coefficient of component i*
μ	*Chemical potential of component i*
β_{ij}	*Model binary interaction parameter in DM model*
ω	*Acentric factor*
β^{AiBj}	*Association volume between site A of component i and site B of component j*
Δ^{AB}	*Strength of interaction between sites A and B.*
Ω	*Numerical constant in the EoS*
ε_0	*Vacuum permittivity*
ε_r	*Relative permittivity (dielectric constant dimensionless)*
ε^{AiBj}	*Association energy between site A of component i and site B of component j*
η	*Reduced density*

Superscript

E	*Excess property*
R	*Residual property*
Sat	*saturated value*
cal	*Calculated property*
exp	*Experimental property*
i,j	*Molecular species*
c	*Critical property*
Ref	*reference property*
L	*Liquid state*
V	*Vapor state*
*	*Property at saturation*
Assoc	*Association*
Res	*residual*

Subscripts

cal	*Calculated property*
exp	*Experimental property*
i, j	*Molecular species*
0	*Reference property*
Cal	*Calculated value*
Exp.	*Experimental value*
c	*critical property*

List of table

List of figures

Introduction

Introduction

Among fossil fuels, natural gas is the cleanest, in terms of CO_2 emission, burn efficiency and amount of air pollutant [1]. Methane is the prevailing element of natural gas; therefore, there are also a variety of impurities. In fact, it contains usually considerable amounts of acid gases (CO_2, H_2S) which can lead to corrosion in equipments and pipelines if water is present. Mercaptans are known as toxic molecules with undesirable odor, and fuel combustion of mercaptan molecules can produce SO_2 which is undesirable chemical, they can cause environmental issues. Acid gases and mercaptans must be removed from natural gas until acceptable standard. The treated natural gas contains as maximum as 2% of CO_2, 2–4 ppm of H_2S and 5–30 ppm of total mercaptans [2]. Chemical absorption with alkanolamines [3] (such as monoethanolamine (MEA), diethanolamine (DEA), methyldiethanolamine (MDEA)) is the most well-established method to separate acid gas from natural gas. Acid gases react with alkanolamines in the absorber to form electrolyte species, mercaptans and hydrocarbons do not react with alkanolamines molecules, and they are physically absorbed by aqueous alkanolamine solution. The context and the absorption process will be presented in chapter 1. The main aim of this thesis is to develop an accurate thermodynamic model to describe alkane, aromatic and Mercaptans (methane, ethane, propane, n-butane, n-pentane, n-hexane, benzene, toluene, and Methyl Mercaptan, Ethyl Mercaptan) solubilities in aqueous alkanolamine solution, to describe acid gases (CO_2,H_2S) solubilities in aqueous alkanolamine solutions, and to predict other crucial properties like: electrolyte concentration, vapor phase composition (mostly water content), and to predict phase diagram for multi-component system containing CO_2-H_2S-alkanolamine-water-hydrocabon-mercaptan.

In addition, some experimental works were carried out. Methyl and Ethyl mercaptan solubility in aqueous MDEA partition coefficient was determined at three pressures up to 7MPa, at two temperatures of 333 and 365 K, by using a static-analytic method [4]. The other part of experimental work concerns the measurement of apparent Henry's law

constants and infinite dilution activity coefficient for different sulphur component (MM, EM, nPM, iPM, nBM, iBM, DMS) in aqueous MEA solution by using gas stripping method [5]. The experimental set-ups and results are shown in chapter 2.

Chapter 3 describes the thermodynamic models involved in this work. Two different approaches have been presented: the symmetric and the dissymmetric approaches. The PR-CPA EoS has been chosen as the symmetric approach. It has an explicit part to account for hydrogen bonding, making it well suited to describe interested systems where water and alkanolamines molecules form hydrogen bonds between them and themselves (self and cross associations). Alkanes are considered as non-associating components. However, due to the presence of –OH or –SH functional group, aromatic and mercaptans are considered as solvated components. Unlike alkanes, aromatics and mercaptans, for CO_2 and H_2S, the chemical reaction between CO_2 / H_2S – alkanolamine are treated as strong cross association between them, the electrolytes formed after chemical reactions are considered as weak electrolyte which are neglected. The Desmukh–Mather model [6] has been chosen as the dissymmetric approach. This model utilizes the extended Debye–Hückel expression to describe all the activity coefficients of electrolyte species for long distance interactions; it uses an EoS and Henry's law constant to represent the vapour phase. This model is widely used in acid gas-amine-water systems modelling, it is considered as a bench mark model to be compared with our PR-CPA EoS.

Chapter 4 summarizes the results of non-reactive components solubilities (including methane, ethane, propane, n-butane, n-pentane, n-hexane, benzene, toluene, and ethyl-benzene) and mercaptans (MM and EM) in aqueous MDEA, DEA and MEA solutions in VLE, LLE, and VLLE conditions will be treated with PR-CPA EoS. Different thermodynamic properties such as the temperature of minimum solubility, water content, and solubility of two alkanes mixtures in aqueous alkanolamine solutions will be predicted by PR-CPA for model validation. Moreover, experimental data measured in this work will be compared with PR-CPA EoS predictions.

In chapter 5, different configurations of the PR-CPA EoS with the pseudo chemical reaction approach will be investigated to better represent the solubility of acid gas solubility

in aqueous alkanolamine solution. CO_2-MDEA-water ternary system is assigned to be the example system to investigate. The PR-CPA EoS performance will compared to Deshmukh–Mather model results for this system. Different thermodynamic properties such as VLE, liquid phase speciation, enthalpy of absorption, and vapor phase composition will be predicted by PR-CPA EoS for model validation. The PR-CPA EoS will be also used to H_2S-MDEA-H_2O, CO_2-MEA-H_2O, and H_2S-MEA-H_2O ternary systems. And different multicomponent systems such as CO_2-H_2S-H_2O-CH_4, CO_2-H_2S-MEA-H_2O, CO_2-H_2S-MDEA-H_2O, CO_2-MDEA-H_2O-CH_4 CO_2-MDEA-H_2O-CH_4-EM systems will be predicted by PR-CPA EoS.

The conclusion and future works will be presented in the end of this PhD. Thesis.

Chapter 1 Acid gas removal from natural gas

1 Acid gas removal from natural gas

Introduction

Chapter 1 describes the general context of natural gas treatment. The natural gas processing is introduced from upstream to downstream. Different technologies of gas treatment are briefly presented, such as adsorption, membrane, low temperature separation, physical absorption, and chemical absorption. This thesis focus on the chemical absorption, the principal of this process and different types of solvent are detailed in this chapter. The importance of thermodynamic model is highlighted during the modelling of absorption column. The objectives of this work is listed in the end of this chapter.

Le chapitre 1 décrit le contexte général du traitement du gaz naturel. Le traitement du gaz naturel est introduit de l'amont vers l'aval. Différentes technologies de traitement des gaz sont brièvement présentées, telles que l'adsorption, la membrane, la séparation à basse température, l'absorption physique et l'absorption chimique. Cette thèse se concentre sur l'absorption chimique, le principe de ce processus et les différents types de solvants sont détaillés dans ce chapitre. L'importance du modèle thermodynamique est mise en évidence lors de la modélisation de la colonne d'absorption. Les objectifs de ce travail sont présentés à la fin de ce chapitre.

1.1 The growth of energy demand of natural gas

The world's population will increase by 1.5 billion people to reach 8.8 billion people by 2035. Over the same period, the world's economy is estimated to be doubled [7]. Consequently, the demand of energy will be strongly increased, new energy sources with lower carbon content are under development. Hence natural gas is a major energy transition to meet growing global needs, it represents 24% of total primary energy in 2014. Natural gas is known as the cleanest of all fossil fuels, because it emits 30% less CO_2 than oil and 50% less than coal to generate the same amount of heat [8]. The demand of natural gas is still increasing, the estimation is 1.8% per year [7], see Figure 1-1.

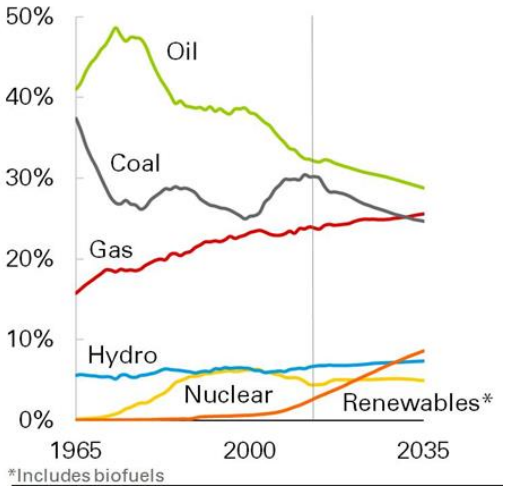

Figure 1-1 Shares of primary energy source from BP[7]

The growth natural gas demand in the world leads to a reassessment of the development potential of natural gas with high acid gas concentration reserves and shale gas reserves that were previously considered economically unsustainable.

1.2 **Natural gas reserves**

Natural gas is formed from the decomposition of plants, animals and micro-organisms. The most widely accepted theory states that fossil fuels are usually formed when organic materials are decayed and compressed under the earth's crust at high pressure and for a very long time (millions of years). Usually, natural gas consist principally of methane (70%-90% on molar composition) and hydrocarbons (ethane, propane, butane, pentane, hexane, and Benzene, Toluene, Ethyl benzene and Xylenes). However, there may exist various impurities in natural gas reserves, we can cite CO_2, H_2S, sulphur components and water. A typical composition of natural gas is shown in Table 1-1.

Table 1-1 : Example of natural gas composition [9]

Components	Composition /mole %
Methane	84.07
Ethane	5.86
Propane	2.20
i-Butane	0.35
n-Butane	0.58
i-Pentane	0.27
n-pentane	0.25
n-Hexane	0.28
n-Heptane and heavier	0.76
Carbon dioxide	1.30
Hydrogen sulphide	0.63
Nitrogen	3.45

The composition of natural gas is related to the type, depth and location of the underground reservoirs of porous sedimentary deposit and the geology of the area. 40% of natural gas reserves are acid gases, i.e. the concentration of CO_2 and H_2S is considerable. Middle

Eastern and central Asian countries have the most important fields, and the concentration of acid gas vary from the location of the natural gas reservoir see Figure 1-2.

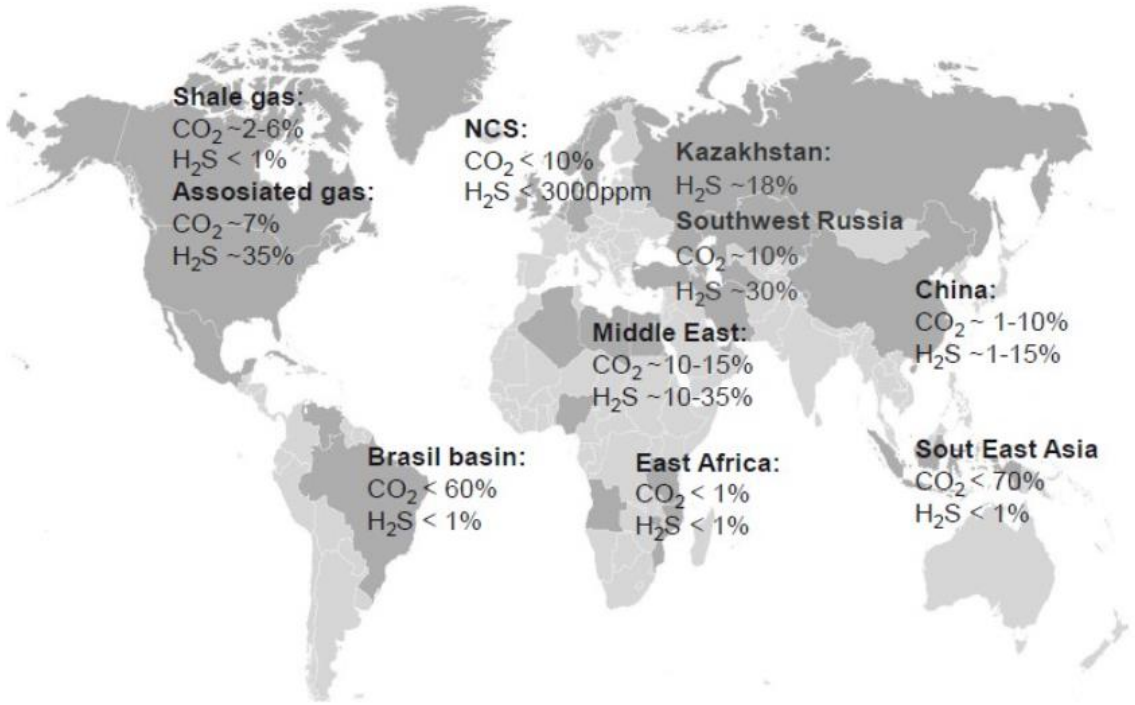

Figure 1-2 Global distribution of CO_2 content in natural gas reserve [10]

Acid gases, majority including CO_2, H_2S and other sulphur species, need to be removed down to sufficiently low levels to meet transportation specification. In fact, acid gases can lead to corrosion in equipments and pipelines if water is present. Corrosion is defined as an irreversible deterioration of a material because of a chemical reaction with its environment. If the reaction continues with the same intensity, the metal can be completely converted into metal salts.

Mercaptans and other sulphur components may also exist in natural gas reserves. Mercaptans are known as toxic molecules with undesirable odour, and fuel combustion of mercaptan molecules can produce Sulphur dioxide SO_2 which is undesirable chemical. SO_2 can cause environmental issues like acid rain.

The treated natural gas must contain as maximum as 2% of CO_2, 2–4 ppm of H_2S and 5–30 ppm (volume) of total mercaptans [2]. To meet this demand, different acid gases

removal technologies have been developed in the last few decades, such as: absorption, adsorption, membrane and low temperature separation technologies. The choice of technology depends on the partial pressure of acid gases in the fuel gas and expected purity of treated gas. Different technologies can be combined in order to benefit from the advantages of each process. Those technologies will be shortly presented in section 1.4.

1.3 **Natural gas processing**

A typical flow diagram of natural gas processing is shown in Figure 1-3. It shows how raw natural gas is processed into sales gas pipelined to the end user markets. It also displays the list of products during to the natural gas processing. The products include [11]:

- Sales gas (mainly methane)
- Ethane
- Natural-gas condensate
- Elemental sulphur
- Natural-Gas Liquids (NGL): propane, butanes and C5+

Raw natural gas is generally collected from a group of gas wells and is treated at the same collection site for water and natural gas condensate removal. The condensate is usually transported to an oil refinery and the water is disposed as waste. Then the raw gas is passed to an acid gas removal plant in order to remove H_2S, CO_2 and other sulphur components (mercaptans, COS, CS_2. Etc). There are many processes available for this purpose, they are briefly introduced in next section, but chemical absorption with amine is the most historical and well established process, it is detailed in next section.

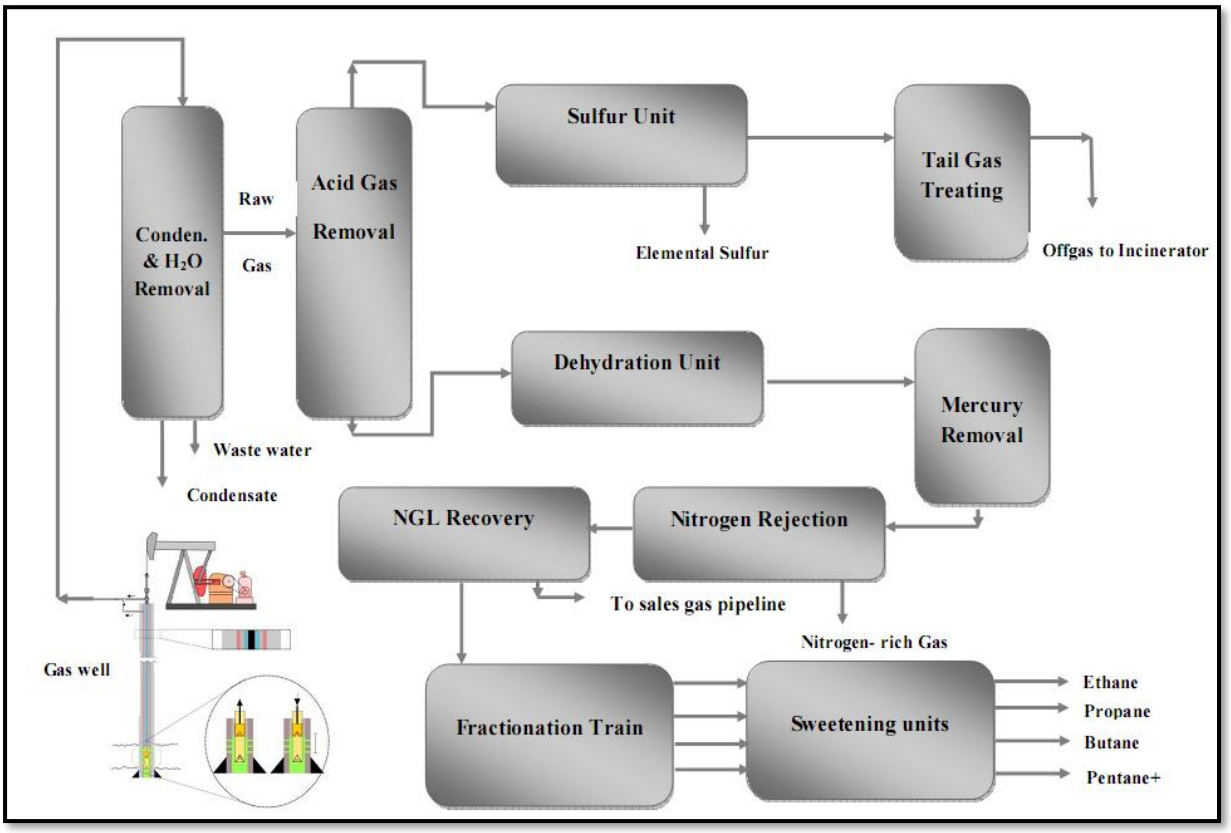

Figure 1-3. Flow diagram of a typical natural gas processing plant [12]

The acid gases are sent to a sulphur recovery unit which converts the H_2S into elemental sulphur or sulphuric acid. The Claus process is by far the most well-known process for sulphur recovery [13].

After passing though dehydration unit, mercury removal unit and nitrogen rejection unit, treated gas is sent to the NGL recovery unit. In this unit, gas can be divided into two parts: one part in gaseous form which contains a lot of methane and ethane, and second part in liquid form which is mainly composed of propane, butane and heavier hydrocarbons (C5 and above). The sales gas is delivered to the customer by pipeline or tanker as liquefied natural gas (LNG).

1.4 Acid gas removal technologies

During the near decades, several technologies such as adsorption, membrane, low temperature separation, physical absorption and chemical absorption have been developed in the aim of acid gas removal from natural gas. Each technology has its advantage and limitation, and is adapted to different situations. The combination of those technologies is also possible. This thesis focus on the chemical absorption process which is the most established one among those technologies.

1.4.1 Adsorption

Pressure Swing Adsorption (PSA) [14] is a gas separation process in which the adsorbent is regenerated by reducing the partial pressure of the adsorbed component. There are three main types of adsorbent: activated carbon, synthetic zeolites and Metal-Organic FrameWorks (MOFs). The main characteristics of an adsorbent are the selectivity, the effective adsorption amount, the mass transfer rate, and the heat of adsorption. The adsorption systems are particularly suited for medium scale processes but not suitable for large scale industrial acid gases capture.

1.4.2 Membrane

Membrane separation processes [15] can separate selectively acid gases from natural gas. They can be applied for high pressure feed gas containing high acid gas concentration. They are based on differences in permeabilities of the gas flowing through the membrane. The permeability of gases is related to the nature of the permanent species (size, shape, and polarity), and the physical-chemical properties of the membrane itself. Nowadays, there are principally two types of membrane which are commercially used for acid gas separation: polymeric membranes and inorganic membranes. Generally, polymeric membranes have good intrinsic transport properties, high processability and low cost[15]. However, inorganic membranes which are more expensive than polymeric membranes are more

preferment in terms of selectivity, temperature and wear resistance, chemically inertness [16].

1.4.3 Low temperature separation

Cryogenic separation is also known as low temperature distillation; it uses a very low temperature for purifying gas mixtures in the separation process [17]. Cryogenic separation is commercially used to liquefy and purify CO_2 from natural gas only containing high CO_2 concentrations (typically greater than 50%). The principle of cryogenic separation is condensation of gases. When the temperature is below the boiling point of CO_2, it begins to condense separate and turns into a liquid state. For other gases in natural gas, each of them will turn to a liquid at a different point, so they can be separated into pure components by using pressure and temperature control. The advantages of this process are the suitability to liquefy and purify the feed gas with high concentration of CO_2 and for producing a liquid CO_2 ready for transportation by pipeline and does not require compression. The main disadvantage of cryogenic separation is that the process is highly energy intensive for regeneration and can significantly decrease the overall plant efficiency when applied to streams with low CO_2 concentration.

1.4.4 Physical absorption

Physical absorption processes [18] are the type of absorption processes where the solvent interacts only physically with acid gases. This process can be used when the feed gas is characterized by high CO_2/H_2S partial pressure and low temperatures. CO_2/H_2S is released at atmospheric pressure. The existence of heavy hydrocarbon in the feed gas restricts the wide use of physical solvent. In addition, low acid gases partial pressures may also discourage the application of physical solvents. The choice of physical solvent is case dependent, for example: methanol is a physical solvent process that has been used for removing CO_2, Selexol [19] and Glycol [20] are effective for capturing both CO_2 and H_2S, Glycerol carbonate [21] has high selectivity for CO_2 over H_2S. The disadvantage of this process is that the solvent is needed to be regenerated at low temperature.

1.4.5 Chemical absorption

Chemical absorption processes are used to remove acid gases by aqueous action chemical reaction between a solvent with the gases. These processes use a solvent, either an alkanolamine (amine process [22]) or an alkali-salt(hot potassium carbonate processes [23]) in an aqueous solution. The amine process is widely used to purify natural gas with a wide range of partial pressure on acid gases, and it has lower equipment and operation cost. The common amine based solvents used for the absorption process are MEA, DEA and MDEA that reacts with the acid gas (CO_2 and H_2S). H_2S and CO_2 can be dissociated from aqueous amine solution by heat.

1.5 Chemical absorption process

1.5.1 1 The principal of chemical absorption process

Absorption with chemical solvents based on amine has been widely used for the removal of acid gas from natural gas in the gas processing industry. Alkanolamines are the most commonly used solvent for acid gas removal process. As shown in Figure 1-4, the amine absorption process consists two columns: “absorber” (contactor) and “regenerator” (stripper). In the absorber, amine solution is in counter current with the feed gas stream, and acid-base reaction takes place between acid gases impurities and amine solution. The treated gas stream leaves at the top of the absorber and goes for further process. At the meantime, the amine solution becomes loaded with acid gases, also called “rich amine”. It should be noted that hydrocarbons and aromatics are also physically dissolved in rich amine solution in the absorber. Therefore, the rich amine solution is sent to one or two flush drums in order to recover dissolved hydrocarbons. The recovered hydrocarbons are used as plant energy source. Before going into the top of regenerator, the rich amine solution is heated by lean amine stream in a heat exchanger. When the rich amine solution flows down from the top of the regenerator to the reboiler, the chemical bends between acid gases and amines are broken by the heat. Acid gases are released and exit from the top

of the regenerator, they can be sent to sulphur recovery units. The lean amine solution leaves from the bottom of the regenerator and then goes though the filtering and skimming unit for removing heavy liquid hydrocarbons.

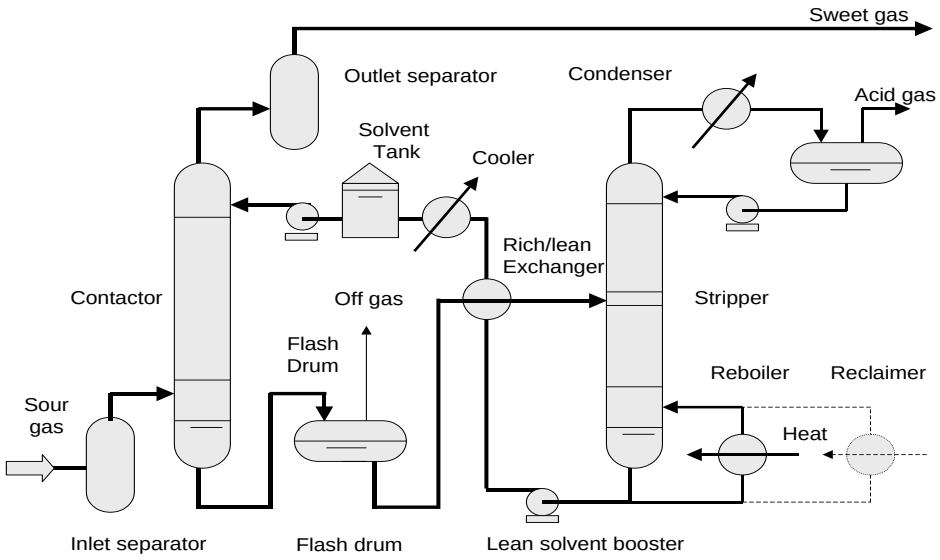

Figure 1-4 Typical Amine Flow Diagram[24]

Since the reactions between acid gases and amines are exothermic, the capacity of absorption is more appreciate at lower temperature. However, the reaction rate is very slow at lower temperature. Typically, in amine process, absorber is operated at 40 °C which is a compromise between absorption capacity and reaction rate. The absorber operating pressure is typically 7 MPa. For the regenerator, although the regeneration of amine is better at higher temperature, high temperature could lead to the degradation of amine molecules and corrosion of equipment. Therefore, the typical operating temperature of the regenerator is around 120 °C. The operational pressure of regenerator is around 0.1-0.2 MPa.

1.5.2 The types of amines

Nowadays, MonoEthanolAmine (MEA), DiEthanolAmine (DEA), and MethyDiEthanolAmine (MDEA) are the most commonly used to purify natural gas, their structures are shown in Figure 1-5.

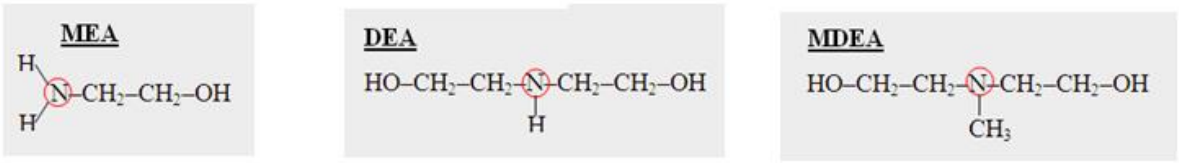

Figure 1-5 Structural formulae for alkanolamines used in gas treating units

Alkanolamines contain both the alcohol functional groups -OH and the amine functional groups -NH. Due to alcohol functional groups, alkanolamines are totally miscible with water. Alkanolamine is basic because of the presence of amine functional groups. Here, R represents the functional group $HOCH_2CH_2$-, MEA has the chemical formula RNH_2, DEA has R_2NH and MDEA has R_2N-CH_3. The reaction between H_2S and the alkanolamines can generally be represented by (we take MEA as an example):

$$RNH_2 + H_2S \Leftrightarrow [RNH_3]^+ + [HS]^- \qquad (0.1)$$

The reactions are instantaneous, and occur with primary, secondary and tertiary amines. However, reactions with CO_2 depend on the nature of the alkanolamine molecule. Primary and secondary amines react with CO_2 and form carbamate, it can be written as (we take MEA as an example):

$$RNH_2 + CO_2 + H_2O \Leftrightarrow [RNH]COO^- + H_3O^+ \qquad (0.2)$$

Ternary alkanolamines (MDEA) cannot directly react with CO_2, because there is no proton on the nitrogen atom. Therefore, CO_2 reacts firstly with water to form carbonic acid (H_2CO_3), and then carbonic acid reacts with the alkanolamine. It can be written as:

$$R_2N - CH_3 + CO_2 + H_2O \Leftrightarrow [R_2N - CH_4]^+ + HCO_3^- \qquad (0.3)$$

Primary and secondary amines react simultaneously with both H_2S and CO_2, tertiary amines react quickly with H_2S but very slowly with CO_2, tertiary amines like MDEA can

be used to selective capture of H_2S [25]. The selective removal and other advantages of MDEA make it the most widely used amine in natural gas treatment industry: lower regeneration energy required compared to MEA and DEA; significantly lower vapour pressure, see Figure 1-6; higher absorption capacity; very low corrosion rate; higher chemical stability, lower capacity for absorption of hydrocarbons [26]. Those advantages of MDEA result in lower energy consumption for solvent regeneration, smaller equipment size and lower plant cost. Moreover, additives such as piperazine can be used to increase the rate of reaction between CO_2 and MDEA, make it suitable for simultaneous removal of H_2S and CO_2 [27]. However, MDEA is more expensive than MEA and DEA.

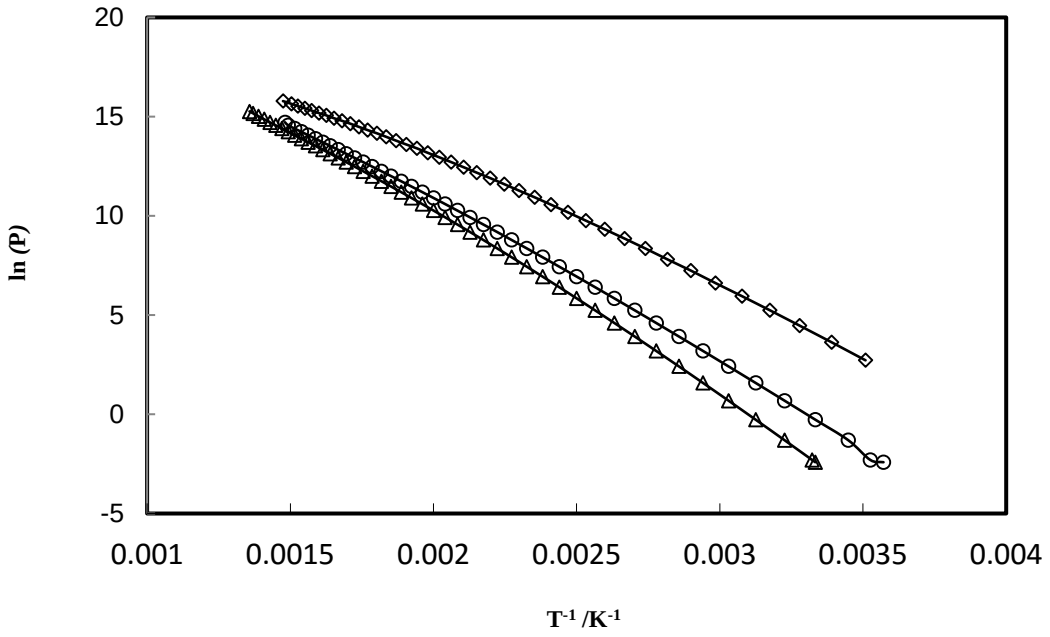

Figure 1-6.Vapour pressures of different alkanolamines as a function of inverse of temperature, data from NIST (◇)=MEA, (○)=DEA, (Δ)=MDEA

MEA is only applied for treatment of gases containing low concentrations of CO_2 and H_2S. The advantages of MEA are: high reactivity and low cost [28,29]. The main disadvantages of MEA are: high corrosiveness, high heat of regeneration, high cost of plant, high vapour

pressure leading to solvent losses by vaporization. MEA may form nonregenerative compound with COS and/or CS_2 [30,31].

DEA is a compromise between MDEA and MEA, it has lower reactivity than MEA, but higher than MDEA. DEA is also less corrosive than MEA, more corrosive than MDEA [32]. Unlike MEA, DEA do not generate nonregenerative compound with COS and/or CS_2. Moreover, DEA has lower vapour pressure than MEA and MDEA.

1.5.3 Modelling of amine absorption columns

The modelling of amine absorption columns is essentially important for process simulation and design in order to meet sell gas specification and minimize capital/operation costs. There are two different approaches are available. One is the equilibrium model, in which the vapour and liquid phases are in the thermodynamic equilibrium. Another is the non-equilibrium model which is also called rate based model accounting the mass transfer rate across the vapour-liquid interface.

1.5.3.1 Equilibrium model

The equilibrium model is the traditional way of analysing the distillation process, which assumes that each gas stream leaving from a tray or a packing segment is in thermodynamic equilibrium with the corresponding liquid stream leaving from the same tray or packing segment. For chemical absorption columns, the chemical reaction must also be taken into account. The whole column is divided into numbers of stages, see Figure 1-7.

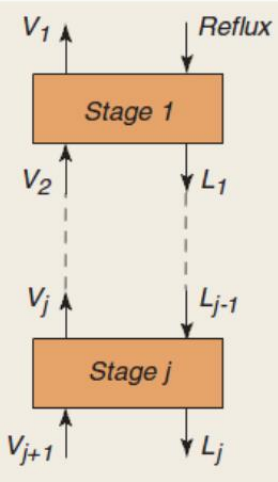

Figure 1-7 Decomposition of the distillation into theoretical stages [33]

Where V is given as the vapour stream flow and L given as the liquid stream flow

Each stage of equilibrium represents an ideal tray or packaging segment. These stages are represented with the equilibrium model with MESH equations. MESH Equations [33] include:

- Material balances
- Equilibrium relationships (to express the assumption that the streams leaving the stage are in equilibrium with each other)
- Summation equations (mole fractions are perverse quantities and won't sum to unity unless you force them to)
- Heat or enthalpy balances (processes conserve energy, as well as mass).

In the reality, the stream leaving from a tray of column is not in thermodynamic equilibrium with the liquid inside. The compositions of streams depend also on the rates of mass transfer from the vapour to the liquid phases. Therefore, correlation parameters such as tray efficiencies or Height Equivalent to a Theoretical Plate (HETP) are needed to fit the gap between the equilibrium-based theoretical description and real column conditions. For tray columns see Figure 1-8, Murphree efficiency [34] is the mostly used one to describe the real trays from the ideal trays in modelling and design, it is expressed as follow:

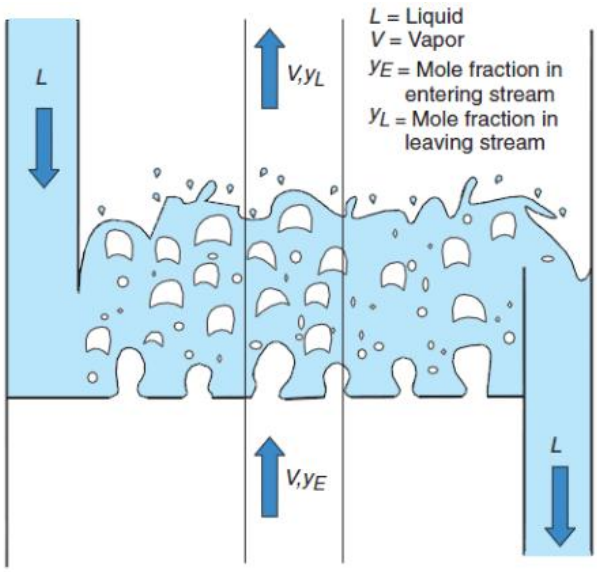

Figure 1-8 Flow patterns on a column tray [33]

$$E_{Murph,i} = \frac{y_{iL} - y_{iE}}{y_{iL}^{*} - y_{iE}} \qquad (0.4)$$

Where * represents thermodynamic equilibrium condition: $y^{*}=K\ x^{*}$, x is the mole composition of liquid phase.

For the packed columns, the HETP is a number that is easy to use in column design. Usually, HETPs are estimated from past experience with similar processes. However, for new processes, this approach cannot be used, and often fails even for old processes.

Thanks to its simplicity, the equilibrium model has been used to simulate and design columns for more than 100 years. However, equilibrium model still has some major weaknesses to be improved. For example, tray efficiency or HETP correlation parameters vary from component to component and from tray to tray, in a multicomponent mixture.

1.5.3.2 Non-equilibrium model (rate-based model)

In order to improve the model and description of column, rate-based model has been developed in recent years. It treats separation processes as mass-transfer-rate-governed processes that they really are. The building block of the non-equilibrium model is shown in Figure 1-9.

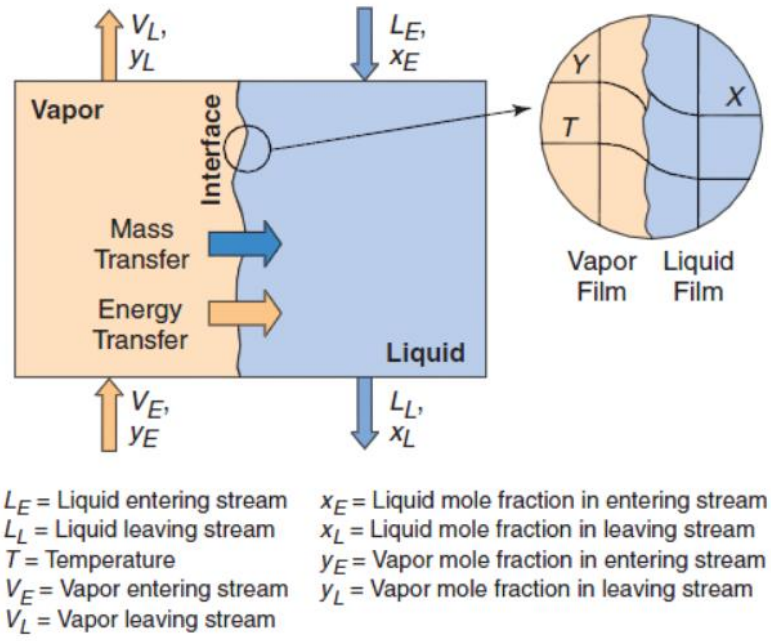

Figure 1-9 1D schematic diagram of a non-equilibrium stage [33]

The equations applied in non-equilibrium model is named as MERSHQ equations [33]:

- M:material balances •
- E: Energy balances
- R: mass and heat transfer rate equations
- S: summation equations
- H: hydraulic equations for pressure drop
- Q: equilibrium equations

Some of these equations are also used in equilibrium model. However, the significant difference of non-equilibrium model from equilibrium model is that the separate balance equations have to be written for each phase [33]. The models describing mass and energy

transfer are crucial to determine the interfacial molar and energy fluxes. The two-film model is the most commonly used one. The two- film model of CO_2 absorption is illustrated in Figure 1-10.

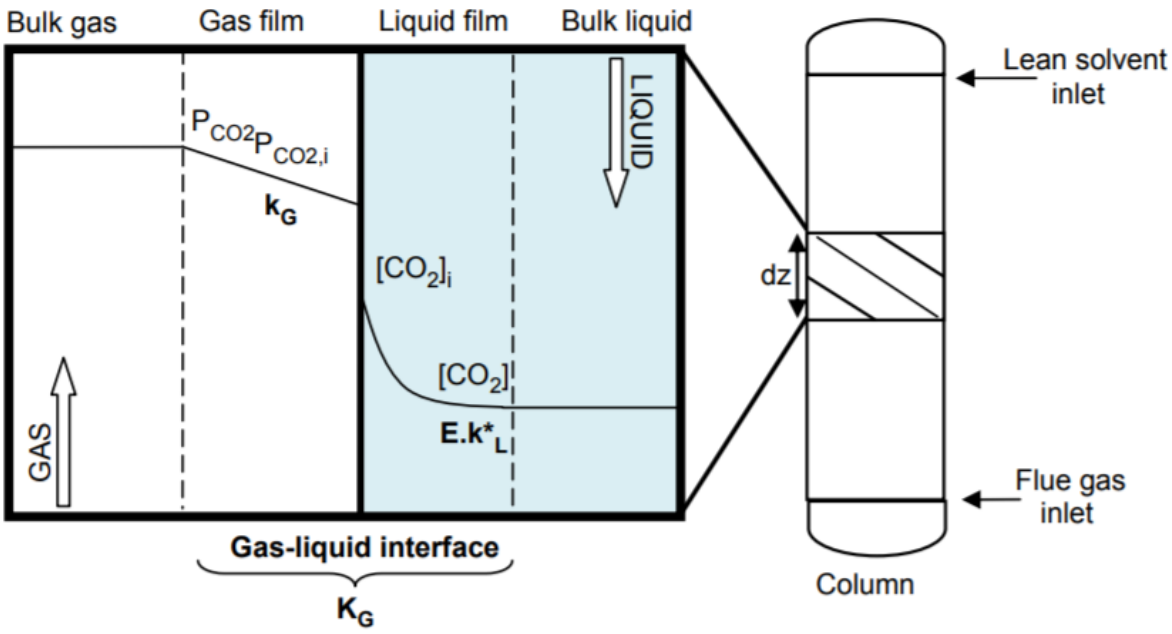

Figure 1-10 Illustration of the gas and liquid mass transfer occurring in a segment of packed column during the absorption process [35]

In two-film model, stationary gas and liquid films are assumed to form on both sides of gas-liquid interface. CO_2 in the gas bulk passes through the gas film, then crosses the gas-liquid interface (where the reactions between CO_2 and amine start to take place), and then enters into the liquid film. According to the two film theory, since the thickness of films is extremely thin, mass transfer within the films is dominated by concentration gradient due to molecular diffusion. The mass transfer relations can be described by following equations:

$$N_{CO_2} = K_G(P_{CO_2} - P^*_{CO_2}) \qquad (0.5)$$

where N_{CO2} is the CO_2 molar flux across the interface, K_G is the overall mass transfer coefficient of CO_2 in gas, P^*_{CO2} is the equilibrium CO_2 partial pressure in the bulk liquid, and P_{CO2} is the CO_2 partial pressure in the bulk gas. P^*_{CO2} is calculated using Henry's law with following Equation:

$$P^*_{CO_2} = H_{CO_2} C^b_{CO_2} \qquad (0.6)$$

Where H_{CO2} is the Henry constant of CO_2 in aqueous solution, C^b_{CO2} is the concentration of CO_2 in the bulk liquid.

According to the two films theory, the overall mass transfer coefficient K_G is expressed by following Equation:

$$\frac{1}{K_G} = \frac{1}{k_G} + \frac{H_{CO_2}}{Ek_l^{'}} \qquad (0.7)$$

With k_G is the mass transfer coefficient in the gas phase, $k_l^{'}$ is the mass transfer coefficient without reaction in the liquid phase and E is the enhancement factor due to chemical reactions.

In real chemical absorption process, thermodynamic equilibrium is rarely reached; it is rather than a complex rate-controlled process that happens far from thermodynamic equilibrium. Non-equilibrium model is able to take into account those phenomenons.

1.6 The importance of the thermodynamic model

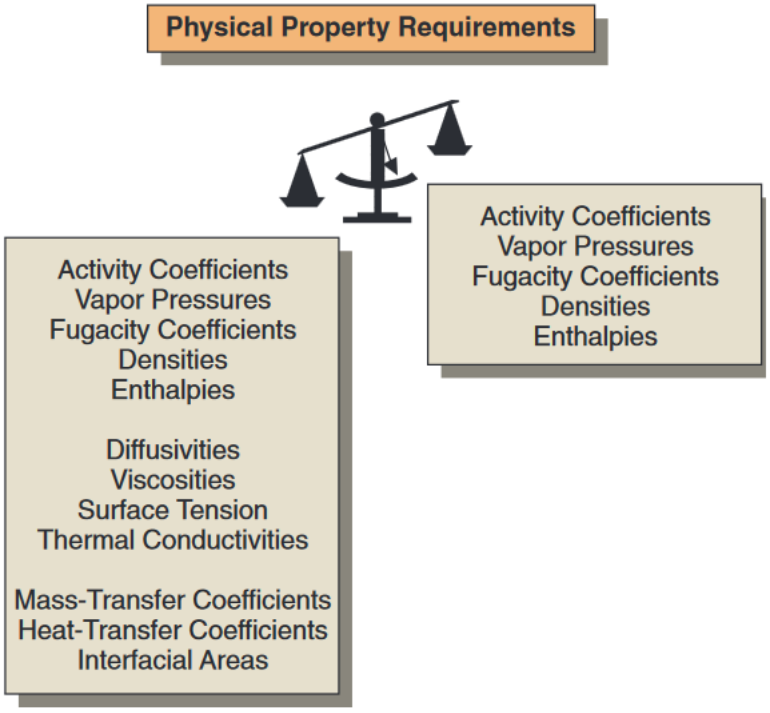

Figure 1-11 physical property needs of equilibrium (right) and non-equilibrium (left) models [33]

Figure 1-11 illustrates the physical property requirements for equilibrium and non-equilibrium models, it can been seen that both equilibrium and non-equilibrium model need thermodynamic properties such as: activity coefficients, vapour pressures, fugacity coefficient, densities and enthalpies. Those thermodynamic properties are provided by reliable thermodynamic model prediction or correlations. Moreover, other physical properties required by non-equilibrium model such as viscosities, surface tension, diffusivities and thermal conductivities need accurate density prediction in the correlations. Thus it is essential that accurate prediction of thermodynamic properties is the key for chemical absorption column design.

1.7 **Scope of this thesis**

Thermodynamic model is of high importance as it is directly linked to the determination of the maximum absorption capacity of the solvent, as a consequence the quantity of solvent to be considered in the columns. An accurate thermodynamic model is able to predict the loose of hydrocarbons (solubility in aqueous alkanolamine solution), the loose of solvent (vapour phase composition), and the speciation of liquid phase. Furthermore, it also describes the absorption/desorption enthalpy behaviour.

A key challenge is to develop a thermodynamic model which is able to accurately predict the above properties with a wide range of temperature, a wide range of amine concentration and a wide range of acid gases loading ratio. The fluids involved in acid gases removal process are: Acid gases (H_2S and CO_2), alkanolamines (MEA, DEA, MDEA), water, Alkane and aromatic hydrocarbons (methane, ethane, propane, n-butane, n-pentane, n-hexane, benzene, toluene) and mercaptans. They make the system very complex, it contains liquid phase speciation, intermolecular association via hydrogen

bonds and chemical reactions. The classical models used for such fluids are reviewed in chapter 3.

Thermodynamic modelling for these systems requires parameter adjustments from experimental data. For acid gas, alkane and aromatic in alkanolamine solutions, various Vapour-Liquid Equilibrium, Liquid-Liquid Equilibrium, Vapour-Liquid-Liquid experimental data are available in the literature or GPA research reports, lists of reference are detailed in chapter 4 and 5. VLE experimental measurement has been carried out concerning MM or EM in aqueous MDEA by using experimental set-up and procedure at CTP, the experimental work is detailed in chapter 2.

`

Chapter 2. Experimental work

2 `Experimental work

Introduction

As explained in Chapter 1, there is a gap of experimental data to validate our model for predicting mercaptans solubility in aqueous alkanolamine solution. In this chapter, the experimental set up and the results for Vapour Liquid Equilibrium data of mercaptans (MM and EM) in aqueous MDEA solution will be represented. Based on the previous work done in CTP [36], the static analytic method has been used for those measurements. The uncertainties of temperature, pressure, and compositions will be estimated. These experimental data are used for model validation, and they will be presented in the Chapter 4.In the context of the choice of solvent for mercaptan removal, I have also participated on the Gas Processor Association project 142. Different sulphur components solubility in 14.6 wt% MEA will be measured in terms of Henry's law constant by using a gas stripping method.

Comme cela est expliqué au chapitre 1, il manque des données expérimentales pour valider notre modèle pour prédire la solubilité des mercaptans dans la solution aqueuse d'alcanolamine. Dans ce chapitre, l'ensemble expérimental et les résultats pour les données d'équilibre liquide-vapeur de mercaptans (MM et EM) dans une solution aqueuse de MDEA seront représentés. Sur la base des travaux antérieurs réalisés dans CTP [36], la méthode analytique statique a été utilisée pour ces mesures. Les incertitudes de température, de pression et de composition seront estimées. Ces données expérimentales sont utilisées pour la validation du modèle et seront présentées dans le chapitre 4. Dans le cadre du choix du solvant pour l'élimination des mercaptans, j'ai également participé au projet GPA 142. La solubilité des composants soufrés dans 14,6% du MEA sera mesurée en termes de constante de loi de Henry en utilisant une méthode de Stripping.

2.1 **Static-analytic method:**

2.1.1 Experimental setup

The static-analytic method is used for Vapour Liquid Equilibrium measurements of ethyl mercaptan and methyl mercaptan, in aqueous MDEA solution. The schematic diagram of this apparatus is presented in Figure 2-1 [36]. The experimental set up contains mainly an equilibrium cell, a ROLSI® [37] capillary sampler and a gas chromatograph.

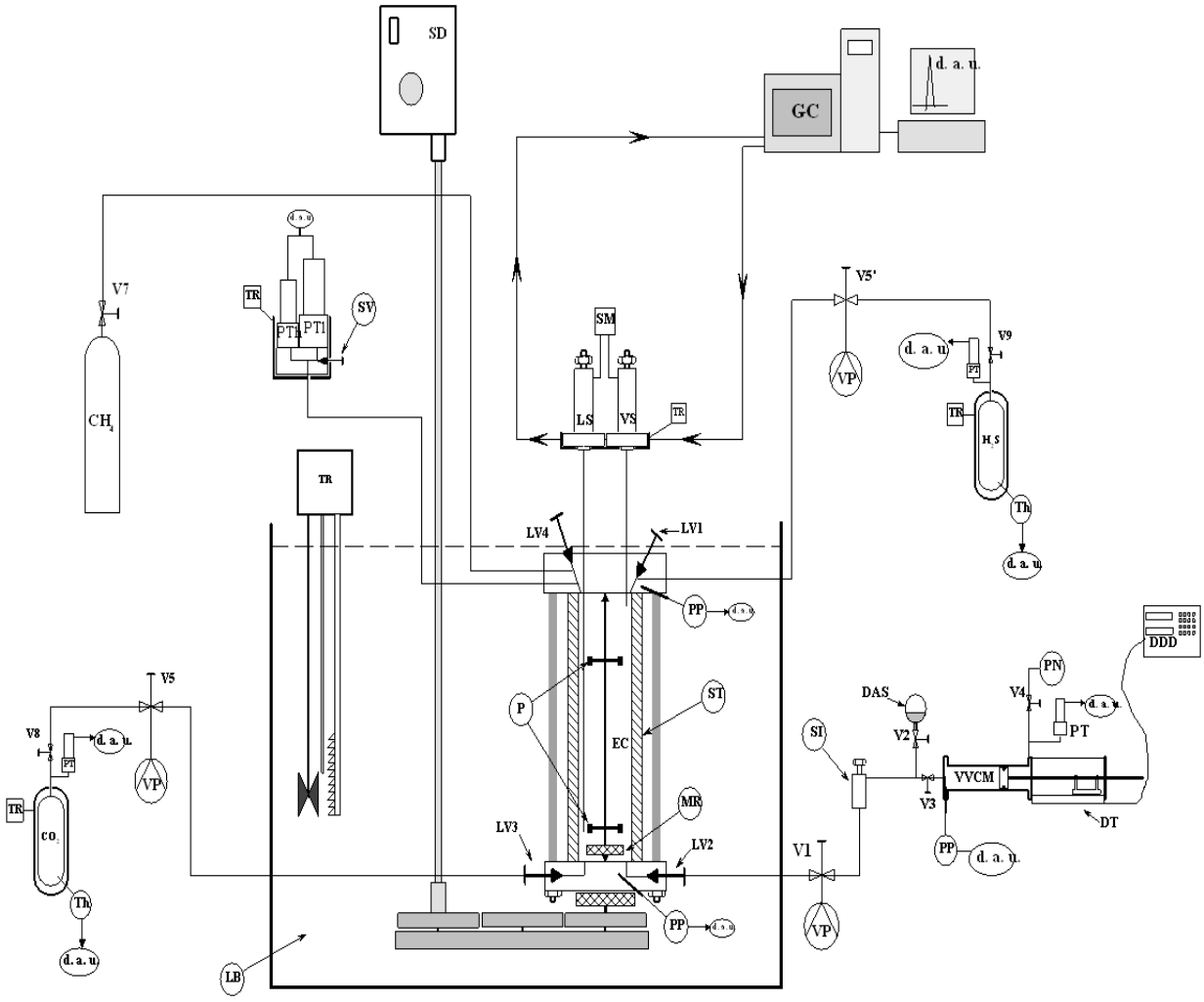

Figure 2-1. Schematic diagram of apparatus: d. a. u. : Data Acquisition Unit ; DDD : Digital Displacement Display ; DM : Degassed Mixture ; DT : Displacement Transducer ; EC : Equilibrium Cell ; GC : Gas Chromatograph ; LB: Liquid Bath; LS : Liquid Sampler ; LVi : Loading Valve ; MR;

Magnetic Rod; P: Propeller; PP : Platinum Probe ; PTh: Pressure transducer for high pressure values; PTl: Pressure transducer for low pressure values; SD : Stirring Device ; SM: Sample Monitoring; CI: Cylindrical tube Injector; TR: Thermal Regulator; Vi: Valve; VP: Vacuum Pump; VS: Vapour Sampler; VVCM: Variable Volume Cell for Mixture.

2.1.1.1 The equilibrium cell

The volume of the equilibrium cell is 34 cm^3.The equilibrium cell is made of a sapphire tube which is held between two stainless steel flanges (top and bottom). These flanges have four valves (LV1, LV2, LV3 and LV4) for gas and liquid loading and cleaning the cell. LV1 is used for H_2S loading. LV2 is the loading Valve for charged alkanolamine solutions, LV3 is the loading valve for CO_2. LV4 is the loading valve for CH_4. This equilibrium cell can be operated within 10 MPa and between 223.15 and 473.15 K. The equilibrium cell is immersed in temperature-constant oil bath with temperature tolerance of ±0.1 K. The temperature in equilibrium cell is represented by the average value of the temperatures at the top and bottom of the cell. These temperatures are measured through two platinum resistance thermometers within 0.02 K accuracy. The pressure in the equilibrium cell is measured by a pressure transducer which is able measure up to 10 MPa. The pressure measurement accuracy is 0.0001 MPa.

2.1.1.2 The ROLSI™ sampler

A typical ROLSI® capillary sampler [37] is shown in Figure 2-2. It consists of a capillary of 0.1 mm internal diameter. The capillary is connected to sample chamber through an aperture. The sample chamber is connected to a gas chromatograph through transfer lines. The sample chamber of the sampler, injector and analytical packed column, are at same pressure where carrier gas (He) is always circulated at a constant flow rate with pressure close to 0.3 MPa. The ROLSI® capillary sampler is able to take samples of several µL by opening the aperture for limited time. With this small amount of sample, we can be confident that thermodynamic equilibrium will not be changed in the equilibrium cell. In fact the sample size is negligible compared to the volume of liquid/vapour phase to be

analysed (between 10-30 mL). The volume of the sample taken by the sampler is qualitatively related to the opening time which can be programmed with a particular value. A heating system is around the sampler to ensure an instantaneous vaporization of liquid samples and to avoid the condensation of the sample steam. Then the sample is sent to the gas chromatograph through a transfer line which is also heated to avoid liquid condensation. The heating temperature of transfer line is higher than the boiling point of MDEA, the heaviest component among components to be analysed.

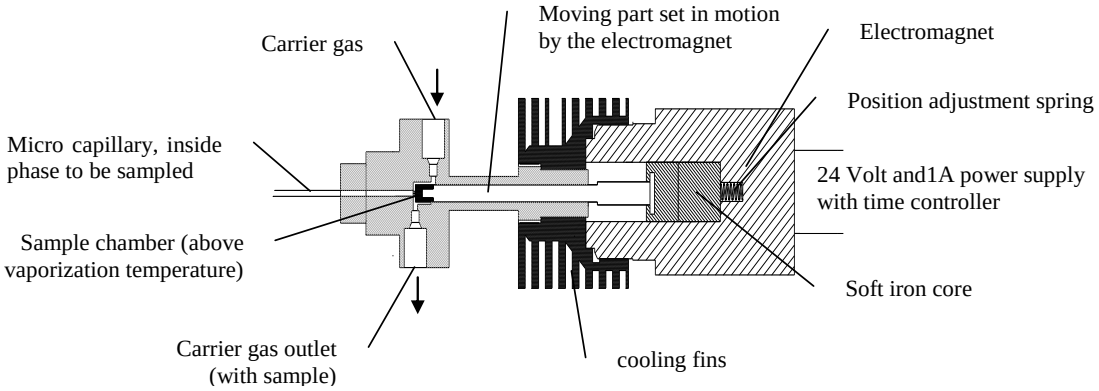

Figure 2-2 Cross sectional view of Electromagnetic ROLSI®

2.1.1.3 Solvent preparation

The chemicals used in this study with their purity are shown in Table 2-1, no further purification has been done for these chemicals. In this study MM/EM are directly added into the prepared aqueous MDEA solution instead of adding MM/EM though the loading valves on the equilibrium cell. It's deal to a better control for concentration of MM/EM in alkanolamine solution. Table 2-2, Table 2-3 and Table 2-4 give the compositions of prepared aqueous solutions.

Table 2-1. Purity and producer of the used substances

Chemical Name	CAS No.	Purity %	Supplier
n-Methyldiethanolamine (MDEA)	105-59-9	99 + GC	Aldrich
Methyl Mercaptan (MM)	74-93-1	99 + / GC	Acros
Ethyl Mercaptan (EM)	75-08-1	99 + / GC	Acros
Water (H_2O)	7732-18-5	Ultra pure	Millipore/ Direct Q
Methane (CH_4)	74-82-8	99.995 / vol.	Messer

Table 2-2 Composition of prepared 25 wt % MDEA aqueous solution with EM (2281ppm)

	water	MDEA	C_2H_5SH (ppm)	uncertainty
M /g/mol	18.02	119.16	62.1356	-
m /g	243.94	81.39	2.0196	0.00005
mass fraction	0.7452	0.2486	0.0062	0.00001
mole fraction	0.94980	0.04792	2281 ppm	0.00001

Table 2-3 Composition of prepared 25 wt % MDEA aqueous solution with EM (1112ppm)

	Water	MDEA	C_2H_5SH(ppm)	uncertainty
M /g/mol	18.02	119.163	62.1356	-
m /g	150.15	50.04	0.6057	0.00005
mass fraction	0.7477	0.2492	0.0030	0.00001
mole fraction	0.9509	0.0479	1112 ppm	0.00001

Table 2-4 Composition of prepared 25 wt % MDEA aqueous solution with MM (2438ppm)

	MDEA	H2O	CH_3SH(ppm)	uncertainty
M /g/mol	119.16	18.02	48.11	-
M /g	46.7699	140.5454	0.9632	0.00005
mass fraction	0.2524	0.7585	0.52	0.00001
mole fraction	0.0478	0.9498	2438 ppm	0.00001

2.1.1.4 Gas chromatography

Figure 2-3 shows the typical configuration of a gas chromatography system. It usually contains: a sample injector, a separation column which is linked to ROLSI® capillary sampler through the transfer line, Thermal Conductivity Detector (TCD) and Flame Ionization Detector (FID) connected in series a simplified analytic circuit, and a multi switch valve which allows loading and cleaning components in the gas chromatography.

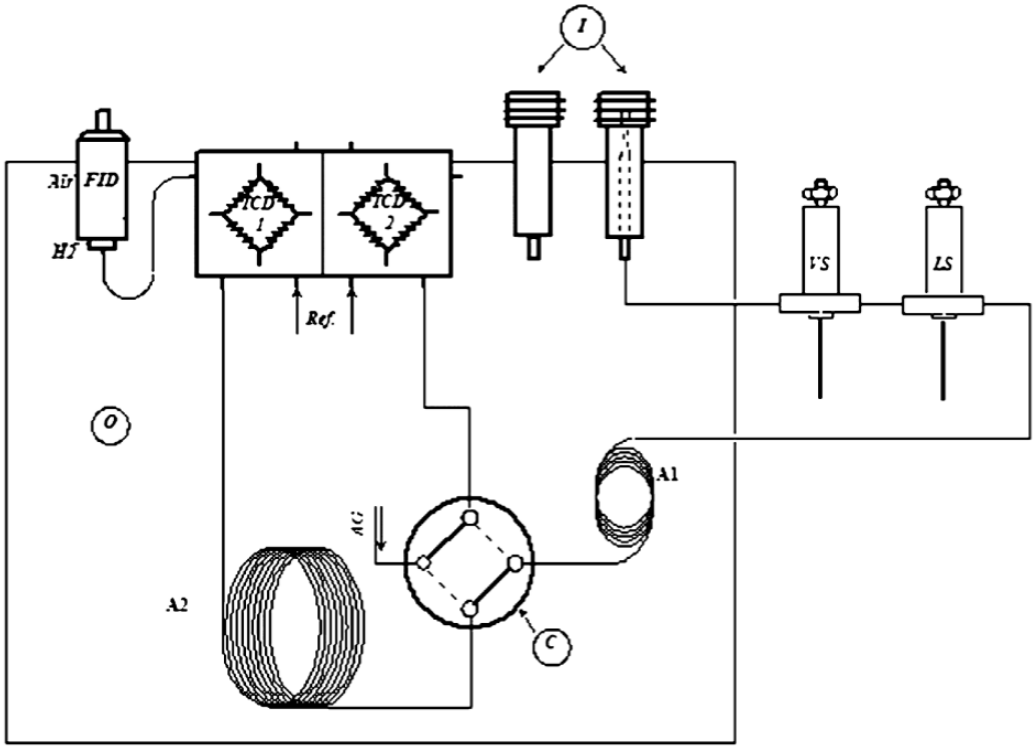

Figure 2-3 Gas chromatograph for liquid and vapor phase analysis (simplified analytical circuit), A1 A2 : Column; AG: auxiliary gas; C: commuting valve; FID: Flame Ionization Detector; I: Injectors; O: Oven; T: Thermal conductivity detector; VS: Vapor phase sampler; LS: Liquid phase sampler.[38]

In this study, a pre-column A1 (same material as the analytical packed column with a shorter length) is added on the multi switch valves in order to avoid the retention of MDEA sampled from the liquid/vapour phase in the analytical packed column. In fact, the MDEA in the sample is adsorbed inside the column even at high temperature (523K) and generate bad peaks. Therefore, CH_4, H_2O, CO_2, and H_2S are separated in the pre-column and send to the analytical packed column by controlling the commuting time of valve C. MDEA will not go into the analytical packed column; the quantity of MDEA can only be calculated by assuming that the ratio between MDEA and water is constant in the liquid phase. The critical parameters for the separation of peaks and the quality of the analysis are the choice of column, temperature of the column, carrier gas nature, flow rate of carrier gas, type and parameters of the detector, their values are shown in Table 2-5. The gradient of temperature programmed in function of time for the oven is represented in Figure 2-4.

Table 2-5 Parameter setting for GC liquid and vapour analysis.

Gas chromatograph	Perichrom, Model 2100
Type of column	Analytical column: Porapack R type (1.2 meter length and 1/8" wide, 80/100 mesh) Pre-column: Porapack R type (0.2 meter length and 1/8" wide, 80/100 mesh)
TCD	T = 453 K Gain : 1, offset =300×10µ Volts Reference gas flow: He: 30 ml/min
FID	T= 523 K, Gain : 10 nA , current=120 mVolts Hydrogen flow : 49 mL/min and air flow : 59 mL/min
Carrier gas: Helium	Gas flow : He: 29.7 mL/min

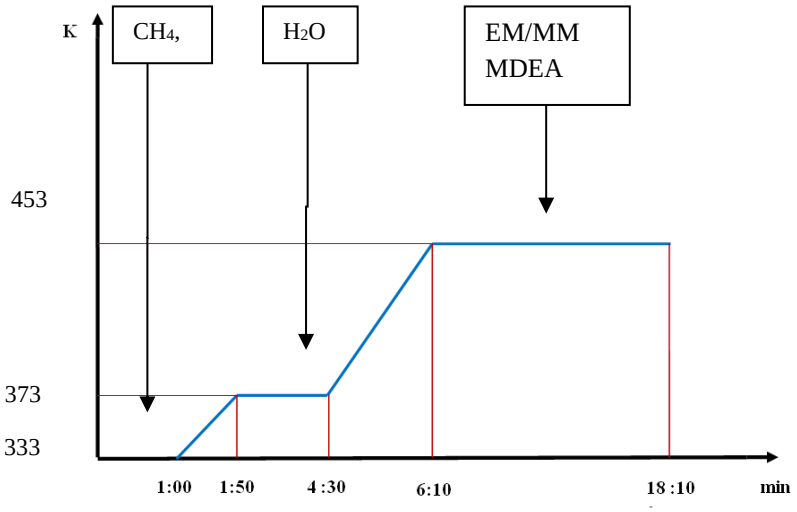

Figure 2-4. Oven temperature programming as a function of time (min) from 333 to 518 K.

2.1.1.5 Calibration of detectors

This calibration is carried out by using 50, 100 and 500 µL automatic syringes (*SGE*, Australia) for gas (CH_4, CO_2, H_2S), 1 and 5 µL syringe for water and MM/EM dissolved

in methanol. The TCD and FID detectors are calibrated by using the method of external standards where a known volume of pure components and known mixture compositions are injected into the GC through the injector (see Figure 2-5). The peak area obtained corresponds to a known quantity of substance.

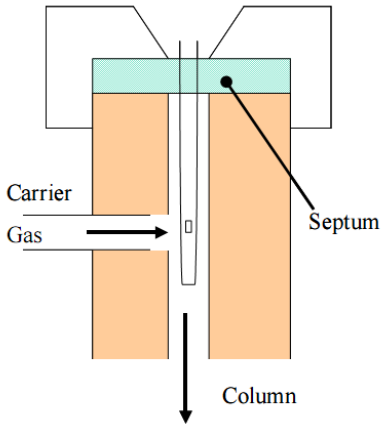

Figure 2-5. GC gas/liquid injector [36]

Calibration curves for different compounds were obtained; they are detailed in APPRENDIX I. A polynomial equation of each curve corresponds to the peak area in function of mole numbers of injected quantity for a given component. The parameters are adjusted and they can estimate the calibration uncertainty. The accuracy of each component in the corresponding phase is shown in Table 2-6.

Table 2-6 Components and accuracy (typical accuracy values)

Component	Phase	Detector (sensitivity)	Accuracy %
CH_4	Vapour	TCD (gain=0.5)	2.5
H_2O	Liquid	TCD (gain=0.5)	1.5
CH_4	Liquid	FID (10nA)	3.5
EM	Liquid/vapour	FID (10nA)	3
MM	Liquid/Vapour	FID (10nA)	1.8

2.1.2 Results

The operation protocol follows the well-established instructions of CTP [36]. The VLE measurement results of 2438 ppm MM: 2438 ppm, 1112 ppm EM and 2281 ppm EM in 25 wt% aqueous MDEA solution are represented in Table 2-7a, 2-7b and 2-7c respectively. The uncertainty of composition in the liquid and vapour phases are also represented, they are calculated by using the method of NIST which is detailed in APPRENDIX II. These data are used for model validation in chapter 4.

Table 2-7a. Vapour Liquid equilibrium data of MM in aqueous MDEA solution (25 wt% MDEA) (global concentration of MM: 2438 ppm). δx corresponds to the standard deviation due to repeatability measurements. u(x) corresponds to the uncertainty u(T)=0.02 K, u(P)=0.0001 MPa

T	P		MM		CH_4		MDEA		H_2O			MM		CH_4	
/K	/MPa	n	x	δx	x	δx	x	δx	x	δx	n	y	δy	y	δy
332.68	2.0033	6	0.00253	2E-05	0.00041	2E-06	0.04777	9E-07	0.94929	2E-05	4	0.04123	1E-04	0.95877	1E-04
332.71	4.0292	6	0.00210	2E-05	0.00084	2E-05	0.04777	2E-06	0.94929	4E-05	5	0.01987	1E-05	0.98013	1E-05
332.69	7.0543	7	0.00167	3E-05	0.00145	1E-05	0.04776	1E-06	0.94912	2E-05	6	0.01013	3E-05	0.98987	3E-05
364.54	1.9405	7	0.00205	3E-05	0.00039	5E-06	0.04780	2E-06	0.94977	4E-05	10	0.05917	9E-05	0.94083	9E-05
364.58	4.0580	7	0.00178	2E-05	0.00087	1E-05	0.04779	1E-06	0.94957	3E-05	4	0.02742	1E-05	0.97258	1E-05
364.60	7.0408	7	0.00157	2E-05	0.00153	1E-05	0.04776	1E-06	0.94914	3E-05	5	0.01503	2E-05	0.98497	2E-05

MM	CH_4	MDEA	H_2O	MM	CH_4
u(x)	u(x)	u(x)	u(x)	u(y)	u(y)
5.10E-05	7.19E-06	9.49E-04	1.89E-02	1.16E-04	1.94E-03
4.28E-05	1.49E-05	9.49E-04	1.89E-02	5.66E-05	1.98E-03
3.30E-05	2.49E-05	9.49E-04	1.89E-02	2.91E-05	2.01E-03
4.07E-05	6.75E-06	9.50E-04	1.89E-02	1.66E-04	1.93E-03
3.57E-05	1.51E-05	9.50E-04	1.89E-02	7.78E-05	1.96E-03
3.09E-05	2.62E-05	9.49E-04	1.89E-02	4.30E-05	2.00E-03

Table 2-7b. Vapour Liquid equilibrium data of EM in aqueous MDEA solution (25 wt% MDEA) (global concentration of EM: 1112 ppm). δx corresponds to the standard deviation due to repeatability measurements. u(x) corresponds to the uncertainty u(T)=0.02 K, u(P)=0.0001 MPa

T	P		EM		CH_4		MDEA		H_2O			EM		CH_4	
/K	/MPa	n	x	δx	x	δx	x	δx	x	δx	n	y	δy	y	δy
333.97	2.0067	5	0.000426	8E-6	0.000456	9E-6	0.04794	4E-7	0.95118	8E-6	20	0.0079	2E-4	0.9921	2E-4
333.98	4.3155	7	0.000475	4E-6	0.001041	2E-5	0.04791	9E-7	0.95057	2E-5	6	0.0045	1E-4	0.9955	1E-4
333.97	6.8929	6	0.00042	2E-5	0.001683	3E-5	0.04788	2E-6	0.95002	3E-5	5	0.00299	9E-5	0.9970	2E-4
364.68	1.1996	5	0.000371	4E-6	0.000450	2E-6	0.04794	2E-7	0.95123	4E-6	9	0.0124	1E-4	0.9876	1E-4
365.71	4.0190	6	0.000367	3E-6	0.001006	9E-6	0.04792	4E-7	0.95071	7E-6	20	0.00719	5E-5	0.99281	5E-5
365.58	7.0163	8	0.000337	1E-5	0.001697	7E-6	0.04788	4E-7	0.95008	9E-6	8	0.00429	5E-5	0.99573	8E-5

EM	CH_4	MDEA	H_2O	MM	CH_4
u(x)	u(x)	u(x)	u(x)	u(y)	u(y)
1.2E-05	6.4E-06	6.4E-04	1.3E-02	4.6E-05	4.1E-03
1.3E-05	1.5E-05	6.4E-04	1.3E-02	2.6E-05	4.1E-03
1.2E-05	2.3E-05	6.4E-04	1.3E-02	1.8E-05	4.2E-03
1.1E-05	6.3E-06	6.4E-04	1.3E-02	7.2E-05	4.1E-03
1.0E-05	1.4E-05	6.4E-04	1.3E-02	4.2E-05	4.1E-03
9.5E-06	2.4E-05	6.4E-04	1.3E-02	2.5E-05	4.1E-03

Table 2-7c. Vapour Liquid equilibrium data of EM in aqueous MDEA solution (25 wt% MDEA) (global concentration of EM: 2281 ppm). δx corresponds to the standard deviation due to repeatability measurements. u(x) corresponds to the uncertainty u(T)=0.02 K, u(P)=0.0001 MPa

T	P		CH_4		H_2O		MDEA		EM		CH_4		H_2O	
/K	/MPa	n	x	δx	x	δx	x	δx	x	δx	y	δx	y	δx
333.30	2.1754	9	0.000378	2E-06	0.951	4E-06	0.048	2E-07	0.00054	3E-06	0.992	2E-05	0.00789	2E-05
333.32	4.0419	7	0.000690	4E-06	0.95	8E-06	0.048	4E-07	0.0005	6E-06	0.995	5E-06	0.00466	5E-06
333.28	6.9601	14	0.001130	7E-06	0.95	7E-06	0.048	4E-07	0.00041	3E-06	0.997	3E-05	0.00297	3E-05
365.12	2.0088	9	0.000374	1E-05	0.951	1E-05	0.048	6E-07	0.00051	3E-06	0.986	3E-05	0.0136	3E-05
365.12	4.041	6	0.000780	2E-05	0.951	2E-05	0.048	9E-07	0.00045	5E-06	0.993	6E-05	0.00704	6E-05
365.12	7.1768	7	0.001270	8E-06	0.951	6E-06	0.048	3E-07	0.00035	4E-06	0.995	2E-05	0.0041	2E-05

EM	CH_4	MDEA	H_2O	MM	CH_4
u(x)	u(x)	u(x)	u(x)	u(y)	u(y)
1.9E-05	6.7E-06	8.2E-04	1.6E-02	5.5E-05	4.9E-03
1.8E-05	1.2E-05	8.2E-04	1.6E-02	3.3E-05	5.0E-03
1.5E-05	2.0E-05	8.2E-04	1.6E-02	2.1E-05	5.0E-03
1.8E-05	6.7E-06	8.2E-04	1.6E-02	9.5E-05	4.9E-03
1.6E-05	1.4E-05	8.2E-04	1.6E-02	4.9E-05	4.9E-03
1.2E-05	2.3E-05	8.2E-04	1.6E-02	2.9E-05	5.0E-03

2.2 The Gas Stripping method

I focused also on the measurement of the Henry's law constant and infinite dilution activity coefficient of sulphur component such as mercaptans, DMS and CS_2. Gas Stripping method (Krummen et al.[5]) was used, this method is based on the variation of vapour phase composition when the highly diluted solute of the liquid mixture in an equilibrium cell is stripped from the solution by a flow of inert gas. The composition of the solute of the leaving gas decreases exponentially as a function of time.

2.2.1 Experimental set up

The schematic diagram of this apparatus is shown in Figure 2-6. In this method, two cells (one dilutor and one saturator) are immersed inside a liquid bath regulated to within 0.01 K. A platinum probe is in contact with the liquid phase of the "dilutor cell" connected to an electronic display, is used for temperature readings. 40 cm^3 of solvent was introduced into the "saturator cell", and about 50 cm^3 of the solvent is introduced into the "dilutor cell" with 10-50 µL of solute (sulphur component). The flow rate of the stripping gas (helium) is controlled by flow regulator. Before entering into the dilutor, helium is injected into the saturator to counteract the loss of solvent in the dilutor. The vapour phase of the dilutor is periodically sampled and analysed using gas chromatography.

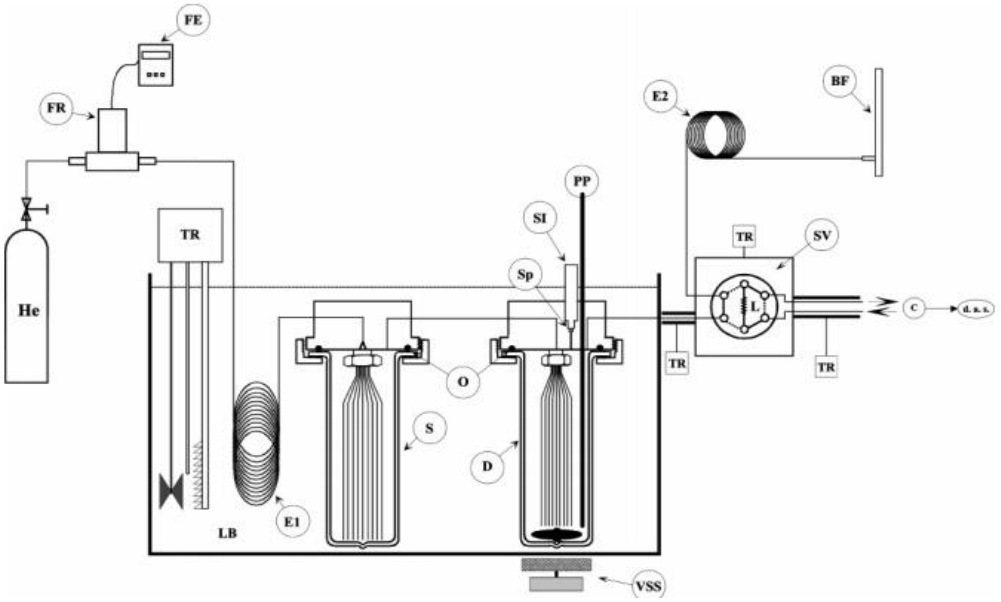

Figure 2-6 Flow diagram of the equipment: BF, bubble flow meter; C, chromatograph; D, dilutor; d.a.s., data acquisition system; He,helium cylinder; E1, E2, heat exchangers; FE, flow meter electronic; FR, flow regulator; L, sampling loop; LB, liquid bath; O, O-ring; PP,platinum resistance thermometer probe; S,

saturator; SI, solute injector; Sp, septum; SV, sampling valve; TR, temperature regulator;VSS, variable speed stirrer

Analytical work was carried out using a gas chromatograph (PERICHROM model PR2100, France) equipped with a Flame Ionization Detector (FID) and a Thermal Conductivity Detector (TCD) connected to a data software system. Helium is used as the carrier gas in this experiment.

- For CS_2, TCD is used as detector, the reference of the analytical column is HAYSEP B, 80/100 Mesh (Silcosteel, length 0.66 m, diameter 2 mm) from RESTEK, France.
- For other components, FID is used as detector, the reference of the analytical column is: 15% APIEZON L, 80/100 Mesh (Silcosteel, length 1.2 m, diameter 2 mm) from RESTEK, France.

2.2.2 Chemicals

The measurements have been carried out for DMS and different mecaptans (methyl mercaptan, ethyl mercaptan, isopropyl mercaptan, n-propyl mercaptan and, n-butyl mercaptan isobutyl mercaptan) in 14.6 wt% aqueous MEA solution at the temperature range of 298-348 K and at 1 atm. Then the measurements have been performed for CS_2 in pure water. However, due to the chemical reaction taking place between water and CS_2, the Henry's law constant cannot be obtained by using gas stripping method (see details in section 2.2.5). The chemicals used are presented in Table 2-8. The composition of prepared solution is presented in Table 2-9.

Table 2-8 CAS Numbers, Purities and Suppliers of Materials.

Chemical Name	CAS No.	Purity %	Supplier
Methyldiethanolamine (MDEA)	105-59-9	99 + / GC	Aldrich
Monoethanolamine (MEA)	109-83-1	99 + / GC	Aldrich
Methyl Mercaptan (MM)	74-93-1	99 + / GC	Aldrich
Ethyl Mercaptan (EM)	75-08-1	99 + / GC	Acros
n-Propyl Mercaptan (n-PM)	107-03-9	99 + / GC	Aldrich
Isopropyl Mercaptan (iPM)	75-33-2	99+	Aldrich
n-Butyl Mercaptan (n-BM)	109-79-5	99 + / GC	Aldrich
Isobutyl Mercaptan (iBM)	513-44-0	99+	Aldrich

Carbon Disulfide	75-15-0	99+	Aldrich
Dimethyl Sulfide (DMS)	75-18-3	99	Fluka
Water (H_2O)	7732-18-5	Ultra pure	Millipore/ Direct Q

Table 2-9 Composition of prepared 14.6 wt % MEA aqueous solution

Quantity	H_2O	MEA
Mass /g	340.86	58.32
Mol. weight /g/mol	18.02	61.08
No. of moles	18.91	0.9548
Mole. fraction	0.9519	0.0481
Mass fraction	0.854	0.146

2.2.3 Henry's Law Constant Calculation

This method does not require any calibration of detectors, because the Henry's Law constant can be obtained by using the evaluation peak areas of the solute in function of time, see Equation(2.1). Zin et al. [39] explained in detail how to obtain this equation.

$$H_i = -\frac{1}{t}\ln\left(\frac{A_i}{(A)_{t=0}}\right)\frac{RTN}{\frac{D}{1-\frac{P_{solv}^{sat}}{P}}+\frac{V_G}{t}\ln\left(\frac{A_i}{(A)_{t=0}}\right)} \qquad (1.1)$$

where D is the carrier gas flow rate ($m^3.s^{-1}$); N is the total number of moles of solvent inside the dilutor cell; VG (m^3) is the volume of the vapour phase inside the dilutor cell; Ai is the chromatograph solute i peak area; t (s) is the time; T (K) is the temperature inside the cell; P is the pressure inside the cell (around atmospheric pressure); P_{sat}^{solv} (Pa) is the saturation pressure of the solvent and R ($J.mol^{-1}.K^{-1}$) is the ideal gas constant. Infinite Dilution Activity Coefficient,γ_i^{∞}, is calculated through Equation(2.2) :

$$\gamma_i^{\infty} = \frac{H_i \, P_{solv}^{sat}}{P_i^{sat}} \qquad (1.2)$$

Where P^{sat} is the vapour pressure of solute i, it is calculated from using following equation with parameters in Table 2-10.

$$P^{sat} = e^{\left(A + \frac{B}{T} + C\ln(T) + DT^{E}\right)} \qquad (1.3)$$

Table 2-10 solutes vapour pressures parameters [39]

Parameters	nBM	iBM	nPM	iPM	MM	EM	DMS	CS2
A	64.649	61.213	61.813	74.676	54.15	65.551	9.1366	59.1005
B	-6262	-5909	-5623	-5272	-4337.7	-5027.4	-2493.7	-4752.1
C	-6.1280	-5.6431	-5.7934	-8.1974	-4.8127	-6.6853	1.8254	-5.7824
D	6.84×10^{-18}	1.48×10^{-17}	6.51×10^{-18}	3.42×10^{-16}	4.5×10^{-17}	6.32×10^{-6}	1.48×10^{-6}	6.36×10^{-6}
E	6	2	6	6	6	2	2	2

2.2.4 Results for different sulphur component in 14.6 wt% MEA

Table 2-11 and Figure 2-7 presents Henry's Law constant values as a function of inverse of temperature for different mercaptan species in 14.6% wt % MEA aqueous solution. The uncertainty of stripping method is estimated from propagation of errors on the uncertainty of the solute peak area determination, the uncertainties on the flow, the uncertainties related to the temperature and pressure, number of moles of solvent and accuracy of the approach, see Equation (2.4). Zin et al. [39] estimated *u(H)/H* to be about 15% which has been considered in this work.

$$u(H_i)/H_i = \sqrt{\begin{aligned}&\left(\frac{\partial H_i}{\partial \alpha}\right)^2_{P,D,T,N,V_G} u(\alpha)^2 + \left(\frac{\partial H_i}{\partial P}\right)^2_{\alpha,D,T,N,V_G} u(P)^2 + \left(\frac{\partial H_i}{\partial D}\right)^2_{\alpha,P,T,N,V_G} u(D)^2 + \\ &\left(\frac{\partial H_i}{\partial T}\right)^2_{\alpha,P,D,N,V_G} u(T)^2 + \left(\frac{\partial H_i}{\partial N}\right)^2_{\alpha,P,D,T,N} u(N)^2 + \left(\frac{\partial H_i}{\partial V_G}\right)^2_{\alpha,P,D,T,N} u(V_G)^2\end{aligned}}$$

(1.4)

.with $\alpha = -\frac{1}{t}\ln\left(\frac{A_t}{(A)_{t=0}}\right)$

Table 2-11 Henry's Law Constant and infinity dilution coefficient for all the studied mercaptans in MEA aqueous solution, u(H)/H=15%, u(γ∞)/ γ∞=15%

DMS			EM		
T/K	*H/ MPa*	*γ∞*	T/K	*H/ MPa*	*γ∞*
298.2	6.0	73.6	298.2	0.78	11.1
308.2	8.7	76.0	308.2	1.77	16.7
318.2	12.8	81.3	318.2	2.73	19.2
328.2	17.5	82.1	328.2	5.34	27.4
338.2	22.8	80.0	338.2	11.0	42.2
348.2	29.1	77.3	348.2	20.5	55.2
MM			iPM		
298.2	0.63	3.1	298.2	2.09	55.8
308.2	1.02	3.7	308.2	3.94	73.9
318.2	1.93	5.2	318.2	8.83	104.8
328.2	3.05	6.2	328.2	13.2	128.0
338.2	5.53	8.7	338.2	26.2	185.5
348.2	9.50	11.7	348.2	49.3	256.5
nBM			iBM		
298.2	1.5	241.5	298.2	2.6	249.7
308.2	3.3	324.7	308.2	4.8	294.8
318.2	5.9	377.5	318.2	10.3	414.9
328.2	12.9	544.9	328.2	19.7	534.6
338.2	22.4	645.3	338.2	36.1	683.1
348.2	41.5	838.3	348.2	71.1	958.6
nPM					
300.3	1.42	58.3			
308.2	2.40	75.1			
318.2	4.59	97.4			
328.2	8.74	129.2			
338.2	15.83	167.6			
348.2	32.70	253.7			

From Figure 2-7 it can be seen that for all sulphur components studied in this work, the Henry's law constant increases with the temperature and Henry's law constant increases with the number of carbon on mercaptan. Which means the solubility of mercaptan in aqueous MEA

decrease with the temperature and the number of carbon, as higher Henry's law constant means lower solubility in the solution.

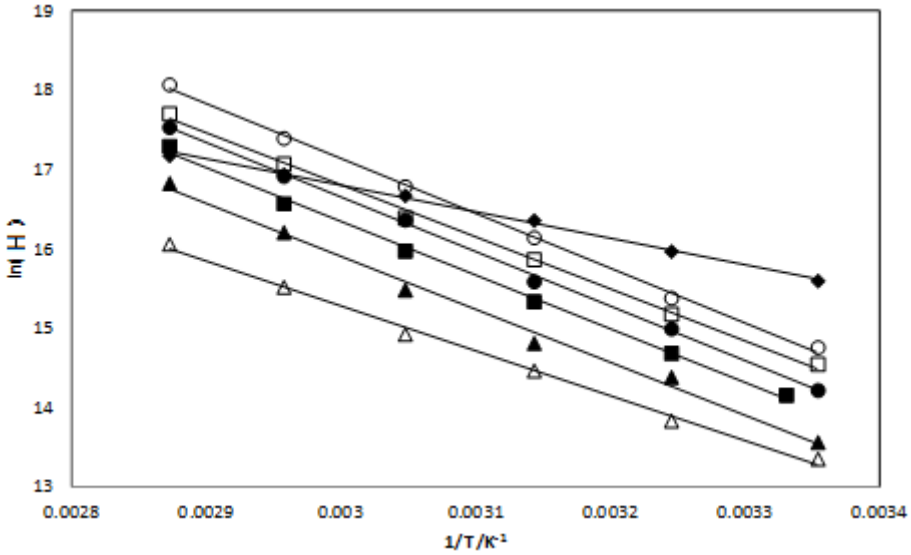

Figure 2-7 Logarithm of Henry's Law Constant of different component in14.6% MEA weight fractions as a function of the inverse of temperature (Δ: MM, ▲: EM, ♦ DMS, ■: nPM; □: iPM, ●: nBM, ○: iBM).

2.2.5 Results for CS2 in different solvents

Table 2-12 presents the values of Henry's law constants in pure water for CS_2.

Table 2-12 Henry's Law Constant for CS_2 in pure water, u(H)=15%, u(γ∞)=15%

	CS_2	
T/K	*H/ MPa*	*γ∞*
298.2	54.1	1125
308.2	116	1680
318.2	214	2198
328.2	319	2387
338.2	500	2776
348.2	722	3694

Then we have tested the CS_2 in 50 wt% MDEA aqueous solution. After introduction of CS_2, Chemical reaction was observed as shown in Figure 2-8; the solution in dilutor became

immediately yellow instead of colourless. Moreover, we can see that the evolution of logarithm of concentration of CS_2 in gas phase doesn't follow a linear trend with time, see Appendix III. We have tested COS and CO_2, which are known as reactive components with amine. Similar results are obtained, see Appendix III. As a conclusion, Henry's Law Constant of CS_2 in alkanolamine cannot be measured by using gas stripping method.

Figure 2-8View of the dilutor cell after introducing CS_2

Chapter 3 Thermodynamic model

3 Thermodynamic model

Introduction

Accurate phase diagrams for Vapour-Liquid-Equilibrium, Liquid-Liquid-Equilibrium and Vapour-Liquid-Liquid-Equilibrium are useful for the design of amine plant for gas purification. Phase diagrams can be predicted by using thermodynamic models which are crucial for acid gas removal industry. In 1981, Deshmukh and Mather [6] developed the first rigorous thermodynamic model for acid gas removal with amine, and it is widely used in the industry for several decades. This model requires large number of parameters concerning different aspects including Henry's law constants, reaction equilibrium constants, activity coefficient model for electrolytes and all of these models require quantity of adjustable parameters. This could be a limitation for the development of thermodynamic models for new amine due to the number of experiments required. The Cubic-Plus-Association Equation of State has been widely used in oil and gas industry, as it takes advantage of cubic EoS like SRK or PR and it can accurately predict the phase behavior for species forming hydrogen bonds, e.g. water and alkanolamines. However, it has never been applied for systems containing chemical reactions. Recently in 2010, an new interesting approach is proposed by Dowell et al. [40], it allows treating chemical reactions as physical association. Both Deshmukh-Mather model and CPA EoS with the new approach will be described in this chapter.

Des diagrammes de phase précis pour l'équilibre vapeur-liquide, l'équilibre liquide-liquide et l'équilibre vapeur-liquide-liquide sont utiles pour la conception d'une usine d'amine pour la purification du gaz naturel. Les diagrammes de phase peuvent être prédits en utilisant des modèles thermodynamiques qui sont cruciaux pour l'industrie de l'élimination des gaz acides. En 1981, Deshmukh et Mather [6] ont développé le premier modèle thermodynamique rigoureux pour l'élimination des gaz acides à l'aide des amines, et ce modèle est largement utilisé dans l'industrie depuis plusieurs décennies. Ce modèle nécessite un grand nombre de paramètres concernant différents aspects incluant les constantes de loi de Henry, les constantes d'équilibre de réaction, le modèle de coefficient d'activité pour les électrolytes et tous ces

modèles nécessitent une quantité de paramètres ajustables. Cela pourrait constituer une limitation pour le développement de modèles thermodynamiques pour une nouvelle amine en raison du nombre d'expériences requises. L'équation d'état Cubic-Plus-Association a été largement utilisée dans l'industrie pétrole et gaz, car elle a des avantages des EoS cubique comme SRK ou PR et elle peut prédire avec précision les comportements des espèces formant des liaisons hydrogène, par exemple. l'eau et les alcanolamines. Cependant, il n'a jamais été appliqué pour des systèmes contenant des réactions chimiques. Récemment en 2010, une nouvelle approche intéressante est proposée par Dowell et al. [40], il permet de traiter les réactions chimiques comme une association physique. Les modèles Deshmukh-Mather et CPA EoS avec la nouvelle approche seront décrits dans ce chapitre.

3.1 **Phase equilibrium calculation**

The Gibbs free energy G is the most useful function of state to study the properties and chemical equilibriums of a system of volume V constituted by N molecules at temperature T and pressure P, G is defined by Equation(3.1):

$$G = U + PV - TS \tag{2.1}$$

Where U is internal energy and S is the entropy

Gibbs free energy is can be also expressed by the chemical potential:

$$G = \sum_{i=1}^{Nc} N_i \mu_i \tag{2.2}$$

Where μ_i: the chemical potential of component i, N_i: the number of component i

The total differential of this expression is:

$$dG = \sum_{i=1}^{Nc} N_i d\mu_i + \sum_{i=1}^{Nc} \mu_i dN_i \tag{2.3}$$

The system is in equilibrium when the Gibbs free energy is the minimum; it is expressed by the Gibbs Duhem Equation (3.4):

$$dG = \sum_{i=1}^{Nc} \mu_i dN_i + Vdp - SdT = 0 \tag{2.4}$$

For an isothermal and isobaric system, we obtain Equation (3.5) and (3.6)

$$dG = \sum_{i=1}^{Nc} \mu_i dN_i = 0 \tag{2.5}$$

$$\mu_i = \left(\frac{\partial G}{\partial N_i} \right)_{T,P,N_{j \neq i}} \tag{2.6}$$

Those equations lead to the equality of chemical potential in all phases (at constant T and P), it can be expressed by Equation (3.7):

$$\mu_i^{phase_1}(T,P,z^{phase_1}) = \mu_i^{phase_2}(T,P,z^{phase_2}) = \mu_i^{phase_3}(T,P,z^{phase3})\cdots = \mu_i^{phase_n}(T,P,z^{phase_n})$$

(2.7)

Considering a mixture of gas, after integrating Equation (3.4) from a reference state at pressure P_0 to another pressure P, for the constituent i, its chemical potential $\mu_i(T,P,z^{phase\ j})$ in phase j can be represented by Equation (3.8):

$$\mu_i^{phase\ j}\left(T,P,z^{phase_j}\right) = \mu_i^{ref}\left(T,P_0\right) + RTln\frac{f_i^{phase\ j}\left(T,P,z^{phase_j}\right)}{f_i^{ref}\left(T,P_0\right)} \qquad (2.8)$$

$$\mu_i^{phase\ j}\left(T,P,z^{phase\ j}\right) = \mu_i^{ref}(T,P_0) + RTln(\phi_i(T,P,z^{phase\ j})) \qquad (2.9)$$

Where μ_i^{ref} is the chemical potential of reference state for component *i* at T and P_0

z is the composition of component i in phase j

f is the fugacity

ϕ_i is the fugacity coefficient of component *i*

Liquid-Liquid Equilibrium, Vapour-Liquid Equilibrium and Vapour-Liquid-Liquid Equilibrium are involved in this work, their phase equilibrium conditions can be generalized by Equations (3.10)(3.11)(3.12):

$$f_i^{phase_1}\left(T,P,z^{phase_1}\right) = f_i^{phase_2}\left(T,P,z^{phase_2}\right) = \cdots = f_i^{phase_n}\left(T,P,z^{phase_n}\right) \qquad (2.10)$$

$$T^{phase_1} = T^{phase_2} = \cdots = T^{phase_n} \qquad (2.11)$$

$$P^{phase_1} = P^{phase_2} = \cdots = P^{phase_n} \qquad (2.12)$$

3.1.1 Vapour Liquid Equilibrium

3.1.1.1 Dissymmetric approach

In this approach, the liquid phase is defined by the activity coefficient model. The vapour phase is represented by Equation of States. The VLE for the gamma-phi approach can be expressed by Equation (3.14), the left side of the equation is the fugacity of the vapour phase and the right side of the equation is the fugacity of the liquid phase:

$$f_i^V = f_i^L \tag{2.13}$$

$$y_i \hat{\Phi}_i^V P = x_i \gamma_i f_i^{*L} \tag{2.14}$$

Where γ_i is the activity coefficient of pure component i, it can be calculated by activity coefficient models such as NRTL [41] and UNIFAC [42]. f_i^{*L} is the fugacity of pure component i calculated in conduction (T, P) by using following Equations:

$$dg = RT \ln f \tag{2.15}$$

$$f_i^{*L} = P_i^{sat} \Phi_i^{sat} \exp\left[\frac{v_i \left(P - P_i^{sat}\right)}{RT}\right] \tag{2.16}$$

Where v_i^L is the molar volume of pure component i at saturation temperature.

However, in the case of infinite dilution, the state of gas molecules absorbed in liquid phase can only be consider as the same as solvent. Gas fugacity can be calculated with Henry's law constant [43]:

$$f_i^L = x_i \gamma_i H_{i,j}(T) \exp\left[\int_{P_j^0}^{P} \frac{v_i^{\infty}}{RT} dP\right] \tag{2.17}$$

Where the Henry constant $H_{i,j}$ of solute i in solvent j is defined by:

$$H_{i,j}(T) = \lim_{x_i \to 0} \frac{f_i^L(T, P^{sat})}{x_i} \tag{2.18}$$

Where γ_i^{∞} is the infinite dilution activity coefficient of component i

3.1.1.2 Symmetric approach

The symmetric approach uses the same Equation of State for both vapour phase and liquid phase. The equilibrium is represented by Equation (3.19):

$$Px_i\phi_i^{liquid}(T,P,x_i) = Py_i\phi_i^{vapor}(T,P,y_i) \qquad (2.19)$$

Where ϕ_i is the fugacity coefficient. It is given by the Equation (3.20):

$$\phi_i(T,P,z_i) = \frac{f_i(T,P,z_i)}{Pz_i} \qquad (2.20)$$

The fugacity coefficient can be calculated by the residual Gibbs energy or the residual Helmholtz energy,:

$$\ln(\phi_i) = \left(\frac{\partial G_i^{Res}}{\partial n_i}\right)_{T,P,n_{j\neq i}} = \left(\frac{\partial A_i^{Res}}{\partial n_i}\right)_{T,V,n_{j\neq i}} + Z - 1 - \ln Z \qquad (2.21)$$

Where *Z* is the compressibility having following expression:

$$Z = \frac{Pv}{RT} \qquad (2.22)$$

As most of Equation of State is explicitly expressed in function of volume, the fugacity coefficient is more conveniently by the residual Helmholtz energy. The residual Helmholtz energy can be determined by an Equation of State, its general expression is given by Equation (3.23):

$$\frac{A^{Res}}{RT} = \frac{1}{RT}\int_{\infty}^{V}\left(\frac{RT}{V} - P\right)dV \qquad (2.23)$$

The van der Waals equation is an Equation of State which is based on the theory where fluids are composed of particles with certain volumes, and particles are influenced by an inter-particle attractive force. It is expressed by Equation (3.24) :

$$P=\frac{RT}{v-b}-\frac{a}{v} \qquad (2.24)$$

Where *a* is the attractive parameter

b is the co-volume parameter

v is the molar volume

Peng-Robinson Equation of State [44] (PR EoS expressed by Equation(3.25)) and Soave-Redlich-Kwong Equation of State [45] (SRK EoS expressed by Equation (3.26)) are modified version of Van der Waals EoS, they are widely applied in the industry.

$$P=\frac{RT}{v-b}-\frac{a(T)}{v(v+b)+b(v-b)} \qquad (2.25)$$

$$P=\frac{RT}{v-b}-\frac{a(T)}{v(v+b)} \qquad (2.26)$$

For a component i, to calculate the attractive parameter $a_i(T)$ and co-volume parameter b_i, both PR EoS and SRK EoS require critical temperature $T_{c,i}$, critical pressure $P_{c,i}$, and acentric factor ω_i.

To calculate the attractive parameter $a_i(T)$ of component i, we can use following Equation:

$$a_i(T)=\Omega_a\frac{R^2T_{c,i}^2}{P_{c,i}}\alpha(T) \qquad (2.27)$$

With Ω_a=0.457236 for PR EoS, Ω_a=0.42748 for SRK EoS, these parameters are determined at critical point by using following Equations:

$$\left(\frac{\partial P}{\partial v}\right)_{Tc}=0 \qquad (2.28)$$

$$\left(\frac{\partial^2 P}{\partial v^2}\right)_{Tc}=0 \qquad (2.29)$$

$\alpha(T)$ is the alpha function, it can be formulated by Equation (3.30):

$$\left[1+\kappa_i\left(1-\sqrt{\frac{T}{T_{c,i}}}\right)\right]^2 \qquad (2.30)$$

For PR EoS: if $\omega_i \leq 0.491$ $\kappa_i = 0.37464+1.54226\,\omega_i-0.26992\,\omega_i^2$;

if $\omega_i > 0.491$ $\kappa_i = 0.379642+1.48503\,\omega_i-0.164423\,\omega_i^2+0.016666\,\omega_i^3$

For SRK EoS: $\kappa_i = 0.48508+1.551716\,\omega_i-0.15613\,\omega_i^2$

To calculate the co-volume parameter b_i of component i, following Equation can be used:

$$b_i = \Omega_b \frac{RT_{c,i}}{P_{c,i}} \qquad (2.31)$$

With Ω_b=0.0777961 for PR EoS, Ω_b=0.08664 for SRK EoS. These parameters are also defined at critical point.

3.1.1.3 The mixing rules

The equations of state for pure component can be applied to mixtures by considering the mutual influence between different compounds with mixing rules. The first form of mixing rules is that of Van der Waals referred to as the classical mixing rule; it gives the following expressions for the parameters of repulsion and attraction of mixture: The classical Van der Waals mixing rules have been employed in this work:

$$a = \sum_i \sum_j x_i x_j a_{ij} \qquad (2.32)$$

$$b = \sum_i \sum_j x_i x_j b_{ij} \qquad (2.33)$$

Where a_{ij} and b_{ij} represent the interaction parameters corresponding to two different species (i ≠j). These parameters are expressed as a function of the attraction and covolume parameters of the pure bodies i and j (denoted by a_i and b_i), Equations (3.34) and(3.35).

$$a_{ij} = \sqrt{a_i a_j}\,(1-k_{ij}) \qquad (2.34)$$

$$b_{ij} = \frac{1}{2}\left(b_i + b_j\right)\left(1 - l_{ij}\right) \qquad (2.35)$$

k_{ij} and l_{ij} are the Binary Interaction Parameters, they can be both adjusted from experimental data. Generally, we only adjust parameter k_{ij} , as it takes into account different interactions between components. The parameter l_{ij} is assumed to be zero.

3.1.2 Vapour Liquid Liquid Equilibrium

VLLE is a three phase equilibrium between two liquid phases L and L' and a vapour phase V. The mixture is characterized by its initial composition z_i, liquid phases composition x_i and x_i', and the vapour phase composition y_i. The material balance equations are given by Equation (3.36) and (3.37):

$$z_i = x_i L + x_i' L' + y_i V \qquad (2.36)$$

$$L + L' + V = 1 \qquad (2.37)$$

With L, L' and V the fraction of each phase.

The phase equilibrium relations between the three phase is:

$$f_i^L\left(T, P, x\right) = f_i^{L'}\left(T, P, z^{L'}\right) = \cdots = f_i^V\left(T, P, y\right) \qquad (2.38)$$

The fugacity of liquid phases can be obtained with an Equation of State or an activity coefficient model. The fugacity of vapour phase is determined by an Equation of State.

The phase equilibrium conditions need to satisfy following constraints:

$$\sum_i x_i = 1 \qquad (2.39)$$

$$\sum_i x_i' = 1 \qquad (2.40)$$

$$\sum_i y_i = 1 \qquad (2.41)$$

This system is able to be resolved by using Newton-Raphson method [46]. And the compositions of each phase can be determined after each iteration. As the initialization of parameters is not always available, the tangent plan method developed by Michelsen [47] is used to analyze the phase stabilities and to have a reasonable initialization value of equilibrium constant K_{eq} which is expressed by:

$$K_{eq} = \frac{y_i}{x_i} \qquad (2.42)$$

3.2 **Thermodynamic models for acid gas removal**

Unlike the phase equilibrium presented in section 3.1, for acid gas treatment, the chemical reaction between CO_2 / H_2S - alkanolamine and the formation of electrolyte species should be considered. The thermodynamic models used to resolve this problem can be grouped into three categories. The first and the simplest are the empirical models. Thanks to their simplicities, they are quite popular for early phase studies. These models utilize simple mathematical correlations for phase equilibria and fitted chemical equilibrium constants [48]. The Kent–Eisenberg model [49] is an example of such a model. This kind of model is unsuitable for predicting the speciation and rigorous energy balances. More rigorous models can be divided into two categories: dissymmetric approach (excess Gibbs energy model) and symmetric approach (Helmholtz energy based models). For the dissymmetric approach, the Desmukh–Mather model [6] has been widely used. This model utilizes the extended Debye–Hückel expression to predict all the activity coefficients of electrolyte species for long distance interactions. And it uses empirical terms to represent short distance interactions. The electrolyte-NRTL model [50] and the electrolyte UNIQUAC model [51] which are more complex activity based models can also be used. For symmetric approach, Fürst and Renon [52] EoS is one of the most widely used. In this work, a new symmetric approach to consider the chemical reaction is developed and the model performance is compared with the widely used dissymmetric model (Desmukh–Mather model).

3.2.1 The Deshmukh–Mather model

In 1981, Deshmukh and Mather [6] developed the first rigorous thermodynamic model for acid gas removal with amine. Thanks to its high computational efficiency, up to 10^6 times faster to evaluate phase equilibria than eNRTL model [53], the Deshmukh-Mather model has been widely used by acid gas removal industry. Weiland et al. [54] applied this model to represent CO_2 and H_2S solubility in aqueous MEA, DEA, DGA and MDEA solutions. Haji-Sulaiman and Aruoa [55] also utilized this model to represent the phase behavior of CO_2 in aqueous DEA and AMP solutions. The solubility of CO_2 in the mixtures of DEA and MDEA has been represented by using Deshmukh and Mather model in Benamor and Aroua's work [56]. Dicko et al. [57] have measured the solubility of CO_2, H_2S and their mixtures in aqueous MDEA solution with methane at 7 MPa, they have modeled those systems with the Deshmukh-Mather model. As a continuity of Dicko et al.'s work, the Deshmukh-Mather model is chosen as a bench mark reference model to compare with the PR-CPA EoS which is presented in section 3.2.2.

The Deshmukh-Mather model included chemical reaction, electrolyte activity model and phase equilibria, CO_2-MDEA-water ternary system is taken as an example to introduce this model.

3.2.1.1 Chemical reactions with MDEA

The chemical equilibria for MDEA-water-CO_2 systems can be governed by the four following reactions:

$$H_2O = OH^- + H^+ \qquad (2.43)$$

$$H_2O + CO_2 = H^+ + HCO_3^- \qquad (2.44)$$

$$HCO_3^- = H^+ + CO_3^{2-} \qquad (2.45)$$

$$MDEAH^+ = H^+ + MDEA \qquad (2.46)$$

For each reaction, a set of parameters from Dicko et al. [57] is available to calculate the equilibrium constant (see ***Table 3-1***). 8 species are involved in the studied system: H_2O, MDEA, CO_2, OH^-, H^+, HCO_3^-, CO_3^{2-}, $MDEAH^+$. The equilibrium constants defined in terms of molalities and activity coefficients are expressed as:

$$K_{H_2O} = \frac{\gamma_{H^+} m_{H^+} \gamma_{OH^-} m_{OH^-}}{a_{H_2O}} \qquad (2.47)$$

$$K_{CO_2} = \frac{\gamma_{H^+} m_{H^+} \gamma_{HCO_3^-} m_{HCO_3^-}}{\gamma_{CO_2} m_{CO_2}} \quad (2.48)$$

$$K_{HCO_3^-} = \frac{\gamma_{H^+} m_{H^+} \gamma_{CO_3^{2-}} m_{CO_3^{2-}}}{\gamma_{HCO_3^-} m_{HCO_3^-}} \quad (2.49)$$

$$K_{MDEA} = \frac{\gamma_{H^+} m_{H^+} \gamma_{MDEA} m_{MDEA}}{\gamma_{MDEAH^+} m_{MDEAH^+}} \quad (2.50)$$

With :

– K_i : Constant of equilibrium

– m_i : molalirity (mol/kg water)

The expressions of the equilibrium constants commonly used are represented by Equation (3.51). Their values are presented in Table 3-1.

$$ln(K_i) = \frac{A}{T^2} + \frac{B}{T} + Cln(T) + D + ET \quad (2.51)$$

Table 3-1 Equilibrium constants for MDEA-CO_2-water ternary system [57]

Constant	$A*10^{-6}$/K^2	$B*10^{-3}$/K	C	D	$E*10^{3}$/K^{-1}	T/K
$K(H_2O)$	0	−13.445	−22.4773	140.932	0	273–498
$K(CO_2)$	−4.710	68.359	188.444	−1203.01	−20.642	273–673
$K(HCO_3^-)$	−3.730	−7.230	−30.6509	175.36	1.314	273–523
K(MDEA)	0	−0.819	10.9756	−79.474	0	278–422

The material balance due to the reactions are characterized by Equations (3.52)(3.53) and (3.54):

$$H_2O: N_w^0 = N_w + N_{HCO_3^-} + N_{CO_3^{2-}} + N_{OH^-} \quad (2.52)$$

$$CO_2: N_{CO_2}^0 = L_{CO_2} N_{MDEA}^0 = N_{CO_2} + N_{HCO_3^-} + N_{CO_3^{2-}} \quad (2.53)$$

$$MDEA: N_{MDEA}^0 = N_{MDEA} + N_{MDEA^+} \quad (2.54)$$

And also the electro-neutrality balance in the liquid phase:

$$N_{MDEAH^+} + N_{H^+} = N_{HCO_3^-} + 2N_{CO_3^{2-}} + N_{OH^-} \quad (2.55)$$

There are 8 equations for 8 species in the liquid phase. These equations are resolved by using Newton-Raphson numerical method [46].

3.2.1.2 Activity coefficients calculation

Activity coefficients are calculated by the Deshmukh–Mather model, this equation associates a Debye-Hückel [58] expression for long-distance interactions and an empirical contribution for short interactions. The Debye-Hückel model allows a good description of the activity coefficients in the diluted solutions. This model has some assumptions and simplifications introduced are as follows:

- The solvent is assimilated to a continuum without structure, it plays only a role to providing a medium of constant relative (dielectric constant)
- The concept of ionic atmosphere is presented to estimate the average effect on the charge of a specific ion of the other ions in spherical symmetry
- This mean effect is estimated by the introduction of an isolated ion in a medium described by a continuous Poisson-Boltzmann distribution [59] of the charge density

Figure 1 illustrates this distribution of the anions and cations. The ionic atmosphere consists of a spherical cloud of ions located around a central ion. This arrangement of the opposing charges makes favourable local formation of ion / counter ion groups.

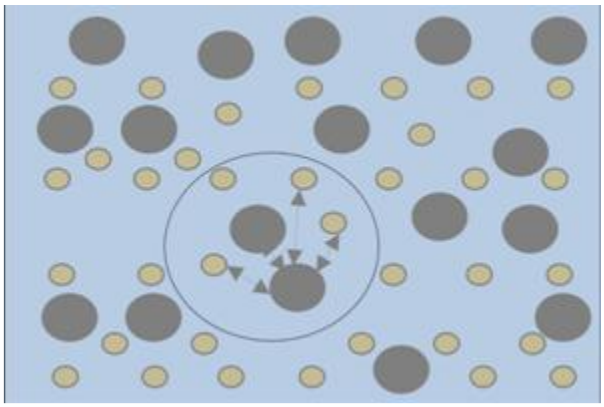

Figure 3-1 Distribution of anions and cations in the ionic atmosphere [60]

It can be expressed by following Equation (3.56):

$$\log(\gamma_i) = \frac{-AZ_i^2 I^{0.5}}{1+BrI^{0.5}} + 2\sum_j \beta_{ij} m_j \qquad (2.56)$$

Where Z_i is the number of charge of ion i , r is the ionic radius, m_j is the molarity of species j in mol/kg water. I is the ionic force, it is given by Equation(3.57). A and B are expressed by Equation (3.58) and (3.59):

$$I = 0.5\sum_j m_j Z_i^2 \qquad (2.57)$$

$$A = \frac{F^3 (2000\rho_{solvent})^{0.5}}{2.303(\varepsilon_0 D_s RT)^{1.5}(8\pi N_A)} \qquad (2.58)$$

$$B = \sqrt{\frac{2000F^3}{\varepsilon_0 D_s RT}} \qquad (2.59)$$

Where F is a constant. Ds is the dielectric constant of water is calculated with Maryott and Smith formula (1951) [61], valid from 273 to 373 K:

$$Ds(T) = 78.54\left(1 - 4.579\times10^{-3}(T-298.15) + 1.19\times10^{-5}(T-298.15)^2 - 2.8\times10^{-7}(T-298.15)^3\right) \quad (2.60)$$

The second term of Equation (2.56) represents the short distance interactions between the different molecular or ionic species. This term is empirical. The interaction parameters β_{ij} exclude the pairs (i, j) of the same sign. The β_{ij} are obtained with a regression of experimental data. According to Dicko et al.[57], only limited pairs of β_{ij} are needed to be fitted from experimental data, they are shown in *Table 3-2***.**The adjusted values are presented in the Chapter 5.

Table 3-3 Adjustable parameters for CO_2-MDEA-water ternary systems.

Couple	β_{ij}/kg-H_2O/kmol
$MDEAH^+$–CO_2	fitted
$MDEAH^+$–HCO_3^-	fitted
MDEA–HCO_3^-	fitted
MDEA–CO_3^{2-}	fitted
MDEA–MDEA	fitted

3.2.1.3 Vapour Liquid Equilibria

Experimental results show that the composition of MDEA in the vapour phase is very low (less than 10^{-4} in molar composition. Therefore in this work we assumed` that MDEA is not present in the vapour phase while calculate VLE. So the VLE for CO_2-MDEA-water are calculated by equalizing fugacity values of liquid phase and vapour phase:

$$\phi_{CO_2} y_{CO_2} P = \gamma_{CO_2} m_{CO_2} H^{P_0}_{CO_2} \exp\left[\frac{\upsilon^{\infty}_{CO_2}(P-P^0)}{RT}\right] \quad (2.61)$$

$$\phi_{H_2O} y_{H_2O} P = a_{CO_2} P^0_{H_2O} \Phi^0{}_{H_2O} \exp\left[\frac{\upsilon_{H_2O}(P-P^0)}{RT}\right] \quad (2.62)$$

The fugacity coefficients are calculated by PR-CPA EoS which wiil be presented in next section, see Equation (3.65). H is the Henry's law constant; P^0_{H2O} is the saturation pressure at reference state. Both of them can be also expressed by Equation (3.63). Their parameters are shown in Table 3-4.

$$ln(H(P_{vap})) = \frac{A}{T^2} + \frac{B}{T} + Cln(T) + D + ET \qquad (2.63)$$

Table 3-4 Parameters for calculating Henry's law constant of solute and saturation pressure of solvent [57]

	A/K	*B*	*C*	*D*/K^{-1}	*E*/K^{-2}	*T*/K
H(CO_2)	−9624.41	−28.7488	192.876	0.01441	0	273–473
P_{vap}(H_2O)	−7206.7	−7.1385	72.55	0	0.000004046	273–650

.gg

3.2.2 The Cubic Plus Association EoS

Due to their simplicity, accuracy and computational efficiency, classical Cubic EoS are widely used in the industry. However, they are not adapted to acid gas removal, because they cannot take into account the association between molecules neither the chemical reaction taken in place between acid gases and amines. In the beginning of 1980s, Wertheim [62] has developed a model for associating molecules. This model is used in the Statistical Associating Fluid Theory EoS [63], it considers perturbation theory and hard sphere model as reference. In 1996, Kontogeorgis et al. [64] has proposed to combine Wertheim's model with adapted radical distribution function and SRK EoS. This model is called Cubic Plus Association EoS (CPA EoS), expressed by Equation (3.64).

$$\frac{A^{CPA}}{RT} = \frac{A^{Cubic}}{RT} + \frac{A^{Association}}{RT} \qquad (2.64)$$

The cubic term can be SRK EoS or PR EoS. We presented in section 3.1.1.2, there is no significant difference between these two EoS. As a continuity of previous work [65], the PR-CPA has been applied in this work, expressed by Equation (3.65). While the PR EoS accounts for the physical interaction contribution between the species, the association term takes into account the specific site-site interaction due to hydrogen bonding. Therefore it is suited to describe studied systems where water and alkanolamines molecules form hydrogen bonds between them and themselves (self and cross associations). Moreover, Dowell et al. [40] have successfully developed a simplified approach which allows treating chemical reactions with the Wertheim term. In this approach, the chemical reactions between alkanolamine and CO_2 have been treated as pseudo-cross association between them.

$$P = \underbrace{\frac{RT}{v-b} - \frac{a(T)}{v(v+b)+b(v-b)}}_{\text{PR}} \underbrace{- \frac{1}{2}\frac{RT}{v}\left(1+\rho\frac{\partial \ln g_r}{\partial \rho}\right)\sum_i x_i \sum_{A_i}\left(1-X_{A_i}\right)}_{\text{Wertheim term}} \qquad (2.65)$$

Where v is the molar volume, b is the molar co volume parameter, $a(T)$ the temperature dependent energy parameter of the equation of state, ρ the molar density ($\rho = 1/v$), g_r the radial distribution function, and X_{Ai} the fraction of sites A on molecule i (hence the subscript Ai) that do not form bonds with other hydrogen bonding sites. X_{Ai} is dependent on the association strength Δ^{AiBj} between it and sights belonging to other molecules of the same or different component, like for example sight B on molecule j named B_j. X_{Ai} is given as

$$X_{A_i} = \frac{1}{1+\rho\sum_j x_j \sum_{B_j} X_{B_j}\Delta^{A_iB_j}} \qquad (2.66)$$

X_{Bj} is the fraction of sites B on molecule j that don't form hydrogen bonds. The association strength Δ^{AiBj} is dependent on the radial distribution function g_r, the association energy ε^{AiBj}, and the association volume β^{AiBj} between sights A_i and B_j. The relation is given by equation:

$$\Delta^{A_iB_j} = g_r\left[\exp\left(\frac{\varepsilon^{A_iB_j}}{RT}\right)-1\right]b_{ij}\beta^{A_iB_j} \qquad (2.67)$$

The equation used to find the radial distribution function is:

$$g_r = \frac{1}{1-1.9\eta} \qquad (2.68)$$

Where η is the reduced fluid density given as:

$$\eta = \frac{1}{4} b\rho \qquad (2.69)$$

Where the co-volume parameter b is assumed to be temperature independent.

3.2.2.1 Pure component

For pure component, the molecules involved in acid gas removal can be divided into two categories:

- Non self association components: alkanes, acid gas, aromatics and mercaptans
- Association components : water, alkanolamine

3.2.2.1.1 Non self associating component

For non self associating component such as alkanes, acid gas, mercaptans and aromatics, the PR-CPA EoS is reduced to PR EoS, their pure component parameters (a_0, b, c_1) can be calculated with critical properties and the acentric factor. For pure substance i, parameters can be obtained by using following Equations:

$$b_i = 0.07780 \frac{RT_c}{P_c} \qquad (2.70)$$

Where b_i is the molar co volume parameter of the PR-CPA EoS

In Equation (2.65), a_i is defined as:

$$a_i = a_{0,i} \left(1 + c_{1,i} \left(1 - \sqrt{\frac{T_i}{T_{c,i}}} \right) \right)^2 \qquad (2.71)$$

Where $a_{0,i}$ and $c_{1,i}$ are parameters of the equation of state for substance *i*.

$$a_{0,i} = 0.45724 \frac{R^2 T_c^2}{P_c} \qquad (2.72)$$

$$c_{1,i} = 0.37464 + 1.54226\omega - 0.26992\omega^2 \qquad (2.73)$$

Pure component parameters for alkanes, acid gas, mercaptans and aromatics are summarized in Table 3-5

Table 3-5 Pure component parameters for non self associating components [66]

Compound	a_0 (bar L^2 mol^{-2})	*b (L/mol)*	c_1	*Tc* /K	*Pc* /MPa	ω
Methane	0.250	2.680	0.392	190.560	0.546	0.0012
Ethane	0.605	4.054	0.525	305.320	4.872	0.0995
propane	1.018	5.631	0.603	369.820	4.248	0.1523
n-butane	1.506	7.248	0.672	425.150	3.794	0.1996
i-butane	1.445	7.249	0.650	407.840	3.639	0.1844
n-pentane	2.069	9.015	0.745	469.700	3.370	0.2515
n-hexane	2.689	10.847	0.814	507.530	3.028	0.3004
CO_2	0.397	2.661	0.701	304.210	7.384	0.2236
H_2S	0.492	2.957	0.517	373.530	8.960	0.0942
MM	0.966	4.209	0.600	469.870	7.212	0.1501
EM	1.427	5.856	0.660	498.800	5.509	0.1918
Benzene	2.039	7.426	0.687	562.000	4.895	0.2100
Ethylbenzene	3.334	11.056	0.818	617.120	3.610	0.2100
Toluene	2.684	9.280	0.764	591.890	4.126	0.2644

3.2.2.1.2 Hydrogen bonding

For associating components (water and alkanolamines), the nomenclature of Huang and Radosz [67] is used to represent the association scheme, see Figure 3-2.

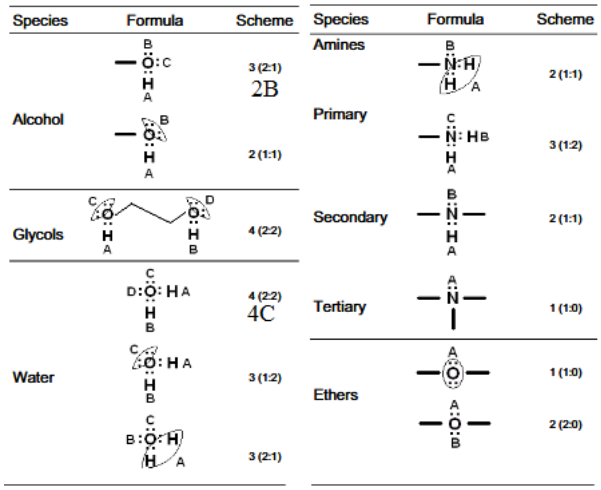

Figure 3-2 Association schemes for associating components [67]

4C is most suitable association scheme for water [68]. However, due to presence of multifunctional groups on alkanolamine, the choice of association scheme is more difficult.

MEA contains one alcohol functional group and one amine functional group, both of them can be best represented by using 2B association scheme, so the 4C association scheme is a natural choice [69],[70].

For DEA 4C association scheme is chosen ie. the two hydroxyl groups are taken into account while the amine group is ignore. Though more advanced association scheme for DEA, such as called 6A and 4D association schemes, have been studied by Avlund et al. [69],[70]. In 6A association scheme, the hydroxyl group and the amine group are each assigned two identical sites. And in 4D association scheme, the hydroxyl group and the amine group have different association parameters. The performances of using 4C, 6A and 4D association schemes are identical for describing the pure component thermodynamic proprieties of DEA and DEA-water binary phase behavior.

The molecular structure MDEA is similar to the one DEA, so we have decided to use 4C association scheme for MDEA as well, furthermore the association parameters of MDEA is assumed as the same as the one of DEA [69],[70].

5 parameters (a_0, b, c_1, ε^{AiBj} and β^{AiBj}) are required to represent thermodynamic properties of water, MDEA, DEA, and MEA; their parameters were regressed by minimizing objective expressed by Equation (3.74):

$$f_{obj,pure} = \sum_{i=1}^{n_{vap}} \left(\left| \frac{P_{sat}^{cal} - P_{sat}^{exp}}{P_{sat}^{exp}} \right| \right)_i + \sum_{i=1}^{n_{\rho}} \left(\left| \frac{\rho_{liq}^{cal} - \rho_{liq}^{exp}}{\rho_{liq}^{exp}} \right| \right)_i \qquad (2.74)$$

Where n_{vap} and n_{ρ} are the number of vapour pressure, and liquid density. P_{sat} is the vapour pressure. ρ_{liq} is the liquid density. P_{sat}^{exp} and ρ_{liq}^{exp} values were generated by using DIPPR correlations from Thermo Data Engine [66]. Pure component parameters are presented in Table 3-6.

Table 3-6. PR CPA parameters for compounds for association compounds considered in this work [66]

Compound	scheme	a_0 /bar L^2 mol^{-2}	b /L mol^{-1}	c_1	ε^{AiBj} /bar.L.mol^{-1}	β^{AiBj}	Tc /K	Range of Tr		ARD%[a]	
								For P_{sat}	For ρ_L	P_{sat}	ρ_L
MEA	4C	1.333	5.467	0.763	168.23	0.0142	647.51	0.42-0.92	0.43-0.61	1.8	0.6
DEA	4C	3.065	9.246	1.02	201.76	0.0083	671.4	0.45-0.88	0.41-0.48	0.3	1.3
MDEA	4C	3.339	11.346	0.695	201.76	0.0083	768	0.39-0.9	0.38-0.63	0.9	2
water	4C	0.123	1.445	0.674	170.48	0.0698	741.6	0.43-0.95	0.43-0.95	1	1.6

[a] ARD% = 1/np× $\Sigma|1 - \chi_i^{calc}/\chi_i^{exp}| \times 100\%$.

3.2.2.2 Mixtures

For mixtures, the classical van der Waals mixing rules as explained in 3.1.1.3 have been chosen in this work. From Equation (2.67) it can be seen that it is necessary to calculate the association

energy and volume parameters to calculate the association strength. Combining rules are involved in case of mixture.

3.2.2.2.1 Combining rules for alkanolamine and water

Alkanolamine and water are both self-associating compounds, the CR-1 combining rule has been chosen among various combining rules in this work. In CR-1 combining rule, the arithmetic mean of the cross-association energy is proportional to the enthalpy of hydrogen bonding while the geometric mean of the cross-association volume is related to the cross-entropy of the hydrogen bonding, see Equation (3.75) and (3.76):

$$\varepsilon^{A_i B_j} = \frac{\varepsilon^{A_i} + \varepsilon^{B_j}}{2} \tag{2.75}$$

$$\beta^{A_i B_j} = \sqrt{\beta^{A_i} \beta^{B_j}} \tag{2.76}$$

3.2.2.2.2 Solvation effect

Due to the C=O, -SH, or -SH functional group on acid gas, mercaptans or aromatics, they could form hydrogen bonding with water or alkanolamine, but they do not cross associate with themselves. Solvation effect between water and acid gas, mercaptans or aromatics have been considered in this work.

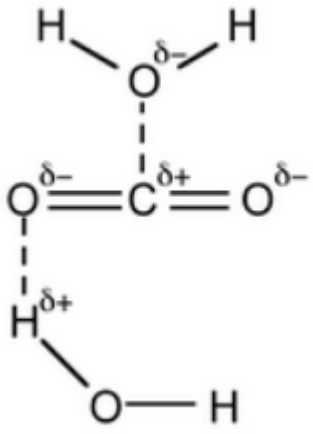

Figure 3-3 Solvation between water carbon dioxide [71]

The modified CR-1 (mCR-1) combining rule is employed to treat the solvation effect in this work, According to this combining rule the cross-association volume $\beta^{A_iB_j}$ is fitted from experimental data and the cross-association energy is equal to the value of the associating component divided by two:

$$\varepsilon^{A_iB_j} = \frac{\varepsilon^{associating}}{2} \qquad (2.77)$$

$$\beta^{A_iB_j} = \beta^{cross}(fitted) \qquad (2.78)$$

3.2.2.3 The new approach to treat Chemical reactions

Conventional configurations for alkanolamine and acid gas are not suitable to represent the chemical reaction between acid gas and alkanolamines. Nevertheless, Dowell et al. [40] have successfully represented the phase behaviour of CO_2-water-MEA ternary systems by using statistical correlation liquid theory for potentials Variable Range (SAFT-VR) without strong consideration of electrolytes species. They proposed that chemical reactions can be treated as associating physical interactions. Association sites that allow the pseudo-chemical reaction of CO_2 and MEA are introduced in the new SAFT models. This approach has been successfully applied to predict CO_2 solubility in MEA, MDEA, DEA, AMP, DEtA as multifunctional alkanolamine [40] [72], and some n-alkyl amines [73] with their SAFT family EoS. Recently, they applied this approach in process simulation and optimization for CO_2 capture by MEA [74]. In their approach is employed to treat the chemical reactions in this work. However the solvation between CO_2 and water has been neglected. But according to Tsivintzelis et al.[75], the solvation effect between CO_2 and water is important to be considered to represent CO_2 - water binary system. The solvation effect between CO_2 and water on CO_2–alkanolamine-water is investigated in this work. Moreover, this work concern also keeping a homogenous thermodynamic model for systems containing H_2S, which has not been investigated with this approach yet. Therefore, new conception of association schemes for acid gas and alkanolamines are developed and investigated in this work, see Figure 3-4.

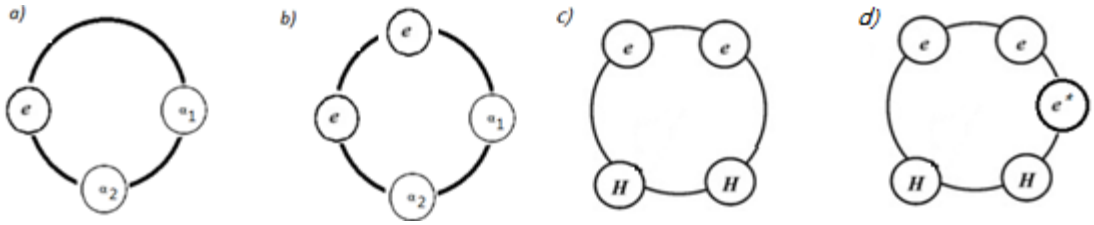

Figure 3-4 association schemes developed in this research

Figure 3-4.a is the association scheme for CO_2, the e site is assigned as a solvation site which allows the cross association between CO_2 and water, α_1 and α_2 are dedicated reaction sites which only react (cross-associate) with the electron site on alkanolamine. Depending on the nature of alkanolamine, 1 α site can be activated for MDEA, and 2 activated for MEA.

Figure 3-4.b is the association scheme for H_2S, the two e sites are given as solvation sites which allows the cross association between H_2S and water, α_1 and α_2 are dedicated reaction sites which are only react (cross-associate) with the electron site on alkanolamine. Depending on the nature of alkanolamine, the 1 α site is activated for MDEA, and 2 activated for MEA.

Figure 3-4.c is the symmetric model of alkanolamine, which is presented in previous section. There are four sites in total including: two e sites and two H sites representing different functional groups. In this symmetric model, there is no distinction between e and H sites, i.e. the association behaviour of the different functional groups are identical.

Figure 3-4.d is the asymmetric model of alkanolamine, one e* site is added based on the symmetric model of alkanolamine. In this asymmetric model, the α sites on acid gas react only with the e* site.

The products after reactions have been considered to be inert. As an example, the reaction between MEA and CO_2 can be represented by Figure 3-5. Reaction products can be determined from a statistical analysis of the molecules not-bonded at given sites, by using Equation (3.79) and (3.80).

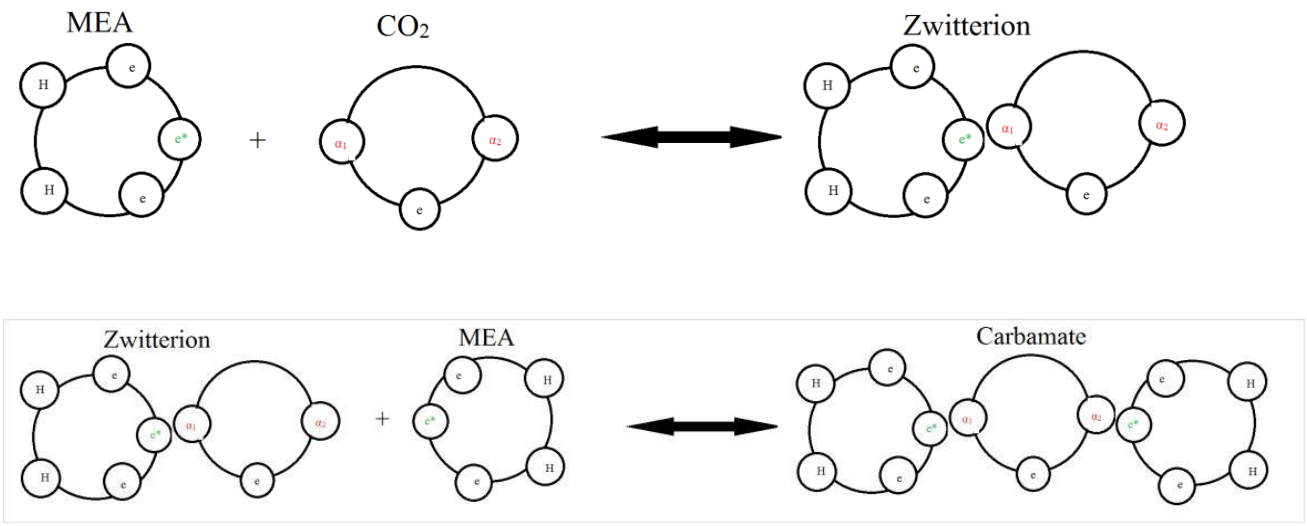

Figure 3-5 Reaction mechanism between CO_2 and MEA (asymmetric model)

$$[MEACOO^{-}]=[x_{CO2}][(1-X^{\alpha 1,CO2})\ (1-X^{\alpha 2,CO2})] \qquad (2.79)$$

$$[HCO_3^{-1}]=[x_{CO2}][X^{\alpha 1,CO2}+1-X^{\alpha 2,CO2}] \qquad (2.80)$$

Where x_{CO2} is the molar concentration of CO_2, which is related to the concentration of alkanolamine and loading ratio. $X^{\alpha i,CO2}$ is the mole fraction of CO_2 not bonded at α_i site.

For alkanolamine and acid gas, their cross-association volume $\beta^{A_iB_j}$ and $\varepsilon^{A_iB_j}$ the cross-association energy are fitted from experimental data, expressed by:

$$\varepsilon^{A_iB_j}=\varepsilon^{cross}(fitted) \qquad (2.81)$$

$$\beta^{A_iB_j}=\beta^{cross}(fitted) \qquad (2.82)$$

k_{ij} is also considered as an adjustable parameter, the influence of k_{ij} and its temperature dependency is studied in this work. ε^{cross}, β^{cross} ,and k_{ij} are fitted at the same time only from acid gas-alkanolamine-water VLE experimental data.

Chapter 4 Modelling of non-reactive systems

4 Modelling of non-reactive systems

Introduction

In this chapter, solubility of non-reactive components including: alkanes (methane, ethane, propane, n-butane, i-butane, n-propane and hexane), aromatics (benzene, toluene, and ethylbenzene), and mercaptans (MM, EM) in different aqueous alkanolamine solutions (MEA, DEA, and MDEA) are modelled with PR-CPA EoS. Alkanolamine-water binary systems are represented with PR-CPA EoS by fitting a temperature independent $k_{ij.}$ Alkanes, aromatics and mercaptans solubility in pure water will be individually studied by considering the presence of solvation effect, if it exists. Then, the solubility of non-reactive components are described by PR-CPA EoS by fitting BIPs (k_{ij} and cross association parameters) between the solute and alkanolamine from ternary experimental data. The PR-CPA EoS is then validated by comparing different thermodynamic properties predicted data with experimental ones which are not used in parameter fitting. We can cite properties such as single component solubility, alkane mixture solubility, vapour phase composition, temperature minimum of solubility, apparent Henry's law constant, etc.

Dans ce chapitre, la solubilité des composants non réactifs incluant: les alcanes (méthane, éthane, propane, n-butane, i-butane, n-propane et hexane), les composés aromatiques (benzène, toluène et éthylbenzène) et les mercaptans (MM, EM) dans différentes solutions aqueuses d'alcanolamine (MEA, DEA et MDEA) sont modélisés avec PR-CPA EoS. Les systèmes binaires alcanolamine-eau sont représentés avec PR-CPA EoS en ajustant un $k_{ij.}$ indépendant de la température. La solubilité des alcanes, des aromatiques et des mercaptans dans l'eau pure sera étudiée individuellement en considérant la présence de l'effet de solvatation, s'il existe. Ensuite, la solubilité des composants non réactifs est décrite par PR-CPA EoS en ajustant les BIP (k_{ij} et cross association paramètres) entre le soluté et l'alcanolamine à partir de données expérimentales ternaires. Le PR-CPA est ensuite validée en comparant différentes propriétés prédites thermodynamiques avec des données expérimentales qui ne sont pas utilisées dans l'ajustement des paramètres. Nous pouvons citer des propriétés telles que la solubilité d'un seul composant, la solubilité du mélange d'alcane, la composition de la phase vapeur, la température minimum de solubilité, la constante de loi de Henry apparente, etc.

4.1 **Alkanolamine-water Binary systems**

Alkanolamine-water binary systems have been studied with CPA EoS by Avlund et al. [69] [70]. According to their successful results, a constant value of k_{ij} is considered to represent alkanolamine-water binary systems. For each alkanolamine-water binary system, we have adjusted the corresponding k_{ij} and a Flash type objective function (Equation (4.1)) has been chosen.

$$f = 100 \times \sum_{i=1}^{n} \left(\left| x_1^{cal} - x_1^{\exp} \right| + \left| y_1^{cal} - y_1^{\exp} \right| \right)_i \qquad (3.1)$$

Where x_1 is the composition of alkanolamine in the liquid phase, y_1 is the composition of alkanolamine in the vapour phase.

Table 4-1 summarizes the adjusted k_{ij} and the references used in PR-CPA EoS for the VLE data treatment of alkanolamine-water systems. For MDEA-water and DEA-water binary systems, as usually, in the vapour phase, the concentration of alkanolamine is very low (order of magnitude of the amine mole fraction around 10^{-6}), only compositions of liquid phase are used to estimate k_{ij}. For MEA-water binary system, both compositions of liquid and vapour phases have been taken into account. From Figure 4-1 and Figure 4-2, it can be seen that PR-CPA EoS with temperature independent k_{ij} is able to accurately represent phase behaviour of alkanolamine-water systems.

Table 4-1. Average Absolute Deviation (AAD) for liquid and vapour composition between PR-CPA EoS adjusted data and experimental ones of water with MEA, DEA or MDEA binary system and k_{ij} values.

	T /K	AAD[a] $x_1 \times 100$	AAD[a] $y_1 \times 100$	k_{ij}	references[b]
MDEA-water	313-450	1.20	0.005	-0.190	[76], [77], [78], [79]
DEA-water	311-473	2.14	-	-0.114	[80], [81]
MEA-water	283-373	1.74	0.23	-0.142	[76], [82], [83]

[a] AAD = $1/NP \times \Sigma| \chi_i^{calc} - \chi_i^{exp}|$; [b] isotherm and isobar VLE data

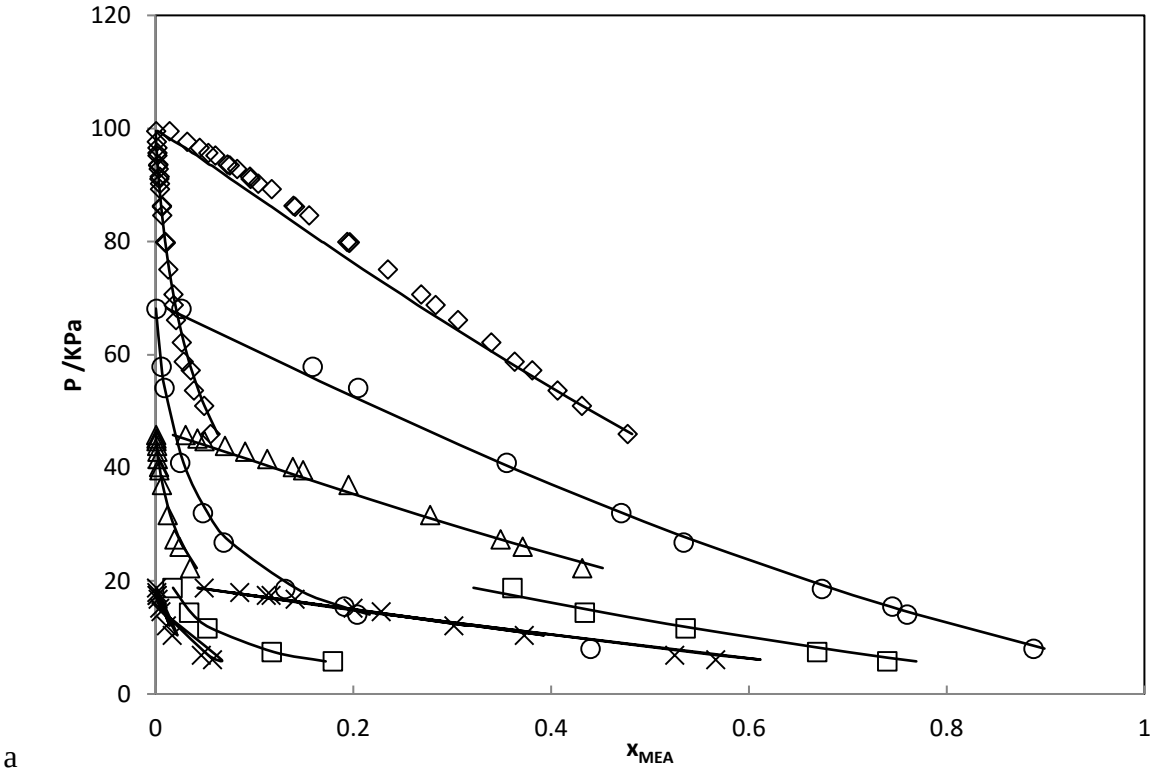

a

Figure 4-1. Comparison between experimental data (symbols) and adjusted ones using PR-CPA EoS (solid lines) for MEA-water binary system; (×) =333 K:Lenard et al. [32], (□)=343 K:Kim et al. [26], (△)=353 K :[26], (○)= 363 K:Tochigi et al. [33], (◇)=373 K [26].

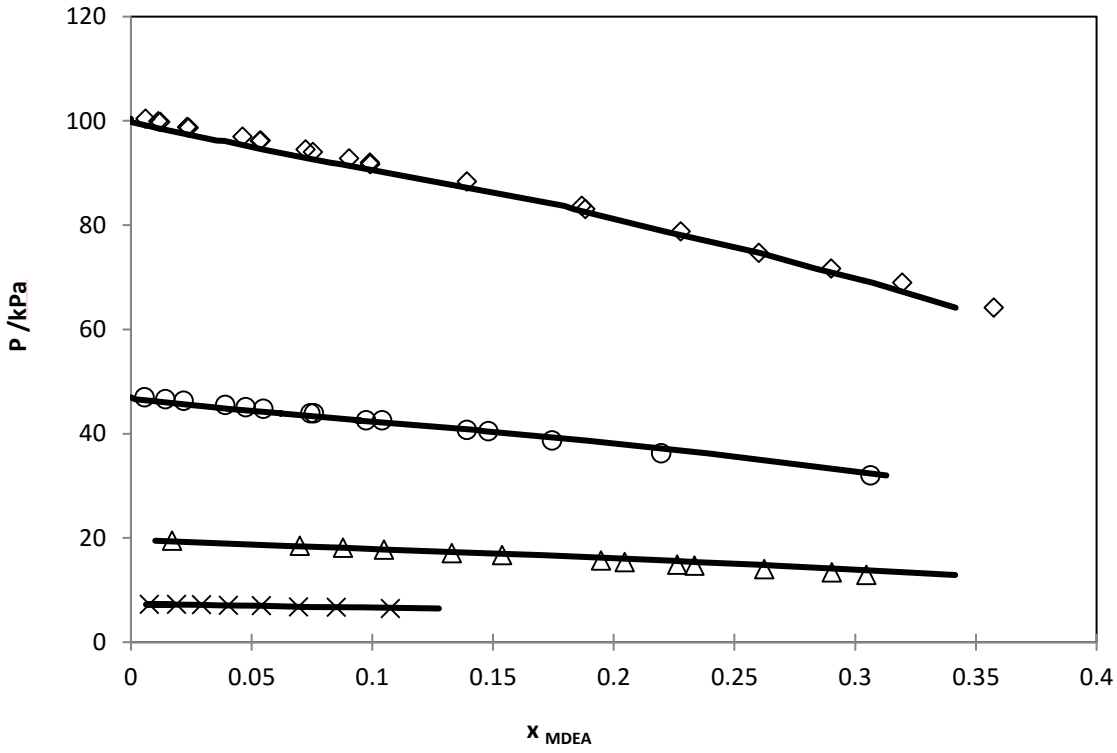

Figure 4-2. Comparison between experimental data (Kim et al. [26], symbols) and adjusted ones using PR-CPA EoS (solid lines) for MDEA-water binary system; (×)=313 K, (△)=333 K, (○)= 353 K, (◇)=373 K.

4.2 Alkane-water-alkanolamine ternary systems

To the best of our knowledge, alkane solubility in alkanolamine solution experimental data is only available in the form of alkane-water-alkanolamine ternary systems. Therefore, 3 BIPs listed in Table 4-2 are required to represent each alkane-water-alkanolamine ternary systems.

Table 4-2 List of BIPs required representing alkane-water-alkanolamine ternary systems.

	Alkanolamine	Water	Alkane
Alkanolamine	NA	Section 4.1	This section[a]
Water		NA	This section[b]
Alkane			NA

a: Fitted from alkane-water-alkanolamine ternary systems data

b: Fitted from alkane-water binary systems data

4.2.1 Alkane-water binary systems

As explained by Hajiw [84], we also consider a second order polynomial equation with temperature (Equation (4.2)) for the BIP to well describe the minimum solubility of alkane in aqueous solution.

.

$$k_{ij} = a + bT + cT^2 \qquad (3.2)$$

a ,*b* ,*c* were estimated by fitting from alkane solubility data, using a Flash type objective function (Equation (4.3)).

$$f_{(obj,hydrocarbon-water)} = 100 \times \sum_{i=1}^{n} \left(\left| \frac{x_1^{cal} - x_1^{\exp}}{x_1^{\exp}} \right| \right)_i \qquad (3.3)$$

Where x_1 is the solubility of hydrocarbon in water.

Table 4-3 summarizes the adjusted k_{ij} and the references used for the VLE data treatment of alkane-water binary systems. The ARD on alkane solubility in water is less than 12 %. Satisfactory results are obtained with our model compared to the ARD (less than 30%) obtained by Oliveira et al. [85] . We suspect that the reason of such deviation is due to their choice of using non temperature dependent k_{ij}.

Table 4-3 Comparison between alkane solubility data water with the calculated ones obtained with PR – CPA EoS and a,b and c parameters values

	T /K	ARD% x_1	a	$b\times10^3$ /K^{-1}	$c\times10^6$ /K^{-2}	References
methane-water	274-623	6	-1.597	8.398	-8.290	[86,87]
ethane-water	259-444	7	-1.517	8.198	-9.236	[88,89]
propane-water	247-422	9	--1.114	6.256	-7.370	[90,91]
n-butane-water	273-423	7	-0.751	4.074	-4.467	[92,93]
i-butane-water	278-363	10	0.198	-2.152	5.205	[94]
n-pentane-water[a]	273-477	12	-0.704	3.932	-4.749	[94–96]
n-hexane-water[a]	273-425	12	-1.026	5.438	-6.565	[95,97]

[a] LLE data were also considered

4.2.2 Alkane solubility in aqueous alkanolamine solution

Previously, we have shown that using regressed k_{ij} for alkanolamine-water and alkane-water binary systems give satisfactory results. To the best of our knowledge, there is no experimental VLE data concerning alkane-alkanolamine binary systems (only one set of data of Methane-MDEA binary system is available in the open literature [98]). Consequently, k_{ij} of alkane-alkanolamine have been fitted using experimental alkane solubility in aqueous alkanolamine solutions.

Both temperature independent and dependent k_{ij} (Equation(3.2)) have been fitted from experimental data by using the same objective function (Equation(3.3)) for treating alkane-water binary systems. In this case x_1 is alkane solubility in aqueous alkanolamine solutions. Results are summarized in Table 4-4. It can be seen that, the model with a temperature independent k_{ij} is able to describe the solubility of alkanes in different aqueous alkanolamine solutions with acceptable ARD (less than 31%). Such deviation can be explained by the choice of using non temperature dependent k_{ij}

Moreover, the model with a temperature dependent k_{ij} is generally able to well describe different alkane solubilities in different aqueous alkanolamine solutions in all range of alkanolamine concentration with ARD less than 10% (except 17% for hexane in aqueous MDEA). In fact,

hexane-aqueous MDEA system has been treated by using two sets of experimental data (Mourakoui et al. [99] and Alheseinat et al.[100]), the ARD% are 8.8% and 32.8%, respectively. Since Alheseinat et al.[100] mentioned that the uncertainty of their experimental data is more than 30%, we consider that this set of data is suspicious. In this work, temperature dependent k_{ij} has been chosen.

Figure 4-3 shows graphically the comparison between PR-CPA EoS and experimental data from Jou et al.[21] for propane solubility in 35 wt % aqueous MDEA solution. The ARD is 5.0% for all sets of experimental data at VLE and LLE conditions. The VLLE interface is correctly represented. Figure 4-4 represents propane solubility in aqueous DEA solution in function of DEA concentration , PR-CPA EoS is in good agreement with experimental data.

Table 4-4 Comparison between experimental data of alkane solubility in aqueous alkanolamine solutions and the adjusted ones obtained with PR-CPA EoS

						T independent k_{ij}			T dependent k_{ij}			
alkanes	alkanolamines	data type	alkanolamine wt %	T /K	P /MPa	kij	ARD%	a	$b\times10^3$ /K^{-1}	$c\times10^5$ /K^{-2}	ARD%	references
Methane	DEA	VLE	5-40	310-394	0.1-20	0.441	6.0	-3.334	21.802	-3.119	4.4	[101]
	MDEA	VLE	35-50	298-423	1-20	0.693	10.5	-0.626	8.506	-1.383	8.4	[98,102,103]
	MEA	VLE	5-40	298-394	0.1-13	0.276	8.4	-6.520	41.059	-6.130	6.5	[101,104]
Ethane	DEA	VLE,VLLE	5-40	283-403	0.1-13	0.305	5.1	-0.544	5.269	-0.810	5.1	[99,105]
	MDEA	VLE	25-50	283-398	0.1-13	0.327	11.2	2.181	-9.183	1.065	6	[102]
	MEA	VLE	5-40	298-398	0.1-12.6	0.194	7.2	-4.193	26.400	-3.935	5.1	[104,105]
Propane	DEA	VLE, VLLE	0-65	298-348	0.1-1.3	0.210	6.6	3.099	-18.490	2.948	5.3	[99,106]
	MDEA	VLE, LLE	25-50	273-423	0.1-19.6	0.351	21.5	0.738	-1.493	0.072	5	[106,107]
	MEA	LLE	0-100	313	1.72	0.113	11	0.113			11	[106]
Butane	DEA	VLLE	35	310-333	0.1-1.3	0.190	8.5	-1.982	12.957	-1.921	5.0	[108]
	MDEA	VLE, LLE	25-50	298-423	0.1-21	0.288	31	0.868	-2.349	0.161	6.2	[93,108]
i-butane	DEA	VLLE	35	310-333	0.1-1.3	0.124	4.5	-0.516	4.665	-0.837	0.3	[99]
	MDEA	VLLE	25-50	298-343	0.4-1.1	0.253	11.3	3.618	26.182	-4.422	8.6	[99]
pentane	DEA	VLLE	35	298-333	0.5	0.132	4.0	1.926	-11.678	1.897	1.3	[99]
	MDEA	VLLE	25-50	298-343	0.5	0.228	7.0	3.545	23.914	-3.789	6.3	[99]
hexane	DEA	VLLE	35	298-353	0.5	0.354	16.6	1.651	-8.393	1.087	7.4	[99]
	MDEA	VLLE	25-62	298-353	0.5	0.195	23.8	0.805	-2.476	0.155	17	[99,100]

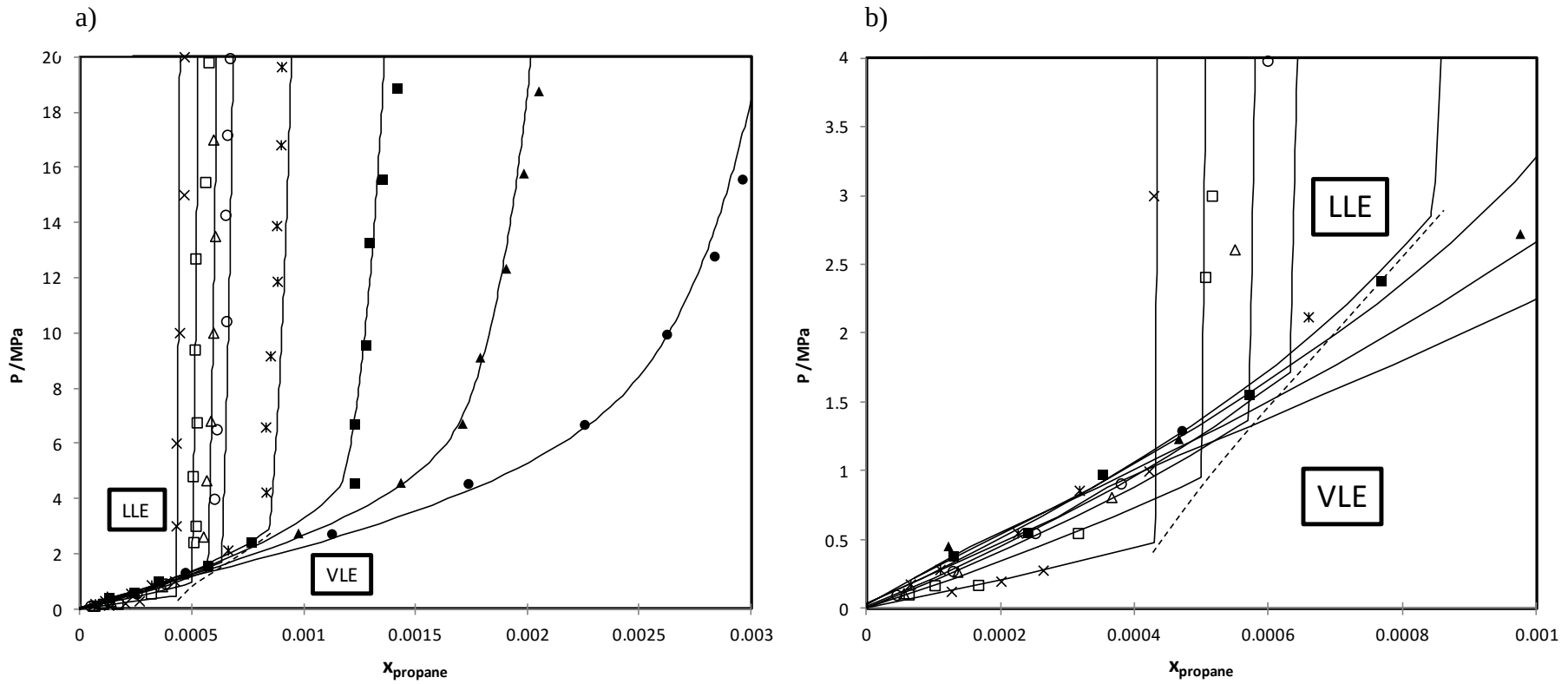

Figure 4-3. (b. is the zoom of a.) Comparison between experimental data from Jou et al. [21] for propane solubility in 35 wt % aqueous MDEA solution and adjusted data using PR-CPA EoS (solid lines). (×) =273 K, (□)=298 K, (△)=313 K (○)=323 K, (*)=348 K, (■)=398 K, (▲)=398 K, (●)=423 K, dashed line: VLLE interface.

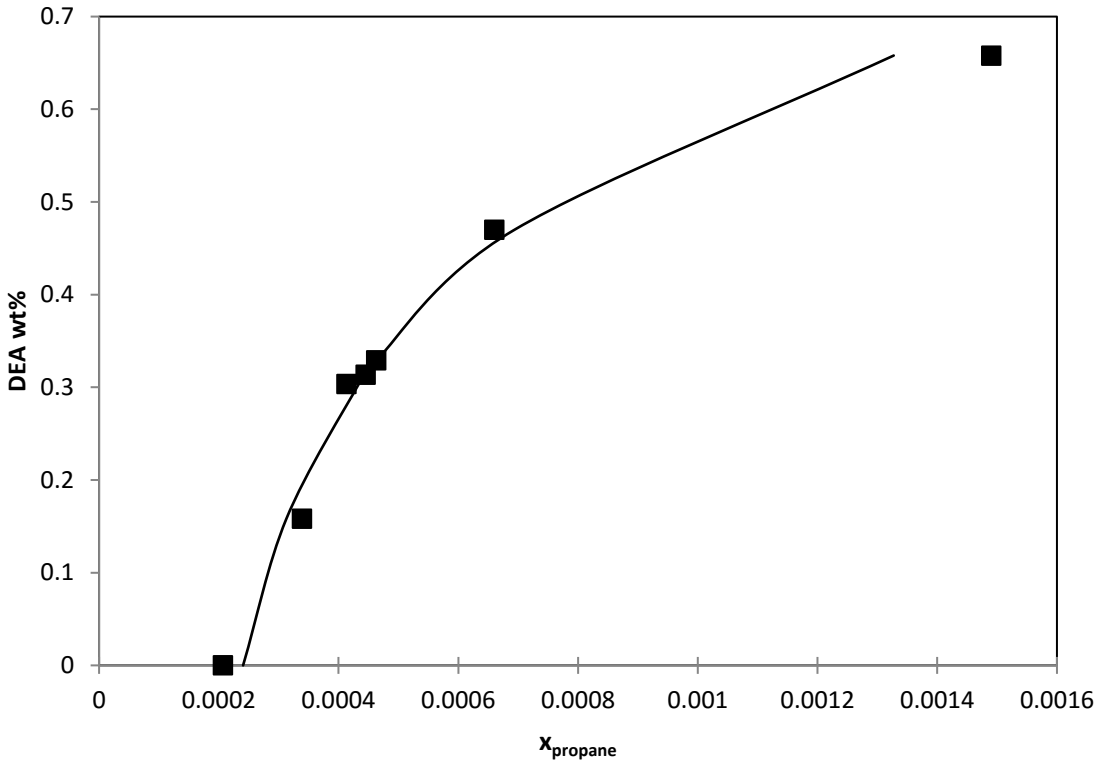

Figure 4-4 Propane solubility in function of DEA concentration (up to 65 wt %) at 313K, 1.724 MPa, symbol :experimental data from Jou et al.[54], solid line: calculated data using PR-CPA EoS

4.2.3 Temperature of minimum solubility of methane

Using our model for methane-water binary system at 5 MPa, we have predicted a temperature of minimum of solubility equals to 407 K. As shown in Figure 4-5, we have predicted the methane solubility as function of temperature (273-405 K) for 3 different aqueous MDEA solutions (25, 35 and 50 wt %) at 7.5 MPa (Since the solubility of methane do not have the same order of magnitude, their values are normalized). We observed that for each aqueous MDEA solution, it exists a temperature of minimum methane solubility. After, we also predict the temperature of minimum of solubility of methane in 3 MDEA aqueous solutions (25, 35 and 50 wt %) and pure water at 3 different pressures 5, 7.5 and 10 MPa, the result is summarized in Table 4-5. In fact, the temperature of methane minimum solubility is influenced by two factors: the concentration of alkanolamine and the pressure.

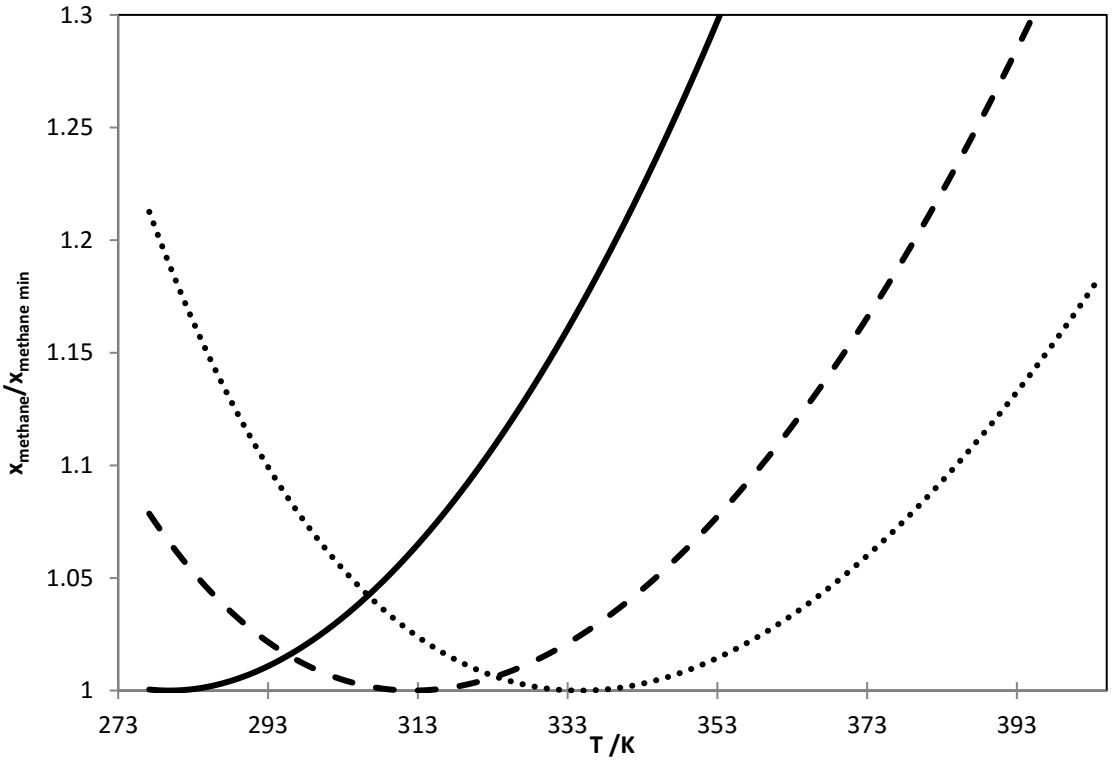

Figure 4-5 PR-CPA EoS prediction on the ratio of methane solubility and the minimum solubility at 75 bar. dotted line=25 wt % MDEA, dashed line=35 wt % MDEA, solid line=50 wt % MDEA

Table 4-5. Methane minimum solubility temperature in aqueous MDEA solution and in pure water predicted by PR-CPA EoS.

P /MPa	**T /K**			
5	407	340	317	286
7.5	402	335	312	280
10	395	330	306	277
wt % MDEA	0	25	35	50

As shown in Figure 4-6, the temperature of the minimum solubility decreases as the MDEA weight percent increases. It could be explained by the fact that the hydrogen bound between water is destroyed by introducing MDEA molecules. Less energy is needed to absorb the

same quantity of methane in a higher MDEA concentration solution. As seen in Figure 4-7, the temperature of methane minimum solubility decreases while the pressure increases. In fact, higher pressure makes methane more soluble. Consequently, lower temperature is required. The same approach can be applied to all alkanes.

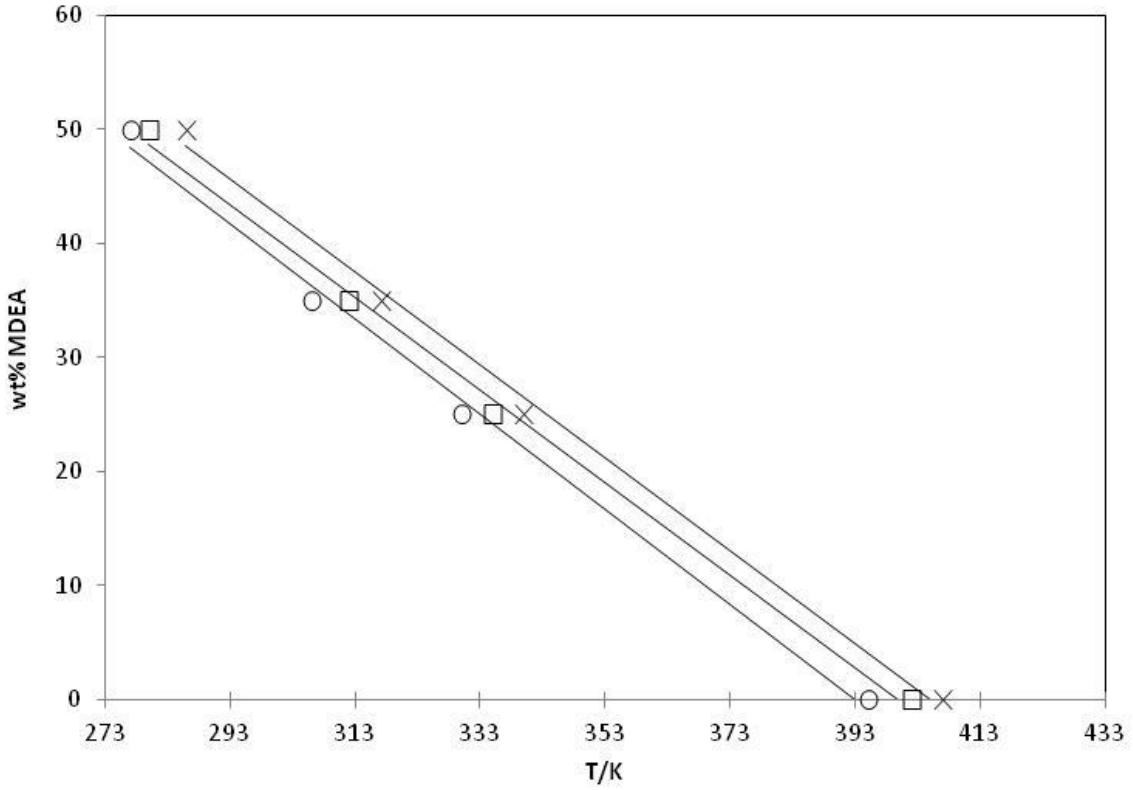

Figure 4-6 PR-CPA EoS prediction of the temperature of minimum solubility of methane as function of MDEA concentration at different pressure, symbols: PR-CPA EoS prediction, (×) =5 MPa, (□)=7.5 MPa, (○)=10 MPa, lines :linear correlation

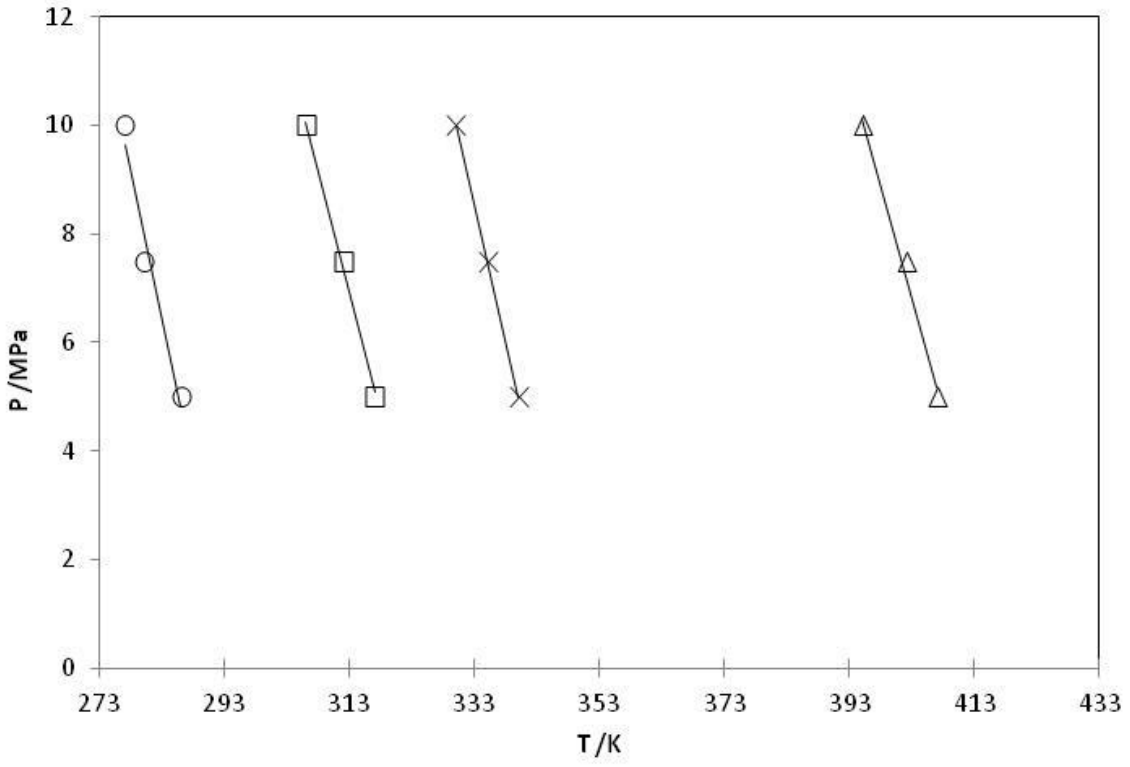

Figure 4-7. PR-CPA EoS prediction of the temperature of minimum solubility of methane as function of pressure in different aqueous MDEA solutions symbols: PR-CPA EoS prediction (□) =50 wt % MDEA, (×)=35 wt % MDEA, (○)=25 wt % MDEA and (Δ)=pure water, lines: linear correlation

4.2.4 Vapour phase prediction

The ability of the model to predict water content was also evaluated. As seen in Figure 4-8, at VLE condition, predicted water contents are in good agreement with the only experimental data found in the literature and measured by Carroll et al. [107] in 1992. The ARDs are less than 20%. However, the model fails to predict water content in LLE condition. After comparison with experimental data of Carroll et al. [107]. The ARDs are less than 124%. The biggest deviations are observed at low temperatures. It is not surprising that EoS fails to predict both VLE and LLE without modifying the mixing rules. We suggest as an alternative solution, to modify the expression of the co-volume *b*, by introducing a binary interaction parameter l_{ij}.

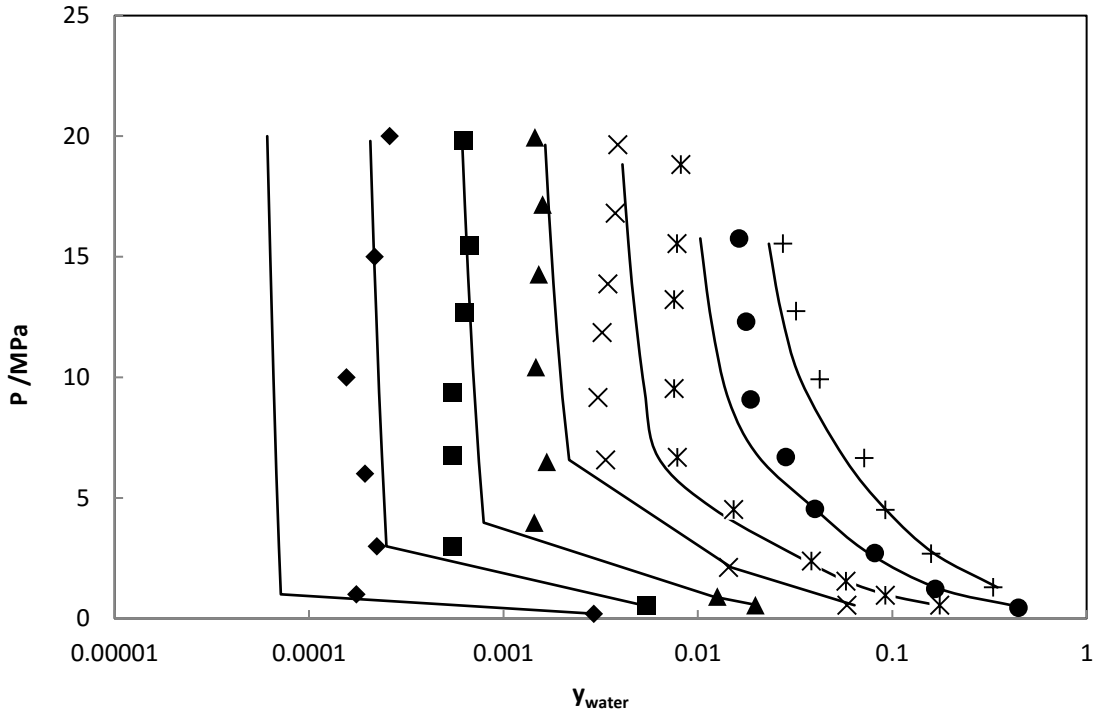

Figure 4-8 Comparison between experimental data from Caroll et al. [107] for water content in propane rich phase of propane-MDEA(35 wt %)-water ternary system and predicted data using PR-CPA EoS (solid lines). (◆) =273K, (■)=298K, (▲)=323K, (×)=348K, (*)=373K, (●)=398K, (+)=423K

MDEA content has been also measured by Carroll et al. [107], the content of MDEA corresponds to few ppm at low temperature. MDEA content is poorly predicted by our model. MDEA content is predicted 10-100 times lower than experimental data at LLE conditions. The only agreement between model and experimental data is at temperature above 373 K and pressure under 5MPa. Mokraoui et al. [99] did not manage to reproduce same work as Carroll et al. [107], for pentane solubility in aqueous MDEA solutions, the concentration of MDEA is less than 10 ppm in the liquid alkane rich phase. We conclude that more MDEA content data is needed for model validation.

We have also evaluated the model performance to predict the water content of this ternary system without k_{ij} for propane-water and propane-MDEA, the ARD on water content is 21% in VLE region. The water content value of propane-water-MDEA ternary system should be much closed to the one of propane-water binary system, as the concentration of MDEA is very low. Therefore, we have predicted the water content without BIP for propane-water

binary system, the ARD is 8.0% compared with the experimental data obtained by Kobayashi et al. [90] and Blanco et al. [109]. We conclude that the MDEA content data from Carroll et al. [107] are suspicious.

4.2.5 Alkane solubility prediction at VLLE conditions

The experimental VLLE data of ethane-MDEA-water, propane-MDEA-water, and n-butane-MDEA-water ternary systems have been used for model validation; they are compared with those predicted with PR-CPA EoS, see

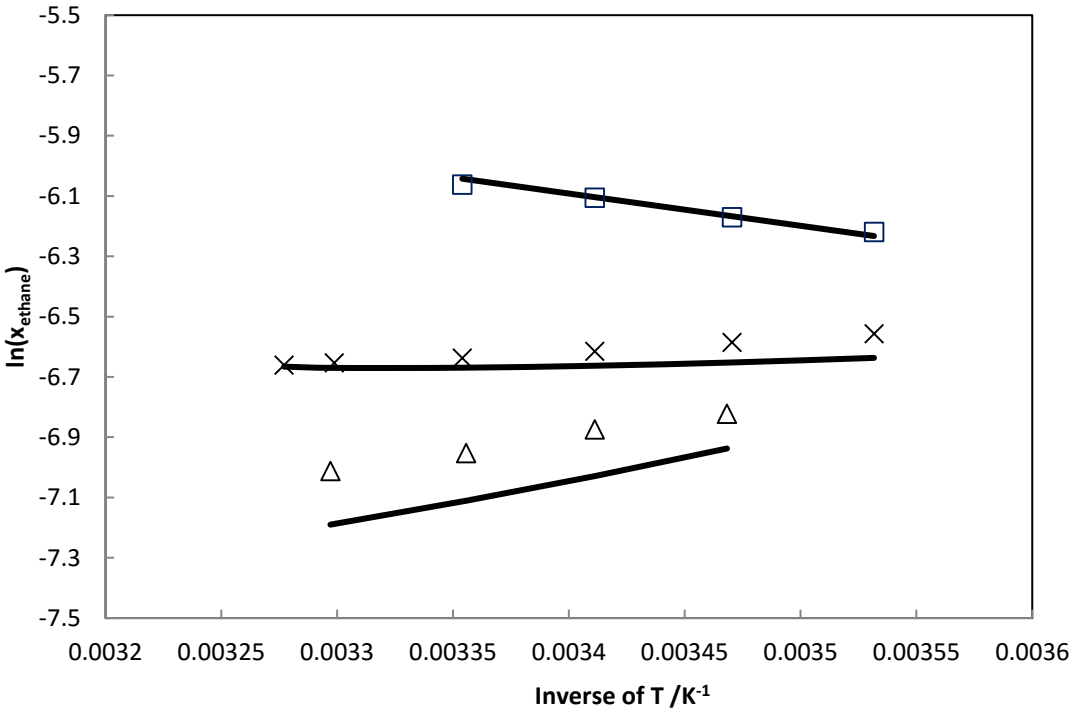

Figure 4-9, Figure 4-10 and Figure 4-11. For ethane-MDEA-water ternary system, the overall ARD for ethane solubility is less than 6% in MDEA with three concentrations (0, 25 and 50 wt %). The largest ARDs (14 %) are observed for ethane solubility in pure water. For propane-MDEA-water ternary system, the ARD for all concentrations of MDEA are less than 2 %. For n-butane-MDEA-water ternary system, PR-CPA EoS can accurately predict n-butane solubility in pure water, 25 wt % MDEA, 35 wt % MDEA and 50 wt % MDEA. The ARDs are less than 8 %.

Moreover, the slope of each curve represents the enthalpy of absorption of solute *i* (ΔH_i^{abs}) given by Equation (4.4)

$$\left(\frac{\partial ln x_i}{\partial \frac{1}{T}}\right)_P = -\frac{\Delta H_i^{abs}}{R} \qquad (3.4)$$

The absorption is endothermic, if the sign of the slope is negative, otherwise exothermic. For propane and n-butane, the absorption is always endothermic because once need energy to destroy the hydrogen bound between water–water, water-MDEA and MDEA-MDEA once alkanes molecules are introduced. However, for ethane, it seems that we have a particular behaviour since there is no tendency of the enthalpy of absorption (exothermic, athermic and endothermic for 0, 25 and 50 wt % MDEA respectively).

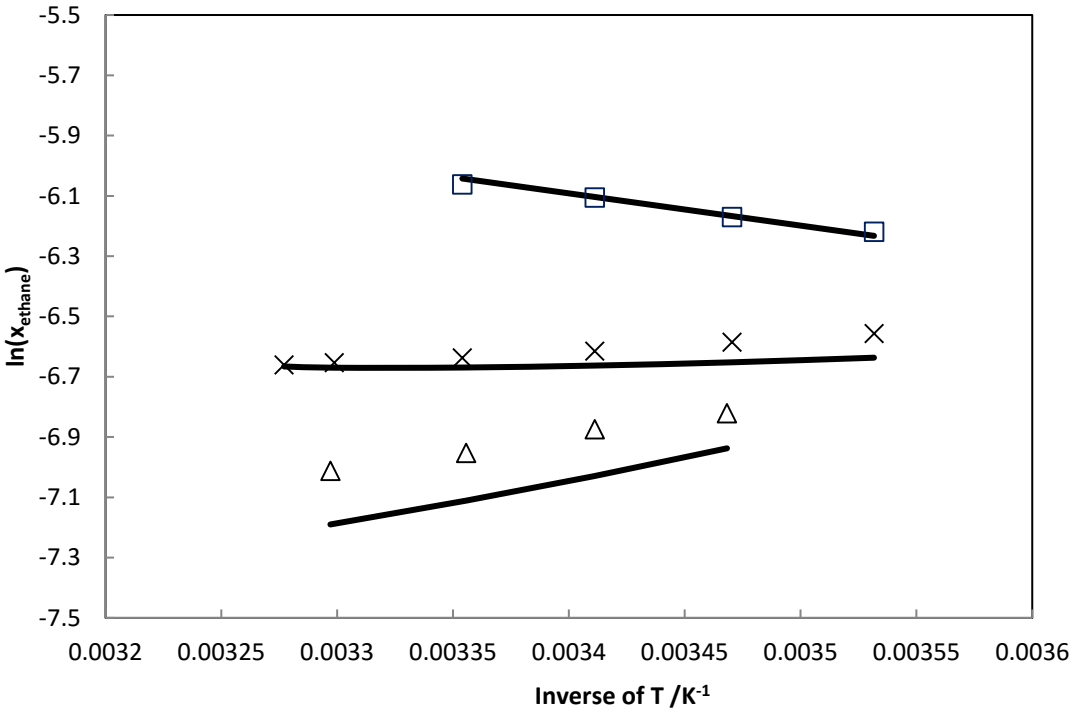

Figure 4-9. Comparison between experimental data from Mokraoui et al. [17] for solubility of ethane in aqueous MDEA solution and predicted data using PR-CPA EoS (solid lines). (Δ) =Pure water, (×)=25 wt % MDEA, (□)=50 wt % MDEA.

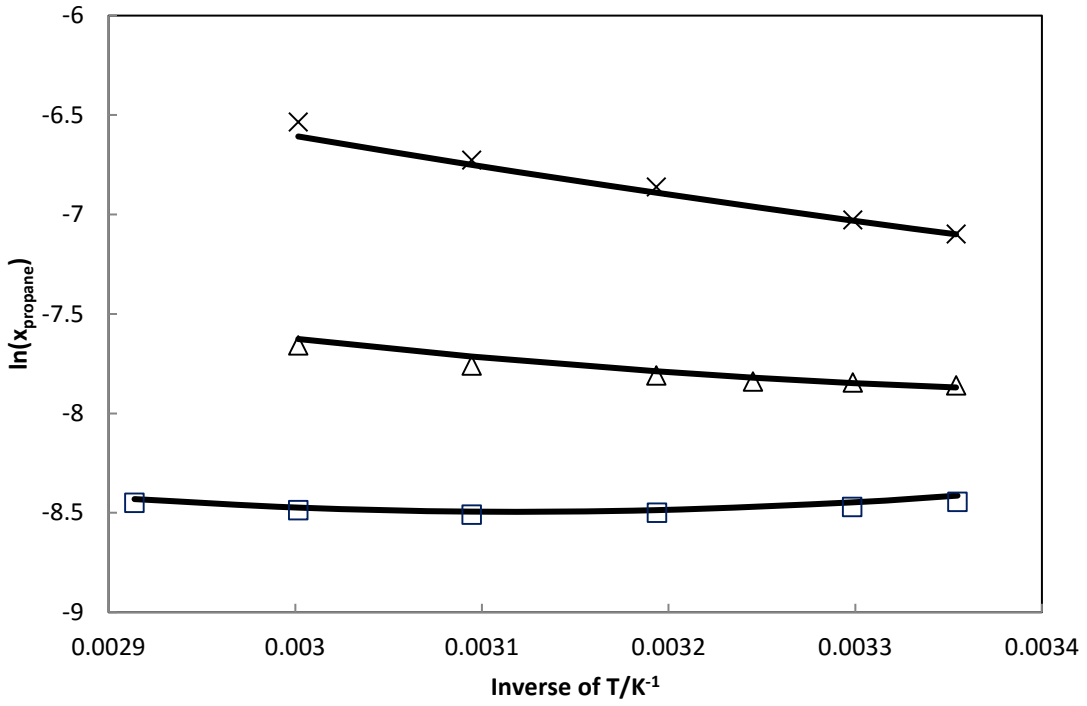

Figure 4-10. Comparison between experimental data from Mokraoui et al. [17] for solubility of propane in aqueous MDEA solution and predicted data using PR-CPA EoS (solid lines). (△) =Pure water, (×)=25 wt % MDEA, (□)=50 wt % MDEA.

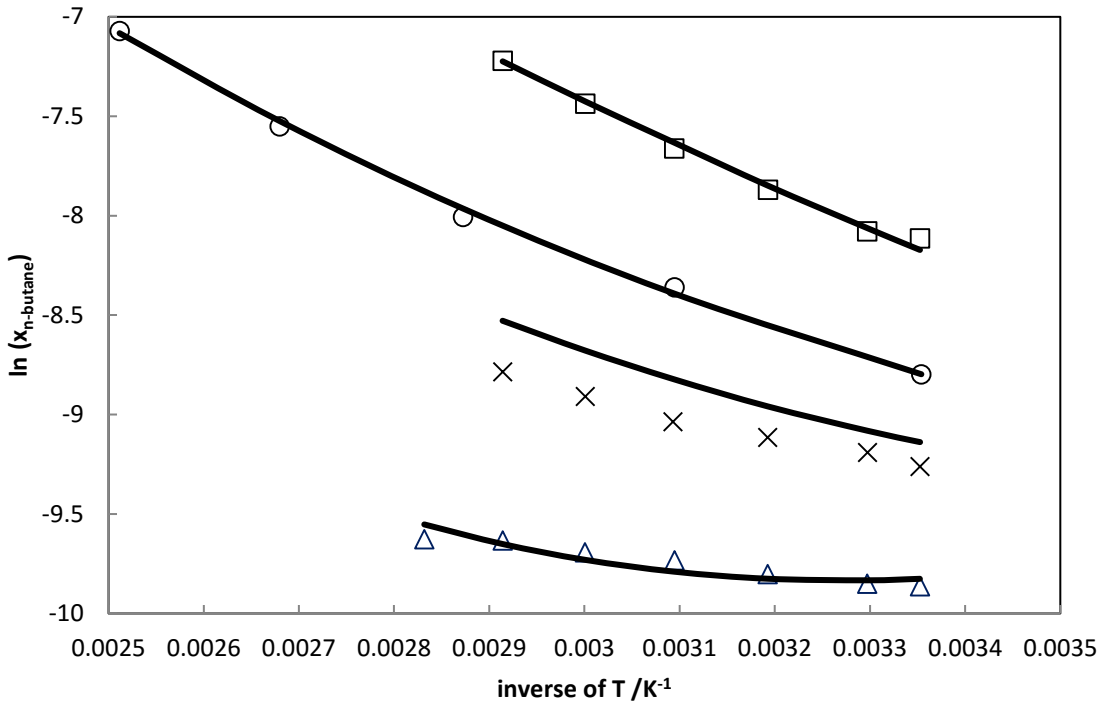

Figure 4-11. Comparison between experimental data from Mokraoui et al. [17], Jou et al. [44] for solubility of nbutane in aqueous MDEA solution and predicted data using PR-CPA EoS (solid lines). (△) =Pure water [17], (×) =25 wt % MDEA [17], (○)=35 wt % MDEA [44], (□)=50 wt % MDEA [17],.

4.2.6 Multi-component alkanes solubilities prediction in aqueous amine solutions

As another model validation test, we have used our model to predict multi-component alkanes solubilities in alkanolamine solutions. Few experimental data for hydrocarbon mixtures solubility in aqueous alkanolamine solutions are available. Mokraoui et al. [4] measured the solubility of two mixtures (MIX1 and MIX2, Table 4-6) in 35 wt % DEA, 25 and 50 wt % MDEA, within temperature range from 298 to 333K and pressure range from 0.6 to 4 MPa. The reported data concern VLE and VLLE conditions.

Table 4-6 Hydrocarbon mixture composition from Mokraoui et al. [99]

Alkanes	Mole Composition	
	MIX1	MIX2
C2	0.5	0.02
C3	0.3	0.5
n-C4	0.1	0.23
i-C4	0.02	0.1
C5	0.05	0.1
C6	0.03	0.05

As for non-associative molecules, the PR-CPA EoS is reduced to PR EoS, the BIP between alkanes is characterized by using constant k_{ij} taken from the work of Gao et al. [110].

From PR- CPA EoS prediction of hydrocarbon mixture solubility in aqueous alkanolamine solutions (Table 4-7), once can notice that the model has good predictability for the main compounds, i.e. ethane and propane for MIX1 and propane for MIX2. The ARDs are less than 30% for ethane and propane. Meanwhile, for C4 to C6, ARDs are much higher.

Table 4-7 PR- CPA EoS prediction of hydrocarbon mixture solubility in aqueous alkanolamine solutions

		T /K	P /MPa	ARD %	
				C2	C3
MIX1	50 wt% MDEA	298-333	0.6-4.2	22	13
	25 wt% MDEA	298-333	0.7-4.0	16	11
	35 wt% DEA	298-333	0.6-4.3	29	17
MIX2	50 wt% MDEA	298-333	0.5-1.3	-	30
	25 wt% MDEA	298-333	0.5-1.3	-	19
	35 wt% DEA	298-333	0.5-1.4	-	9

4.3 **Aromatic-water-alkanolamine ternary systems**

Aromatic solubility experimental data is only available in the form of aromatic-water-alkanolamine ternary systems. The only available alkanolamine-aromatic binary systems experimental data is the one for MEA-Benzene binary system [111]. Therefore, modelling of aromatic solubility in alkanolamine solution is treated using the same way for alkane solubility in alkanolamine solutions. 3 BIPs listed in Table 4-8 are required to represent each aromatic-water-alkanolamine ternary systems.

Table 4-8 List of BIPs required representing alkane-water-alkanolamine ternary systems.

	Alkanolamine	Water	aromatic
Alkanolamine	NA	Section 4.1	This section[a]
Water		NA	This section[b]
aromatic			NA

a: Fitted from aromatic-water-alkanolamine ternary systems data

b: Fitted from aromatic-water binary systems data

4.3.1 Aromatics-water binary systems

Aromatics are considered as not self-associating, but they are able to cross associate with water. 2B solvation scheme has been chosen for all aromatics. In this case, three BIPs are involved: cross association volume β^{AiBj} and cross association energy ε^{AiBj} and k_{ij} . As we explained in section **3.2.2.2.2**, the m-CR1 combining rules are applied. ε^{AiBj} is equals to the half of $\varepsilon^{AH2OBH2O}$, however, k_{ij} and β^{AiBj} are considered as adjustable parameters. The corresponding objective function is expressed as:

$$f = 100 \times \sum_{i=1}^{n} \left(\frac{\left| x_1^{cal} - x_1^{exp} \right|}{x_1^{exp}} + \frac{\left| y_1^{cal} - y_1^{exp} \right|}{y_1^{exp}} \right)_i \qquad (3.5)$$

Where x_1 is aromatic solubility in water, y_1 is water content in the aromatic rich phase. Again as alkane-water binary systems, Oliveira et al [85] proposed to use temperature independent binary interaction parameter k_{ij} to describe aromatic solubility in liquid water rich phase and water in liquid aromatic rich phase. However, with a constant k_{ij}, the minimum of aromatic solubility in water was failed. Hajiw et al. [65] studied aromatic solubility in pure water by using GC-PR-CPA EoS, they showed that a temperature dependent k_{ij} is needed to well describe the minimum solubility of aromatics in aqueous solution. This k_{ij} is the same as the one used for alkane-water binary systems, and expressed by Equation(3.2). In the open literature, mutual solubilities of aromatics and water in a broad range of temperature from 270 to 470 K at LLE condition. Few VLE experimental data is available with temperature > 550 K, which is far out of the acid gas treatment operation condition. Therefore, only LLE data are involved in parameter adjustment. The optimized parameters are summarized in Table 4-9.

Table 4-9 comparison between experimental data on aromatic solubility in water and adjusted data with PR-CPA EoS, β and a,b,c parameters values

Binary	ARD%		$\beta^{AwaterBaromatic}$	kij			Reference
	$x_{aromatic}$	x_{water}		a	$b\times10^3/K^{-1}$	$C\times10^6/K^{-2}$	
benzene-water	10	13	0.043	-0.369	2.092	-2.321	[112] [113]
ethylbenzene-water	3.1	4.7	0.062	-0.493	2.437	-2.773	[114,115]
toluene-water	19.1	18.1	0.015	-0.516	2.524	-3.026	[113,116]

Figure 4-12 shows the results of benzene solubility in the aqueous phase at LLE conditions, all data have been presented on the same figure whatever the pressure is. It can be seen that the solubility of benzene is well described by PR-CPA EoS in a wide range of temperature from 279 to 455 K. The temperature of minimum solubility is accurately represented by the model at 279 K. However, at high temperature (>400 K), the deviation is becoming larger and larger. The water content in the benzene rich phase is also well represented by PR-CPA EoS as shown in Figure 4-13. As for the solubility of benzene in water, the model has better performance at lower temperature (<400 K). It can be explained by the fact that the quantity of experimental data involved in parameter fitting is less available at high temperature than at low temperature.

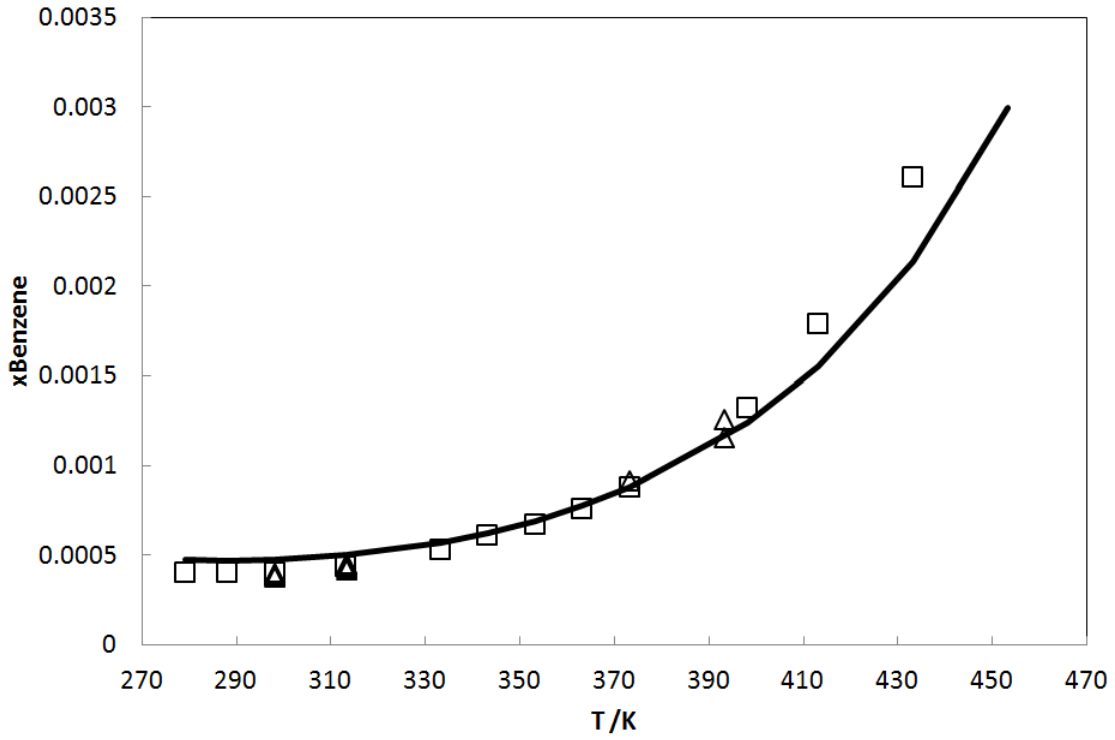

Figure 4-12 Comparison between experimental data (symbols) and adjusted ones using PR-CPA EoS (solid lines) for benzene solubility in water; (□): Jou et al. [113], (△) : Valtz et al.

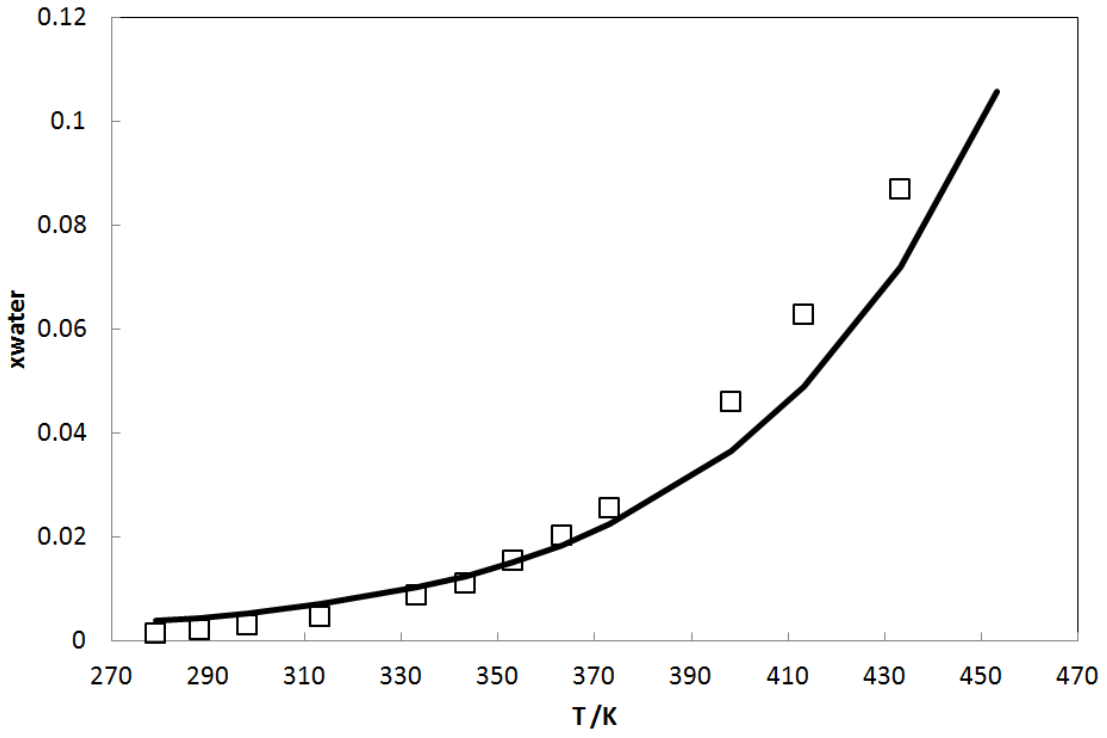

Figure 4-13 Comparison between experimental data (symbol) and adjusted ones using PR-CPA EoS (solid lines) for water solubility in benzene rich phase; (□): Jou et al. [113]

4.3.2 Aromatic solubility in aqueous alkanolamine solution

Previously, we have shown that regressed k_{ij} for alkanolamine-water and aromatic-water systems give satisfactory results. To represent phase behavior of aromatic-water-alkanolamine systems, k_{ij} and cross association volume $\beta^{AalkanolamineBaromatic}$ between aromatic and alkanolamine has been fitted from experimental aromatic solubility data in aqueous alkanolamine solutions. The corresponding objective function is the same as the one used for alkane-water-alkanolamine ternary systems, it is expressed by Equation (3.3). In this case, x_1 is aromatic solubility in aqueous alkanolamine solutions.

As aromatic-water binary systems, a k_{ij} of second order polynomial expression function of temperature for aromatic-alkanolamine is chosen for aromatic-alkanolamine binary systems (Equation(3.2)). Valtz et al.[112] have represented aromatic solubility data in different alkanolamine solutions at different pressures where the pressure was adjusted by methane. In their study, they have considered that aromatic solubility is not affected by dissolved methane in the liquid phase. However, Coquelet et al.[114], Valtz et al. [116] and Valtz et al.[117] have recalculated the real aromatic solubility data by taking into account the influence of methane. Consequently, these new aromatic solubility data are used in this work. Table 4-10 summarizes adjusted k_{ij} and model deviations. The PR-CPA EoS is able to describe with ARD<13%.

Figure 4-14 shows that PR-CPA EoS is able to predict benzene solubility in a wide range of temperature (298-398K). It is important to highlight that benzene solubility is calculated with the same parameters for all the three aqueous solutions (pure water, 25 and 50 wt% MDEA).

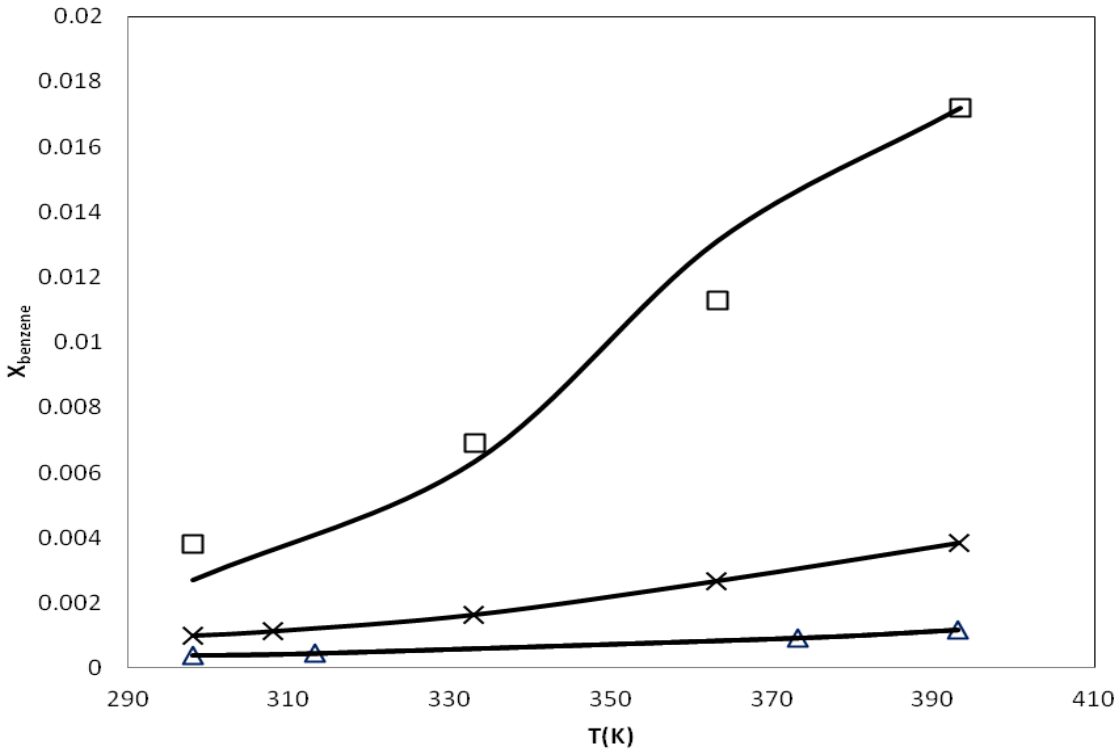

Figure 4-14 Solubility of benzene in aqueous MDEA solution at VLLE condition. Experimental data: Valtz et al.[117]. (△) Pure water; (×) 25 wt % MDEA; (□) 50 wt % MDEA. Solid lines: PR-CPA model prediction

Table 4-10 comparison experimental data of aromatic solubility in aqueous alkanolamine solutions with PR-CPA EoS

amine	aromatic	amine wt %	T/K	P /MPa	kij a	kij $b\times10^{3}/K^{-1}$	kij $c\times10^{6}/K^{-2}$	ARD%	$\beta^{AamineBaromatic}$	Reference
MEA	toluene	14.6	298-353	0.509-0.516	-0.389	3.789	-8.000	2	0.0507	[116]
DEA	toluene	35	298-353	0.5.9-0.533	-0.3878	3.550	-6.657	1	0.0628	[116]
	benzene	25/50	298-393	0.016-0.5.00	-0.071	2.113	-6.246	12	0.0269	[117]
MDEA	toluene	25/50	298-393	0.007-0.5.00	0.507	-1.700	0.900	11	0.0087	[116]
	ethylbenzene	50	333	0.5000	0.069	0.069			0.0530	[114]

4.4 Mercaptan-water-alkanolamine-methane quaternary systems

To the best of our knowledge, mercaptan solubility in alkanolamine solution experimental data is only available in the literature in the form of mercaptan-water-alkanolamine-methane quaternary systems. Therefore, 6 BIPs listed in Table 4-11 are required to represent each mercaptan-water-alkanolamine-methane quaternary systems.

Table 4-11 List of BIPs required representing mercaptan-water-alkanolamine-methane quaternary systems.

	Mercaptan	Alkanolamine	Water	Methane
Mercaptan	NA	this section[a]	this section[b]	this section[c]
Alkanolamine		NA	Section 4.1	Section 4.2
Water			NA	Section 4.2
Methane				NA

a: Fitted from mercaptan-water-alkanolamine-methane quaternary systems data

b: Fitted from mercaptan-water binary systems data

c: Fitted from mercaptan-methane binary systems data

All the BIPs concerning mercaptans with other components are adjusted from experimental data. The objective function used in this study is given by Equation (3.3). Where x_1 is the composition of mercaptans in the aqueous phase.

4.4.1 Mercaptan-methane binary systems

There is no solvation effect between methane and mercaptans, k_{ij} for methane-MM and methane-EM binary systems are adjusted from experimental data of Awan et al. [118]. Temperature independent k_{ij} are considered for these two systems, the value of k_{ij} and ARD are reported in Table 4-12.

Table 4-12: BIPs values and ARD of liquid (x) composition between PR-CPA EoS adjusted data and experimental ones obtained for methane (1) with MM or EM binary system.

	T /K	ARD x_1	k_{ij}	reference
methane-EM	272-313	3.2	0.0933	[118]
methane-MM	243-363	1.2	0.0898	[118]

The phase diagram of methane-EM binary system at 272 K is shown in Figure 4-15, it can be seen that the composition of EM calculated by the model is in good agreement with experimental data. Figure 4-16 shows the phase diagram of methane-MM binary system at 304

K, we can observe that MM liquid and vapour compositions are well described by PR-CPA EoS.

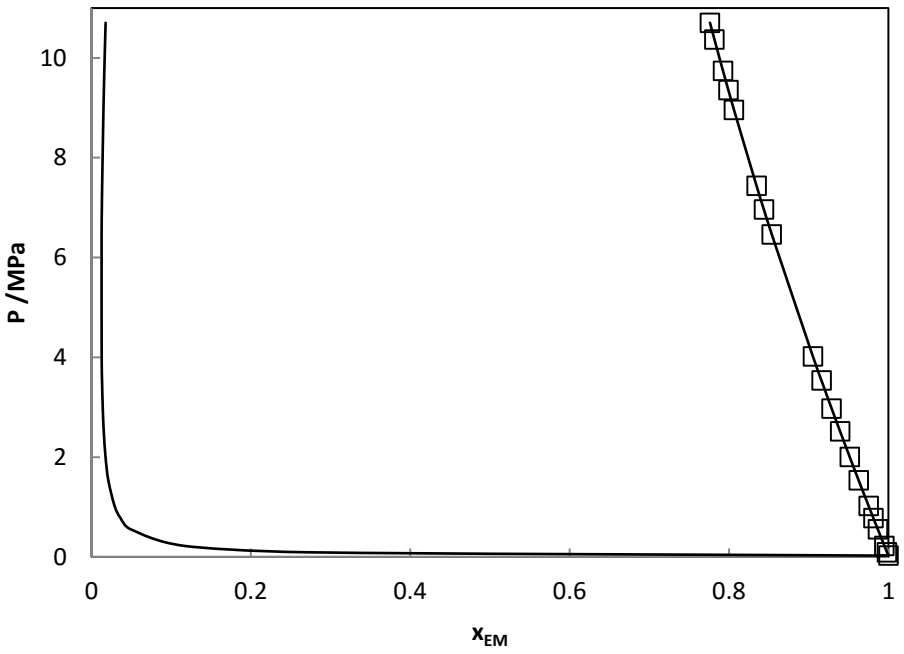

Figure 4-15 Phase diagram (P-x-y) of methane-EM binary system at 272K, symbol: experimental data [118], Lines: adjusted data obtained with PR-CPA EoS.

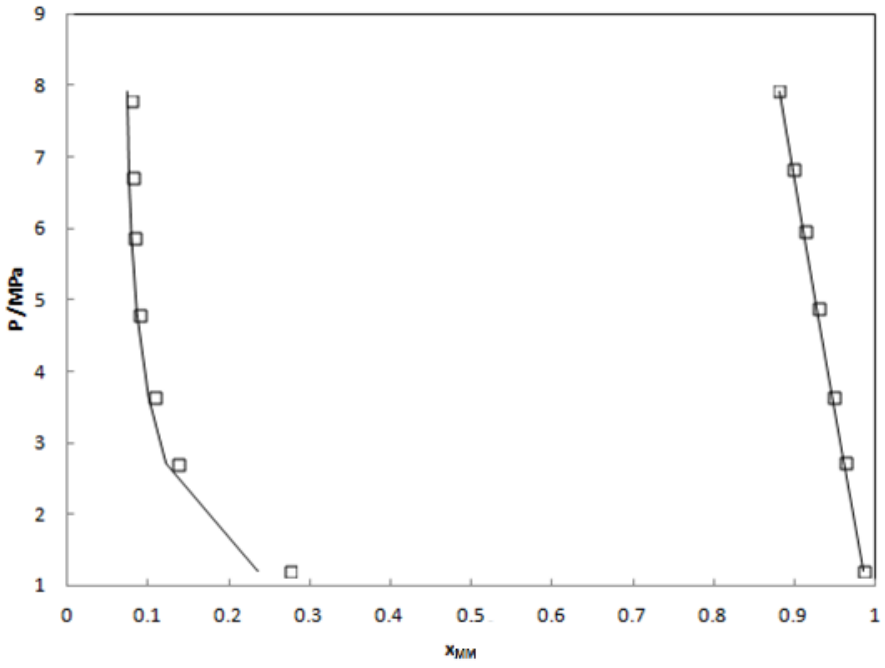

Figure 4-16 Phase diagram (P,x,y)of methane-MM binary system at 304K, symbol: experimental data [118], Lines: adjusted data obtained with PR-CPA EoS.

4.4.2 Mercaptan-water binary systems

Awan et al. [119] showed that it is better to consider the solvation effect between mercaptan and water. In this study, cross association energy between mercaptan and water is equal to the half of the value of water. We have adjusted the cross association volume and k_{ij} from experimental data. The results are shown in Table 4-13. Figure 4-17 shows the phase diagram of water-MM binary system at 470 K, the solubility of MM in water is well described by PR-CPA EoS, however, the composition of MM in the vapour phase at high pressure seems to be overestimated. Regarding the shape of the phase diagram, we may suspect a LLE at higher pressure. That may explain the overestimation of our model as parameters are adjusted from VLE data.

Table 4-13 : BIPs values and ARD of liquid (x) composition between PR-CPA EoS adjusted data and experimental ones obtained for water (1) with MM or EM binary system.

	T /K	ARD x_1	BIP	β^{AiBj}	ε^{AiBj} /bar.L.mol-1	reference
water-EM	310-588	2.3	0.02726	0.0627	83.275	[118,120]
water-MM	310-588	9	0.000365	0.0124	83.275	[120]

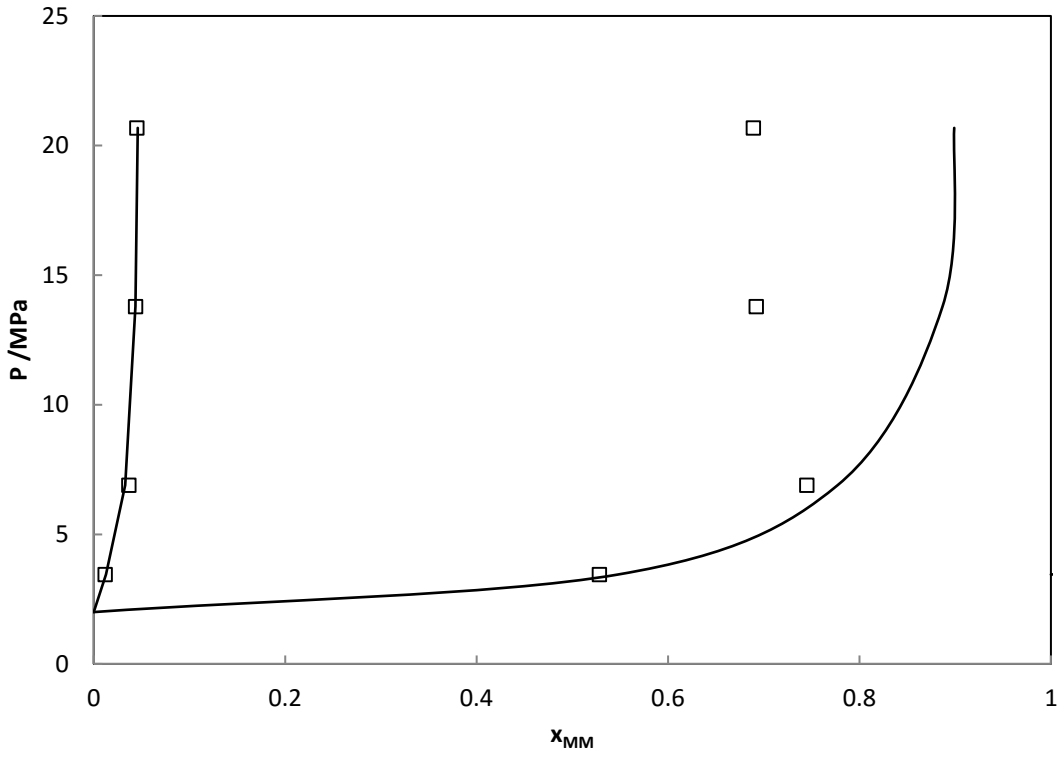

Figure 4-17 Phase diagram (P,x,y)of water-MM binary system at 470K, symbol: experimental data from Awan et al. [118], Lines: adjusted data obtained with PR-CPA EoS.

4.4.3 Mercaptan solubility in aqueous alkanolamine solution with pressure adjusted by methane

To the best of our knowledge, there are no available experimental data for mercaptan-alkanolamine binary systems, meaning that BIPs are not available also. Nevertheless, we fitted these parameters from experimental data of mercaptan–water-alkanolamine ternary systems. Because of the data is only available at two temperatures 313 and 343 K, it is difficult to consider the temperature dependence of k_{ij}. Therefore, a temperature independent k_{ij} has been chosen. On the other hand, solvation effect may exist between mercaptans and alkanolamines, however, due to the limited quantity of experimental data, it is more consistent to fit a single parameter k_{ij} instead of two parameters k_{ij} *and* β^{AiBj} at the same time. Moreover, compared with the quantity of water, the quantity of alkanolamine is minority, for example, for 25 wt% MDEA aqueous solution, the molar composition of MDEA is 0.048 against 0.952 on water. Therefore, we neglected the solvation effect between alkanolamines and mercaptans. The adjusted k_{ij} and ARD are shown in Table 4-14.

Table 4-14 k_{ij} values and ARD of liquid (x) composition between PR-CPA EoS adjusted data and experimental ones obtained for MM or EM with water-alkanolamine systems.

	T /K	ARD x_1	Amine concentration (wt%)	k_{ij}	reference
Water-MDEA-EM-methane	313 and 343	9	50	-0.0553	[121]
Water-MDEA-MM- methane	314 and 343	18	50	-0.047	[121]
Water-DEA-EM- methane	313 and 343	15	35	-0.075	[121]
Water-DEA-MM- methane	314 and 343	14	35	-0.098	[121]

From Figure 4-18 and Figure 4-19, we can see that EM or MM solubilities calculated by PR-CPA EoS are in good agreement with experimental data. Moreover, it is interesting to notice that methane solubilities and EM or MM vapour composition are also well described, the respective ARD are 5% and 15%.

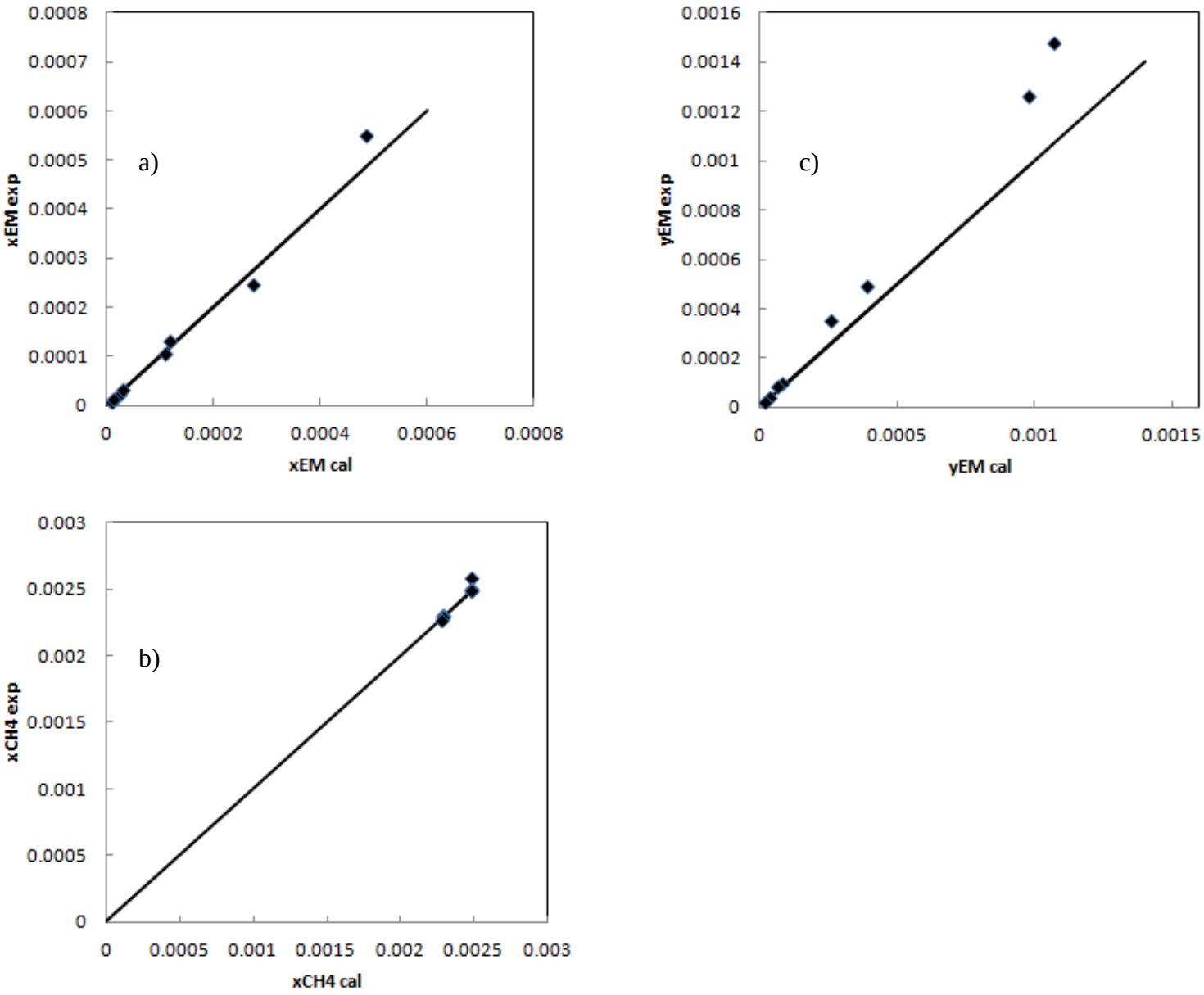

Figure 4-18 Comparison between experimental data from Jou et al. [121] and ones obtained with PR-CPA EoS for EM-water –MDEA system (50 wt% MDEA): a. EM solubility, b. Methane solubility and c. EM composition in vapour phase.

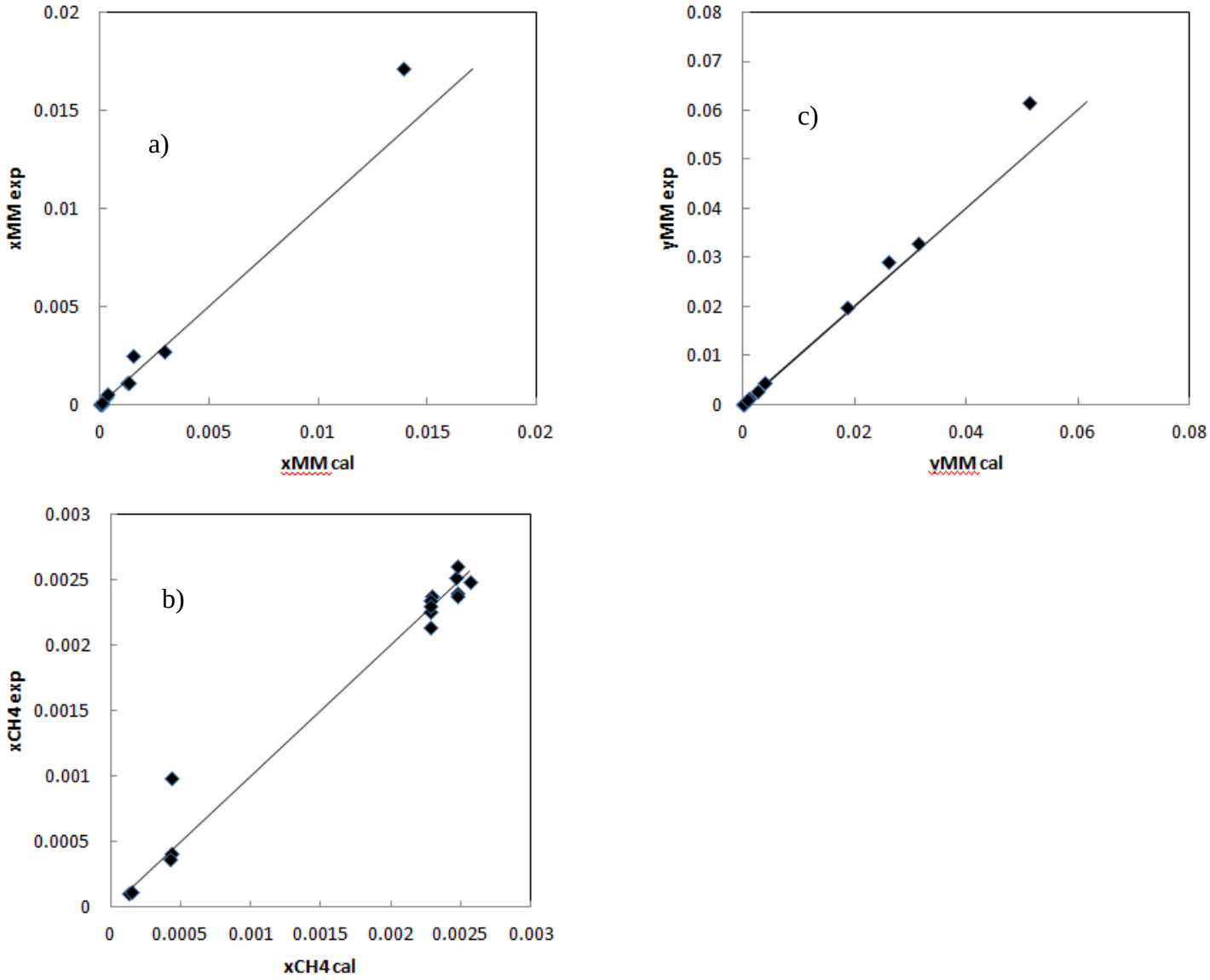

Figure 4-19 Comparison between experimental data from Jou et al. [121] and ones obtained with PR-CPA EoS for MM-water –MDEA system (50 wt% MDEA): a. MM solubility, b. Methane solubility and c. MM composition in vapour phase.

4.4.4 Model validation: comparison with our new experimental results

Apparent Henry's law constant of mercaptans in aqueous amine solutions is crucial for the choice of absorption solution, since it is directly linked to the solubility of mercaptan. The relation between apparent Henry's law constant (H_i), solubility (liquid composition x_i), pressure (P) and vapour phase composition (y_i) is given by Equation (4.6) :

$$H_i(T, P, x_i, y_i) = \frac{Py_i}{x_i} \qquad (3.6)$$

The experimental results obtained for EM-MDEA-water-methane and MM-MDEA-water-methane are shown in Chapter 2 We have predicted apparent Henry's law constant with PR-CPA EoS. For EM-MDEA-water-methane systems, as shown in Figure 4-20, the apparent Henry's constant in function of pressure, temperature and EM initial composition has been successfully predicted. When the temperature increase, EM is less soluble in the aqueous MDEA solution, because desorption is more appreciated at higher temperature. It is interesting to notice that, for every condition, EM becomes less soluble while pressure increases. Similar results have been found for MM-MDEA-water-methane, shown in Figure 4-21. We have also compared bubble point of EM and MM in 25 wt% MDEA, the ARD are 22% and 18% respectively.

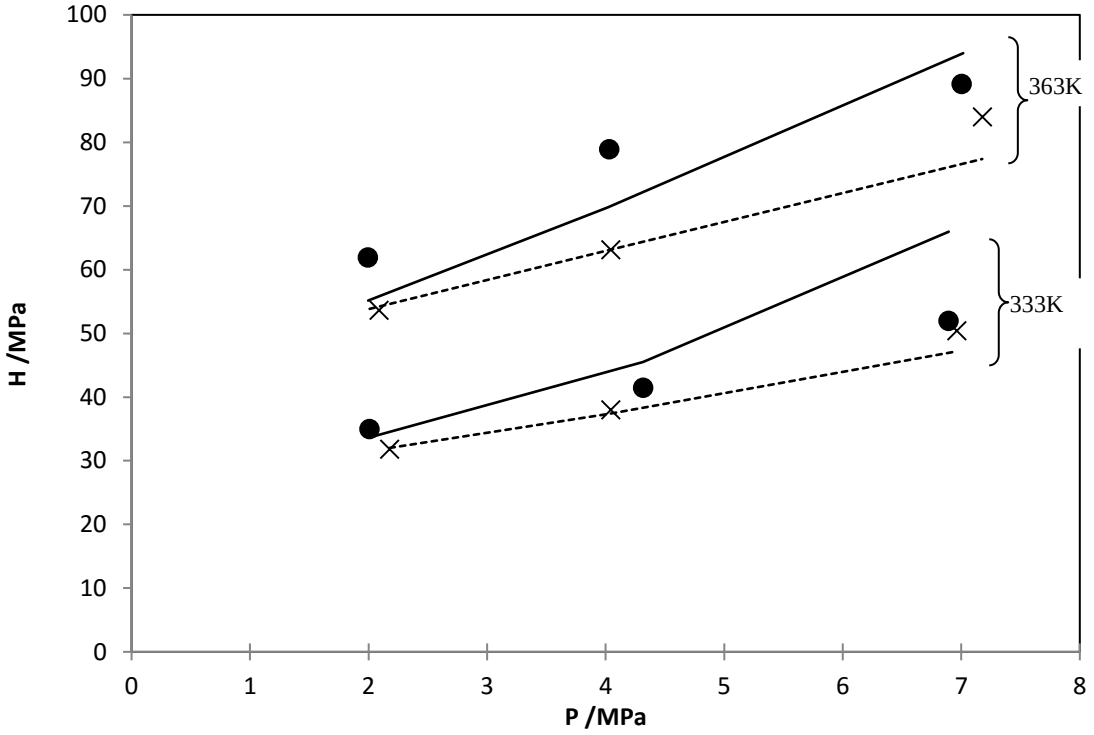

Figure 4-20 Henry's law constant in function of pressure for EM in aqueous MDEA solution. Symbols: experimental data this work (×) = 2000 ppm EM, (●) = 1000 ppm EM, Solid lines: model prediction for systems with 1000 ppm EM, dotted lines model prediction for systems with 2000 ppm EM.

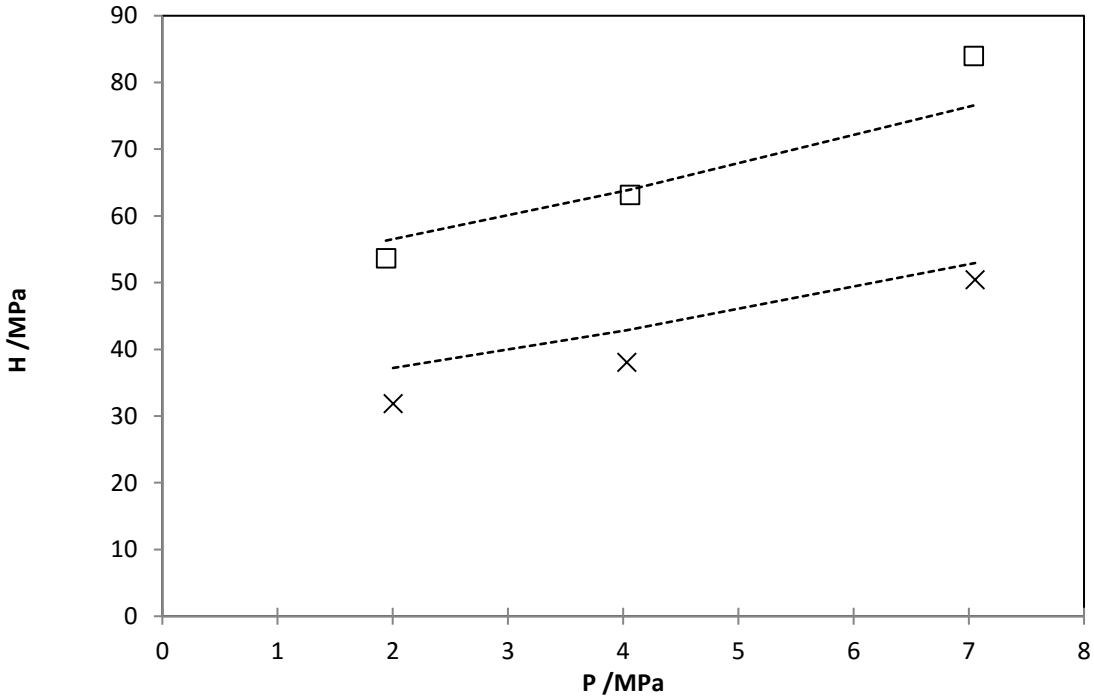

Figure 4-21 Henry's law constant in function of pressure for MM in aqueous MDEA solution. Symbols: experimental data obtained with 1 000 ppm of MM as initial composition in this work (×) = 333 K , (□) = 365 K . Dotted lines model prediction

Conclusion

Solubility of non-reactive components including: alkanes (methane, ethane, propane, n-butane, i-butane, n-propane and hexane), aromatics (benzene, toluene, and ethylbenzene), and mercaptans (MM, EM) in different aqueous alkanolamine solutions (MEA, DEA, and MDEA) will have been successfully represented by PR-CPA EoS within ARD of 18%, see following figure:

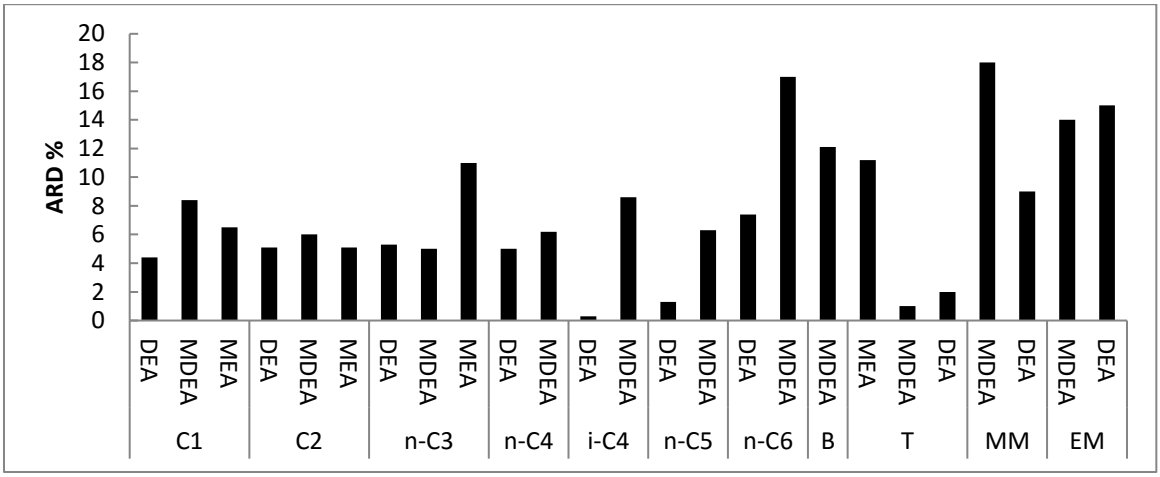

Figure 4-22 Deviations of hydrocarbon and mercaptan solubility in aqueous alkanolamine solution. C1=methane, C2=ethane, C3=propane, C4=butane, C5=pentane, C6=hexane, B=benzene, T=toluene, MM=methyl mercaptan, EM=ethyl mercaptan

Alkane mixture solubility, vapour phase composition, temperature minimum of solubility, and Henry's law constant for multicomponent systems have been accurately predicted by PR-CPA.

Chapter 5 Modelling of reactive systems

5 Modelling of reactive systems

Introduction

We have introduced the simplified approach with PR-CPA EoS to treat the chemical reactions between acid gases and alkanolamine in chapter 3. In this Chapter, firstly, we will choose the best configuration for representing the solubility of acid gas solubility in aqueous MDEA and MEA solution. CO_2-MDEA-water ternary system is assigned to be the example system to investigate the choice of association scheme (symmetric or asymmetric) for MDEA, the influence of k_{ij} between CO_2-MDEA, and the influence of solvation effects between water-CO_2. For model validation, different thermodynamic properties such as VLE, liquid phase speciation, enthalpy of absorption, and vapour phase composition will be predicted by PR-CPA EoS and compared with experimental data. Moreover PR-CPA EoS performance will be compared to Deshmukh–Mather model. The PR-CPA EoS will be applied on H_2S-MDEA-H_2O, CO_2-MEA-H_2O, and H_2S-MEA-H_2O ternary systems. And different multicomponent systems such as CO_2-H_2S-H_2O-CH_4, CO_2-H_2S-MEA-H_2O, CO_2-H_2S-MDEA-H_2O, CO_2-MDEA-H_2O-CH_4 CO_2-MDEA-H_2O-CH_4-EM systems will be predicted by PR-CPA EoS and compared to experimental data to validate the model.

Nous avons introduit l'approche simplifiée avec PR-CPA EoS pour traiter les réactions chimiques entre les gaz acides et l'alcanolamine dans le chapitre 3. Dans ce chapitre, nous allons d'abord choisir la meilleure configuration pour représenter la solubilité des gaz acides dans les solutions aqueuses de MDEA et MEA. Le système ternaire CO2-MDEA-eau est assigné comme système d'exemple pour étudier le choix du schéma d'association (symétrique ou asymétrique) pour MDEA, l'influence de k_{ij} entre CO2-MDEA et l'influence des effets de solvatation entre l'eau et le CO_2. Pour la validation du modèle, différentes propriétés thermodynamiques telles que la VLE, la spéciation en phase liquide, l'enthalpie d'absorption et la composition en phase vapeur seront prédites par PR-CPA EoS et comparées aux données expérimentales. De plus, les performances de PR-CPA EoS seront comparées au modèle Deshmukh-Mather. Le PR-CPA sera appliqué sur les systèmes ternaires H_2S-MDEA-H_2O, CO_2-MEA-H_2O, and H_2S-MEA-H_2O. Et différents systèmes multicomposants tels que les systèmes CO_2-H_2S-H_2O-CH_4, CO_2-H_2S-MEA-H_2O, CO_2-H_2S-MDEA-H_2O, CO_2-MDEA-H_2O-CH_4 CO_2-MDEA-H_2O-CH_4-EM seront prédits par PR-CPA EoS et comparé aux données expérimentales pour valider le modèle.

.Modeling of CO_2-MDEA-water ternary system

5.1.1 CO_2-water Binary system

Before investigating the solubility of CO_2 in aqueous alkanolamine solution, the solubility of CO_2 in pure water is studied by using PR-CPA EoS. Rodriguez et al.[122] have neglected the solvation effects between CO_2 and water with SAFT-VR EoS when they treat CO_2 solubility in different alkanolamine solutions. However, according to Tsivintzelis et al.[75], the solvation effect between CO_2 and water is important to be considered to represent CO_2 - water binary systems. To understand the influence of solvation effect, BIPs has been fitted both with and without solvation:

- Without solvation: As the same case of alkane solubility in water, we also consider a second order polynomial equation with temperature (Eq .5.1) for the k_{ij} to describe the solubility of CO_2 in water.
- With solvation: k_{ij} is still adjustable, two cross association parameters (ε^{AiBj} and β^{AiBj}) are involved. According to mCR-1 combining rule, the value of ε^{AiBj} is assumed as non adjustable; it takes the value from experimental data [75]. β^{AiBj} is a adjustable parameter.

All parameters were estimated by fitting CO_2 solubility data and using a Flash type objective function expressed by following equation:

$$f = 100 \times \sum_{i=1}^{n} \left(\frac{\left| x_1^{cal} - x_1^{exp} \right|}{x_1^{exp}} \right)_i \qquad (4.1)$$

Table 5-1 summarizes the adjusted parameters and ARD for the VLE data treatment of CO_2-water binary systems. Both with and without solvation between CO_2 and water can well represent CO_2-water binary systems. Figure 5-1 shows graphically the comparison between model adjustment and experimental data from Valtz et al. [123].

Table 5-1 BIP values and ARD of liquid (x) compositions between PR-CPA EoS adjustment and experimental data for CO_2-water binary system.

			k_{ij}				
	T /K	ARD x_{CO2}	a	b×10^3 /K^{-1}	c×10^6 /K^{-2}	β^{AiBj}	reference
CO_2-water Without solvation	278-479	6.2	-0.768	4.1492	-5.1396	NA	[123–125]
CO_2-water With solvation	278-479	5.4	0.0052	0.397	NA	0.0136	

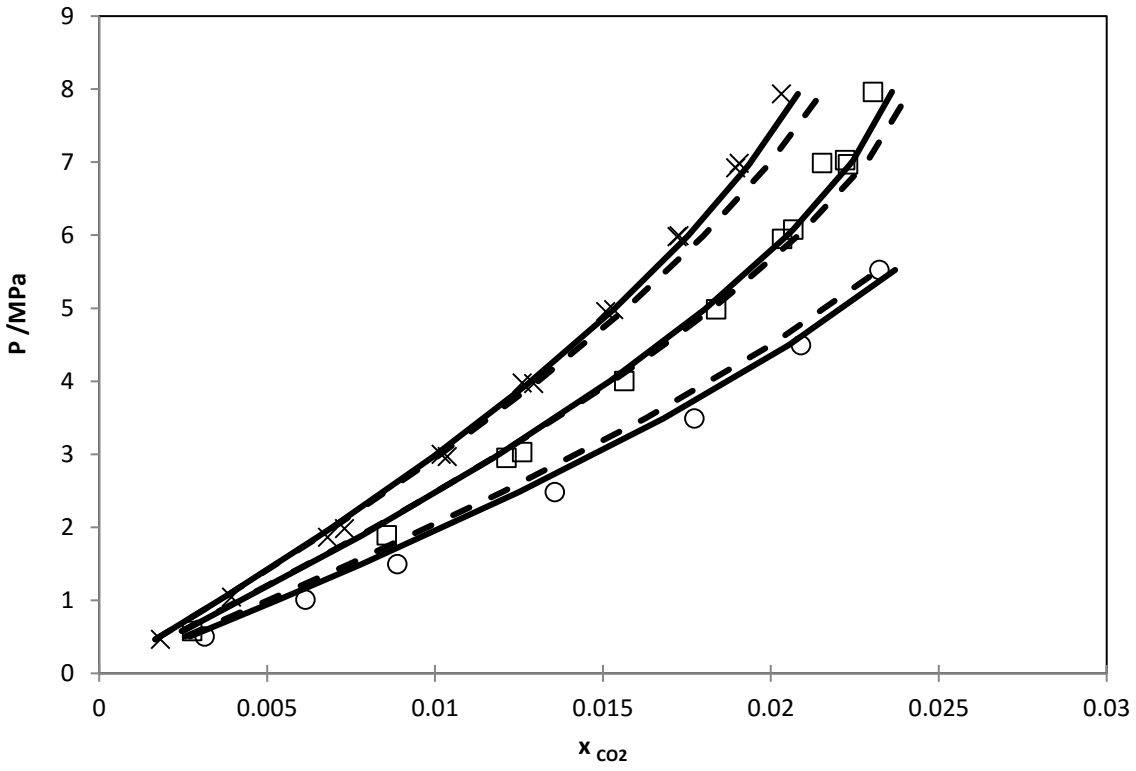

Figure 5-1 Comparison of experimental CO_2 solubility in water and adjusted values by PR-CPA EoS, solid line: without solvation, dotted lines: with solvation. symbol: experimental data from Valtz et al. [123] ; (○)=298 K , (□)=308 K (*)=318 K,

5.1.2 The choice of model parameters for CO_2-MDEA-water ternary system

In order to have the best model performance to represent acid gas solubility in alkanolamine solution, different model configurations including the association scheme of MDEA, the influence of k_{ij} between CO_2-MDEA and the solvation effect between CO_2-water will be discussed in this section. All BIP used in parameter fitting are summarized in Table 5-2. The experimental data used in this section is the ones used by Rodriguez et al.[122].

Table 5-2 PR-CPA binary parameters for CO_2-MDEA-water ternary system

Binary	k_{ij}[a]			β^{AiBj}	ε^{AiBj} /bar.L.mol-1
	a	b×10^3 /K^{-1}	c×10^6 /K^{-2}		
water-MDEA	-0.190			NA	NA
CO2-water(with solvation)	0.0052	0.397		0.0136	86.3
CO_2-water(without solvation)	-0.768	4.1492	-5.1396	NA	NA
CO_2-MDEA symmetric	*	*	*	*	*
CO_2-MDEA asymmetric	*	*	*	*	*

a: $k_{ij} = a + b \cdot T + c \cdot T^2$

*: Parameters to be estimated

The objective function is used and given by following equation.

$$f = 100 \times \sum_{i=1}^{n} \left(\frac{\left| P^{cal} - P^{exp} \right|}{P^{exp}} \right)_i \qquad (4.2)$$

Where P is the total pressure of CO_2-MDEA-H_2O ternary systems.

5.1.2.1 The association scheme of MDEA

In this study we used two different approaches (explained in chapter 3) to represent MDEA. There are two adjustable parameters β^{AiBj} and ε^{AiBj} to represent the "cross association" between CO_2 and MDEA, the k_{ij} between CO_2-MDEA is set to zero for both approaches. The results are shown in Table 5-3. In this step, the solvation effect between water-CO_2 has not been considered for either approach, i.e. the physical e site on CO_2 is not active.

Table 5-3 Comparison of symmetric and asymmetric approach for CO_2-MDEA binary system with PR-CPA EoS.

	T /K	wt % MDEA	ARD %	β^{AiBj}	ε^{AiBj} /bar.L.mol^{-1}
CO_2-MDEA symmetric	313-413	19 and 32	49	0.01256	205.85
CO_2-MDEA Asymmetric	313-413	19 and 32	32	0.00695	356.51

Figure 5-2 shows the comparison of experimental CO_2 solubility in MDEA-water solution with 32% MDEA and adjusted ones with two different approaches. It can be noticed that the symmetric approach fails to represent the total pressure of CO_2-MDEA-water systems. Nevertheless, the same systems can be correctly represented by using the asymmetric approach. At lower temperature the model fits well the tendency of experimental data, but at higher temperature, the deviation is larger. The same behavior has also been found by Dowell et al. [40], where they compared the symmetric approach with asymmetric approach for MEA at 313 K. Therefore, the asymmetric approach is chosen for the following studies.

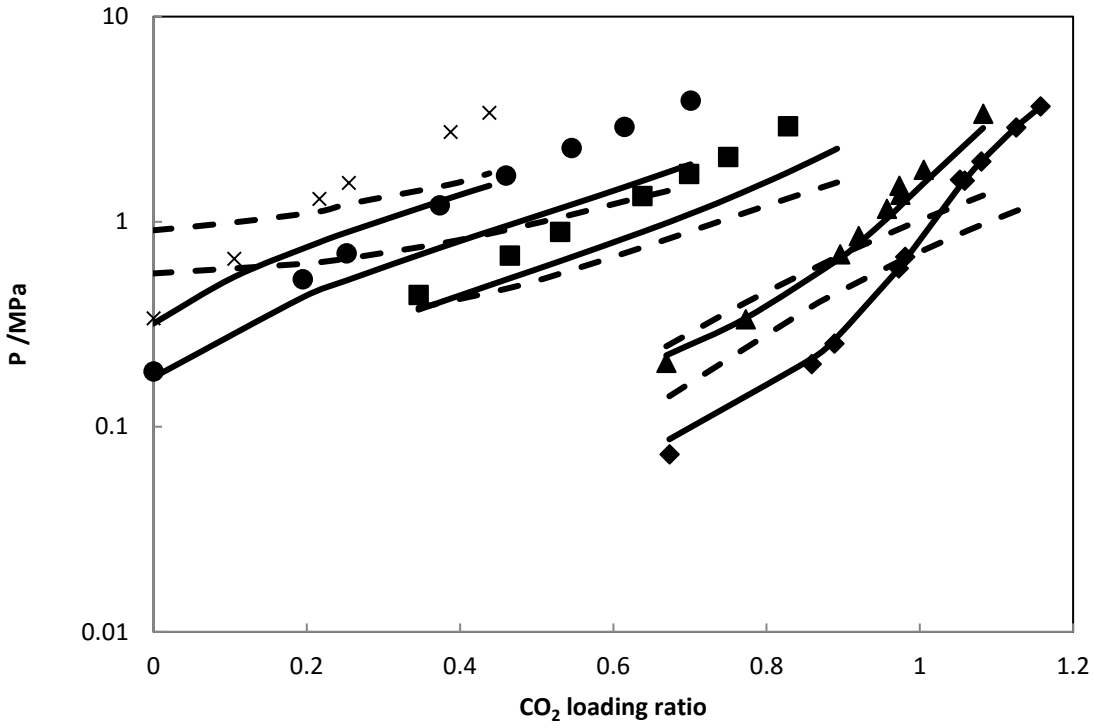

Figure 5-2 Comparison of total pressure of CO_2-MDEA-water ternary system with 32 wt% MDEA and adjusted values obtained with PR-CPA EoS. Solid lines: with asymmetric approach, Dotted Lines: with symmetric approach. Symbols: experimental data from Kuranov et al. [126]**. (◆)=313 K, (▲)=333 K, (■)=373 K,(●)=393 K，(×)=413 K**

5.1.2.2 k_{ij} between CO_2-MDEA

In previous section, we demonstrated that the asymmetric association scheme for MDEA is significantly better than the symmetric one. However, there are still large deviations especially at higher temperatures. According to Rodriguez et al.[122], k_{ij} between CO_2 and MDEA could be also an adjustable parameter to represent the physical interaction between CO_2 and MDEA. However, for MDEA-CO_2 binary system, we consider the k_{ij} between MDEA-CO_2 is adjustable in this section. Therefore, we have 5 parameters to adjust: a, b, c, β^{AiBj} and ε^{AiBj}. The ARD and optimized parameter are summarized in Table 5-4 . The solvation effect between CO_2 and water is still not considered.

Table 5-4 Influence of k_{ij} on the asymmetric approach

	k_{ij}						
	T /K	ARD %	a	b×10^3 /K^{-1}	c×10^6 /K^{-2}	β^{AiBj}	ε^{AiBj} /bar.L.mol^{-1}
CO_2-MDEA With $k_{ij}=0$	313-413	32	0	0	0	0.00695	356.51
CO_2-MDEA With temperature dependent k_{ij}	313-413	14	6.94	40.9	6.46	0.00493	326.52

Figure 5-3 shows the influence of k_{ij} between CO_2-MDEA on total pressure of CO_2-MDEA-water systems. Using a temperature dependent kij gives a significant improvement at higher temperature. The ARD is 14 % for a temperature range of 313-413 K, and MDEA concentration between 19 and 32 wt %. As a consequence, temperature dependent k_{ij} is considered for subsequent studies.

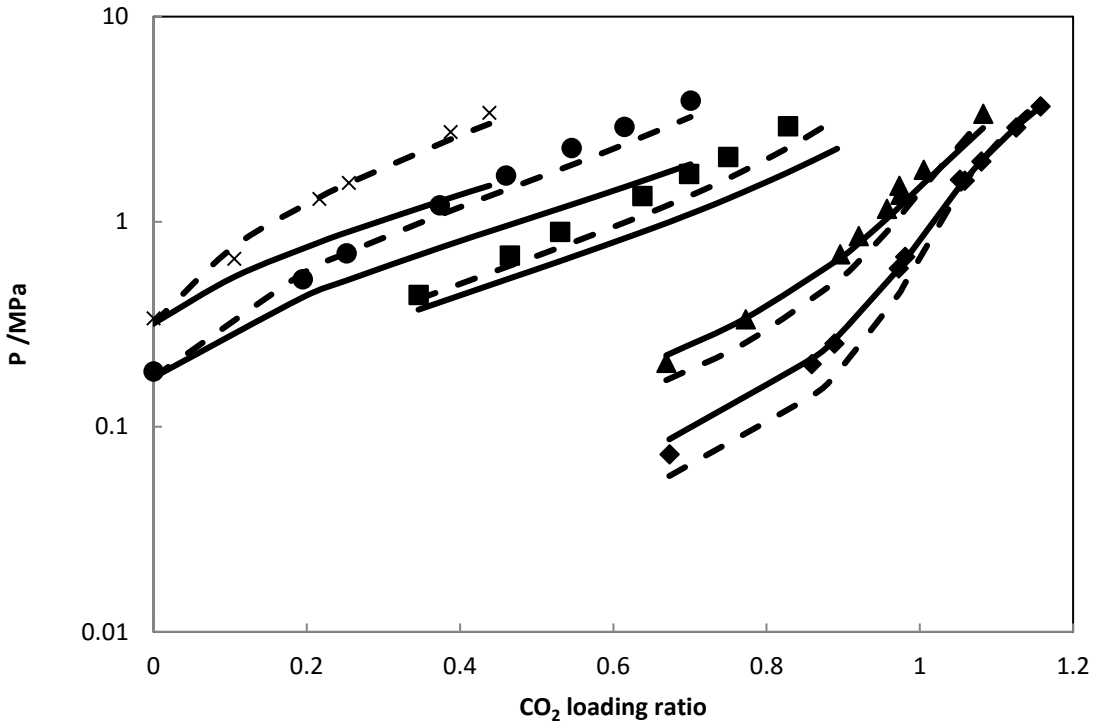

Figure 5-3 Comparison of total pressure of CO_2-MDEA-water ternary system with 32 wt% MDEA and adjusted values obtained with PR-CPA EoS. Solid lines: with k_{ij}=0, Dotted Lines: with adjusted k_{ij}. Symbols: experimental data from Kuranov et al. [126]**. (◆)=313 K, (▲)=333 K, (■)=373 K, (●)=393 K，(×)=413 K**

5.1.2.3 The solvation effect between CO_2-water

After comparison in previous section, we consider that the asymmetric approach with a temperature dependent k_{ij} gives best accuracy to represent CO_2-MDEA-water ternary systems. In this section, we investigate the influence of solvation effect between CO_2-water on CO_2-MDEA-water ternary system. The comparison of ARD and adjusted values are summarized in Table 5-5

Table 5-5 Influence of k_{ij} on the asymmetric approach

	T /K	ARD %	k_{ij}			β^{AiBj}	ε^{AiBj} /bar.L.mol^{-1}
			a	b×10^3 /K^{-1}	c×10^6 /K^{-2}		
CO_2-MDEA (with CO_2-water solvation)	313-413	11	6.51	-40.4	68.7	0.00486	340.97
CO_2-MDEA (without CO_2-water solvation)	313-413	14	6.94	40.9	6.46	0.00493	326.52

Figure 5-4 and Figure **5-5** shows the influence of solvation effect between CO_2-water on CO_2-MDEA-water ternary systems for 32 and 19 wt % MDEA respectively. For 32 wt % MDEA, both approaches can well represent the experimental data. The difference is very small; the two curves are nearly superposed. However, for 19 wt % MDEA, the one with CO_2-water solvation gives much better results, especially at lower temperature. The solvation between CO_2- water should be taken into account to treat CO_2 – MDEA-water ternary system.

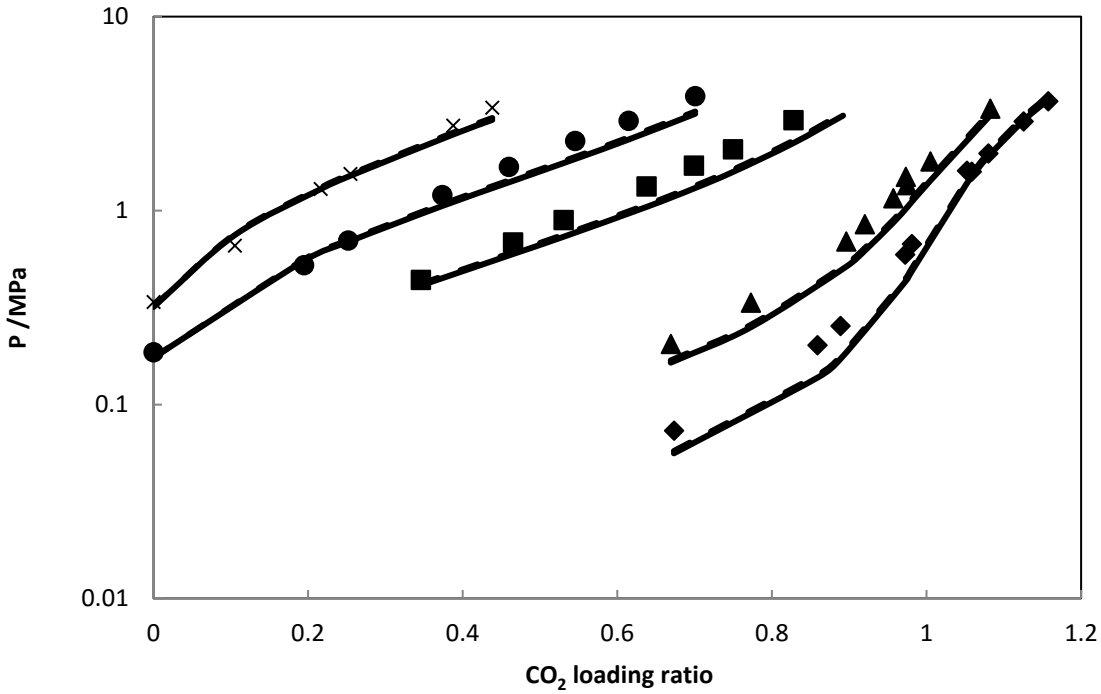

Figure 5-4 Comparison of total pressure of CO_2-MDEA-water ternary system with 32 wt% MDEA and adjusted values obtained with PR-CPA EoS. Solid lines: with CO_2-water solvation, Dotted Lines: without CO_2-water solvation. Symbols: experimental data from Kuranov et al. [126]**. (◆)=313 K, (▲)=333 K, (■)=373 K, (●)=393 K，(×)=413 K**

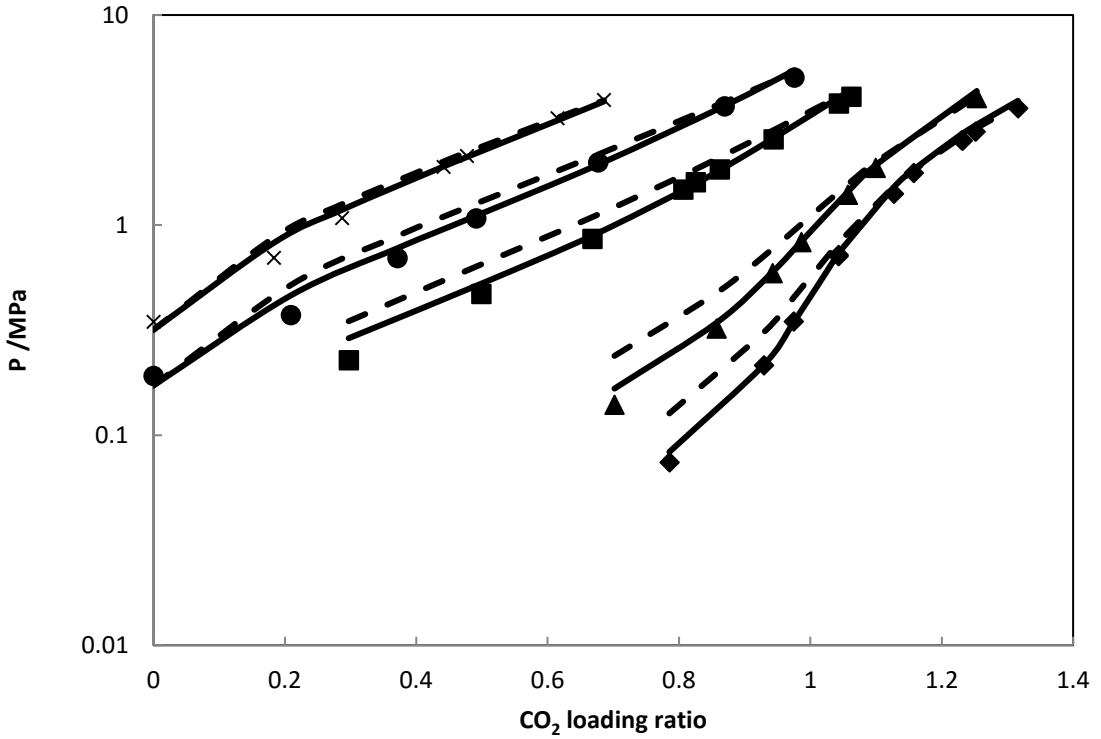

Figure 5-5 Comparison of total pressure of CO_2-MDEA-water ternary system with 19 wt% MDEA and adjusted values obtained with PR-CPA EoS. Solid lines: with CO_2-water solvation, Dotted Lines: without CO_2-water solvation. Symbols: experimental data from Kuranov et al. [126]**. (◆)=313 K, (▲)=333 K, (■)=373 K, (●)=393 K，(×)=413 K**

5.1.3 Model prediction

5.1.3.1 CO_2 solubility

Experimental data with 25 wt % MDEA [127] is used to validate the model prediction. These data are at a temperature range of 298K-348K, as we showed in 4.1.2.3, the solvation effect between CO_2-water is more accurate at lower temperature in 19 wt % MDEA. In this section, we predict with and without CO_2-water solvation effect; the results are shown in Figure 5-6. It can be seen that, the total pressure is correctly predicted by our model with or without CO_2-water solvation. Without CO_2-water solvation effect, the deviation is larger when CO_2 loading ratio is lower (<0.6), the ARD% is 30. However, with solvation effect, the model prediction is more accurate in all range of CO_2 loading ratio and temperature, the ARD is 12%.

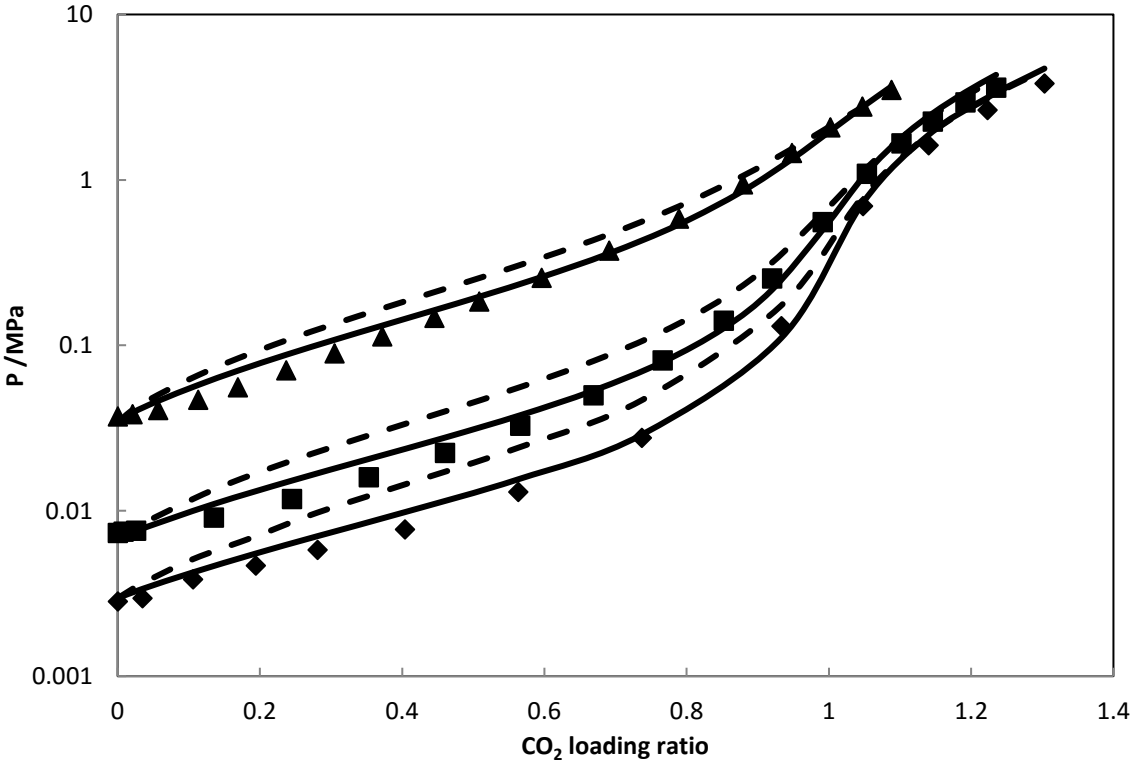

Figure 5-6 Prediction of total pressure of CO_2-MDEA-water ternary system with 25 wt% MDEA with PR-CPA EoS. Solid lines: with CO_2-water solvation, Dotted Lines: without CO_2-water solvation. Symbols: experimental data from Sidi-Boumedine et al. [127]**. (◆)=298 K, (▲)=313 K, (■)=348 K**

5.1.3.2 Liquid phase speciation

Another important aspect in the model validation is the description of the degree of speciation of the system. The main products of reactions in the model are the $MDEAH^+$ and HCO^-_3, the concentration of these products can be deduced from the ratio of unbounded α sites on the CO_2, see following equations:

$$[MDEA^+] = [x_{CO2}][(1 - X^{\alpha 1,CO2})] \quad (4.3)$$

$$[HCO_3^{-1}] = [x_{CO2}][X^{\alpha 1,CO2}] \quad (4.4)$$

Where x_{CO2} is the model concentration of CO_2 in the liquid phase

The analysis of the degree of speciation for CO_2-MDEA-H_2O at 313 K is presented in Figure 5-7. PR-CPA EoS provides very good predictions of the composition in MDEA and bicarbonate at different temperatures.

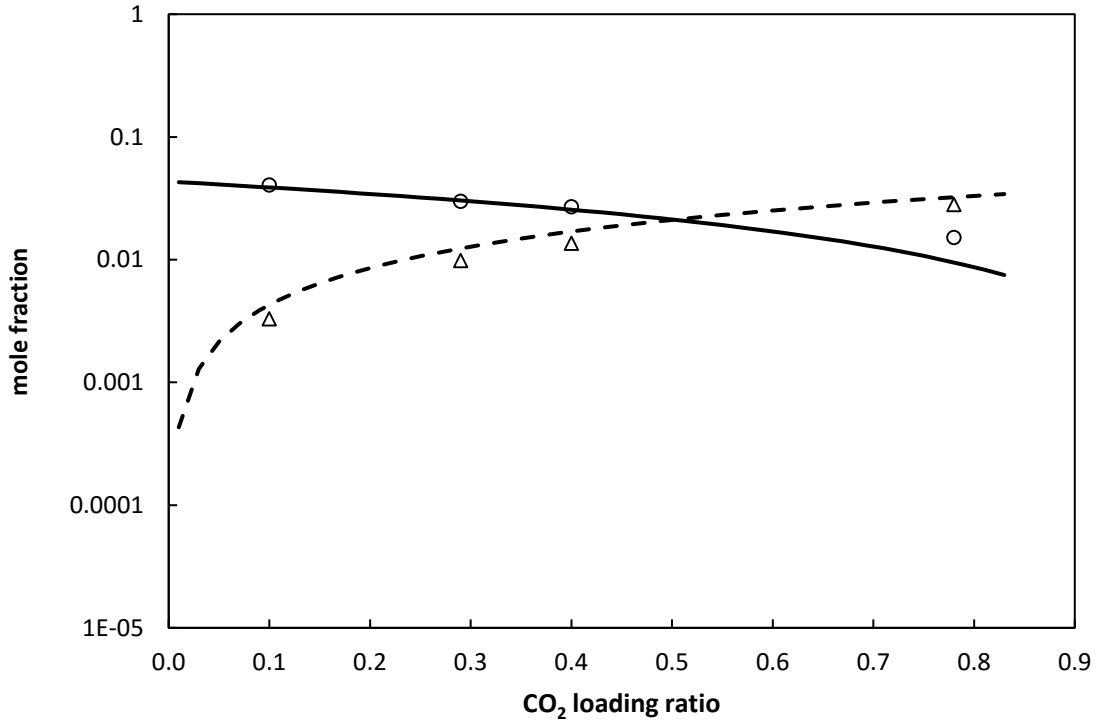

Figure 5-7 Prediction of liquid phase electrolytes speciation of CO_2-MDEA-water ternary system with 30 wt % MDEA at 313K. Solid line: MDEA, dotted line: HCO_3^{-1} symbol: experimental data from Jakobsen et al. [128]: (Δ)=HCO_3^{-1}, (○)=MDEA

5.1.3.3 Enthalpy of absorption

In the context of acid gas removal processes, another important aspect to consider is the enthalpy of absorption of CO_2, as the major source of heat in the system is the heat released when CO_2 is absorbed by MDEA. As for the heat of absorption, the enthalpy of the standard state (ΔHo,heat of reaction) was obtained by calculating the heat of absorption generated per one mole of CO_2. The heat of absorption is not greatly affected by pressure [129]. The enthalpy of absorption is calculated by using following equation:

$$\Delta H_{abs} = \left(\frac{d \ln(P)}{d1/T} \right)_x \qquad (4.5)$$

The comparison between the PR-CPA EoS predictions and the experimental data of the enthalpy of absorption of CO_2 in MDEA is shown in Figure 5-8. With 20 wt% MDEA, temperature from 298 to 333 K, which is a typical temperature range for CO_2 absorbers, PR-CPA is able to accurately predict the enthalpy of absorption of CO_2. The overall ARD is 14.5 %. However the increase of $-\Delta H_{abs}$ with temperature is not correctly predicted with PR-CPA EoS. These experimental data should be reviewed by comparing with others.

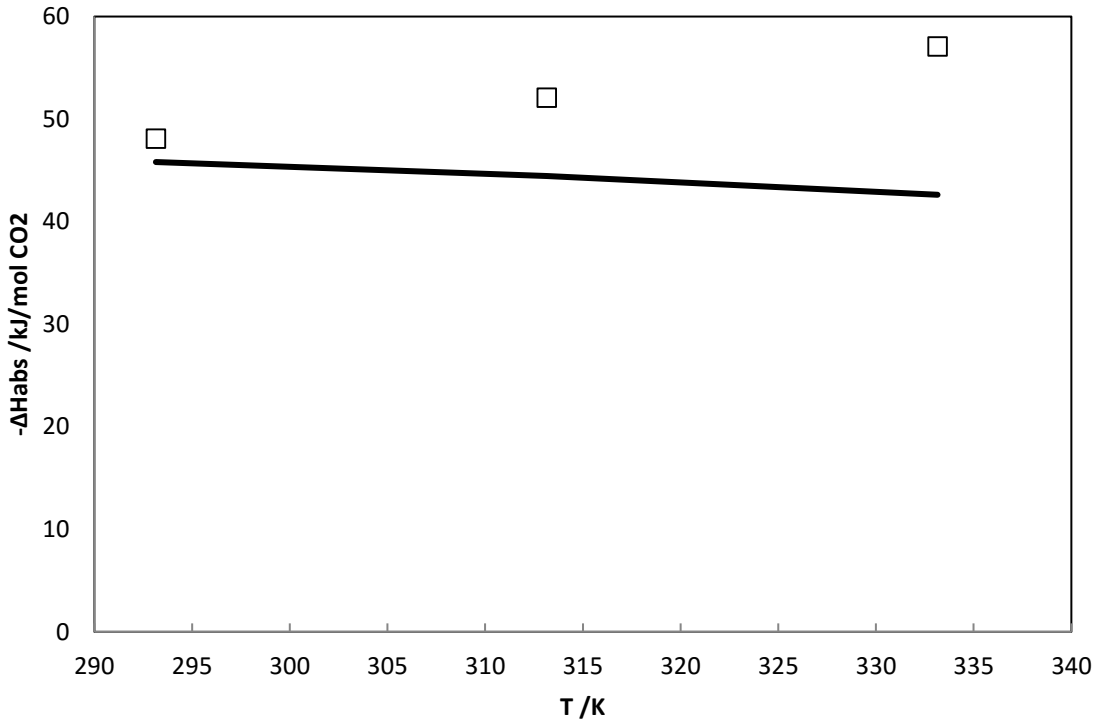

Figure 5-8 Prediction of enthalpy of absorption of CO_2-MDEA-water ternary system with 20 wt % MDEA. Lines: PR-CPA EoS prediction, symbols: experimental data from Gupta et al. [130]

5.1.4 Comparison with Deshmukh–Mather model

In section 5.1.2, we showed that PR-CPA EoS is able to accurately represent the phase behaviour of CO_2–MDEA-water ternary system with a simplified approach to treat the chemical reactions and without considering the presence of different electrolytes species. In this section, we compare results with Deshmukh–Mather model [6] adjustment, which is detailed in Chapter 3.

According to Dicko et al. [57], with the aim of limiting the number of parameters to be adjusted, 5 parameters are considered as adjustable. The objective function is as the same as PR-CPA EoS, it is expressed by Equation (4.2). Optimized parameters are shown in Table 5-6. The ARD is 19 %, which is higher than PR-CPA.

Table 5-6 Adjusted parameters for CO_2-MDEA-water ternary system

Couple	β_{ij}/kg-H_2O/kmol
$MDEAH^+$–CO_2	-7.585
$MDEAH^+$–HCO_3^-	-6.015
MDEA–HCO_3^-	48.366
MDEA–CO_3^{2-}	33.92
MDEA–MDEA	-177.12

Figure 5-9 andFigure **5-10** show the comparison of PR-CPA and Deshmukh–Mather model for CO_2 in 32 and 19 wt % MDEA aqueous solution respectively. At lower temperature (T<393 K), both model are able to represent CO_2 total pressure in function of CO_2 loading ratio. However, at 413 K, Deshmukh–Mather Model fails to describe of experimental curve. Benamor and Aroua [56] refined Deshmukh–Mather model for CO_2-MDEA-water ternary system by using temperature dependent β_{ij}. Like section 5.1.3.1, we did not use the set of experimental data with 25 wt % MDEA in parameter adjustment. The comparison between two models predictions is shown in Figure 5-11. It can be seen that both models can predict the tendency of experimental data. PR-CPA EoS is more accurate to predict total pressure of CO_2-MDEA-water systems. Deshmukh–Mather model over predict the total pressure in all range of CO_2 loading ratio, the ARD is 21 %. However, at 298 K, Deshmukh–Mather is unable to calculate the total pressure. It can be explained by that it is out of the range of temperature 313-413 K in adjustment and

the chosen chemical equilibrium constants are not validate in the extremity of such range of temperature.

Because of the limitation of Deshmukh–Mather model and better accuracy with PR-CPA EoS, the last is chosen for the study on H_2S-MDEA-water, H_2S-MEA-water and CO_2-MEA-water ternary system and multi component systems in following sections.

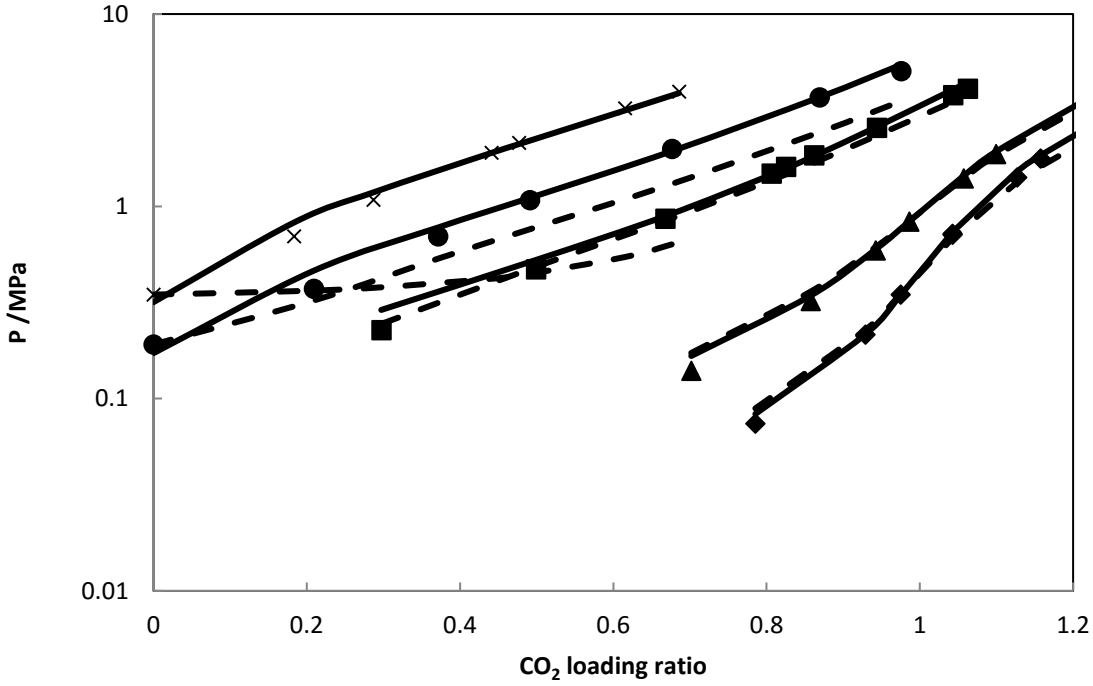

Figure 5-9 Comparison of total pressure of CO_2-MDEA-water ternary system with 32 wt% MDEA and adjusted values obtained with PR-CPA .Solid lines: PR-CPA EoS, Dotted Lines: DM model. Symbols: experimental data from Kuranov et al. [126]**. (◆)=313 K, (▲)=333 K, (■)=373 K, (●)=393 K，(×)=413 K**

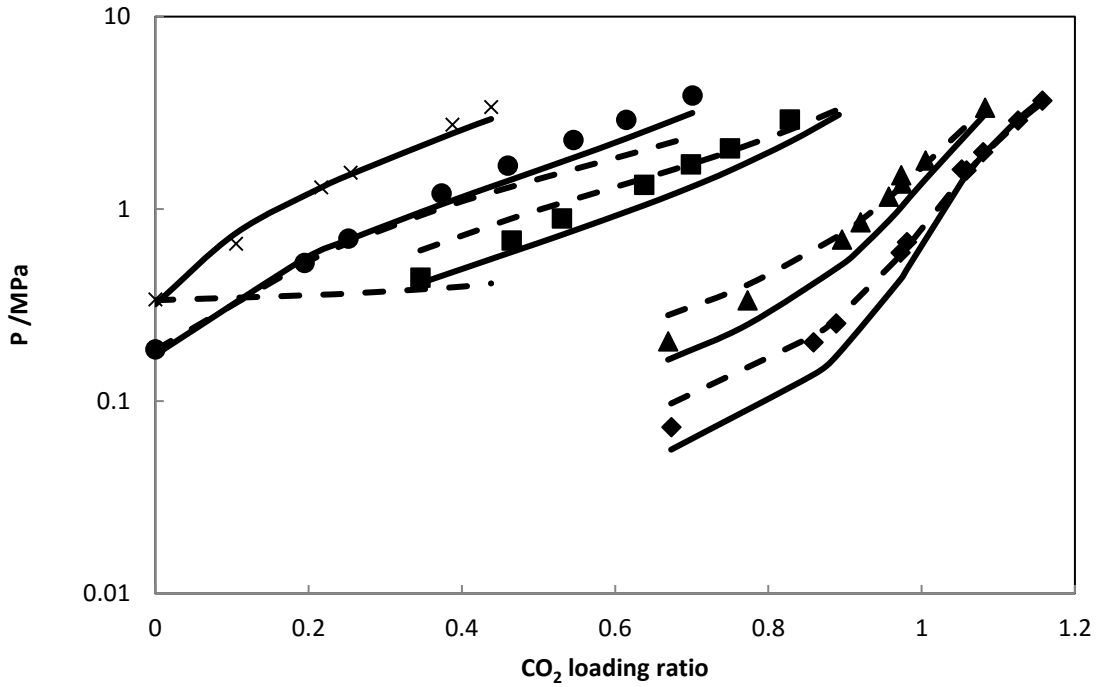

Figure 5-10 Comparison of total pressure of CO2-MDEA-water ternary system with 19 wt% MDEA and adjusted values obtained with PR-CPA EoS .Solid lines: PR-CPA, Dotted Lines: DM model. Symbols: experimental data Kuranov et al. [126]**. (◆)=313 K, (▲)=333 K, (■)=373 K, (●)=393 K，(×)=413 K**

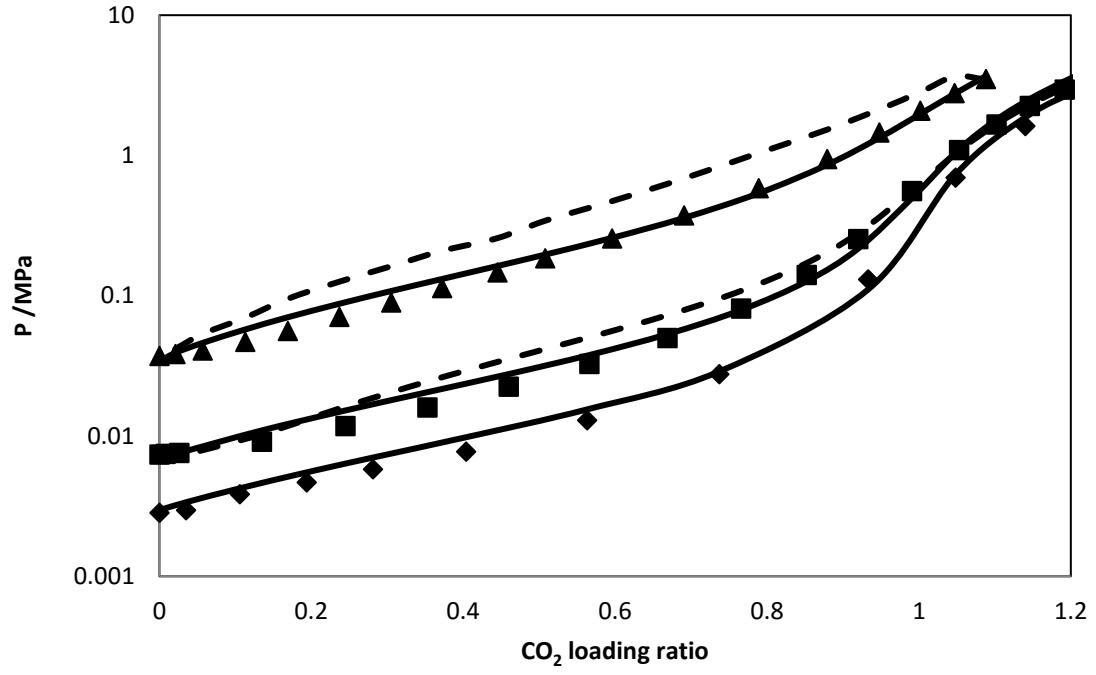

Figure 5-11 Prediction of total pressure of CO_2-MDEA-water ternary system with 25 wt% MDEA. solid lines: PR-CPA EoS, Dotted Lines: DM model. Symbols: experimental data from Sidi-Boumedine et al. [127]**. (◆)=298 K, (▲)=313 K,(■)=348 K**

5.2 Modeling of H_2S-MDEA-water ternary system

5.2.1 H_2S-water Binary system

In section 5.1, we demonstrated that the solvation effect between CO_2 and water cannot be neglected. Therefore, in this section, we consider the solvation effect between H_2S and water (we did not adjust parameters without solvation effect). Therefore, k_{ij} is adjustable, two cross association parameters (ε^{AiBj} and β^{AiBj}) are involved. ε^{AiBj} is assumed to be a non adjustable parameter with an experimental value set at 108.78 [131]; β^{AiBj} is an adjustable parameter. These parameters were estimated by fitting H_2S solubility data and using the same objective function in section 5.1.1. Table 5-7 summarizes the adjusted parameters and ARD for the VLE data treatment of H_2S-water binary system. Figure 5-12 shows the comparison between model adjustment and experimental data. Our model can well represent H_2S-water binary system for both liquid and vapour phases with a constant k_{ij} and cross association parameters.

Table 5-7 k_{ij} value and ARD of liquid (x) compositions between PR-CPA EoS adjusted data and experimental ones obtained for H_2S –water binary system.

	T /K	ARD x_{H2S}	k_{ij}	β^{AiBj}	ε^{AiBj} /bar.L.mol^{-1}	Reference
H_2S-water	283-443	2.1	0.0998	0.01427	108.78	[132,133]

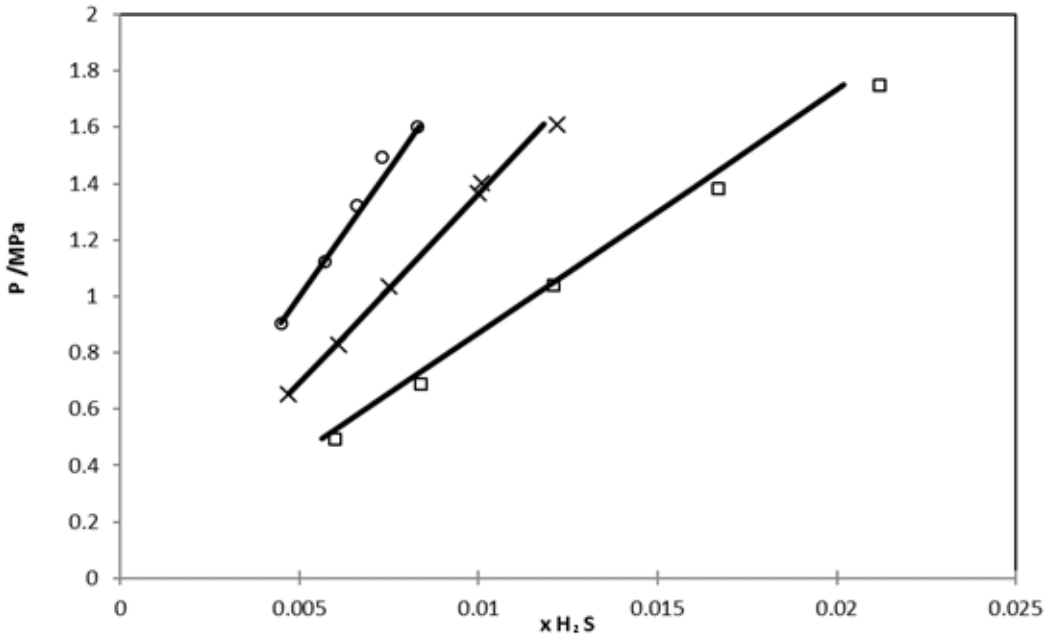

Figure 5-12 Comparison of experimental H_2S solubility in water and adjusted values obtained with PR-CPA, symbol: experimental data from Selleck et al. [133]; (□)=311K (x)=344K, (○)=377 K , solid lines: PR-CPA EoS.

5.2.2 H_2S solubility in aqueous MDEA

To the best of our knowledge, there is no available experimental data for H_2S-MDEA binary systems. Using the same method in previous section, parameters for H_2S-MDEA binary system has been fitted from ternary experimental data. The same number of parameters and the same objective function are employed. There are available ternary experimental data with various concentration of MDEA from 0.20 to 0.488 [127] [134]. The range of loading rate of H_2S is up to 1.933. However, in industrial application the loading rate of H_2S is normally less than 1.00. Therefore, we have chosen experimental data only with loading rate of H_2S less than 1.00 for parameter estimations. The objective function is the same as which used in section 5.1 Optimized parameters values are summarized in Table 5-8, the overall ARD is 13% in a temperature range from 311 to 388 K.

Table 5-8 Adjusted Binary Interaction Parameters of PR-CPA for H_2S-MDEA-water ternary system

Binary	k_{ij}[a]			β^{AiBj}	ε^{AiBj} /bar.L.mol-1
	a	b×10^3 /K^{-1}	c×10^6 /K^{-2}		
water-MDEA	-0.190				
H_2S-water	0.0998	0.397		0.01427	108.78
H_2S-MDEA	0.8489	-2.834	8.461	0.01846	316.42

a: $k_{ij} = a + b \cdot T + c \cdot T^2$

Figure 5-13 and Figure 5-14 show the comparison between the total pressure of H_2S-MDEA-water ternary system and the adjusted one obtained with PR-CPA at different MDEA concentrations (20 and 48 wt %). It can be highlight that PR-CPA can accurately represent the total pressure of H_2S-MDEA-water ternary system with temperature range from 311 to 388K, and H_2S loading ratio from 0 to 0.988.

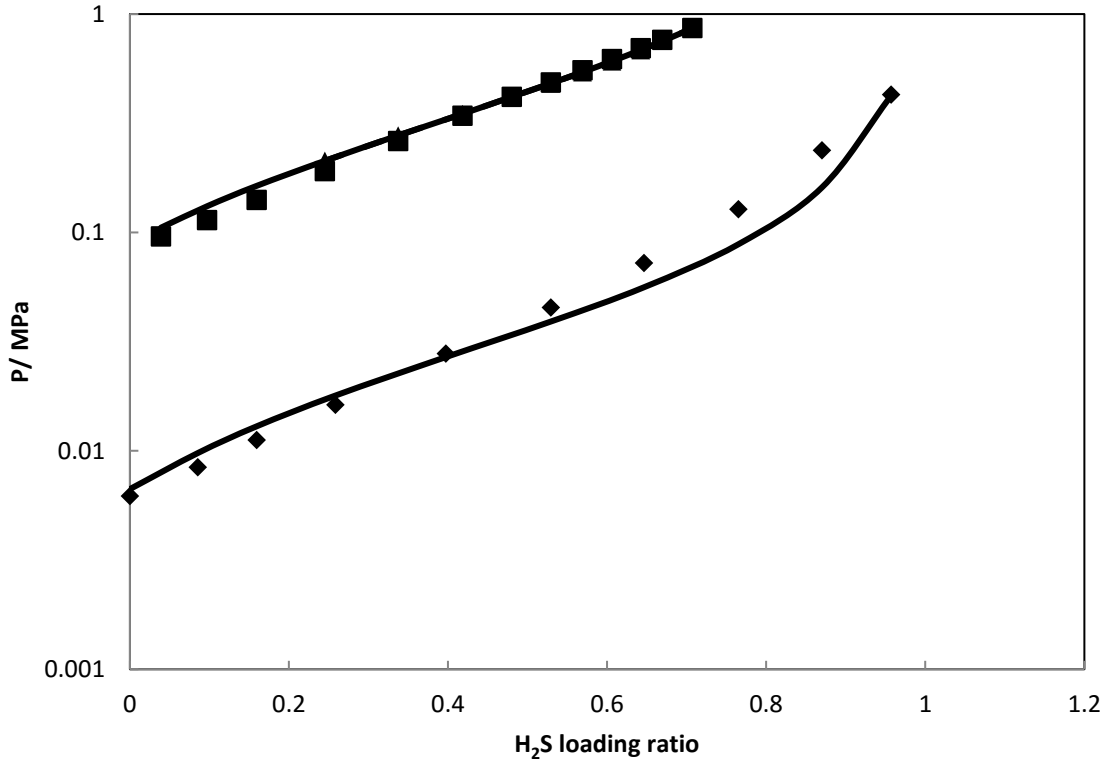

Figure 5-13 Comparison of total pressure of H_2S-MDEA-water ternary system with 48 wt% MDEA and adjusted values obtained with PR-CPA EoS. Symbols: experimental data from Sidi-Boumedine et al. [127] **. Solid lines: PR-CPA EoS adjusted data. (◆)=313K, (■)=373 K.**

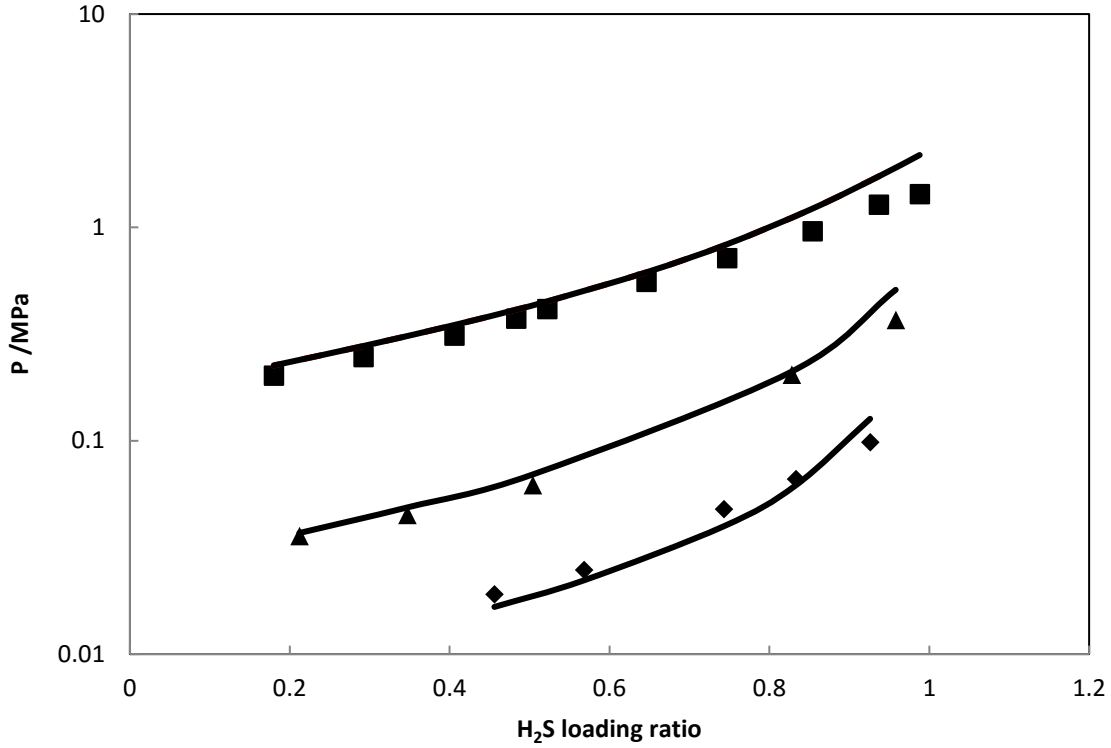

Figure 5-14 Comparison of total pressure of H_2S-MDEA-water ternary system with 20 wt% MDEA and adjusted values obtained with PR-CPA EoS. Symbols: experimental data from Bhairi et al. [134] **. Solid lines: PR-CPA EoS adjusted data. (◆)=311 K, (▲)=338 K, (■)=388 K.**

5.2.3 Model prediction

We used the set of experimental data with 20 wt % and 48 wt % MDEA to adjust parameters. Experimental data obtained at 35 wt % MDEA [135] are used to validate the model prediction. The result is shown in Figure 5-15. It can be seen that, the tendency of total pressure is correctly predicted by our model, the ARD is 17 %. However, the total pressure is overestimated for low H_2S loading ratio (<0.2).

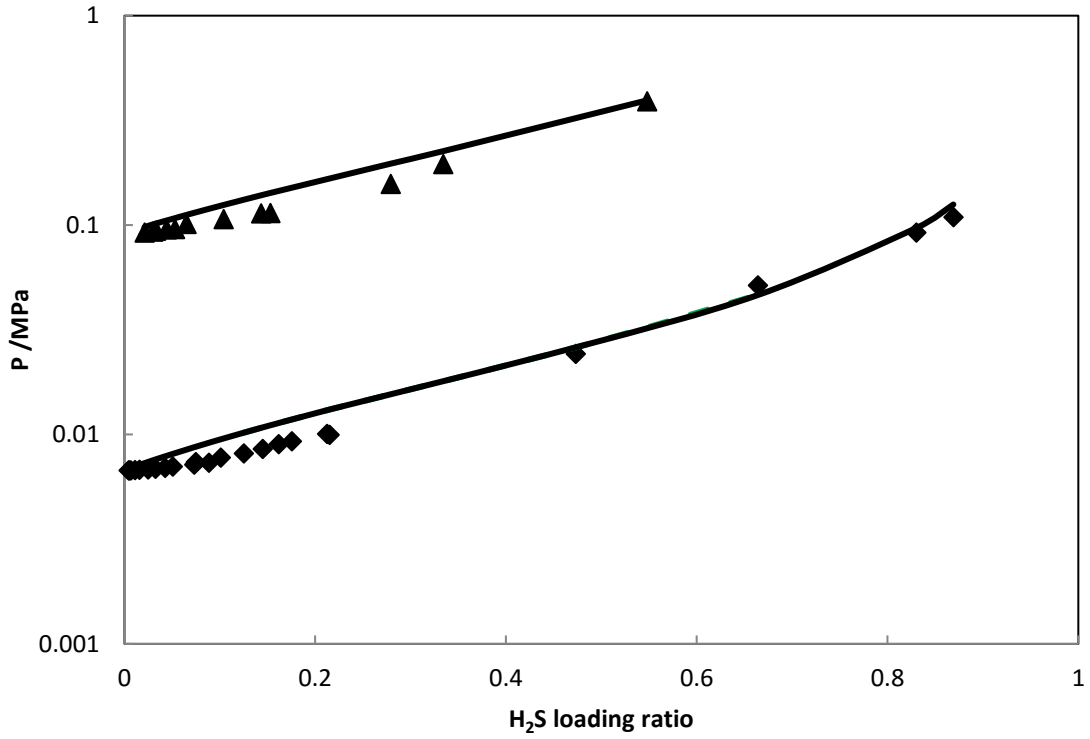

Figure 5-15 Prediction of total pressure of H_2S-MDEA-water ternary system with 35 wt% MDEA. Symbols: experimental data from Jou et al. [135] **. Solid lines: PR-CPA EoS. (◆)=313 K, (▲)=373 K.**

5.3 Modeling of CO_2-MEA-water ternary system

In section 5.1, we showed that the PR-CPA EoS with the asymmetric association scheme and the consideration of CO_2 solvation effect is able to accurately represent the solubility of CO_2 in aqueous MDEA solution. MEA is also a widely used solvent in acid gas removal process, the difference between MEA and MDEA is that a second reaction forming carbomate should be considered. Therefore, the two α sites are both active in this case, and two additional parameters $\beta^{AiBj'}$ and $\varepsilon^{AiBj'}$ are involved in order to represent the formation of carbomate. The chemical reactions taking place are represented in chapter 3.

The k_{ij} between CO_2-MDEA is assigned with temperature dependent. All binary parameters used in parameter fitting are summarized in Table 5-2. The objective function is used and given by Equation (1.1). The results are shown in Table 5-3.

Table 5-9 PR-CPA binary parameters for CO_2-MDEA-water ternary system

Binary	k_{ij}[a]			β^{AiBj}	ε^{AiBj} /bar.L.mol^{-1}	$\beta^{AiBj'}$	$\varepsilon^{AiBj'}$ /bar.L.mol^{-1}
	a	b×10^3 /K^{-1}	c×10^6 /K^{-2}				
water-MEA	-0.142			NA	NA		
CO_2-water	0.0052	0.397		0.0136	86.3		
CO_2-MDEA	-6.99	29.90	-23.73	0.00411	408.62	0.00106	361.17

a: $k_{ij} = a + b \cdot T + c \cdot T^2$

Figure 5-13 shows the comparison between the total pressure of CO_2-MEA-water ternary system and the adjusted one obtained with PR-CPA with 30 wt% MEA concentrations. It can be highlight that PR-CPA can accurately represent the total pressure of CO_2-MEA-water ternary system with temperature range from 298 K to 398K, and CO_2 loading ratio from 0 to 0.95.

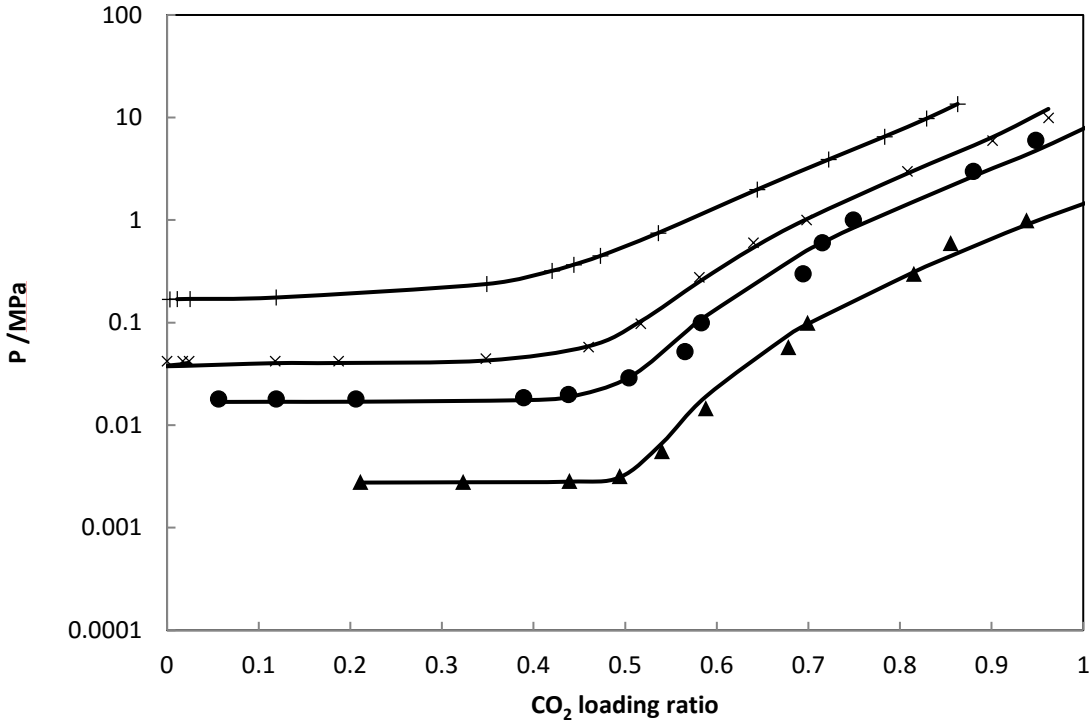

Figure 5-16 Comparison of total pressure of CO_2-MEA-water ternary system with 30 wt% MEA and adjusted values obtained with PR-CPA. Solid lines: experimental data from Jou et al. [136]**. (▲)=298 K, (●)=333 K， (×)=353 K, (+)=393 K**

5.3.1 Model prediction

5.3.1.1 Liquid phase speciation

As we explained in chapter 3, although chemical equilibrium constants are not needed in the PR-CPA EoS, the concentration of different electrolytes were calculated by using the fraction of molecules of CO_2 not bonded at the site α ($X^{\alpha,CO2}$) by using following Equations:

$$[MEACOO^{-}] = [x_{CO2}][(1-X^{\alpha 1,CO2})\,(1-X^{\alpha 2,CO2})] \qquad (4.6)$$

$$[HCO_3^{-1}] = [x_{CO2}][X^{\alpha 1,CO2}+1-X^{\alpha 2,CO2}] \qquad (4.7)$$

Where x_{CO2} is the model concentration of CO_2 in the liquid phase

The PR-CPA EoS is able to accurately predict the speciation of acid gas reacting with aqueous alkanolamine solutions. Figure 5-17 shows the excellent agreement between PR-CPA prediction and experimental data for the speciation for carbomate and bicarbonate for CO_2-MEA-water ternary system at 313 K.

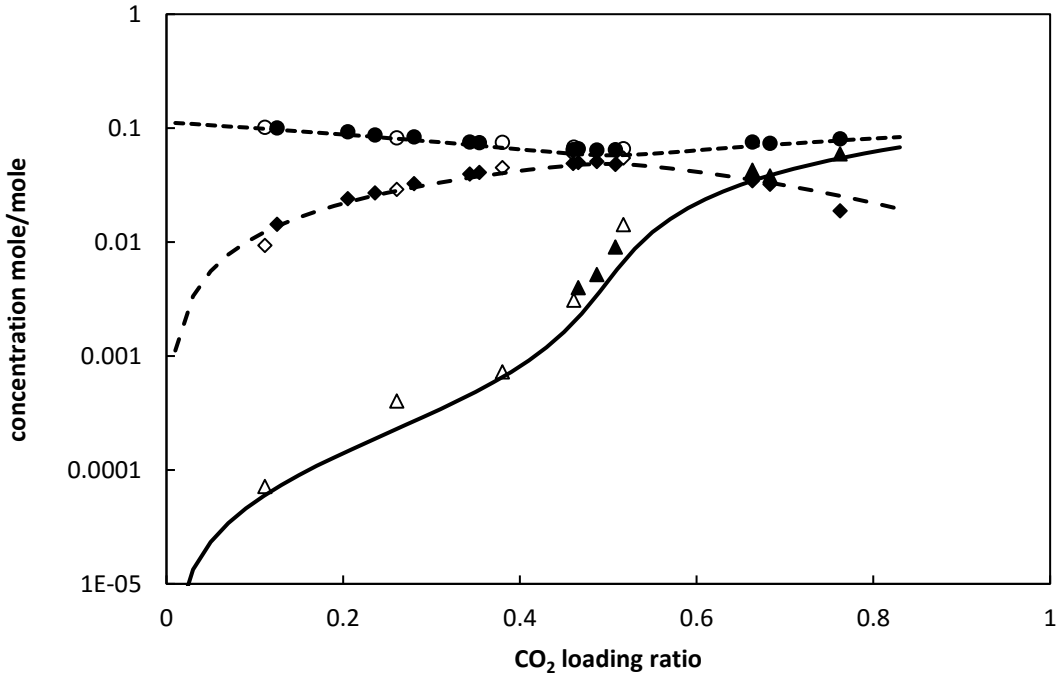

Figure 5-17 Prediction of liquid phase electrolytes speciation of CO_2-MEA-water ternary system with 30 wt % MEA at 313.15 K. Solid line: HCO_3^{-1}, dashed line: $MEACOO^-$, dotted line: $MEA+MEAH^+$, symbols: experimental data from Hilliard et al. [137] **(△)=HCO_3^{-1},(◇)= $MEACOO^-$ (○)=$MEA+MEAH^+$ from Hilliard** [138]**, (▲)=HCO_3^{-1},(◆)= $MEACOO^-$ (●)=$MEA+MEAH^+$.**

5.3.1.2 Vapour phase concentration

MEA is much more volatile compared to MDEA, accurate prediction of MEA concentration in the vapour phase is necessary for process designer to estimate the quantity of loss of solvent. Moreover, the water content is crucial for the design of drying units. Figure 5-18 and Figure **5-19** show that the PR-CPA EoS has also excellent ability to predict vapour phase composition on water and MEA at 333 and 313 K respectively.

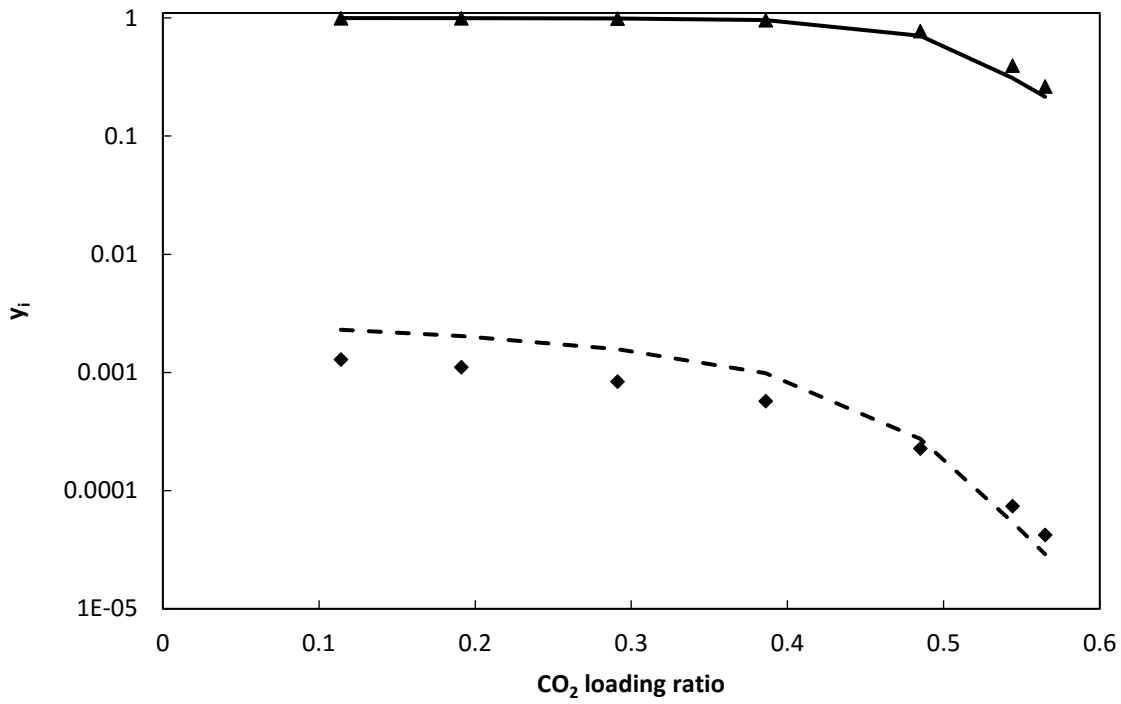

Figure 5-18 Prediction of vapour phase composition of CO_2-MEA-water ternary system with 30 wt % MEA at 333.15 K Lines predicted by PR-CPA EoS, Solid line: y_{water}, dashed line:y_{MEA}, symbol: experimental data from Hilliard et al. [138] **(▲)=y_{water},(◆)= y_{MEA}**

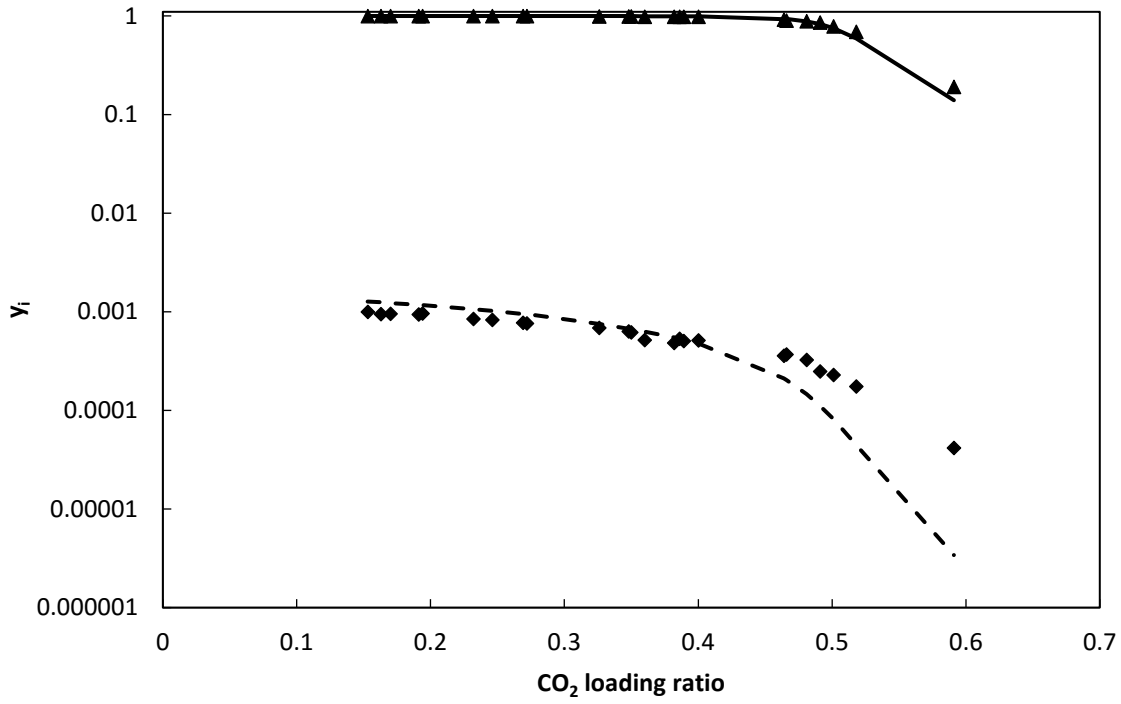

Figure 5-19 Prediction of vapour phase composition of CO_2-MEA-water ternary system with 30 wt % MEA at 313.15 K Lines predicted by PR-CPA EoS, Solid line: y_{water}, dashed line:y_{MEA}, symbol: experimental data from Hilliard et al. [138] **(▲)=y_{water},(◆)= y_{MEA}**

5.3.1.3 Enthalpy of absorption

The enthalpy of absorption of CO_2 in aqueous MEA is predicted by PR-CPA EoS at 313 and 393 K shown in Figure 5-20 and Figure 5-21 respectively. At 313 K, which is a typical operational temperature in the absorber, it can be seen that the enthalpy of absorption is accurately predicted when the CO_2 loading ratio is lower than 0.4, ie. before the formation of carbomate. However, the PR-CPA EoS underestimates the enthalpy of absorption by 49% when the carbomate is formed. At 393 K, which is an operational temperature in the disrober, the enthalpy of absorption can be considered as the opposite value of enthalpy of desorption. The trend of enthalpy of absorption variation in function of CO_2 loading ratio is correctly predicted. The value is underestimated by 25 kJ/mol CO_2 in all range of CO_2 loading ratio. Brand [139] has investigated the enthalpy of absorption of CO_2 in aqueous MEA solution with the SAFT-VR EoS. These values of enthalpy of absorption are underestimated by 50 kJ/mol CO_2. As a solution, they proposed to reduce the deviation by adding a constant which seems to be not very consistent.

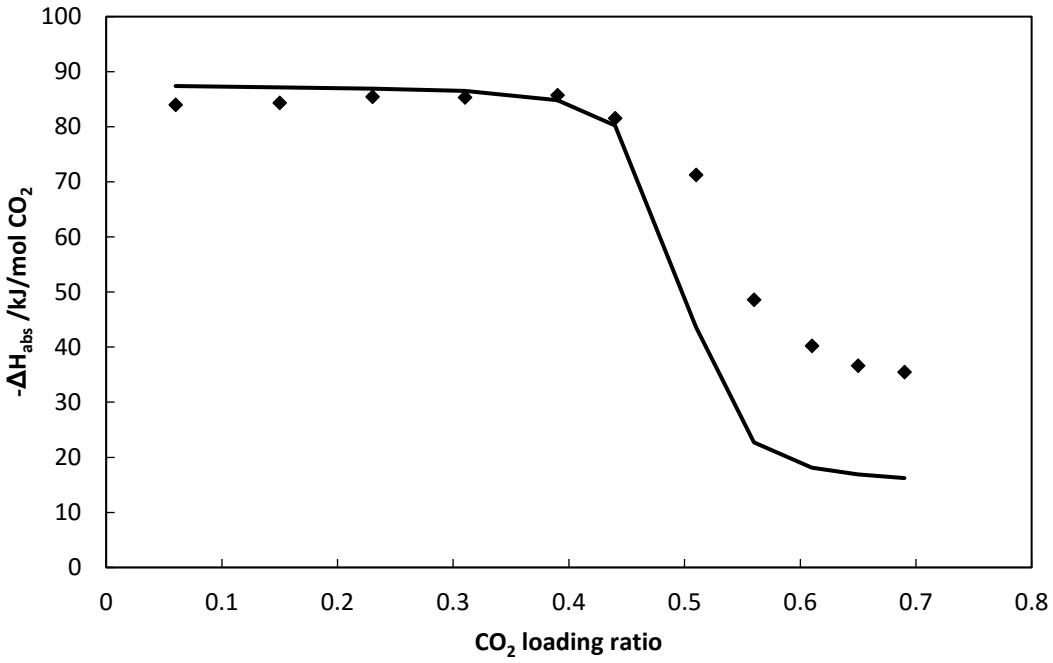

Figure 5-20 Prediction of enthalpy of absorption of CO_2-MEA-water ternary system with 30 wt % MEA at 313.15, Solid line PR-CPA EoS, symbol: experimental data from Hilliard et al. [138]

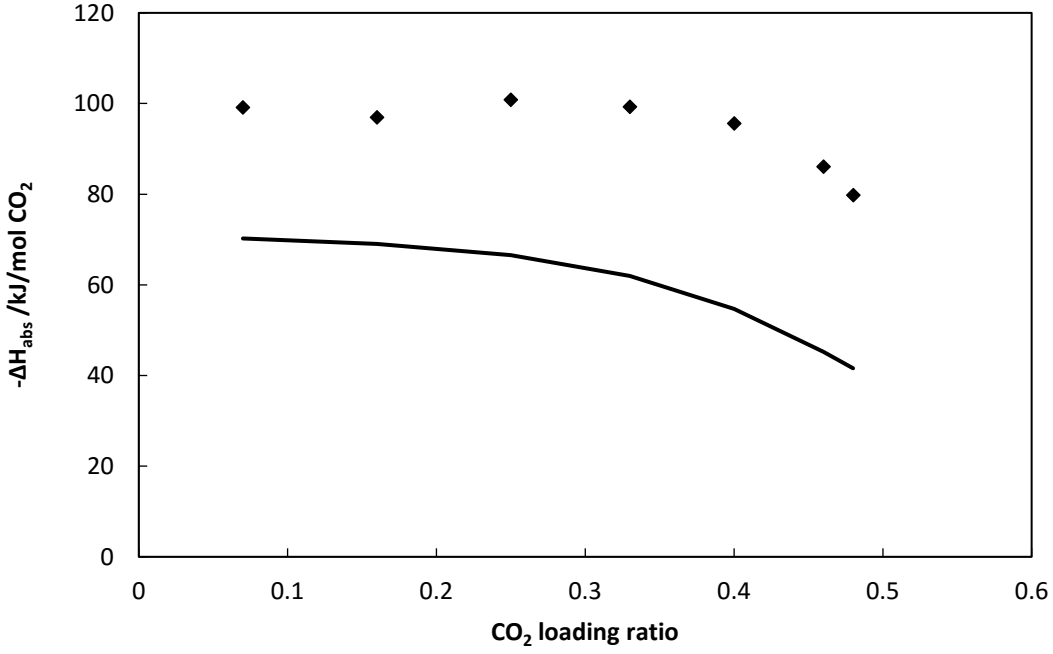

Figure 5-21 Prediction of enthalpy of absorption of CO_2-MEA-water ternary system with 30 wt % MEA at 393.15, Solid line PR-CPA EoS, symbol: experimental data from Hilliard et al. [138]

5.4 **Modelling of H_2S-MEA-water ternary system**

The reaction mechanism of H_2S-MEA is considered as the same as CO_2-MEA. Therefore, the two α sites on H_2S are both active and are represented by two sets of β^{AiBj} and ε^{AiBj}. The k_{ij} between H_2S-MEA is also considered as temperature dependent. All binary interaction parameters used in parameter fitting are summarized in Table 5-10. According to the open literature, the experimental data of H_2S-MEA-water system are only available in form of partial pressure of H_2S in function of H_2S loading ratio, the objective function is used and given by following Equation. The results are shown in Table 5-10.

$$f = 100 \times \sum_{i=1}^{n} \left(\frac{\left| P^{cal} - P^{exp} \right|}{P^{exp}} \right)_i \qquad (4.8)$$

Where P is the H_2S partial pressure of H_2S-MEA-H_2O ternary systems.

Table 5-10 PR-CPA EoS binary parameters for CO2-MDEA-water ternary system

Binary	$k_{ij}{}^a$			β^{AiBj}	ε^{AiBj} /bar.L.mol-1	$\beta^{AiBj'}$	$\varepsilon^{AiBj'}$ /bar.L.mol-1
	a	b×10^3 /K^{-1}	c×10^6 /K^{-2}				
water-MEA	-0.190			NA	NA		
H_2S-water	-0.768	4.1492	-5.1396	NA	NA		
H_2S-MEA	-6.426	38.15	-49.94	0.00380	411.51	0.0170	178.26

a: $kij = a + b \cdot T + c \cdot T^2$

Figure 5-22 shows the comparison between H_2S partial pressure of H_2S-MEA-water ternary system and the adjusted one obtained with PR-CPA EoS with 30 wt% MEA concentrations. It can be seen that PR-CPA EoS can accurately represent H_2S partial pressure of H_2S-MEA-water ternary system within temperature range from 298 to 393K, when H_2S loading ratio is greater than 0.2. However, the PR-CPA EoS overestimate H_2S partial pressure when the H_2S loading rate is low (<0.2).

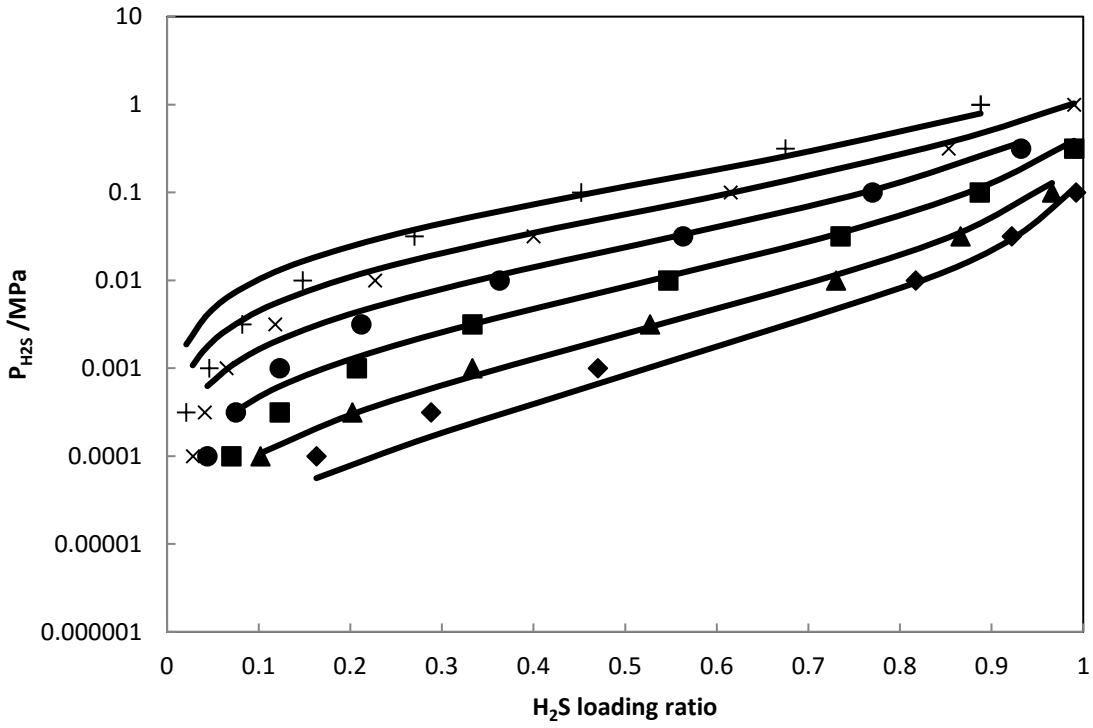

Figure 5-22 Comparison of H_2S partial pressure of H_2S-MEA-water ternary system with 30 wt% MEA and adjusted values obtained with PR-CPA. Solid lines: experimental data from Lee et al. [140]**. (♦)=298 K, (▲)=313 K, (■)=333K, (●)=353 K， (×)=373 K, (+)=393 K**

5.5 Multicomponent system prediction

5.5.1 CH_4-CO_2-H_2S-H_2O quaternary system

CH_4-CO_2-H_2S-H_2O quaternary system is important to evaluate PR-CPA EoS prediction performance. In this section, we compare the model prediction with experimental data from Huang et al [141] for two different mixtures in a wide range of temperature (from 310 to 449 K). The composition of mixtures is represented in Table 5-11.

Table 5-11 Initial composition of CH_4-CO_2-H_2S-H_2O mixtures

	Mole fraction	
component	Mixture 1	Mixture 2
H_2O	0.5	0.5
CO_2	0.05	0.3
H_2S	0.4	0.05
CH_4	0.05	0.15

Table 5-12 shows the model deviation of each component in liquid phase and vapour phases for mixtures 1 and 2, PR-CPA EoS has good prediction performance with maximum ARD<20%. Li et al. [142] has reduced the model deviation to 10 % with PR-CPA EoS by considering the solvation effect of methane with other components, though it is not physically correct.

Table 5-12 ARD of PR-CPA EoS prediction for CH_4-CO_2-H_2S-H_2O quaternary system [141]

	T /K	P /MPa	ARD %							
			x_{CO2}	x_{CH4}	x_{H2O}	x_{H2S}	y_{CO2}	y_{CH4}	y_{H2O}	y_{H2S}
Mixture 1	310-449	4.8-17.3	3.9	13.4	0.1	14.9	0.6	1.3	12.2	2.4
Mixture 2			7.2	18.4	0.2	20	0.7	1.2	11.3	1.9

5.5.2 CO_2-H_2S-H_2O-alkanolamine quaternary system

CO_2 and H_2S are usually both present in the natural gas reserve. It is important to have an accurate thermodynamic model which is able to accurately predict partial pressures of CO_2 and H_2S in aqueous alkanolamine solution. With parameters from previous sections, the PR-CPA EoS prediction is compared with experimental data of CO_2-H_2S-H_2O-MEA [140] and CO_2-H_2S-H_2O-MDEA [143]. Within temperature range from 311 to 393 K, Figure 5-23 and Figure

5-24 describe excellent agreement between PR-CPA EoS prediction and experimental data [140] for H_2S and CO_2 respectively in MEA. Satisfactory results have been found for MDEA.

Two tails students t-test have been carried out for those systems, the P value is between 0.001 and 0.073, it demonstrate the model prediction is in good agreement with experimental data.

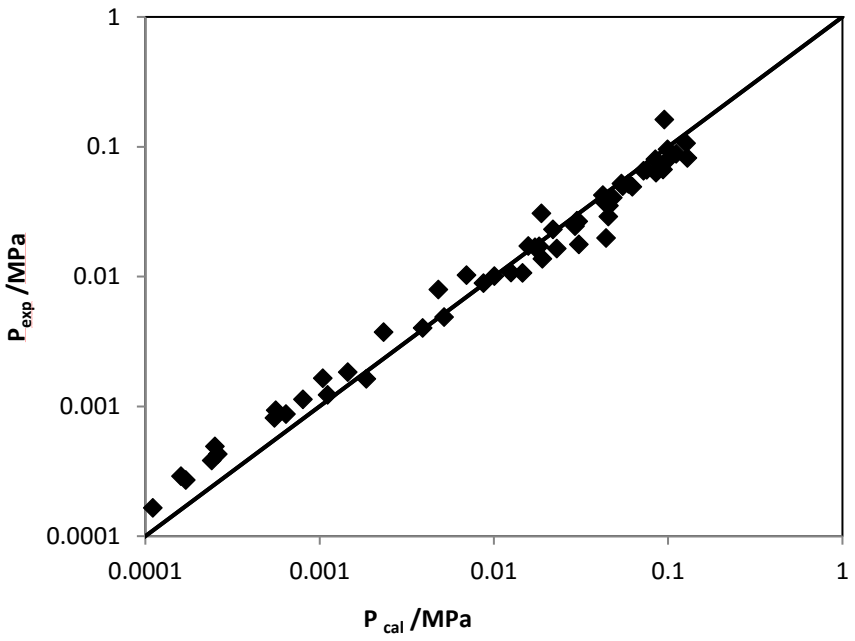

Figure 5-23 Prediction of H_2S partial pressure in a CO_2-H_2S-water-MEA(15 wt%) quaternary system : experimental data from Lee et al. [140]. P=0.001 for student t-test

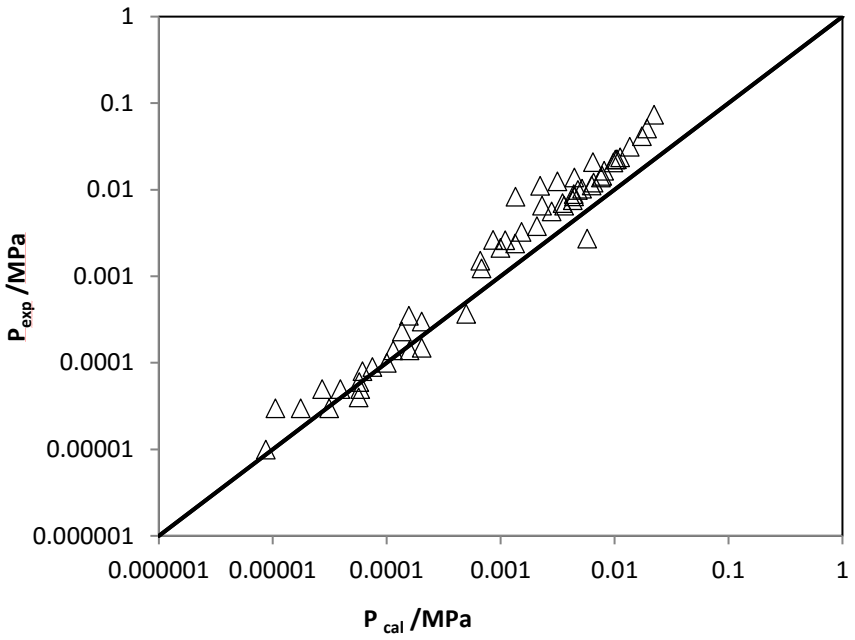

Figure 5-24 Prediction of CO_2 partial pressure in a CO_2-H_2S-water-MEA(15 wt%) quaternary system : experimental data from Lee et al. [140]. P=0.033 for student t-test

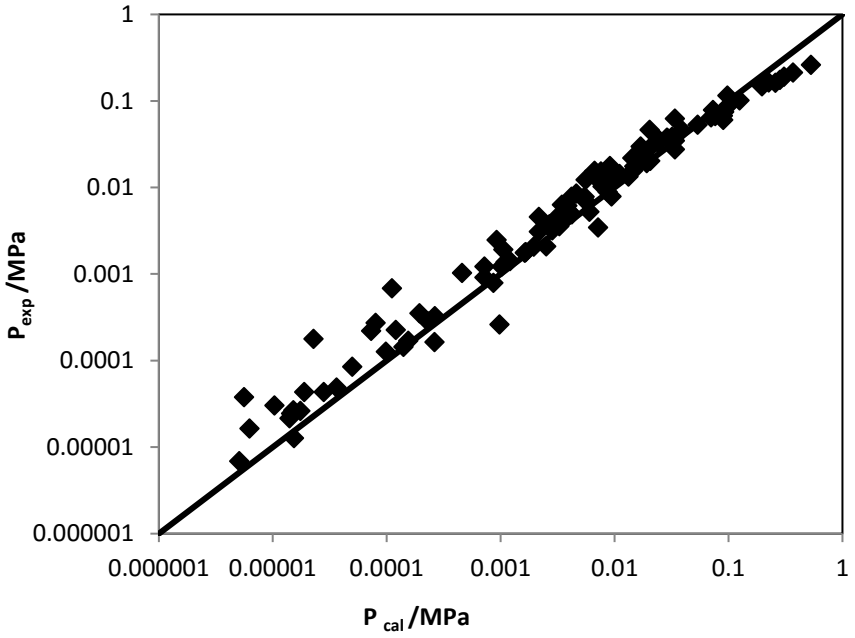

Figure 5-25 Prediction of CO_2 partial pressure in a CO_2-H_2S-water-MDEA(50 wt%) quaternary system : experimental data from Jou et al. [143]. P=0.057 for student t-test

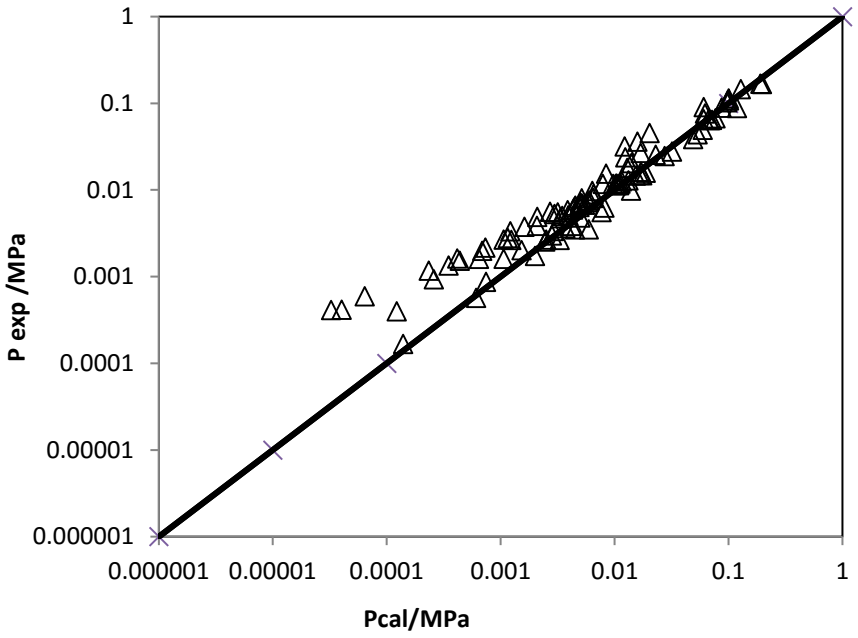

Figure 5-26 Prediction of H_2S partial pressure in a CO_2-H_2S-water-MDEA(50 wt%) quaternary system : experimental data from Jou et al. [143] P=0.073 for student t-test

5.5.3 CO_2-H_2O-MDEA-CH_4 quaternary system

In previous sections, we showed that PR-CPA EoS is able to accurately describe the phase behaviour of CO_2-MDEA-water and CH_4-MDEA-water ternary system. In the context of acid gas removal from natural gas, it is necessary to validate the model with the presence of methane. In this work, CO_2-MDEA-water-CH_4 quaternary system has been chosen. Pure component parameters and binary interaction parameters have the same values that we determined in previous sections.

Since available experimental data in the open literature do not provide any initial global composition (z), it is not possible to predict by using Flash calculation. However, the concentration of MDEA and the solubility of CH_4 and CO_2 are presented [144]. Therefore, prediction has been done by bubble point calculation to compare the vapour phase composition. Table 5-13 summarizes the experimental data from Addicks et al. [144] and the prediction by PR-CPA EoS. It can be seen that the evolution of y_{CO2} has been correctly predicted in function of temperature and CO_2 loading ratio. y_{CO2} is better predicted at higher temperature than at lower temperature. y_{H2O} and y_{MDEA} are also predicted by our model. Due to experimental

equipment limits, water and MDEA compositions in the vapour phase are not available in the open literature; it is not possible to compare the predicted y_{MDEA} and y_{H2O} with experimental data. We have presented renormalized y_{CO2} and y_{CH4} without considering MDEA and water presence in the vapour phase. However, the total pressure is always underestimated; the deviation is about 25 % in general. In fact, the predicted total pressure is very sensible to methane composition in the liquid phase, +1% x_{CH4} can almost lead to +1% total pressure.

Table 5-13 Experimental data [144] and model prediction data for CO_2-MDEA-water-CH_4 quaternary system at 10 MPa with 30 wt % MDEA

T /K	*Pexp /Mpa*	*CO_2 loading ratio*	x_{water}	x_{MDEA}	x_{CO2}	x_{CH4}
313.15	10	0.2586	0.9231	0.0599	0.0154	0.0016
313.15	10	0.6203	0.9035	0.0586	0.0364	0.0015
353.15	10	0.6895	0.9000	0.0584	0.0403	0.0013
353.15	10	0.7713	0.8957	0.0581	0.0448	0.0013
353.15	10	0.8347	0.8926	0.0579	0.0483	0.0012

Pcal /MPa	$y_{water\ cal}$	$y_{MDEA\ cal}$	$y_{CO2\ exp}$	$y_{CO2\ cal}$	$y_{CO2\ cal\ re*}$	$y_{CH4\ exp}$	$y_{CH4\ cal}$	$y_{CH4cal\ re*}$
7.84	0.0011	1.20E-07	0.0011	0.0025	0.0025	0.9989	0.9964	0.9975
7.65	0.0012	4.20E-07	0.0048	0.0122	0.0122	0.9952	0.9866	0.9878
7.29	0.0076	1.10E-05	0.0778	0.0886	0.0893	0.9222	0.9037	0.9106
7.19	0.0079	1.30E-05	0.1056	0.1299	0.1309	0.8944	0.8622	0.8691
7.07	0.0082	1.60E-05	0.1441	0.1825	0.1840	0.8559	0.8093	0.8160

*Renormalized value (neglecting the presence of water and MDEA in the vapour phase)

5.5.4 EM-CO_2-MDEA-water-CH_4 multi-component system

EM-CO_2-MDEA-water-CH_4 multi-component system is chosen as to evaluate the model performance for predicting mercaptan solubility in loaded alkanolamine solution. Experimental data of various mercaptan-CO_2-amine-water-CH_4 has been measured in CTP and are available

in the ongoing GPA research report 142 [145]. Pure component parameters and binary interaction parameters are taken from previous sections.

Table 5-14 summarizes the experimental data and the prediction by PR-CPA EoS. The composition of EM in the vapour phase is accurately predicted, the ARD is 5%. Moreover, the order of magnitude of y_{CO2} is correctly predicted. y_{H2O} and y_{MDEA} are also predicted by our model. Water and MDEA compositions in the vapour phase are not available; we cannot compare the predicted data with experimental ones. We have been renormalized y_{EM}, y_{CO2} and y_{CH4} without considering MDEA and water presence in the vapour phase. Due to the sensibility of methane solubility, the total pressure of EM-CO_2-MDEA-water-CH_4 is underestimated by 30%.

Table 5-14 Experimental data from Boonaert et al. [145] and mode prediction by PR-CPA for EM-CO_2-MDEA-water-CH_4 system at 7 MPa with 25 wt % MDEA

T /K	P_{exp} */MPa*	*CO_2 loading ratio*	x_{H2O}	x_{MDEA}	x_{CO2}	x_{EM}	x_{CH4}
333.35	7.008	0.155	0.944	0.04760	0.00740	0.00030	0.00104
333.35	7.035	0.309	0.937	0.04720	0.01460	0.00027	0.00091
365.12	7.056	0.14	0.944	0.04760	0.00668	0.00026	0.00110
365.12	6.984	0.253	0.939	0.04740	0.01199	0.00025	0.00097

Pcal /MPa	$y_{H2O\ cal}$	$y_{MDEA\ cal}$	$y_{CO2\ exp}$	$y_{CO2\ cal}$	$y_{CO2\ cal\ re\ *}$	$y_{EM\ exp}$	$y_{EM\ cal}$	$y_{EM\ cal\ re\ *}$	$y_{CH4\ exp}$	$y_{CH4\ cal}$	$y_{CH4\ cal\ re\ *}$
4.97	0.0041	3.32E-07	0.0013	0.0040	0.0040	0.0039	0.0041	0.0041	0.9950	0.9870	0.9911
4.03	0.0050	4.81E-07	0.0043	0.0109	0.0110	0.0042	0.0038	0.0038	0.9910	0.9800	0.9849
5.14	0.0137	2.77E-06	0.0067	0.0111	0.0113	0.0045	0.0044	0.0044	0.9890	0.9700	0.9835
4.36	0.0161	3.76E-06	0.0120	0.0256	0.0260	0.0049	0.0044	0.0045	0.9780	0.9530	0.9686

*Renormalized value (neglecting the presence of water and MDEA in the vapour phase)

Conclusion

The asymmetric association scheme for MDEA, temperature dependent k_{ij}, and consideration of solvation effect between CO_2-water with PR-CPA EoS is the best configuration to represent CO_2-MDEA-water ternary system. With optimized parameter fitting from experimental data, different thermodynamic properties such as VLE, liquid phase speciation, enthalpy of absorption, and vapor phase composition have been successfully predicted by PR-CPA EoS. PR-CPA EoS is more accurate than DM model in terms of model accuracy and number of parameters. The PR-CPA EoS has been extended to H_2S-MDEA-H_2O, CO_2-MEA-H_2O, and H_2S-MEA-H_2O ternary systems, we obtained satisfactory results. Different multicomponent systems including CO_2-H_2S-H_2O-CH_4, CO_2-H_2S-MEA-H_2O, CO_2-H_2S-MDEA-H_2O, CO_2-MDEA-H_2O-CH_4 CO_2-MDEA-H_2O-CH_4-EM systems have also been correctly predicted by PR-CPA EoS.

PR-CPA EoS can be extended to other acid gas-amine-water systems, especially for new amine development. Different types of data such as chemical equilibrium constant, mixture liquid density and dielectric constant are not necessarily required by PR-CPA EoS. Because only VLE experimental data concerning acid gas solubility in water, amine-water, and acid gas solubility in aqueous amine are enough to estimate PR-CPA EoS parameters.

The PR-CPA EoS has some limitations, for example, the reactions between acid gases and water have been neglected, and as a result the pH value of the loaded solvent cannot be calculated with present PR-CPA EoS. As a solution, the reactions between acid gases and water can be treated as strong associations by adding dedicated associations sites on water and acid gases. Though we assumed that the electrolytes have no influence on acid gas-water-alkanolamine systems, the PR-CPA EoS is not able to correctly present the phase behaviour of those systems when the loading ratio of acid gas is greater than 1. PR-CPA EoS will be combined with explicit electrolyte terms such as (MSA, Born [52]) to investigate the influence of electrolyte activity.

Conclusion and future work

Conclusion and future work

In this thesis, the phase behaviour of mixtures related to acid gas removal from natural gas has been investigated. The PR-CPA EoS have been applied on non-reactive systems to describe the solubilities of hydrocarbons (including methane, ethane, propane, n-butane, n-pentane, n-hexane, benzene, toluene, and ethyl-benzene) and mercaptans (including methyl mercaptan and ethyl mercaptan) in aqueous MDEA, DEA and MEA solutions in VLE, LLE, and VLLE conditions. Pure compounds parameters of associating compounds are determined by regression from experimental data. The model describes both pure component liquid density and vapour pressure within ARD < 3%. Then, PR-CPA EoS is applied to model phase equilibria of mercaptan-water, alkanolamine-water and hydrocarbons-water binary systems. It shows good agreement for these binaries systems. Experimental data of hydrocarbons/mercaptans in aqueous alkanolamine solutions (solubility) are used to correlate BIPs of corresponding hydrocarbons-alkanolamine and mercaptans-alkanolamines binary systems. With optimized parameters, hydrocarbons and mercaptans solubilities in aqueous alkanolamine solutions are successfully described by the model; the ARDs are under 10% for alkanes, 18% for aromatics and 20% for mercaptans. The temperature of minimum solubility was successfully predicted. Water content was also accurately predicted in VLE conditions (ARDs are less than 12%) but not in LLE conditions. Solubility of two alkanes mixtures in aqueous alkanolamine solutions were studied in this work. The model is able to predict main components solubility (The ARDs are less than 20%)

For reactive systems, in the acid gas-alkanolamine-water ternary systems, electrolyte species are formed after chemical reactions. In this work, the electrolyses are not treated explicitly. The reaction is therefore represented by the incorporation of α sites on CO_2 or H_2S to the e* site which represents the amine site on alkanolamine molecule. Depending on the reaction mechanism, the number of active α sites on acid gas can be equal to one or two. Parameters between acid gas and alkanolamine (temperature dependent BIP, $\beta^{e^*\alpha}$, $\varepsilon^{e^*\alpha}$) have been fitted from CO_2/H_2S-alkanolamine-water ternary systems experimental data. Different configurations concerning association scheme of alkanolamine, temperature dependency of BIP and solvation effect between water and acid gas have been compared with an example of CO_2-MDEA-water ternary system. The asymmetric association scheme for MDEA, temperature dependent k_{ij}, and consideration of solvation effect between CO_2-water with PR-CPA EoS is the best configuration. Using optimized configuration and parameters, the solubility of CO_2/H_2S in aqueous MDEA/MEA solutions were adequately predicted. For CO_2-MDEA-water ternary

system, PR-CPA EoS was compared with the Desmukh–Mather model which is known as a classical model for acid gas treatment. PR-CPA EoS is more accurate than DM model in terms of model accuracy (The ARDs is less than 11% and 19% respectively) and number of parameters. Only BIPs are needed by PR-CPA EoS, however, the DM model requires different types of parameters such as chemical equilibrium constant, dielectric constant, Henry's law constant and adjustable parameters like β_{ij}. With optimized parameter fitted from experimental data, different thermodynamic properties such as VLE, liquid phase speciation, enthalpy of absorption, and vapour phase composition have been successfully predicted by PR-CPA EoS.

The PR-CPA EoS has been validated by comparing with multi-component systems experimental data such as: mixture of hydrocarbons with water-DEA and water-MDEA H_2S-CO_2-water-CH_4, H_2S-CO_2-MDEA-water, H_2S-CO_2-MDEA-water-CH_4, CO_2-MDEA-water-CH_4-EM, CO_2-MDEA-water-CH_4-MM, H_2S-MDEA-water-CH_4-EM, H_2S-MDEA-water-CH_4-MM, CO_2-H_2S-MDEA-water-CH_4-EM, CO_2-H_2S-MDEA-water-CH_4-EM. ARD comparison, or student test are carried out for those systems Overall, the PR-CPA EoS is able to accurately predict the vapour phase composition. MM and EM solubility in aqueous MDEA solution have been measured in this work and successfully predicted by PR-CPA EoS.

As future work, PR-CPA EoS will be applied on other mercaptan (such as n-Propyl Mercaptan and n-Butyl Mercaptan)-water-amine systems with or without the presence of acid gases. Some experimental data concerning those systems are already available in Gas Processor Association research reports. It is interesting to extend the PR-CPA EoS with the pseudo-chemical reaction approach on other existing amines, such as alkyl-amine and other physical absorption amines (such as glycols). Moreover, because of the advantage on the number of parameter compared to other kind of thermodynamic models, it is also interesting to use PR-CPA EoS in new amine development in the context of acid gas treatment.

Thermodynamic models serve process simulation; it is interesting to integrate the PR-CPA EoS into commercial process simulation software such as Aspen and Prosim will allow us to investigate the model performance on the whole acid gas treatment process. Furthermore, chemical reactions in general can be treated as strong association by PR-CPA EoS. PR-CPA EoS is potentially a powerful tool for reactive distillation.

Appendix I calibrations

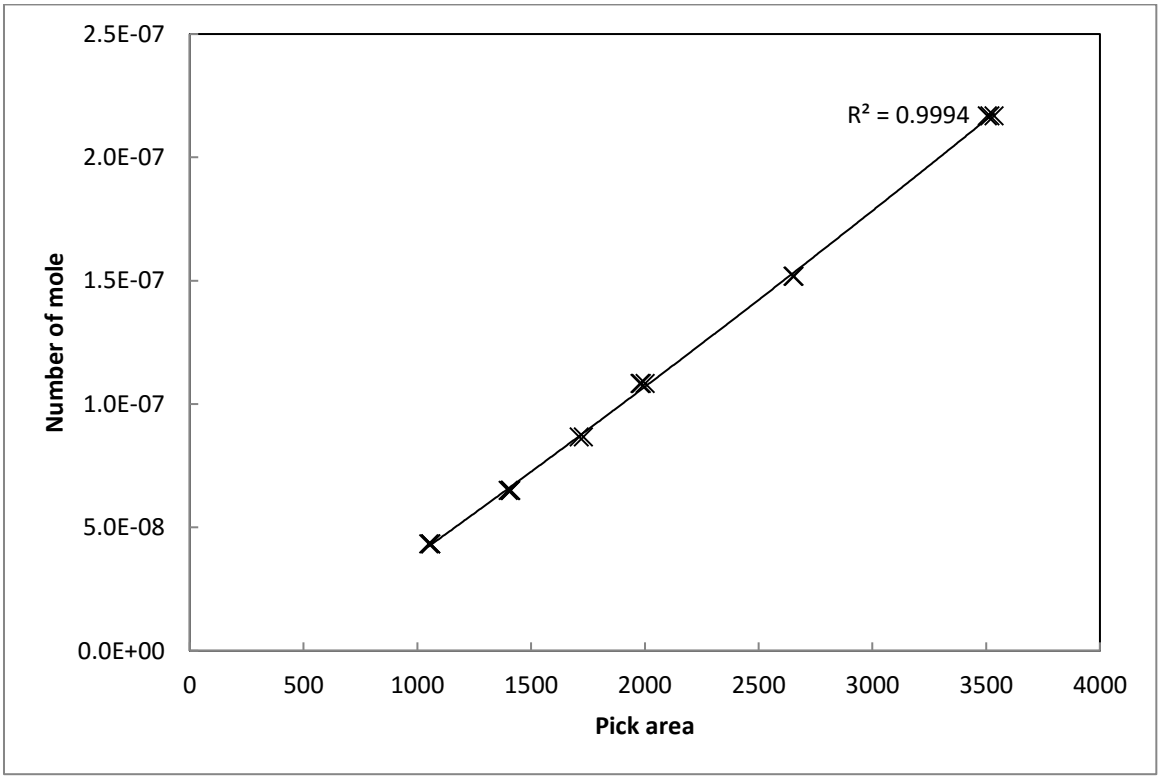

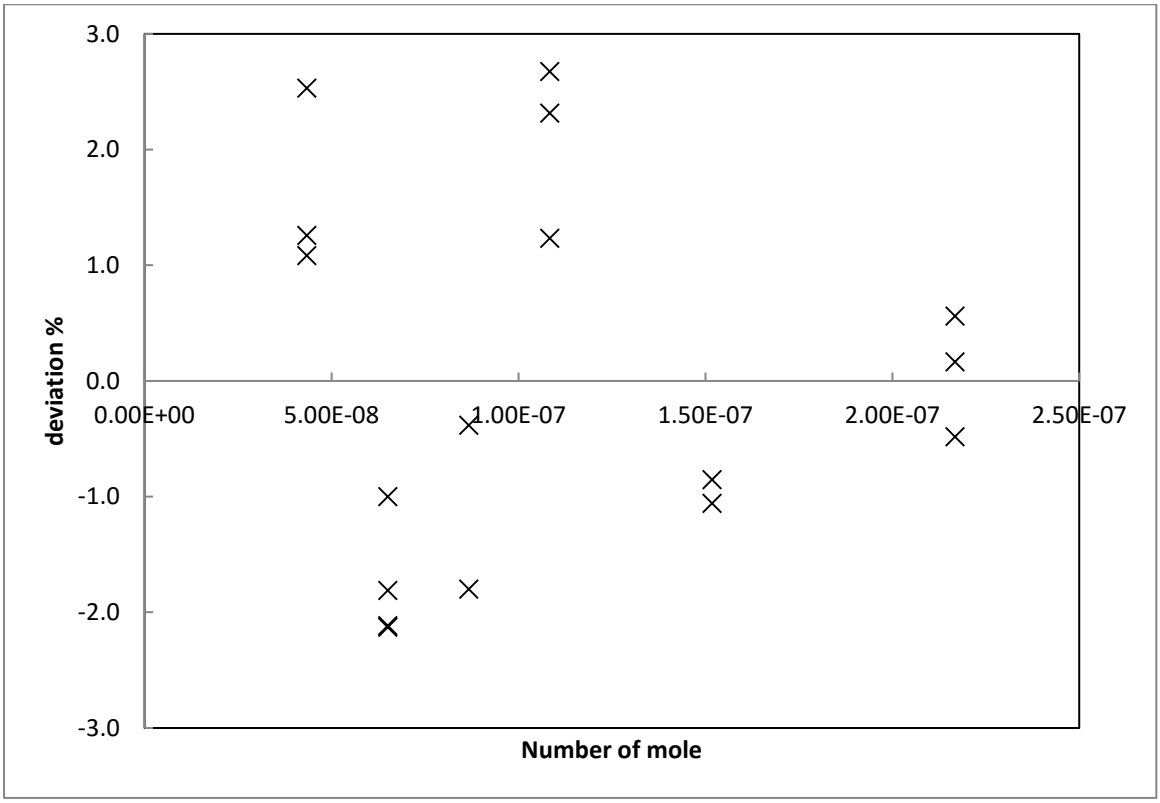

A-0-1 FID calibration and deviation for EM

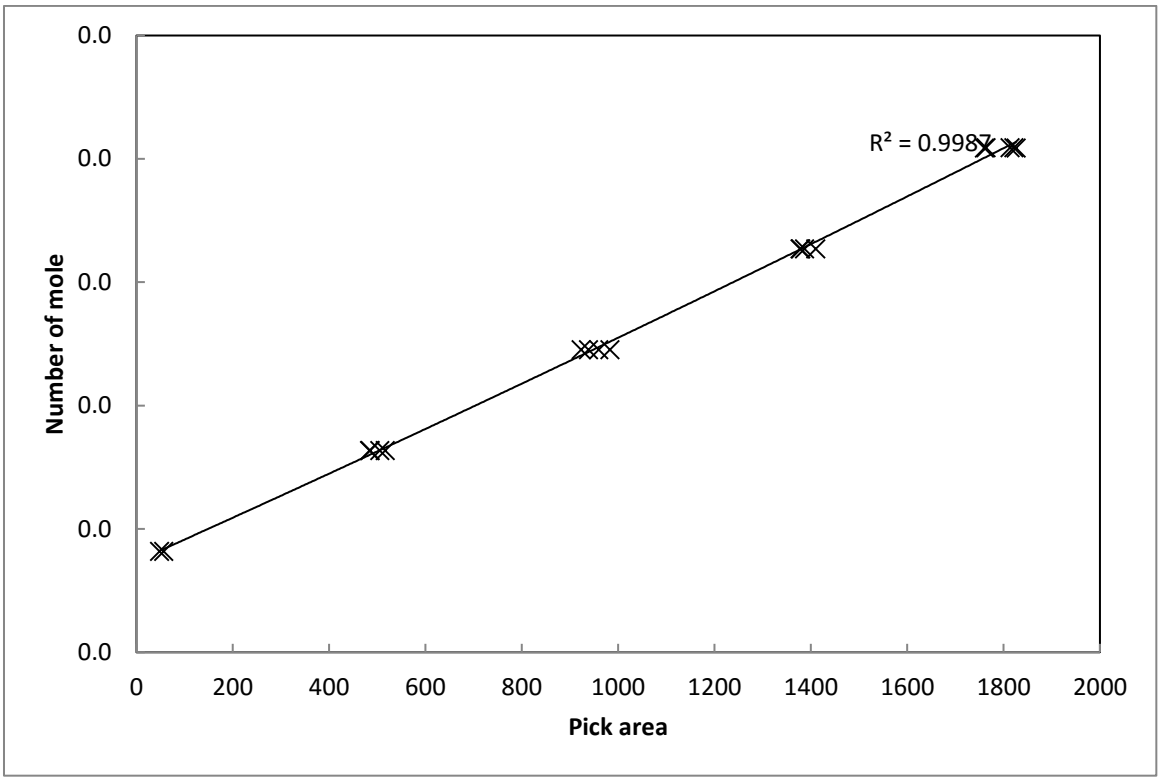

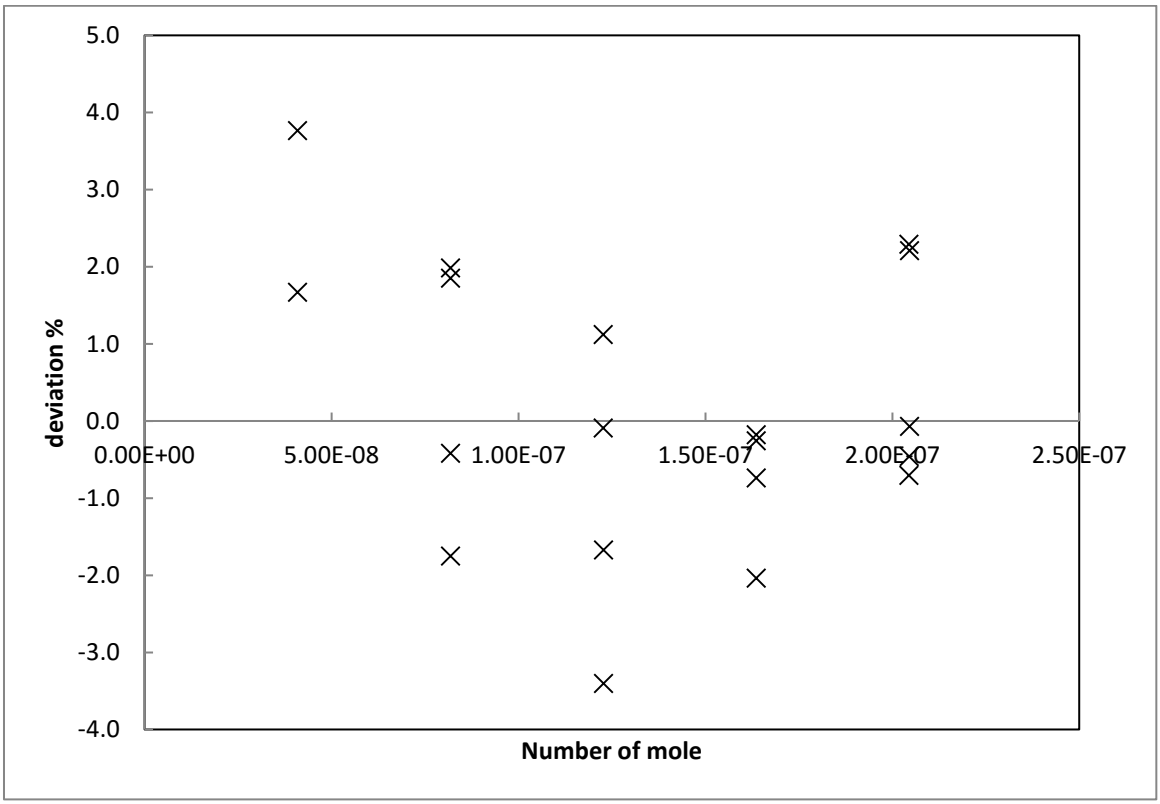

A-0-2 FID calibration and deviation for CH_4

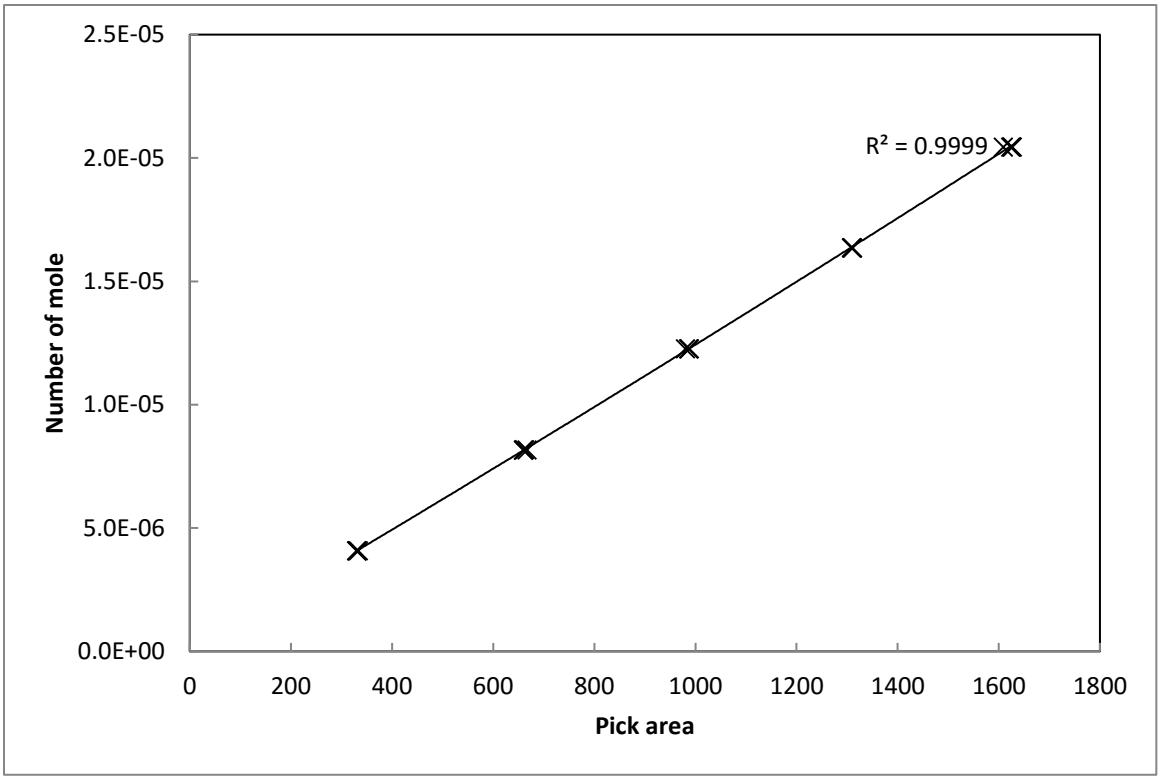

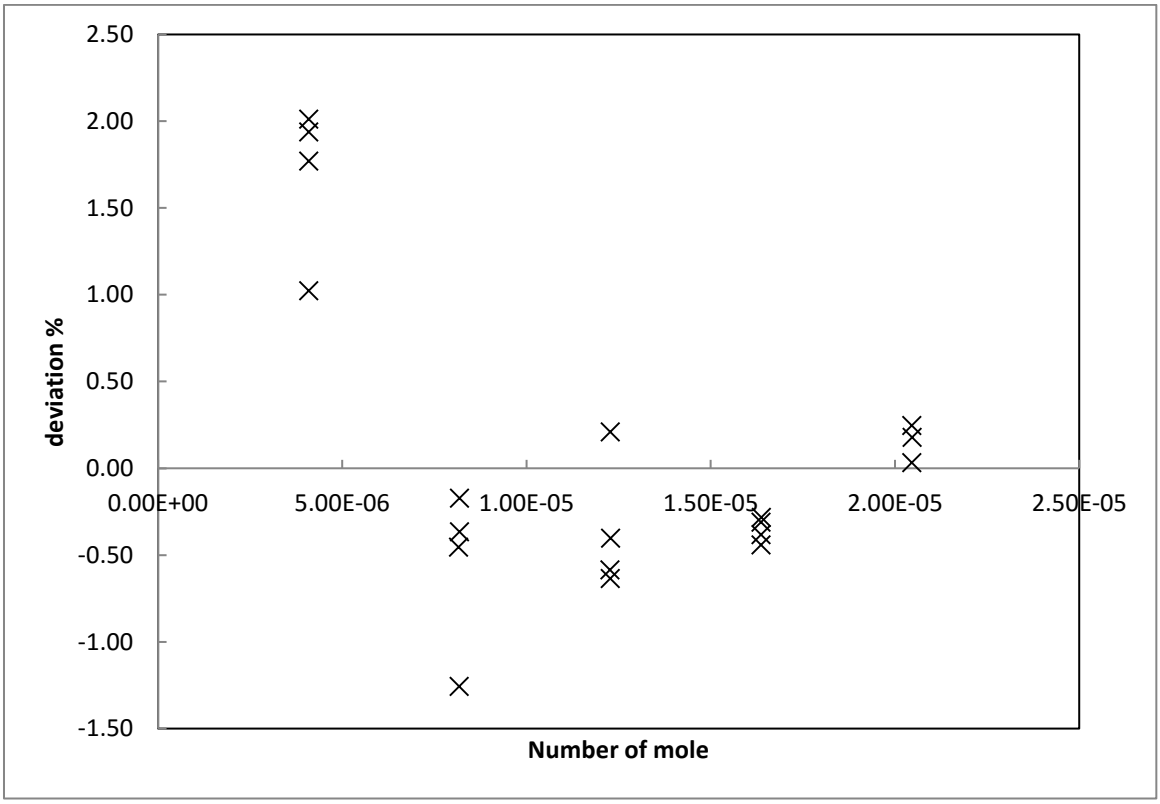

A-0-3 TCD calibration and deviation for CH_4

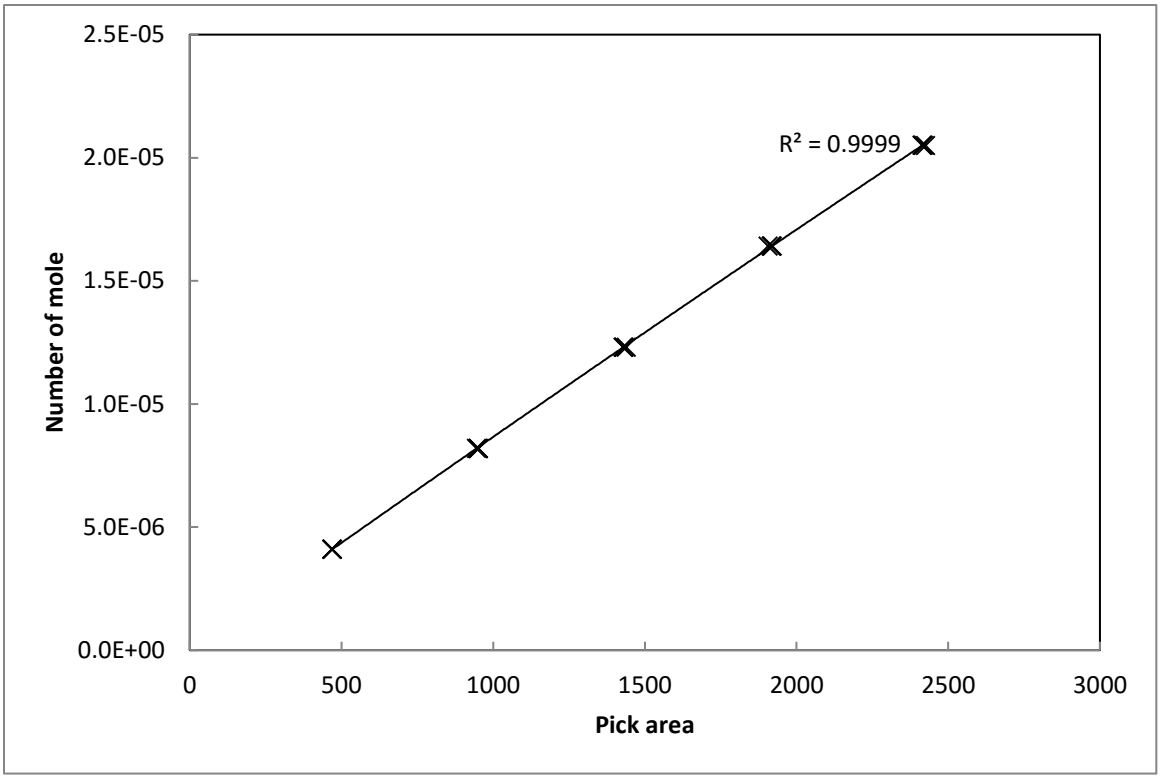

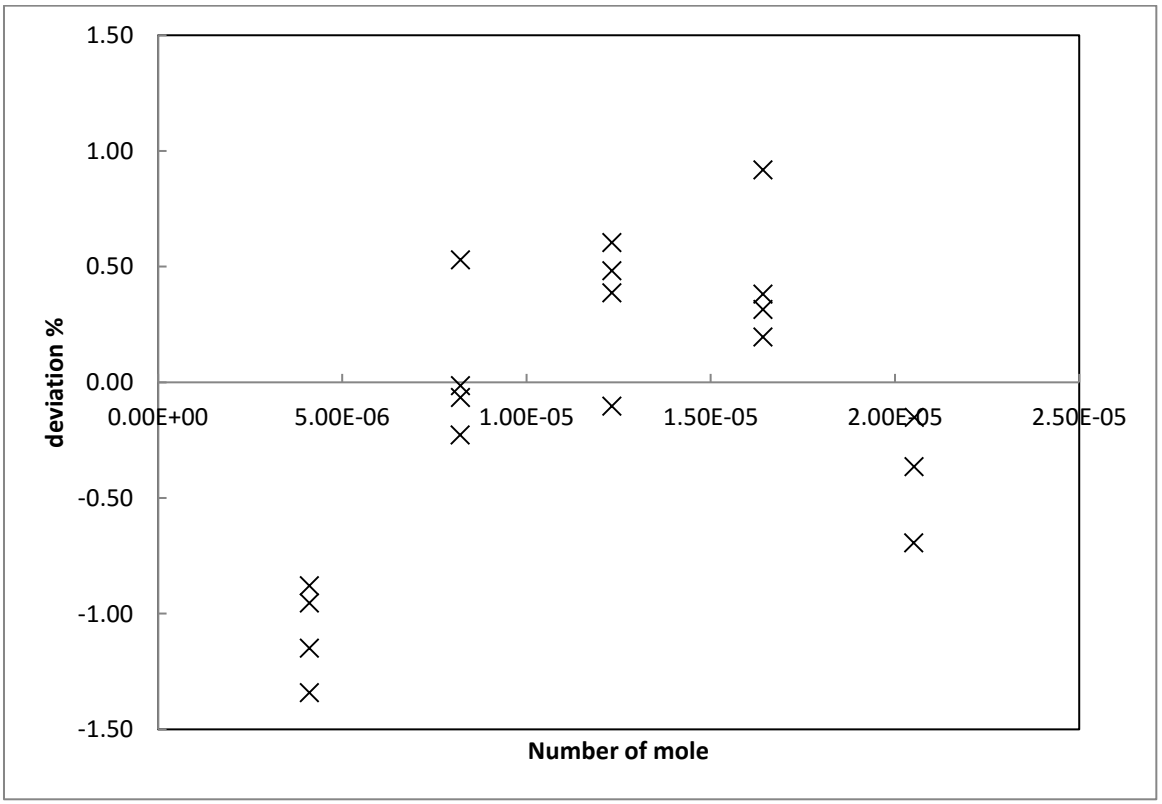

A-0-4 TCD calibration and deviation for MM

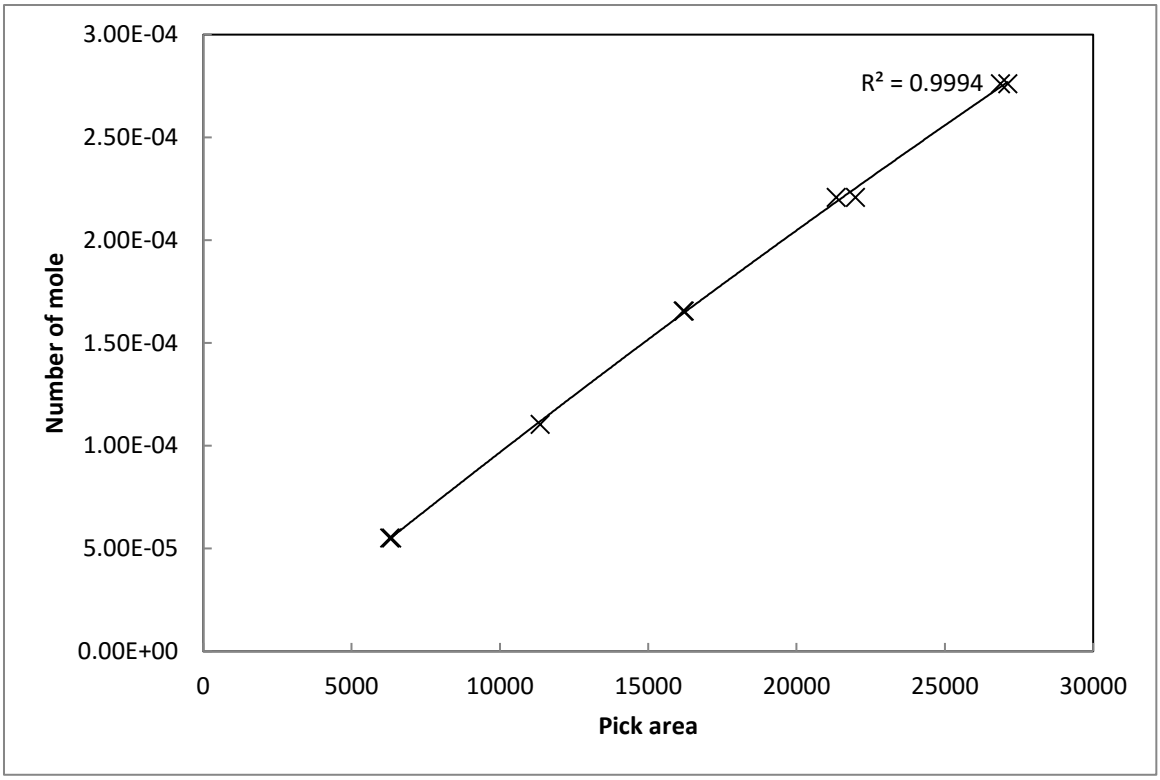

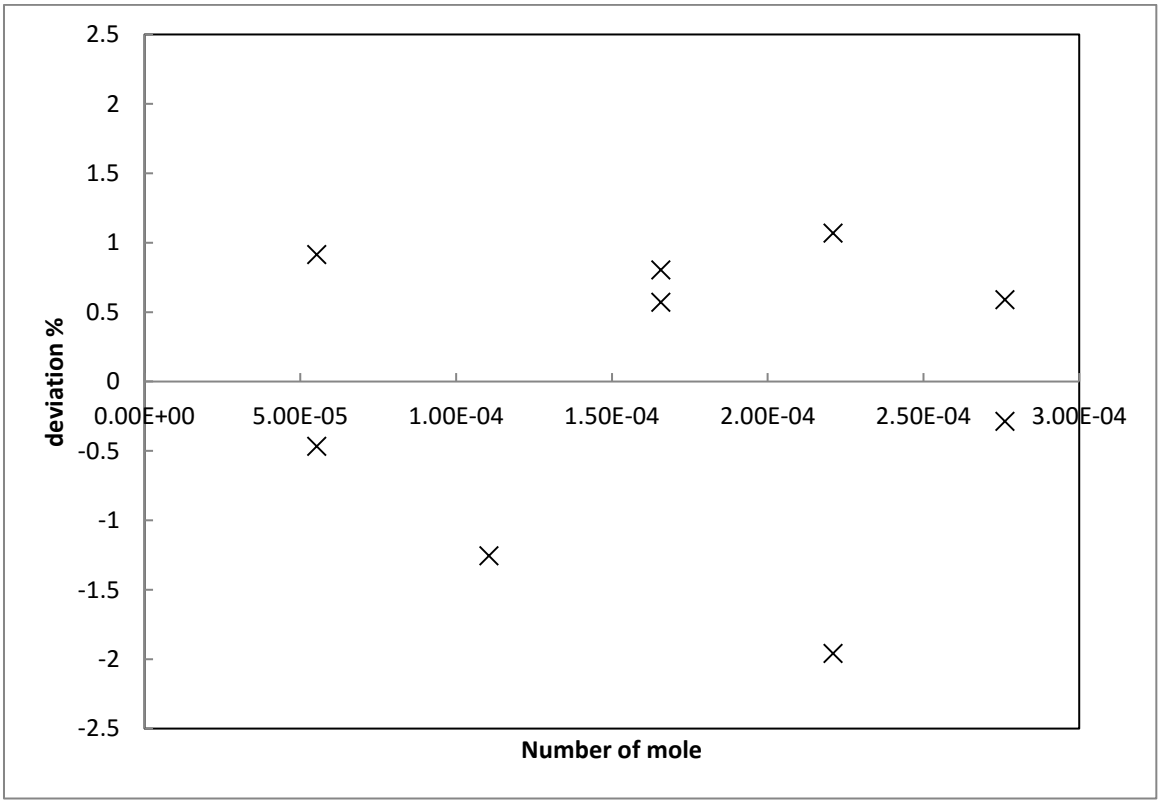

A-0-5 TCD calibration and deviation for water

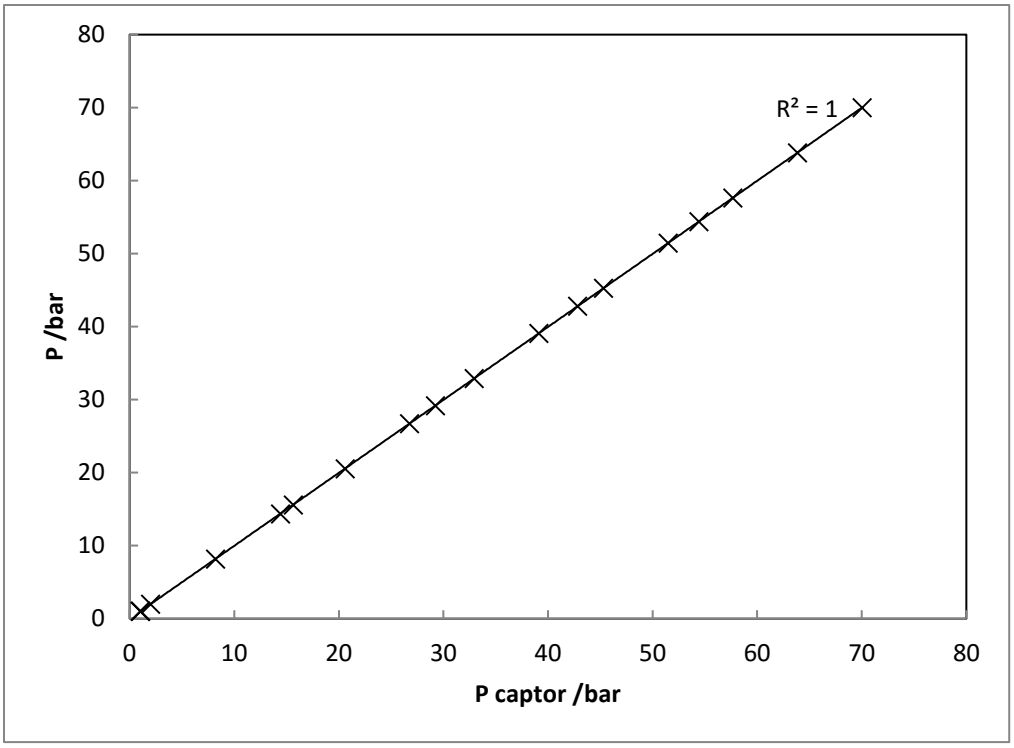

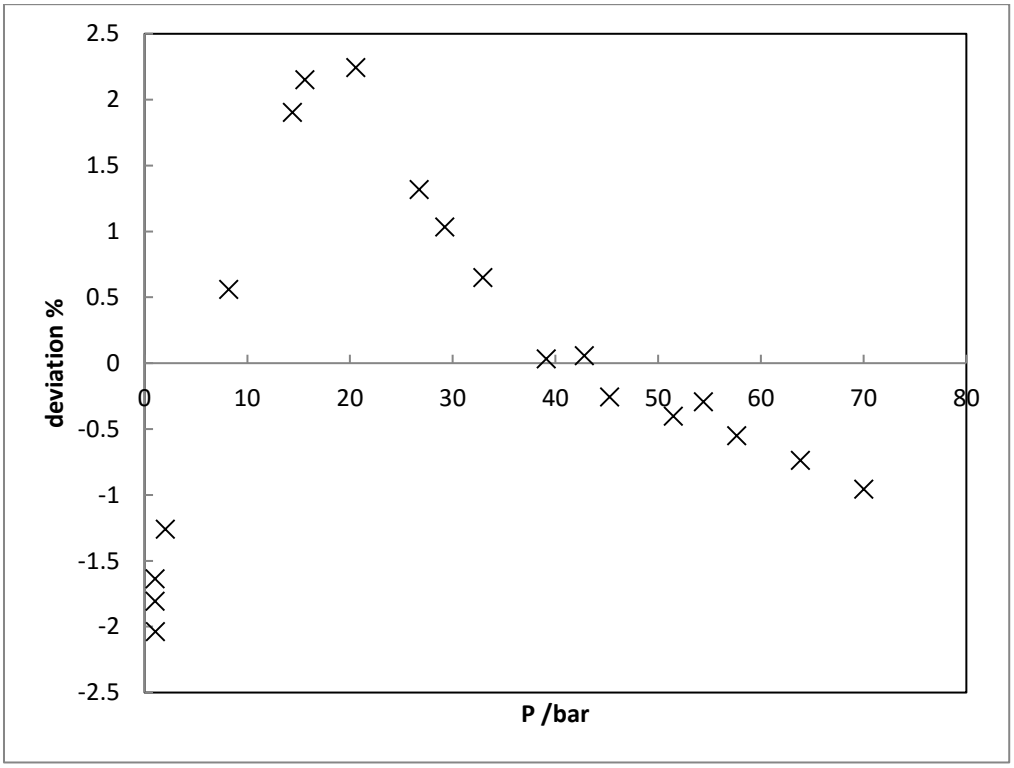

A-0-6 pressure calibration and deviation

Appendix II uncertainty calculation

There are two main sources of uncertainties: uncertainties due to calibration and uncertainty due to repeatability. The uncertainty due to calibration is of Type B. It means that after calibration we do not get directly the uncertainty but the accuracy. A statistic distribution has to be chosen. In term of probability it is common to consider a rectangular statistic distribution. The rectangular distribution is given as $u_{calib}(\theta) = \frac{b}{\sqrt{3}}$. b is defined as the half-width between the upper and lower error limits (so the value of the accuracy). This value is obtained after polynomial regression between value given by the sensor and the reference value. For a normal distribution, ± u encompasses about 68 % of the distribution; for a rectangular distribution, ± u encompasses about 58 % of the distribution.

During an experiment, to determine the value of one quantity (T, P or mole numbers) we have to consider all values acquired. It follows a calculation of average values and standard deviation u. The averaging of repeated readings yields a mean θ_{avg} with a standard deviation u. As before, this can be statistically converted to an uncertainty due to repeatability of the measurements, via:

$$u_{rep}(\theta) = \frac{\delta}{\sqrt{n}} = \sqrt{\frac{1}{n(n-1)}\sum_{i=1}^{n}(\theta_i - \theta_{avg})^2} \qquad \text{(A.1)}$$

where, $\theta_{avg} = \frac{1}{n}\sum_{i=1}^{n}\theta_i$

and n is the number of repeated quantity measurements. A Gaussian type of distribution is the likely behavior here, since the repeated readings are likely to fall close to the mean (with maybe one or two values falling from the mean). This is known as a type A evaluation (systematic uncertainty), where only statistical methods are required to interpret the uncertainty. Eq. (2) presents the combined standard temperature uncertainty, u_c (T).

$$u_c(\theta) = \pm\sqrt{u_{calib}(\theta)^2 + u_{rep}(\theta)^2} \qquad \text{(A.2)}$$

with subscripts calib, rep denoting that of calibration, repeatability.

The determination of the uncertainty of the composition required the uncertainty of each mole numbers. The uncertainty of the mole fraction is determined after calibration of the GC detectors (Equations A.3 and A.4).

$$x_i = \frac{n_i}{\sum_i^{ncomp} n_i} \tag{A.3}$$

$$u(x_i) = \sqrt{\sum_i^{ncomp} \left(\frac{\partial x_i}{\partial n_i} \right)_{i \neq j}^2 u^2(n_i)} \tag{A.4}$$

For example, for a binary system, one can calculate $u(x_1) = x_1(1-x_1)\sqrt{\left(\frac{u(n_1)}{n_1}\right)^2 + \left(\frac{u(n_2)}{n_2}\right)^2}$.

Uncertainty on apparent Henry's law constant can be calculated from uncertainty on mole fraction (both vapor and liquid phases) and uncertainty on pressure. Equation A.5 details the expression.

$$u(H_i) = H_i * \sqrt{\left(\frac{u(P)}{P}\right)^2 + \left(\frac{u(x_i)}{x_i}\right)^2 + \left(\frac{u(y_i)}{y_i}\right)^2} \tag{A.5}$$

Appendix III Chromatograph of COS, CS_2 and CO_2 in aqueous 50 wt% MDEA solution

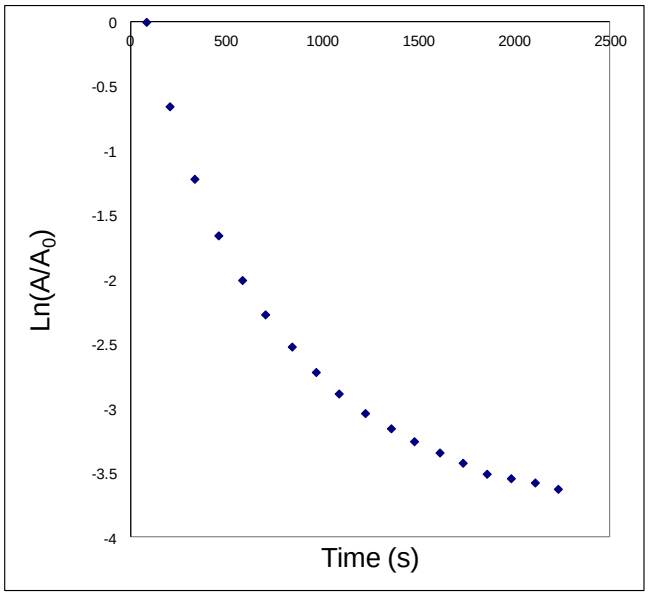

Figure 0-1 Chromatograph solute peak area (A) as a function of time for CS_2 in 50 wt% MDEA aqueous solution at 328 K.

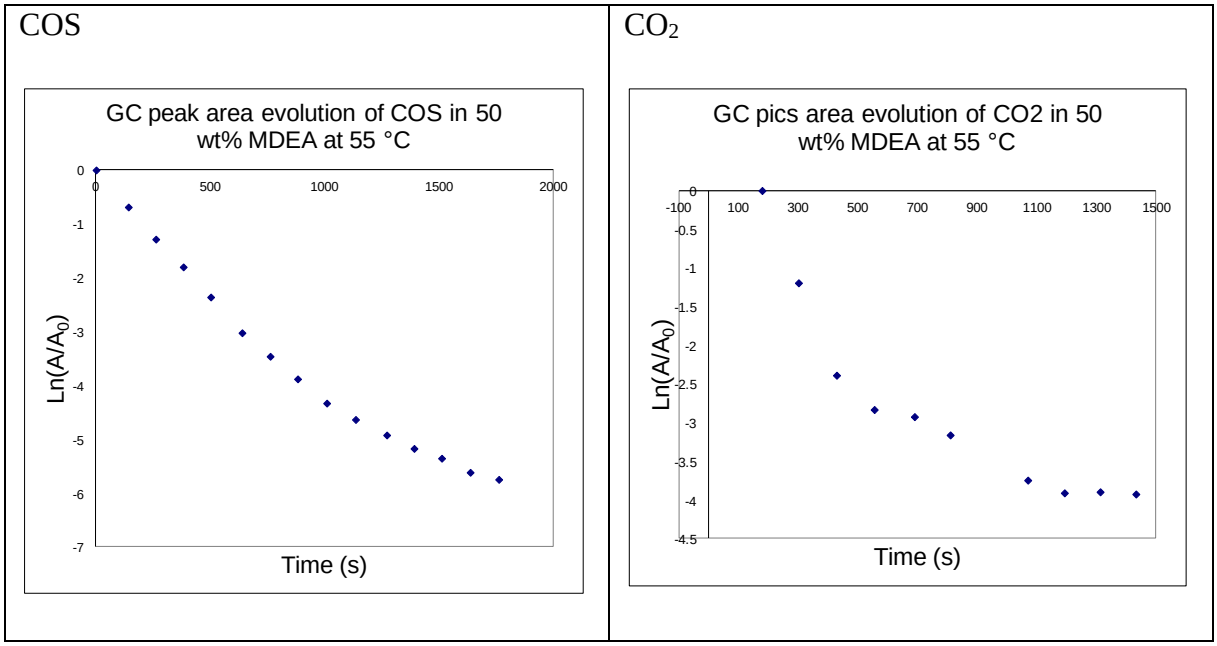

Figure 0-2 Chromatograph solute peak area (A) as a function of time for COS and CO_2 in 50 wt% MDEA aqueous solution at 328 K

Appendix IV List of publication

Published Journal:

T. Wang, E. El Ahmar, C. Coquelet, Alkane solubilities in aqueous alkanolamine solutions with CPA EoS, Fluid Phase Equilibria. 434 (2017) 93–101.

Oral presentation:

T. Wang, **E. El Ahmar**, C. Coquelet, S. Huang, Measurement and modeling of mercaptans solubility in aqueous alkanolamine solutions, 2017 GPA midstream convention 2017, Saint Antonio, USA

T. Wang, E. El Ahmar, C. Coquelet, Thermodynamic aspects for acid gas removal from natural gas, CETCCUS 2017, Clermont Ferrand, France

Poster presentation:

T. Wang, E. El Ahmar, C. Coquelet, Prediction of hydrocarbons solubility in aqueous alkanolamine solution with CPA, PPEPPD 2016, Porto, Portugal

T. Wang, E. El Ahmar, C. Coquelet, G. Kongtogeorgis, Modeling of CO_2-MDEA-water systems using the CPA equation of state with a simplified approach, CERE DTU seminar 2017, Lyngby, Denmark

Reference

[1] How much carbon dioxide is produced when different fuels are burned? - FAQ - U.S. Energy Information Administration (EIA), (n.d.). https://www.eia.gov/tools/faqs/faq.cfm?id=73&t=11 (accessed October 21, 2016).

[2] E. Huguet, B. Coq, R. Durand, C. Leroi, R. Cadours, V. Hulea, A highly efficient process for transforming methyl mercaptan into hydrocarbons and H2S on solid acid catalysts, Appl. Catal. B Environ. 134–135 (2013) 344–348. doi:10.1016/j.apcatb.2013.01.037.

[3] A.L. Kohl, R.B. Nielsen, Chapter 2 - Alkanolamines for Hydrogen Sulfide and Carbon Dioxide Removal, in: Gas Purif. Fifth Ed., Gulf Professional Publishing, Houston, 1997: pp. 40–186. http://www.sciencedirect.com/science/article/pii/B9780884152200500021 (accessed August 1, 2016).

[4] Christophe Coquelet, Javeed A. Awan, Eric Boonaert, Alain Valtz, Pascal Theveneau, Dominique Richon, Vapor-Liquid Equilibrium Studies of Organic Sulfur Species in MDEA, DEA Aqueous Solutions, GPSA Houst. (2012).

[5] M. Krummen, D. Gruber, J. Gmehling, Measurement of Activity Coefficients at Infinite Dilution in Solvent Mixtures Using the Dilutor Technique, Ind. Eng. Chem. Res. 39 (2000) 2114–2123. doi:10.1021/ie990830p.

[6] R.D. Deshmukh, A.E. Mather, A mathematical model for equilibrium solubility of hydrogen sulfide and carbon dioxide in aqueous alkanolamine solutions, Chem. Eng. Sci. 36 (1981) 355–362. doi:10.1016/0009-2509(81)85015-4.

[7] Statistical Review of World Energy | Energy economics | BP Global, Bp.Com. (n.d.). http://www.bp.com/en/global/corporate/energy-economics/statistical-review-of-world-energy.html (accessed November 1, 2016).

[8] Natural Gas - U.S. Energy Information Administration (EIA), (n.d.). https://www.eia.gov/naturalgas/ (accessed November 1, 2016).

[9] B. Guo, A. Ghalambor, Chapter 2 - Properties of Natural Gas, in: Nat. Gas Eng. Handb. Second Ed., Gulf Publishing Company, 2005: pp. 13–33. doi:10.1016/B978-1-933762-41-8.50009-5.

[10] W.F.J. Burgers, P.S. Northrop, H.S. Kheshgi, J.A. Valencia, Worldwide development potential for sour gas, Energy Procedia. 4 (2011) 2178–2184. doi:10.1016/j.egypro.2011.02.104.

[11] What are natural gas liquids and how are they used? - Today in Energy - U.S. Energy Information Administration (EIA), (n.d.). https://www.eia.gov/todayinenergy/detail.php?id=5930 (accessed October 9, 2017).

[12] Natural-gas processing, Wikipedia. (2017). https://en.wikipedia.org/w/index.php?title=Natural-gas_processing&oldid=799116006 (accessed October 9, 2017).

[13] G.P. Association, others, GPSA engineering data book, Gas Process. Suppliers Assoc. Tulsa OK. (1998).

[14] Process for separating a binary gaseous mixture by adsorption, n.d. http://www.google.com/patents/US3155468 (accessed July 21, 2017).

[15] S. Sridhar, B. Smitha, T.M. Aminabhavi, Separation of Carbon Dioxide from Natural Gas Mixtures through Polymeric Membranes—A Review, Sep. Purif. Rev. 36 (2007) 113–174. doi:10.1080/15422110601165967.

[16] H.P. Hsieh, Inorganic Membranes for Separation and Reaction, Elsevier, 1996.

[17] J. Gale, H. Herzog, J. Braitsch, P.S. Northrop, J.A. Valencia, Greenhouse Gas Control Technologies 9The CFZ^{TM} process: A cryogenic method for handling high- CO2 and H2S gas reserves and facilitating geosequestration of CO2 and acid gases, Energy Procedia. 1 (2009) 171–177. doi:10.1016/j.egypro.2009.01.025.
[18] B. Burr, L. Lyddon, A comparison of physical solvents for acid gas removal, in: 87th Annu. Gas Process. Assoc. Conv. Grapevine TX March, 2008: pp. 2–5. https://www.bre.com/PDF/A-Comparison-of-Physical-Solvents-for-Acid-Gas-Removal-REVISED.pdf (accessed July 21, 2017).
[19] J.E. Johnson, A.C.J. Homme, Selexol solvent process reduces lean, high-CO2 natural gas treating costs, Energy Prog. 4 (1984) 241–248.
[20] A. Henni, P. Tontiwachwuthikul, A. Chakma, Solubilities of Carbon Dioxide in Polyethylene Glycol Ethers, Can. J. Chem. Eng. 83 (2005) 358–361. doi:10.1002/cjce.5450830224.
[21] M. Okutsu, T. Kitsuki, Process for the preparation of glycerol carbonate, US6495703 B1, 2002. http://www.google.ch/patents/US6495703 (accessed October 9, 2017).
[22] A.L. Kohl, R. Nielsen, Gas Purification, Gulf Professional Publishing, 1997.
[23] G.T. Rochelle, J. Cullinane, Polyamine/alkali salt blends for carbon dioxide removal from gas streams, US8070856 B2, 2011. http://www.google.ch/patents/US8070856 (accessed July 21, 2017).
[24] N. Sadegh, Acid Gas Removal from Natural Gas with Alkanolamines, Technical University of Denmark, 2013.
[25] M. Bolhàr-Nordenkampf, A. Friedl, U. Koss, T. Tork, Modelling selective H2S absorption and desorption in an aqueous MDEA-solution using a rate-based non-equilibrium approach, Chem. Eng. Process. Process Intensif. 43 (2004) 701–715. doi:10.1016/S0255-2701(03)00011-4.
[26] B. Shimekit, H. Mukhtar, Natural gas purification technologies-major advances for CO2 separation and future directions, INTECH Open Access Publisher Croatia, Europe, 2012. http://cdn.intechopen.com/pdfs/35293.pdf (accessed April 3, 2017).
[27] F. Closmann, T. Nguyen, G.T. Rochelle, MDEA/Piperazine as a solvent for CO2 capture, Energy Procedia. 1 (2009) 1351–1357. doi:10.1016/j.egypro.2009.01.177.
[28] W.M. Budzianowski, Energy Efficient Solvents for CO2 Capture by Gas-Liquid Absorption: Compounds, Blends and Advanced Solvent Systems, Springer, 2016.
[29] Removal of CO2 and H2S Using Aqueous Alkanolamine Solusions | Amine | Carbon Dioxide, Scribd. (n.d.). https://www.scribd.com/document/253420556/Removal-of-CO2-and-H2S-Using-Aqueous-Alkanolamine-Solusions (accessed March 6, 2018).
[30] S.B. Fredriksen, K.-J. Jens, Oxidative Degradation of Aqueous Amine Solutions of MEA, AMP, MDEA, Pz: A Review, Energy Procedia. 37 (2013) 1770–1777. doi:10.1016/j.egypro.2013.06.053.
[31] M.S. Islam, R. Yusoff, B.S. Ali, M.N. Islam, M.H. Chakrabarti, Degradation studies of amines and alkanolamines during sour gas treatment process, Int. J. Phys. Sci. 6 (2011) 5877–5890.
[32] M.S. DuPart, T.R. Bacon, D.J. Edwards, Understanding corrosion in alkanolamine gas treating plants, Part 2, Hydrocarb. Process. 72 (1993) 89.
[33] R. Taylor, R. Krishna, H. Kooijman, Real world modeling of distillation, Chem. Eng. Prog. 99 (2003) 28–39.
[34] E.V. Murphree, Rectifying Column Calculations., Ind. Eng. Chem. 17 (1925) 747–750. doi:10.1021/ie50187a044.
[35] M. Saimpert, G. Puxty, S. Qureshi, L. Wardhaugh, A. Cousins, A new rate based absorber and desorber modelling tool, Chem. Eng. Sci. 96 (2013) 10–25. doi:10.1016/j.ces.2013.03.013.

[36] Christophe Coquelet, Javeed A. Awan, E. Boonaert, Alain Valtz, Pascal Théveneau, Dominique Richon, VAPOR-LIQUID EQUILIBRIUM STUDIES OF ORGANIC SULFUR SPECIES IN MDEA, DEA AQUEOUS SOLUTIONS, GPA Res. Rep. (2010).
[37] P. Guilbot, A. Valtz, H. Legendre, D. Richon, Rapid on-line sampler-injector: a reliable tool for HT-HP sampling and on-line GC analysis, Analusis. 28 (2000) 426–431. doi:10.1051/analusis:2000128.
[38] S. Mokraoui, M.K. Hadj-Kali, A. Valtz, D. Richon, New Vapor–Liquid–Liquid Equilibrium Data for Ethane and Propane in Alkanolamine Aqueous Solutions, J. Chem. Eng. Data. 58 (2013) 2100–2109. doi:10.1021/je400340s.
[39] R.M. Zin, C. Coquelet, A. Valtz, M.I.A. Mutalib, K.M. Sabil, Measurement of Henry's Law constant and infinite dilution activity coefficient of isopropyl mercaptan and isobutyl mercaptan in (methyldiethanolamine (1) + water (2)) with w1 = 0.25 and 0.50 at temperature of (298 to 348) K using inert gas stripping method, J. Chem. Thermodyn. 93 (2016) 193–199. doi:10.1016/j.jct.2015.10.005.
[40] N. Mac Dowell, F. Llovell, C.S. Adjiman, G. Jackson, A. Galindo, Modeling the Fluid Phase Behavior of Carbon Dioxide in Aqueous Solutions of Monoethanolamine Using Transferable Parameters with the SAFT-VR Approach, Ind. Eng. Chem. Res. 49 (2010) 1883–1899. doi:10.1021/ie901014t.
[41] H. Renon, J.M. Prausnitz, Local compositions in thermodynamic excess functions for liquid mixtures, AIChE J. 14 (1968) 135–144. doi:10.1002/aic.690140124.
[42] A. Fredenslund, R.L. Jones, J.M. Prausnitz, Group-contribution estimation of activity coefficients in nonideal liquid mixtures, AIChE J. 21 (1975) 1086–1099. doi:10.1002/aic.690210607.
[43] I.R. Krichevsky, J.S. Kasarnovsky, Thermodynamical Calculations of Solubilities of Nitrogen and Hydrogen in Water at High Pressures, J. Am. Chem. Soc. 57 (1935) 2168–2171. doi:10.1021/ja01314a036.
[44] D.-Y. Peng, D.B. Robinson, A New Two-Constant Equation of State, Ind. Eng. Chem. Fundam. 15 (1976) 59–64. doi:10.1021/i160057a011.
[45] G. Soave, Equilibrium constants from a modified Redlich-Kwong equation of state, Chem. Eng. Sci. 27 (1972) 1197–1203. doi:10.1016/0009-2509(72)80096-4.
[46] J.-F. Bonnans, J.C. Gilbert, C. Lemaréchal, C.A. Sagastizábal, Numerical optimization: theoretical and practical aspects, Springer Science & Business Media, 2006. http://books.google.com/books?hl=en&lr=&id=88X5vN3ybvgC&oi=fnd&pg=PA3&dq=info:tBvcaJpsOKwJ:scholar.google.com&ots=J3914jg5q2&sig=TSTQC_lO__6SmkFyD04HEHOSMrU (accessed September 21, 2017).
[47] M.L. Michelsen, The isothermal flash problem. Part I. Stability, Fluid Phase Equilibria. 9 (1982) 1–19. doi:10.1016/0378-3812(82)85001-2.
[48] M.L. Posey, G.T. Rochelle, A Thermodynamic Model of Methyldiethanolamine−CO2−H2S−Water, Ind. Eng. Chem. Res. 36 (1997) 3944–3953. doi:10.1021/ie970140q.
[49] R.L. Kent, B. Elsenberg, BETTER DATA FOR AMINE TREATING., Hydrocarb. Process. 55 (1976) 87–90.
[50] C. ‐C. Chen, H.I. Britt, J.F. Boston, L.B. Evans, Local composition model for excess Gibbs energy of electrolyte systems. Part I: Single solvent, single completely dissociated electrolyte systems, AIChE J. 28 (1982) 588–596. doi:10.1002/aic.690280410.
[51] K. Thomsen, P. Rasmussen, Modeling of vapor-liquid-solid equilibrium in gas-aqueous electrolyte systems, Chem. Eng. Sci. 54 (1999) 1787–1802. doi:10.1016/S0009-2509(99)00019-6.
[52] W. Fürst, H. Renon, Representation of excess properties of electrolyte solutions using a new equation of state, AIChE J. 39 (1993) 335–343. doi:10.1002/aic.690390213.

[53] S. Ma'mun, J.P. Jakobsen, H.F. Svendsen, O. Juliussen, Experimental and Modeling Study of the Solubility of Carbon Dioxide in Aqueous 30 Mass % 2-((2-Aminoethyl)amino)ethanol Solution, Ind. Eng. Chem. Res. 45 (2006) 2505–2512. doi:10.1021/ie0505209.
[54] R.H. Weiland, T. Chakravarty, A.E. Mather, Solubility of carbon dioxide and hydrogen sulfide in aqueous alkanolamines, Ind. Eng. Chem. Res. 32 (1993) 1419–1430. doi:10.1021/ie00019a016.
[55] M.Z. Haji-Sulaiman, M.K. Aroua, Equilibrium of CO2 in aqueous diethanolamine (DEA) and Amino Methyl Propanol (AMP) solutions, Chem. Eng. Commun. 140 (1996) 157–171.
[56] A. Benamor, M.K. Aroua, Modeling of CO2 solubility and carbamate concentration in DEA, MDEA and their mixtures using the Deshmukh–Mather model, Fluid Phase Equilibria. 231 (2005) 150–162. doi:10.1016/j.fluid.2005.02.005.
[57] M. Dicko, C. Coquelet, C. Jarne, S. Northrop, D. Richon, Acid gases partial pressures above a 50 wt% aqueous methyldiethanolamine solution: Experimental work and modeling, Fluid Phase Equilibria. 289 (2010) 99–109. doi:10.1016/j.fluid.2009.11.012.
[58] E. Hückel, Zur Theorie der Elektrolyte, in: Ergeb. Exakten Naturwissenschaften, Springer, Berlin, Heidelberg, 1924: pp. 199–276. doi:10.1007/978-3-642-94260-0_9.
[59] A.D. MacGillivray, Upper Bounds on Solutions of the Poisson—Boltzmann Equation near the Limit of Infinite Dilution, J. Chem. Phys. 56 (1972) 80–83. doi:10.1063/1.1676941.
[60] B. Maribo-Mogensen, G.M. Kontogeorgis, K. Thomsen, Comparison of the Debye–Hückel and the Mean Spherical Approximation Theories for Electrolyte Solutions, Ind. Eng. Chem. Res. 51 (2012) 5353–5363. doi:10.1021/ie2029943.
[61] A.A. Maryott, E.R. Smith, Table of dielectric constants of pure liquids, U.S. Govt. Print. Off., 1951.
[62] M.S. Wertheim, Fluids with highly directional attractive forces. I. Statistical thermodynamics, J. Stat. Phys. 35 (1984) 19–34. doi:10.1007/BF01017362.
[63] W.G. Chapman, K.E. Gubbins, G. Jackson, M. Radosz, SAFT: Equation-of-state solution model for associating fluids, Fluid Phase Equilibria. 52 (1989) 31–38. doi:10.1016/0378-3812(89)80308-5.
[64] G.M. Kontogeorgis, E.C. Voutsas, I.V. Yakoumis, D.P. Tassios, An Equation of State for Associating Fluids, Ind. Eng. Chem. Res. 35 (1996) 4310–4318. doi:10.1021/ie9600203.
[65] M. Hajiw, A. Chapoy, C. Coquelet, Hydrocarbons – water phase equilibria using the CPA equation of state with a group contribution method, Can. J. Chem. Eng. 93 (2015) 432–442. doi:10.1002/cjce.22093.
[66] Frenkel, M.; Chirico, R. D.; Diky, V. V.; Yan, X.; Dong, Q.; Muzny,, C., NIST ThermoData Engine, NIST Standard Reference Database 103, Version 1.0; National Institute of Standards and Technology, Standard Reference Data Program: Gaithersburg, MD, 2004., (n.d.).
[67] S.H. Huang, M. Radosz, Equation of state for small, large, polydisperse, and associating molecules, Ind. Eng. Chem. Res. 29 (1990) 2284–2294. doi:10.1021/ie00107a014.
[68] G.M. Kontogeorgis, I. V. Yakoumis, H. Meijer, E. Hendriks, T. Moorwood, Multicomponent phase equilibrium calculations for water–methanol–alkane mixtures, Fluid Phase Equilibria. 158–160 (1999) 201–209. doi:10.1016/S0378-3812(99)00060-6.
[69] A.S. Avlund, D.K. Eriksen, G.M. Kontogeorgis, M.L. Michelsen, Application of association models to mixtures containing alkanolamines, 20 Years SAFT Equ. StateRecent Adv. ChallengesSymposium. 306 (2011) 31–37. doi:10.1016/j.fluid.2011.02.005.

[70] A.S. Avlund, G.M. Kontogeorgis, M.L. Michelsen, Modeling Systems Containing Alkanolamines with the CPA Equation of State, Ind. Eng. Chem. Res. 47 (2008) 7441–7446. doi:10.1021/ie800040g.
[71] Carbon Dioxide, (n.d.). https://cnx.org/contents/zRIF4Y7d@2/Carbon-Dioxide (accessed October 13, 2017).
[72] C.V. Brand, J. Rodríguez, A. Galindo, G. Jackson, C.S. Adjiman, Validation of an absorber model of carbon dioxide capture in an aqueous amine solvent developed based on the SAFT-VR framework, in: I.A.K. and R. Srinivasan (Ed.), Comput. Aided Chem. Eng., Elsevier, 2012: pp. 930–934. doi:10.1016/B978-0-444-59506-5.50017-1.
[73] N. Mac Dowell, F.E. Pereira, F. Llovell, F.J. Blas, C.S. Adjiman, G. Jackson, A. Galindo, Transferable SAFT-VR Models for the Calculation of the Fluid Phase Equilibria in Reactive Mixtures of Carbon Dioxide, Water, and n-Alkylamines in the Context of Carbon Capture, J. Phys. Chem. B. 115 (2011) 8155–8168. doi:10.1021/jp107467s.
[74] C.V. Brand, E. Graham, J. Rodríguez, A. Galindo, G. Jackson, C.S. Adjiman, On the use of molecular-based thermodynamic models to assess the performance of solvents for CO2 capture processes: monoethanolamine solutions, Faraday Discuss. 192 (2016) 337–390. doi:10.1039/C6FD00041J.
[75] I. Tsivintzelis, G.M. Kontogeorgis, M.L. Michelsen, E.H. Stenby, Modeling phase equilibria for acid gas mixtures using the CPA equation of state. Part II: Binary mixtures with CO2, Fluid Phase Equilibria. 306 (2011) 38–56. doi:10.1016/j.fluid.2011.02.006.
[76] I. Kim, H.F. Svendsen, E. Børresen, Ebulliometric Determination of Vapor−Liquid Equilibria for Pure Water, Monoethanolamine, N-Methyldiethanolamine, 3-(Methylamino)-propylamine, and Their Binary and Ternary Solutions, J. Chem. Eng. Data. 53 (2008) 2521–2531. doi:10.1021/je800290k.
[77] S. Xu, S. Qing, Z. Zhen, C. Zhang, J.J. Carroll, Vapor pressure measurements of aqueous N-methyldiethanolamine solutions, Fluid Phase Equilibria. 67 (1991) 197–201. doi:10.1016/0378-3812(91)90055-C.
[78] E. Voutsas, A. Vrachnos, K. Magoulas, Measurement and thermodynamic modeling of the phase equilibrium of aqueous N-methyldiethanolamine solutions, Fluid Phase Equilibria. 224 (2004) 193–197. doi:10.1016/j.fluid.2004.05.012.
[79] C. Dell'Era, P. Uusi-Kyyny, E.-L. Rautama, M. Pakkanen, V. Alopaeus, Thermodynamics of aqueous solutions of methyldiethanolamine and diisopropanolamine, Fluid Phase Equilibria. 299 (2010) 51–59. doi:10.1016/j.fluid.2010.08.026.
[80] S. Horstmann, P. Mougin, F. Lecomte, K. Fischer, J. Gmehling, Phase Equilibrium and Excess Enthalpy Data for the System Methanol + 2,2'-Diethanolamine + Water, J. Chem. Eng. Data. 47 (2002) 1496–1501. doi:10.1021/je020085e.
[81] Z. Cai, R. Xie, Z. Wu, Binary Isobaric Vapor−Liquid Equilibria of Ethanolamines + Water, J. Chem. Eng. Data. 41 (1996) 1101–1103. doi:10.1021/je960118o.
[82] J.-L. Lenard, R.W. Rousseau, A.S. Teja, Vapor-Liquid Equilibria for Mixtures of 2-aminoethanol+ water, AIChE Symp. Ser. 86 (1990) 1–5.
[83] K. Tochigi, K. Akimoto, K. Ochi, F. Liu, Y. Kawase, Isothermal Vapor−Liquid Equilibria for Water + 2-Aminoethanol + Dimethyl Sulfoxide and Its Constituent Three Binary Systems, J. Chem. Eng. Data. 44 (1999) 588–590. doi:10.1021/je980068i.
[84] M. Hajiw, Hydrate Mitigation in Sour and Acid Gases, phdthesis, Ecole Nationale Supérieure des Mines de Paris, 2014. https://pastel.archives-ouvertes.fr/tel-01139496/document (accessed August 29, 2016).
[85] M.B. Oliveira, J.A.P. Coutinho, A.J. Queimada, Mutual solubilities of hydrocarbons and water with the CPA EoS, Fluid Phase Equilibria. 258 (2007) 58–66. doi:10.1016/j.fluid.2007.05.023.

[86] J. Gao, D.-Q. Zheng, T.-M. Guo, Solubilities of Methane, Nitrogen, Carbon Dioxide, and a Natural Gas Mixture in Aqueous Sodium Bicarbonate Solutions under High Pressure and Elevated Temperature, J. Chem. Eng. Data. 42 (1997) 69–73. doi:10.1021/je960275n.
[87] Y. Wang, B. Han, H. Yan, R. Liu, Thermal Measurements, A Selection of Papers Presented at the International and III Sino-Japanese Symposium on Thermal MeasurementsSolubility of CH4 in the mixed solvent t-butyl alcohol and water, Thermochim. Acta. 253 (1995) 327–334. doi:10.1016/0040-6031(94)02011-C.
[88] S. Mao, Z. Zhang, J. Hu, R. Sun, Z. Duan, An accurate model for calculating C2H6 solubility in pure water and aqueous NaCl solutions, Fluid Phase Equilibria. 238 (2005) 77–86. doi:10.1016/j.fluid.2005.09.014.
[89] A. Chapoy, C. Coquelet, D. Richon, Measurement of the Water Solubility in the Gas Phase of the Ethane + Water Binary System near Hydrate Forming Conditions, J. Chem. Eng. Data. 48 (2003) 957–966. doi:10.1021/je0202230.
[90] R. Kobayashi, D. Katz, Vapor-Liquid Equilibria For Binary Hydrocarbon-Water Systems, Ind. Eng. Chem. 45 (1953) 440–446. doi:10.1021/ie50518a051.
[91] A. Chapoy, S. Mokraoui, A. Valtz, D. Richon, A.H. Mohammadi, B. Tohidi, Solubility measurement and modeling for the system propane–water from 277.62 to 368.16 K, Fluid Phase Equilibria. 226 (2004) 213–220. doi:10.1016/j.fluid.2004.08.040.
[92] J.G. Le Breton, J.J. McKetta Jr, Low-pressure solubility of n-butane in water, Hydrocarb Proc Petr Ref. 43 (1964) 136–138.
[93] F.-Y. Jou, J.J. Carroll, A.E. Mather, F.D. Otto, Phase equilibria in the system n-butane-water-methyldiethanolamine, Proc. Seventh Int. Conf. Fluid Prop. Phase Equilibria Chem. Process Des. 116 (1996) 407–413. doi:10.1016/0378-3812(95)02912-5.
[94] S. Mokraoui, C. Coquelet, A. Valtz, P.E. Hegel, D. Richon, New Solubility Data of Hydrocarbons in Water and Modeling Concerning Vapor−Liquid−Liquid Binary Systems, Ind. Eng. Chem. Res. 46 (2007) 9257–9262. doi:10.1021/ie070858y.
[95] L.C. Price, Aqueous Solubility of Petroleum as Applied to Its Origin and Primary Migration, AAPG Bull. 60 (1976) 213–244.
[96] Gillespie, Wilson, Gas Process. Assoc. RR-48. (1982).
[97] C. Marche, C. Ferronato, J. Jose, Solubilities of n-Alkanes (C6 to C8) in Water from 30 °C to 180 °C, J. Chem. Eng. Data. 48 (2003) 967–971. doi:10.1021/je025659u.
[98] F.-Y. Jou, A.E. Mather, Solubility of Methane in Methyldiethanolamine, J. Chem. Eng. Data. 51 (2006) 1429–1430. doi:10.1021/je060118g.
[99] S. Mokraoui, A. Valtz, C. Coquelet, D. Richon, Mutual solubility of hydrocarbons and amines, GPA Res. Rep. (2007).
[100] E. Alhseinat, R. Danon, C. Peters, F. Banat, Solubility of Hexane in Aqueous Solutions of Methyldiethanolamine, J. Chem. Eng. Data. (2015). doi:10.1021/acs.jced.5b00240.
[101] J.J. Carroll, F.-Y. Jou, A.E. Mather, F.D. Otto, The solubility of methane in aqueous solutions of monoethanolamine, diethanolamine and triethanolamine, Can. J. Chem. Eng. 76 (1998) 945–951. doi:10.1002/cjce.5450760512.
[102] F.-Y. Jou, J.J. Carroll, A.E. Mather, F.D. Otto, Solubility of Methane and Ethane in Aqueous Solutions of Methyldiethanolamine, J. Chem. Eng. Data. 43 (1998) 781–784. doi:10.1021/je980003f.
[103] K.A.G. Schmidt, F.-Y. Jou, A.E. Mather, Solubility of Methane in an Aqueous Methyldiethanolamine Solution (Mass Fraction 50 %), J. Chem. Eng. Data. 53 (2008) 1725–1727. doi:10.1021/je700734p.
[104] J.D. Lawson, A.W. Garst, Hydrocarbon gas solubility in sweetening solutions: methane and ethane in aqueous monoethanolamine and diethanolamine, J. Chem. Eng. Data. 21 (1976) 30–32. doi:10.1021/je60068a011.

[105] F.-Y. Jou, A.E. Mather, Solubility of Ethane in Aqueous Solutions of Monoethanolamine and Diethanolamine, J. Chem. Eng. Data. 51 (2006) 1141–1143. doi:10.1021/je060031v.
[106] F.-Y. Jou, H.-J. Ng, J.E. Critchfield, A.E. Mather, Solubility of propane in aqueous alkanolamine solutions, Proc. Ninth Int. Conf. Prop. Phase Equilibria Prod. Process Des. 194–197 (2002) 825–830. doi:10.1016/S0378-3812(01)00647-1.
[107] J.J. Carroll, F.-Y. Jou, A.E. Mather, F.D. Otto, Phase equilibria in the system water-methyldiethanolamine-propane, AIChE J. 38 (1992) 511–520. doi:10.1002/aic.690380405.
[108] J. Critchfield, Hydrocarbon/water and hydrocarbon/ aqueous amine, Mutual Solubilities, (n.d.) TP-29, August 2003, Gas Processors Association, Tulsa, Ok.
[109] S.T. Blanco, I. Velasco, E. Rauzy, S. Otín, Water dew points of binary nitrogen+water and propane+water mixtures. Measurement and correlation, Fluid Phase Equilibria. 161 (1999) 107–117. doi:10.1016/S0378-3812(99)00164-8.
[110] G. Gao, J.-L. Daridon, H. Saint-Guirons, P. Xans, F. Montel, A simple correlation to evaluate binary interaction parameters of the Peng-Robinson equation of state: binary light hydrocarbon systems, Fluid Phase Equilibria. 74 (1992) 85–93. doi:10.1016/0378-3812(92)85054-C.
[111] J.L. Gustin, H. Renon, Heats of mixing of binary mixtures of N-methylpyrrolidinone, ethanolamine, n-heptane, cyclohexane, and benzene by differential flow calorimetry, J. Chem. Eng. Data. 18 (1973) 164–166. doi:10.1021/je60057a022.
[112] A. Valtz, P. Guilbot, D. Richon, Amine BTEX solubility, GPA Res. Rep. (2002).
[113] F.-Y. Jou, A.E. Mather, Liquid−Liquid Equilibria for Binary Mixtures of Water + Benzene, Water + Toluene, and Water + p-Xylene from 273 K to 458 K, J. Chem. Eng. Data. 48 (2003) 750–752. doi:10.1021/je034033g.
[114] C. Coquelet, A. Valtz, D. Richon, Solubility of ethylbenzene and xylene in pure water and aqueous alkanolamine solutions, J. Chem. Thermodyn. 40 (2008) 942–948. doi:10.1016/j.jct.2008.01.021.
[115] L. Peng, Q. Wang, B. Shen, C. Chen, Z. Xiong, Liquid–Liquid Equilibrium for the Ternary System Water + Ethylbenzene + Acetophenone and Water + Ethylbenzene + 1-Phenylethanol, J. Chem. Eng. Data. 59 (2014) 4090–4098. doi:10.1021/je500726x.
[116] A. Valtz, C. Coquelet, D. Richon, Solubility data for toluene in various aqueous alkanolamine solutions, J. Chem. Thermodyn. 39 (2007) 426–432. doi:10.1016/j.jct.2006.07.027.
[117] A. Valtz, C. Coquelet, D. Richon, Solubility data for benzene in aqueous solutions of methyldiethanolamine (MDEA) and of diglycolamine (DGA), Thermochim. Acta. 443 (2006) 245–250. doi:10.1016/j.tca.2006.01.012.
[118] J.A. Awan, I. Tsivintzelis, C. Coquelet, G.M. Kontogeorgis, Phase Equilibria of Three Binary Mixtures: Methanethiol + Methane, Methanethiol + Nitrogen, and Methanethiol + Carbon Dioxide, J. Chem. Eng. Data. 57 (2012) 896–901. doi:10.1021/je2011049.
[119] J.A. Awan, I. Tsivintzelis, M.P. Breil, C. Coquelet, D. Richon, G.M. Kontogeorgis, Phase Equilibria of Mixtures Containing Organic Sulfur Species (OSS) and Water/Hydrocarbons: VLE Measurements and Modeling Using the Cubic-Plus-Association Equation of State, Ind. Eng. Chem. Res. 49 (2010) 12718–12725. doi:10.1021/ie101470b.
[120] P. Gillespie, G. Wilson, Sufur Compounds and Water VLE and Mutual Solubility MESH-H2O; ETSH-H2O; CS2-H2O; and COS-H2O, GPA Res. Rep. (1984).
[121] F.-Y. Jou, A.E. Mather, Phase Equilibria and Kinetics of Sulfur Species-Hydrocarbon-Aqueous Amine Systems, GPA Res. Rep. (1998).
[122] J. Rodriguez, N.M. Dowell, F. Llovell, C.S. Adjiman, G. Jackson, A. Galindo, Modelling the fluid phase behaviour of aqueous mixtures of multifunctional alkanolamines and

carbon dioxide using transferable parameters with the SAFT-VR approach, Mol. Phys. 110 (2012) 1325–1348. doi:10.1080/00268976.2012.665504.
[123] A. Valtz, A. Chapoy, C. Coquelet, P. Paricaud, D. Richon, Vapour–liquid equilibria in the carbon dioxide–water system, measurement and modelling from 278.2 to 318.2 K, Fluid Phase Equilibria. 226 (2004) 333–344. doi:10.1016/j.fluid.2004.10.013.
[124] F. Lucile, P. Cézac, F. Contamine, J.-P. Serin, D. Houssin, P. Arpentinier, Solubility of Carbon Dioxide in Water and Aqueous Solution Containing Sodium Hydroxide at Temperatures from (293.15 to 393.15) K and Pressure up to 5 MPa: Experimental Measurements, J. Chem. Eng. Data. 57 (2012) 784–789. doi:10.1021/je200991x.
[125] L.W. Diamond, N.N. Akinfiev, Solubility of CO2 in water from −1.5 to 100 °C and from 0.1 to 100 MPa: evaluation of literature data and thermodynamic modelling, Fluid Phase Equilibria. 208 (2003) 265–290. doi:10.1016/S0378-3812(03)00041-4.
[126] G. Kuranov, B. Rumpf, N.A. Smirnova, G. Maurer, Solubility of Single Gases Carbon Dioxide and Hydrogen Sulfide in Aqueous Solutions of N-Methyldiethanolamine in the Temperature Range 313−413 K at Pressures up to 5 MPa, Ind. Eng. Chem. Res. 35 (1996) 1959–1966. doi:10.1021/ie950538r.
[127] R. Sidi-Boumedine, S. Horstmann, K. Fischer, E. Provost, W. Fürst, J. Gmehling, Experimental determination of carbon dioxide solubility data in aqueous alkanolamine solutions, Fluid Phase Equilibria. 218 (2004) 85–94. doi:10.1016/j.fluid.2003.11.014.
[128] J.P. Jakobsen, J. Krane, H.F. Svendsen, Liquid-Phase Composition Determination in CO2−H2O−Alkanolamine Systems: An NMR Study, Ind. Eng. Chem. Res. 44 (2005) 9894–9903. doi:10.1021/ie048813+.
[129] Y.E. Kim, J.A. Lim, S.K. Jeong, Y.I. Yoon, S.T. Bae, S.C. Nam, Comparison of Carbon Dioxide Absorption in Aqueous MEA, DEA, TEA, and AMP Solutions, Bull. Korean Chem. Soc. 34 (2013) 783–787. doi:10.5012/bkcs.2013.34.3.783.
[130] M. Gupta, E.F. da Silva, A. Hartono, H.F. Svendsen, Theoretical study of differential enthalpy of absorption of CO2 with MEA and MDEA as a function of temperature, J. Phys. Chem. B. 117 (2013) 9457–9468. doi:10.1021/jp404356e.
[131] I. Tsivintzelis, G.M. Kontogeorgis, M.L. Michelsen, E.H. Stenby, Modeling phase equilibria for acid gas mixtures using the CPA equation of state. I. Mixtures with H2S, AIChE J. 56 (2010) 2965–2982. doi:10.1002/aic.12207.
[132] J.I. Lee, A.E. Mather, Solubility of Hydrogen Sulfide in Water. Ber. Bunsen-Ges, Physical, 1977.
[133] F.T. Selleck, L.T. Carmichael, B.H. Sage, Phase Behavior in the Hydrogen Sulfide-Water System, Ind. Eng. Chem. 44 (1952) 2219–2226. doi:10.1021/ie50513a064.
[134] A.M. Bhairi, Experimental Equilibrium Between Acid Gases and Ethanolamine Solutions, (1984). https://shareok.org/handle/11244/18756 (accessed May 16, 2017).
[135] F.-Y. Jou, J.J. Carroll, A.E. Mather, F.D. Otto, The solubility of carbon dioxide and hydrogen sulfide in a 35 wt% aqueous solution of methyldiethanolamine, Can. J. Chem. Eng. 71 (1993) 264–268. doi:10.1002/cjce.5450710213.
[136] F.-Y. Jou, A.E. Mather, F.D. Otto, The solubility of CO2 in a 30 mass percent monoethanolamine solution, Can. J. Chem. Eng. 73 (1995) 140–147. doi:10.1002/cjce.5450730116.
[137] W. Böttinger, M. Maiwald, H. Hasse, Online NMR spectroscopic study of species distribution in MEA–H2O–CO2 and DEA–H2O–CO2, Fluid Phase Equilibria. 263 (2008) 131–143. doi:10.1016/j.fluid.2007.09.017.
[138] M.D. Hilliard, A predictive thermodynamic model for an aqueous blend of potassium carbonate, piperazine, and monoethanolamine for carbon dioxide capture from flue gas, Thesis, 2008. https://repositories.lib.utexas.edu/handle/2152/3900 (accessed June 21, 2017).

[139] C. Brand, CO2 capture using monoethanolamine solutions : development and validation of a process model based on the SAFT-VR equation of state, (2013). http://spiral.imperial.ac.uk/handle/10044/1/18081 (accessed July 5, 2017).
[140] J.I. Lee, F.D. Otto, A.E. Mather, The solubility of H2S and CO2 in aqueous monoethanolamine solutions, Can. J. Chem. Eng. 52 (1974) 803–805. doi:10.1002/cjce.5450520617.
[141] S.S.-S. Huang, A.-D. Leu, H.-J. Ng, D.B. Robinson, The phase behavior of two mixtures of methane, carbon dioxide, hydrogen sulfide, and water, Fluid Phase Equilibria. 19 (1985) 21–32. doi:10.1016/0378-3812(85)85033-0.
[142] Cubic-plus-association equation of state for water-containing mixtures: Is "cross association" necessary? - Li - 2009 - AIChE Journal - Wiley Online Library, (n.d.). http://onlinelibrary.wiley.com/doi/10.1002/aic.11784/pdf (accessed March 25, 2015).
[143] F.-Y. Jou, F.D. Otto, A.E. Mather, The solubility of mixtures of H2S and CO2 in an mdea solution, Can. J. Chem. Eng. 75 (1997) 1138–1141. doi:10.1002/cjce.5450750618.
[144] J. Addicks, G.A. Owren, A.O. Fredheim, K. Tangvik, Solubility of Carbon Dioxide and Methane in Aqueous Methyldiethanolamine Solutions, J. Chem. Eng. Data. 47 (2002) 855–860. doi:10.1021/je010292z.
[145] Eric Boonaert, Alain Valtz, Tianyuan Wang, Elise El Ahmar, Christophe Coquelet, GPA Proj. (2016).

Résumé

Parmi les combustibles fossiles, le gaz naturel est le plus propre, en termes d'émissions de CO2, d'efficacité énergétique et de quantité de polluants atmosphériques émis. Le méthane est l'élément principal du gaz naturel; néanmoins, il contient des quantités considérables de gaz acides (CO2, H2S) qui peuvent entraîner la corrosion des équipements et des pipelines si de l'eau est présente. Les mercaptans sont d'autres composés soufrés présents dans le gaz naturel dont combustion peut produire du SO2 qui est un produit chimique indésirables causant des problèmes environnementaux. Les gaz acides et les mercaptans doivent être retirés du gaz naturel jusqu'à une norme acceptable. Le gaz naturel traité contient jusqu'à 2% de CO2, 2-4 ppm de H2S et 5-30 ppm de mercaptans. L'absorption chimique avec des solvants aqueuses comportant des alcanolamines [3] (comme la monoéthanolamine (MEA), la diéthanolamine (DEA), la méthyldiéthanolamine (MDEA)) est la méthode la plus bien malteuse pour séparer les gaz acides du gaz naturel. Les gaz acides réagissent selon une réaction acide base dans l'absorbeur pour former des espèces électrolytes. Les mercaptans et les hydrocarbures ne réagissent pas avec les molécules d'alcanolamines, et sont physiquement absorbés. Le modèle thermodynamique a une grande importance pour la conception du procédé de traitement des gaz acide, car il va permettre de déterminer l'Equilibre Liquide Vapeur et faire les bilans d'énergie. Des modèles thermodynamiques fiables peuvent permettre aux concepteurs non seulement de confirmer leurs limites réglementaires, mais aussi de minimiser la perte de composants précieux comme les hydrocarbures.
Dans ce travail, un modèle thermodynamique a été développé pour prédire:

·Les solubilités des alcanes (méthane, éthane, propane, n-butane, n-pentane, n-hexane), aromatiques (ethylbenzène, benzène, toluène) et mercaptans (MM, EM) dans une solution aqueuse d'alcanolamine

· Les solubilités des gaz acides (CO2, H2S) dans des solutions aqueuses d'alcanolamine et d'autres propriétés cruciales telles que: la concentration d'électrolyte, la composition en phase vapeur (principalement le conteneur d'eau)

· Les diagrammes de phase pour les systèmes multi-composants contenant du CO2-H2S-alcanolamine-eau-hydrocabon-mercaptan.

Les paramètres du model ont été déterminés avec les données expérimentales disponibles dans la littérature et les nouvelles données mesurées.

Mots Clés

Abstract

Among fossil fuels, natural gas is the cleanest, in terms of CO2 emission, burn efficiency and amount of air pollutant. Methane is the prevailing element of natural gas; therefore, there are also a variety of impurities. In fact, it contains usually considerable amounts of acid gases (CO2, H2S) which can lead to corrosion in equipments and pipelines if water is present. Mercaptans are known as toxic molecules with undesirable odor, and fuel combustion of mercaptan molecules can produce SO2 which is undesirable chemical, they can cause environmental issues. Acid gases and mercaptans are needed to be removed from natural gas until acceptable standard. The treated natural gas contains as maximum as 2% of CO2, 2–4 ppm of H2S and 5–30 ppm of total mercaptans. Chemical absorption with alkanolamines [3] (such as monoethanolamine (MEA), diethanolamine (DEA), methyldiethanolamine (MDEA)) is the most well-established method to separate acid gas from natural gas. Acid gases react with alkanolamines in the absorber to form electrolyte species, mercaptans and hydrocarbons do not react with alkanolamines molecules, and they are physically absorbed by aqueous alkanolamine solution. Then the loaded solution can be regenerated by heating in the stripper.
Thermodynamic model is of high importance for the conception of the process, as it is linked directly to the accurate determination of the Vapor-Liquid Equilibrium and energy balances. Reliable thermodynamic models can allow designers not only to confirm their regulatory limits, but also to minimize the loss of valuable hydrocarbons components.
In this work a thermodynamic model has been developed to describe:

·Alkane (methane, ethane, propane, n-butane, n-pentane, n-hexane), aromatic (ethylbenzene, benzene, toluene) and mercaptans (MM,EM) in aqueous alkanolamine solution

·Acid gases (CO2,H2S) solubilities in aqueous alkanolamine solutions, and other crucial properties like: electrolyte concentration, vapor phase composition(mostly water contant)

·The phase diagram for multi-component system containing CO2-H2S-alkanolamine-water-hydrocabon-mercaptan

The parameters of the model were determined with the experimental data available in the literature and the new measured data.

Keywords

Gas Processing, absorption, phase diagrams, modeling, experimental work, amine